
Control of Spiral Waves in Reaction-Diffusion Systems Using Response Function

Submitted by **Saad Mohammed Almuaddi**,
to the University of Exeter as a thesis for the degree of
Doctor of Philosophy in Mathematics, in **October 2019**.

This thesis is available for Library use on the understanding that it is copyright material and that no quotation from the thesis may be published without proper acknowledgement.

I certify that all material in this thesis which is not my own work has been identified and that no material has previously been submitted and approved for the award of a degree by this or any other University.

Signature:

ABSTRACT

This thesis is motivated by the desire to understand spiral wave dynamics in reaction-diffusion systems with particular focus on the FitzHugh-Nagumo model. We attempt to control the behaviour of spiral waves using controller dynamics. Response functions characterise the behaviour of spiral waves under perturbations, and so it is natural to use these for control purposes. In this project, we consider perturbations of the FitzHugh-Nagumo equation using control functions with different support. We calculate the response functions using the adjoint linear system of the FitzHugh-Nagumo equation with 1D controller dynamics and also characterise the control functions with the smallest support function which can be used to control the system in periodic and meander regimes. We find the minimum size of the support function that the radius is comparable to the region of the non zero response function.

ACKNOWLEDGEMENT

First of all, I would like to thank all the people who provided me with their precious help and support during the course of my doctoral journey. My deep and sincere gratitude goes to my supervisor, Professor Peter Ashwin, for his continuous support, guidance and availability. Without his help and constant feedback, this thesis would not have been possible and it has been an honour studying under his supervision. In addition, I would like to thank my other supervisor, Professor Vadim Biktashev, for his guidance and feedback on my work. Also, I would like to thank Dr. Chris Ferro and Professor Matt Collins for their advice and support. My sincere appreciation also goes to all my colleagues and other members of the College of Engineering, Mathematics and Physical Sciences for such a warm academic atmosphere. Special thanks go to Abdullah Aldurayhim, Ibrahim Alraddadi, Harun Baldemir, Burhan Bezekci, Courtney Quinn, Bert Wuyts, Bonnie Liefting, Damian Smug, Hassan Alkhayun, Christopher Marcotte, Robert Carroll, Jordon Moore and many others. I would also like to express my gratitude to Paul Ritchie and Karl Nyman for their help in proofreading my thesis. I also wish to thank all the members of the University of Exeter and Saudi Society for helping me cope with homesickness during these years away from home. I would like to thank the Department of Mathematics at the Imam Abdulrahman Bin Faisal University for their support and encouragement. Finally, I would like to express my deepest gratitude to every single member of my family, especially my parents, my wife Azzah and my son Mohammed. I owe them much more than I would ever be able to express. I dedicate this

thesis to my father Mohammed and my mother Sarah.

CONTENTS

	Page
List of Tables	9
List of Figures	11
1 Introduction	15
1.1 Mathematical Reaction-Diffusion Equations and Initial Concepts	15
1.2 Brief Historical Background and Motivation	16
1.3 Rotation, Meander and Control of the Spiral Wave Tip Trajectory	21
1.4 Dynamical Systems Approach to Spiral Waves	23
1.4.1 Stability of Equilibrium Points	23
1.4.2 Stability of Periodic Solutions	27
1.5 Adjoint Linear System for Ordinary Differential Equations	32
1.6 Perturbed Nonlinear Systems and the Adjoint Linear System	34
1.7 Basic Concepts of the Euclidean Group of Symmetries	36
1.8 Summary of the Thesis, Highlighting New Material	38
2 The FitzHugh-Nagumo System and Spiral Waves	40
2.1 The FitzHugh-Nagumo Model on the Plane	40
2.2 Numerical Solutions of the FitzHugh-Nagumo Model	41
2.3 Simulation of Spiral Waves	47

2.4	Trajectory of the Spiral Wave Tip	51
3	Stability of the Spiral Wave, Symmetries and Response Functions	57
3.1	Numerical Solutions of the Linearised FitzHugh-Nagumo System and Response Functions	57
3.2	Symmetries and Drift of the Spiral Waves	64
3.3	Linear stability of the Spiral Wave	77
3.4	Angular Velocity and Wavelength of the Spiral Wave	82
4	Control of Spiral Waves Using Proportional Feedback Control	91
4.1	Proportional Feedback Control for the FitzHugh-Nagumo Model	92
4.2	Examples of Spiral Wave Behaviour under Proportional Feedback Control	94
4.3	Control Parameter Regions for Successful Control	99
4.4	Criteria for Successful Control	104
4.5	Region of Successful Control for Model Parameters	106
4.6	Examples of Unsuccessful Control of the Spiral Wave Behaviour	107
4.7	Proportional Feedback Control with Localised Control Action	111
4.7.1	Control Using a Fixed-Localised Control Action	112
4.7.2	Control Using a Tip-Localised Control Action	113
5	Stability of Spiral Waves with Localised Control Action	115
5.1	Study the Dynamical Stability Spiral Wave Solution for Different Values of Radius	116
5.2	Computing Response Function in the Small Perturbation	117
6	Conclusion	125
6.1	Summary of the Results	125
6.2	Further Work and Open Questions	126

CONTENTS

A Computing Winfree's Diagram	129
B Algorithm of Semi-implicit method for the FitzHugh-Nagumo model	163
C Finding the Minimum Distance to the Hyperplane	176
Bibliography	185

LIST OF TABLES

TABLE	Page
3.1 The table shows the iteration of the approximate angular velocity c^m for the FitzHugh-Nagumo model.	89

LIST OF FIGURES

FIGURE	Page
1.1 A sample experimental picture of a spiral wave in the heart.	19
2.1 Diagram of kinetic function and equilibrium point	43
2.2 Initial condition for u and v components ($\epsilon = 0.3, \beta = 0.75$)	48
2.3 Rigid rotation of the numerical solution of a non-linear system for u component.	49
2.4 Meander of the numerical solution of the non-linear system for u component.	49
2.5 Meander of the spiral wave for u component ($\epsilon = 0.15, \beta = 0.77$).	50
2.6 Hypermeander of the spiral wave for u component ($\epsilon = 0.02, \beta = 1.2$).	50
2.7 Diagram of Spiral wavelength ($\epsilon = 0.3, \beta = 0.75$)	51
2.8 Isolines of spiral wave for components u and v	52
2.9 The diagram of the tip location for the rigid rotation	54
2.10 Diagram of parameters ϵ and β	55
2.11 Diagram of parameters ϵ and β such that the total length of x and y axes is equal to 100 and 50.	56
2.12 Diagram of specific parameters ϵ and β such that the total length of x and y axes is equal to 150 and 50.	56
3.1 Rigid rotation of the numerical solution of the linear system for c component.	61
3.2 Meander of the numerical solution of the linear system for component c	62

3.3	Rigid rotation of the numerical solution of the adjoint linear system for k component.	63
3.4	Meander of the numerical solution of the adjoint linear system for k component.	64
3.5	Diagram of minimal values α_1, α_2 and α_3 , tow and infinity norm.	76
3.6	Diagram of forward linear solution \mathbf{v}^m for rigid rotation.	76
3.7	Diagram of $\alpha_1 \frac{\partial u}{\partial x}$ for rigid rotation.	77
3.8	Diagram of $\alpha_2 \frac{\partial u}{\partial y}$ for rigid rotation.	77
3.9	Diagram of $\alpha_3 \frac{\partial u}{\partial t}$ for rigid rotation.	78
3.10	Diagram of the polar coordinate system (r, Θ) for component χ and the spiral wave solution for component χ in the disk.	88
3.11	Diagram showing the periodic time for the spiral wave.	90
4.1	Diagram referring to functions $x_{tip}(t)$ and $y_{tip}(t)$ with parameters $\alpha = 0.5, \beta = 0.75$ and $\epsilon = 0.3$	95
4.2	Successful control of the behaviour of the spiral wave in a periodic regime using the parameters $\beta = 0.85$ and $\epsilon = 0.25$	96
4.3	The diagram for functions $r_0(t), r(t), \tilde{f}(t)$ and $r_0(t) - r(t)$ describes the values for the successful control of the spiral wave behaviour.	97
4.4	Successful transition of the rigid rotation of the spiral wave to the centre for the u component.	98
4.5	Example of spiral wave in a meander regime for the u component.	98
4.6	Successful transition from the meandering spiral wave to the rigid rotation for the component u	99
4.7	The parameters $\beta = 0.75$ and $\epsilon = 0.3$ are for the region of the values α_1 and α_2 in the periodic regime.	101
4.8	The parameters $\beta = 0.8$ and $\epsilon = 0.292$ are for the region of the values α_1 and α_2 in the meander regime.	102

4.9	The diagram of the stable and unstable spiral wave solutions for the different size of the bounded domain.	103
4.10	The diagram indicates the global successful control as grid points for the whole parameters ϵ and β	107
4.11	Rigid rotation by the proportional feedback control is not obtained with this parameter for the meandering spiral wave for component u	108
4.12	Diagram referring to functions $r_0(t)$, $\tilde{f}(t)$ and $r(t)$ where the behaviour of the spiral wave is not controlled.	109
4.13	The forcing function in a periodic regime does not make the spiral wave motion stable as a rigid rotation.	109
4.14	Spiral rigid rotation as an example of the effect of the bounded domain on the meandering spiral wave for the u component.	111
4.15	Successful control method using the fixed-localised control action and the tip-localised control action.	113
5.1	The relation between the different values of radius R and the largest eigenvalues γ using local support function.	117
5.2	The average solutions of the adjoint linear system in the $x-y$ Cartesian plane for the periodic regime.	119
5.3	The average solutions of the adjoint linear system using $\cos\theta_{m_1}$ and $\sin\theta_{m_1}$ for the periodic regime.	121
5.4	Successful control for parameters $\epsilon = 0.25$ and $\beta = 0.8288$ is shown using the average of adjoint eigenfunctions $k(x, y, t)$ and $s(x, y, t)$	121
5.5	The left eigenfunction of The linear system of FHN with controller model in cartesian coordinate is for component k_0	122
5.6	The average solutions of the adjoint linear system (??) of FHN with controller model in cartesian coordinate using $\cos\theta_{m_1}$ and $\sin\theta_{m_1}$	123

5.7 The diagram of amplitude of length \hat{A}_R for the average solutions $\hat{\rho}_1$ and $\hat{\rho}_2$ of the adjoint linear system (??) of FHN with the controller model. 123

A.1 Diagram showing the curvature $K(t)$ in the periodic regime. 132

A.2 Diagram showing the curvature $K(t)$ in the meander regime. 133

A.3 The figure shows rigid and meander regions using a signed curvature K 134

INTRODUCTION

This chapter begins with an introduction to the reaction-diffusion (RD) equations that generate spiral wave solutions. Briefly, we discuss the history of spiral waves and some applications. We also give some detail about the motivation of study controlling the drift of a spiral wave tip. Finally, we present the important concepts regarding to stability condition of dynamical solutions.

1.1 Mathematical Reaction-Diffusion Equations and Initial Concepts

A reaction-diffusion equation is a nonlinear partial differential equation that includes a reaction function and a diffusion term. The reaction function supplies local dynamics, while the diffusion part (the diffusive transport) propagates information. By interplay of local dynamics and diffusive transport, the spiral waves are observed in excitable media [39]. In general, a reaction-diffusion equation on an infinite domain can be formulated

as follows:

$$\mathbf{u}_t = \mathbf{f}(\mathbf{u}) + \mathbf{D}\nabla^2\mathbf{u}, \quad (1.1)$$

where $\mathbf{u} : \mathbb{R}^{d+1} \rightarrow \mathbb{R}^\ell$ represents a pattern $\mathbf{u}(\mathbf{x}, t)$ such that $\mathbf{x} \in \mathbb{R}^d, t \in \mathbb{R}, \mathbf{u}_t = \frac{\partial \mathbf{u}}{\partial t}, \nabla^2 \mathbf{u} = \sum_{j=1}^d \frac{\partial^2 \mathbf{u}}{\partial x_j^2}$ is the diffusion part and $\mathbf{f} : \mathbb{R}^\ell \rightarrow \mathbb{R}^\ell$ is a smooth function that represents the reaction kinetics. The vector \mathbf{x} represents position and the variable t is time. The matrix $\mathbf{D} \in \mathbb{R}^{\ell \times \ell}$ is the diffusivity and the reaction function (kinetic term) is $\mathbf{f}(\mathbf{u})$. The reaction function $\mathbf{f}(\mathbf{u})$ is a nonlinear function. In this thesis, we consider homogeneous constant diffusivity \mathbf{D} that is a diagonal matrix with non-negative elements that do not depend on the space and time variables. We also restrict the vector \mathbf{x} to be in 2D Euclidean space ($d = 2$) and deal with spiral wave solutions in the (x, y) plane.

1.2 Brief Historical Background and Motivation

Probably the most significant occurrences of spiral waves in nature can be found in cardiac tissue in the case of cardiac malfunction. By studying spiral wave movements, we can gain a better understanding of how the heart functions and potentially, how to treat cardiac malfunctions [13, 19].

An important development of spiral waves occurred in 1946 with the works of Wiener and Rosenblueth; their spiral wave solution is described in [87]. Spiral waves (rotating waves) are defined as propagating waves (travelling waves) that rotate in the plane about a centre point (the spiral wave core): see Winfree [84]. Wiener and Rosenblueth used ideas of the excitable media for cardiac arrhythmias motivated by problems in the sinoatrial node (SA) of the right atrium. Through their work, they managed to understand mathematically some cardiac arrhythmia [13, 51].

In 1952, reaction-diffusion equations were studied by Turing [83]. From 1960 to 1969, there was a growing interest in RD systems; for example, Belousov and Zhabotinski

observed spiral wave patterns in chemical reactions and created a new model called the Belousov Zhabotinski (BZ) reaction. This model in 1D was simplified [64, 67, 82] as follows:

$$\begin{aligned}\frac{\partial U}{\partial t} &= U(1 - U - r_1 V) + \frac{\partial^2 U}{\partial x^2}, \\ \frac{\partial V}{\partial t} &= -b_1 UV + \frac{\partial^2 V}{\partial x^2},\end{aligned}$$

where U and V are dynamical variables with parameters b_1 and r_1 . The BZ reaction is used by mathematicians as an example of an RD system with spiral waves. It is also used as model for biological and dynamical spiral wave phenomena [77].

The collaborative work of Hodgkin and Huxley focused on the excitability of nerve cells and made a tremendous contribution in the field of physiology. They derived a series of equations now called Hodgkin-Huxley (HH) equations; this model consists of four equations [44]:

$$c \frac{dP}{dt} = I_{ex} - g_{Na} (P - P_{Na}) - g_K (P - P_K) - g_L (P - P_L), \quad (1.2a)$$

$$\frac{dN}{dt} = \alpha_N (1 - N) - \beta_N N, \quad (1.2b)$$

$$\frac{dM}{dt} = \alpha_M (1 - M) - \beta_M M, \quad (1.2c)$$

$$\frac{dH}{dt} = \alpha_H (1 - H) - \beta_H H. \quad (1.2d)$$

Equation (1.2) describes sodium with symbol (Na) and potassium with symbol (K), P is the membrane potential voltage and the constant c is the capacitance. Moreover, I_{ex} is an externally applied current, and L is a leak branch. In addition, g_{Na} , g_K and g_L are constant. The constants α_N , β_N , α_M , β_M , α_H and β_H are rate constants that determine the rate transitions between permissive and non-permissive gates. The functions N , M and H are gating variables that represent the activation of the potassium and sodium current.

In 1961, FitzHugh focused on the HH model to describe the electrophysiology of the nervous system and simplified the HH system (1.2) to two equations with dependent

variables P and Q :

$$\begin{aligned}\frac{dP}{dt} &= I_{ex} + P - \frac{P^3}{3} - Q, \\ \frac{dQ}{dt} &= \epsilon (P - c_1 - c_2 Q),\end{aligned}\tag{1.3}$$

where P and Q are dynamical variables and c_1 , c_2 and ϵ are positive constant parameters. The main reason to reduce to two variables is to make the system simple enough in order for it to be solved analytically. FitzHugh observed that the P -nullcline had the form of a cubic function and the Q -nullcline had the shape of a straight line [21, 27, 28]. In 1962, Nagumo et al. illustrated FitzHugh's model (1.3) and also computed the numerical solution of FitzHugh's system in 1D such that they investigated the model (1.3) for an equivalent circuit [66]. As a result, the model (1.3) was named the FitzHugh-Nagumo (FHN) system. This model can be used as a reaction term for an RD equation. Indeed, the spiral wave solutions are observed in the FHN equation [6]. In the 1970s, Arthur Winfree demonstrated the meander behaviour of spiral waves for the FitzHugh-Nagumo system [89]. There has been a significant amount of research that has discussed spiral waves for the FHN system. For example, research focused on how to initiate spiral waves or how to transit the rigid rotation of spiral waves into a meander or hypermeander (these patterns will be discussed explicitly in Section 1.2) [92]. Winfree first measured cardiac excitability and also modified the BZ system to be an excitable dynamical reaction instead of oscillatory. He was also the first to explain trigger waves propagating in the BZ model [40, 91]. Zhabotinsky and Zaikin observed the oscillation of the reaction diffusion system experimentally and noted a periodic propagation from concentric spiral waves in chemical reactions [98]. Furthermore, Allesie, Bonk and Schopman first observed spiral waves in the atrial muscle of rabbit hearts with heartbeat problems as shown in Figure 1.1. They deduced that fibrillation of the heart affects blood movement in the heart [2]. Understanding the heart's behaviour is important to recognise many aspects of arrhythmias through visualization of the electrical wave dynamics of the heart.

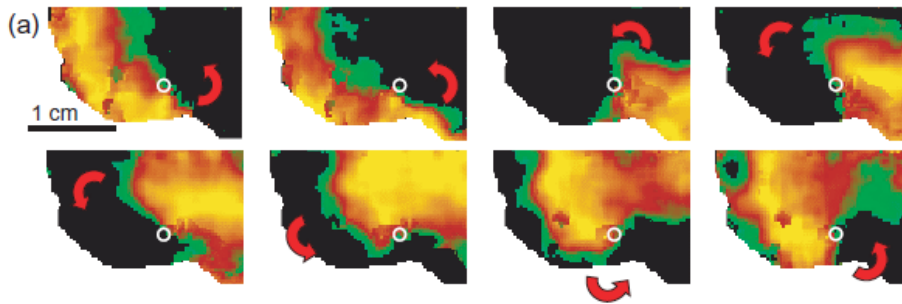


Figure 1.1: The picture, which is taken from [19], shows the visualisation of a spiral wave in experimental cardiac tissue. The spiral wave dynamics rotates rigidly counterclockwise with different membrane voltages in a heart tissue. The orange colour demonstrates high voltage, whereas the green colour indicates lower voltage. Voltages in between are shown by a red colour.

Therefore, we need to use a dynamical system in order to elucidate the mechanisms of visualization techniques. This leads us to improve our understanding of the dynamics of cardiac tissue. As we discussed previously, the HH equations focus on nerve cells such as neurons in the human brain. Therefore, if the magnitude of the sodium or potassium ion flow is low, then neurons in the human brain will not be stimulated [45]. This leads to decreasing cognitive ability. The HH model can help us to understand the mechanisms of membrane potential which is electrical activity. Since the FHN system is derived from the HH model, it is also helpful to understand the dynamics of cells. The modified FHN system is often applied as a general system for excitable media. This is because this system can be amenable to analyse phenomena of the dynamics compared with the HH model [69]. Since the heart consists of muscle cells which have a similar property of nerve cells, we can investigate wave propagation of electrical activity in systems of excitable cells using the FHN system. 10 years later, Gorelova and Bures noted an exciting spiral wave in the retinal tissue in the eyes through using optical characteristics by microscopic observation [35]. Later, in 1990, Jakubith, et al. researched chemical reactions and investigated spatiotemporal patterns with the oscillatory oxidation of carbon dioxide using the BZ system. Based on their experiments, they managed to observe spiral waves through photoemission electron microscopy [46].

In 1991, Winfree classified the behaviour patterns of spiral waves for FitzHugh-Nagumo system if constant parameters are properly adapted in an acceptable range such as rigid rotation, meander, hypermeander (these shapes will be discussed in more detail in Section 2.2). He was the first person to study the behaviour of spiral waves for FHN and contributed to translate related information of dynamical spiral waves from Russian to English [89, 92, 99]. In 2000, Agladze and Steinbock experimentally observed patterns of spiral waves on the rust of steel plates subjected to acid and air such that spiral wave patterns can be noted by the eye on a steel surface [1]. Since 1970, dynamical spiral waves have been studied in the fields of biology, physics and chemistry. Indeed, important works on the behaviour of spiral waves have been produced on the reaction diffusion system. In his book *When Time Breaks Down* [90], Winfree investigated this topic in four sections. In the first section, he introduced and also interpreted the fibrillation in the heart. Moreover, he also discussed circadian rhythms and heartbeat. In the next section, he talked about dynamical spiral waves if the heart has problems in terms of heartbeat. In the third part, he expanded ideas of the previous sections in three dimensions; for example, scroll waves. In the final part of the book, he provided a summary and raised questions regarding several unsolved issues [78, 90]. Similarly, Murray illustrated the dynamical spiral waves of the reaction diffusion equation, which is useful for undergraduate and postgraduate students [65]. Keener and Sneyd, *Mathematical Physiology*, reviewed the Hodgkin-Huxley model and the FitzHugh-Nagumo system in Chapter 9, and explained how to solve FHN and HH equation in one dimension. Also, they briefly discussed spiral waves in Chapter 10 [52].

In recent years, several researchers have noted the roles of Euclidean symmetries in the motion of spiral wave solutions. Euclidean symmetries consist of translations, rotations and reflections. For instance, Barkely noted that many features of spiral wave dynamics can be understood by Euclidean symmetry [93]. Other researchers have

investigated adjoint eigenfunctions (response functions) for dynamical spiral waves such that the response functions of spiral wave solutions are numerically found by the adjoint linearised problem. Response functions effectively show a localised response in the vicinity of the spiral wave core [16]. This work is significant to address the dynamics of spiral wave individually. For example, Biktasheva et al. studied the response function of an adjoint linear system and also found the solutions near the spiral core for the excitable FitzHugh-Nagumo model [14]. Marcotte et al. focused on the spectrum (eigenvalues), numerically computing the eigenvalues of the adjoint operator for the reaction-diffusion Karma model to understand spiral waves for this model [61]. Moreover, Schlesner et al. were mainly interested in the study of the control of dynamical spiral wave tip for the FHN system [75] in order for spiral wave to be controlled. In this project, we focus on the control of the behaviour of a spiral wave for the FHN system and so investigate different types of control. Response functions are discussed for the control of spiral tip in Chapter ???. The overall purpose of this study is explained in Section 1.3.

1.3 Rotation, Meander and Control of the Spiral Wave Tip Trajectory

It is helpful to examine the dynamics of different types of spiral wave. The first type is called a rigid rotation (stationary rotation) of the tip trajectory (tip path) such that the rigid rotation can be defined as the rotation of a spiral wave which moves around the centre point [76]. In other words, when a spiral wave rigidly rotates, its shape remains constant around the centre point of rotation at equilibrium. The second type is called a meander (quasi periodic or non-stationary rotation) of the spiral wave which is a complicated motion. A meander is a type of motion where the tip path of the spiral wave does not remain on a circle as rigid rotation, but it has many small loops like a

flower where the number of "petals" on the flower varies with the system parameters [92]. Usually, the tip trajectory does not exactly repeat. Nevertheless, in exceptional cases it can. The last type of behaviour is when the movement of the spiral wave is called hypermeander whereby the spiral tip trajectory consists of complex small loops and irregular movements. The difference between the meander and the hypermeander is that the tip trajectory of the meander for the spiral wave is regular whereas the tip path of the hypermeander is irregular [32, 37, 76].

As outlined in [32, 37], if the heart has problems with the sinoatrial node (the cardiac muscle cells that set the rhythm of the heart and play the role of pacemaker) then spiral waves can appear in the cardiac muscle tissue. Spiral waves help us to identify cardiac problems such as ventricular fibrillation where the heart does not pump blood properly. In ventricular tachycardia, the sinoatrial node in the right atrium beats too rapidly which can result in fibrillation. It is worth mentioning that a spiral wave in the heart tissue leads to uncoordinated contraction of heart muscle and hence to a loss of effectiveness of the pumping action. Because of this, presence of spiral waves in heart tissue is a significant cause of death [7]. Since electrical waves within the cardiac tissue move as spiral waves.

To control the behaviour of spiral waves, Schlesner et al. [75] propose using a proportional feedback control. As explained in Chapter 4, a perturbation $\mathbf{h}(t)$ is applied to the whole domain. This function can be compared to the electric shocks (defibrillation) used to force heartbeats to become regular [75]. Fibrillation is associated with spiral waves in the heart tissue so by controlling or removing spiral waves, it is possible to treat fibrillation. Standard methods involve applying electric shocks to the whole heart to remove all spiral waves and therefore all heartbeat irregularities. However, this method affects all cardiac cells and can cause serious damage to heart tissue, certain cells can be destroyed and the problem may not be solved. In future, it may be possible to apply

shocks, not on the whole heart itself but on specific parts of the heart to reduce the damage caused by defibrillation. Controlling or removing the spiral wave is an important issue in the treatment of cardiac problems. A first step to this is to remove spiral waves by controlling the spiral tip through a perturbation function, as it will be elaborated in Chapter 4 [75]. Ideally, we want to find less intrusive ways to remove the spiral wave and so to give improved methods of defibrillation.

This thesis focuses on numerical simulations and control of the dynamics of spiral wave solutions of the FHN equation. It also relates the control of spiral waves to the eigenfunction of an adjoint linear operator as a response function. Finally, we attempt to demonstrate effective factors that lead to a successful control method and also discuss the dynamical spiral wave solution using numerical methods.

1.4 Dynamical Systems Approach to Spiral Waves

This section reviews some of the methods used to study the stable and unstable solutions of the nonlinear systems. It also discusses the relationship between nonlinear and linear systems in both autonomous and non-autonomous models. Although we state these ideas for ODEs, much of them carry over to PDEs such as RD equations. In particular we can study the stability of the solutions by investigating the eigenvalues of linear systems. These ideas are explained in Subsections 1.4.1 and 1.4.2.

1.4.1 Stability of Equilibrium Points

Let us consider a continuous time nonlinear system posed as follows:

$$\frac{d\mathbf{x}(t)}{dt} = \mathbf{f}(\mathbf{x}(t)), \quad (1.4)$$

with initial condition $\mathbf{x}(0) = \mathbf{x}_0$ where

$$\mathbf{f}: \mathbf{E} \rightarrow \mathbb{R}^n, \quad \mathbf{x} \in \mathbb{R}^n, \quad \mathbf{E} \subset \mathbb{R}^n, \quad n \in \mathbb{N}, \quad t \geq 0,$$

such that \mathbf{E} is open. We write the solution of system (1.4) as $\mathbf{x}(t) = \varphi(t, \mathbf{x}_0)$. Suppose that solution $\mathbf{x}(t) = \mathbf{x}_*$ of equation (1.4) is an equilibrium, that is

$$\mathbf{f}(\mathbf{x}_*) = 0.$$

Now, we want to understand the stability of the fixed point \mathbf{x}_* in equation (1.4) by examining the eigenvalues of the linearised system. Let

$$\mathbf{x} = \mathbf{x}_* + \mathbf{y},$$

where \mathbf{y} is a perturbation. By using a Taylor series expansion, we have

$$\begin{aligned} \mathbf{f}(\mathbf{x}_* + \mathbf{y}) &= \mathbf{f}(\mathbf{x}_*) + \frac{\partial \mathbf{f}(\mathbf{x}_*)}{\partial \mathbf{x}_*} \mathbf{y} + \mathcal{O}(|\mathbf{y}|^2), \\ &\approx \frac{\partial \mathbf{f}(\mathbf{x}_*)}{\partial \mathbf{x}_*} \mathbf{y}, \end{aligned}$$

such that assuming \mathbf{f} is sufficiently smooth. Hence, the linearised system (1.4) about the equilibrium \mathbf{x}_* is

$$\frac{d\mathbf{y}(t)}{dt} = \mathbf{A}\mathbf{y}(t), \tag{1.5}$$

where

$$\mathbf{A} = \left. \frac{\partial \mathbf{f}(\mathbf{x})}{\partial \mathbf{x}} \right|_{\mathbf{x}=\mathbf{x}_*}$$

is the matrix of first order partial derivatives of the function $\mathbf{f}(\mathbf{x})$ (Jacobian matrix) [68].

We say that the equilibrium point \mathbf{x}_* is *Liapunov stable* if for any neighbourhood $N(\mathbf{x}_*)$, then there is a neighbourhood $M(\mathbf{x}_*)$, such that any solution of system (1.4) beginning in neighbourhood $N(\mathbf{x}_*)$ stays in $M(\mathbf{x}_*)$ for all $t \geq 0$ [81, p.196]. In other words,

$$\mathbf{x}(0) \in N(\mathbf{x}_*) \implies \mathbf{x}(t) \in M(\mathbf{x}_*), \quad \forall t \geq 0.$$

Moreover, \mathbf{x}_* is *asymptotically stable* if it is Liapunov stable and if there exists a neighbourhood $M(\mathbf{x}_*)$ such that

$$\lim_{t \rightarrow \infty} \mathbf{x}(t) = \mathbf{x}_*,$$

for all $\mathbf{x}(0) \in M(\mathbf{x}_*)$. We can understand the stability of point $\mathbf{y} = 0$ for system (1.5) in terms of the eigenvalues of the matrix A . If we have eigenvalues $\lambda_j \in \mathbb{C}$ of \mathbf{A} for $j = 1, \dots, n$ and with corresponding eigenvectors $\mathbf{v}_j \in \mathbb{R}^n$, that is,

$$\mathbf{A}\mathbf{v}_j = \lambda_j \mathbf{v}_j, \quad (1.6)$$

then suppose n_s, n_u and $n_c \in \mathbb{N}$ are chosen such that eigenvalues λ_n are split into three groups according to the sign of the real part of λ_j [68]. First, we assume the first n_s eigenvalues satisfy

$$\operatorname{Re}(\lambda_j) < 0, \quad j \in \{1, \dots, n_s\}, \quad (1.7)$$

and we define the stable subspace

$$\mathbf{E}^s = \operatorname{Span}\{\mathbf{v}_1, \dots, \mathbf{v}_{n_s}\}.$$

The second group of n_u eigenvalues satisfy

$$\operatorname{Re}(\lambda_j) > 0, \quad j \in \{n_s + 1, n_s + 2, \dots, n_s + n_u\}, \quad (1.8)$$

and we define the unstable subspace

$$\mathbf{E}^u = \operatorname{Span}\{\mathbf{v}_{n_s+1}, \dots, \mathbf{v}_{n_s+n_u}\}.$$

The third group of eigenvalues λ_j satisfy the following condition (1.9):

$$\operatorname{Re}(\lambda_j) = 0, \quad j \in \{n_s + n_u + 1, n_s + n_u + 2, \dots, n_s + n_u + n_c\}, \quad (1.9)$$

and we define the centre subspace

$$\mathbf{E}^c = \operatorname{Span}\{\mathbf{v}_{n_s+n_u+1}, \dots, \mathbf{v}_{n_s+n_u+n_c}\}.$$

Note that the eigenvalues in this case are called neutral modes (neutral eigenvalues).

This leads us to define that the vector space \mathbb{R}^n is as follows [38, 68]:

$$\mathbb{R}^n = \mathbf{E}^s \oplus \mathbf{E}^u \oplus \mathbf{E}^c.$$

If we have

$$n = n_s, \quad n_u = n_c = 0,$$

then we can show that the linear system (1.5) is asymptotically stable for all j [41]. If the linear system is stable, then note that,

$$\mathbb{R}^n = \mathbf{E}^s.$$

Moreover, if we have

$$n = n_s + n_u, \quad n_c = 0, \quad n_s \geq 1, \quad n_u \geq 1, \quad (1.10)$$

there exist only negative and positive real parts of eigenvalues. Then, the linear system (1.5) will be unstable of saddle type. This means that some trajectories starting from the initial condition $\mathbf{y}(t_0)$ will diverge from the equilibrium point. If the linear system (1.5) has the centre subspace \mathbf{E}^c , then a stationary point of the linear dynamical system is not ruled by either the stable or unstable manifold as the neutral mode does not present stable or unstable solutions [38].

Finally, stability of the linear system near an equilibrium point $\mathbf{y}_\star = 0$ can be used to understand stability of the equation for the original nonlinear system (1.4) using the following Hartman-Grobman theorem, also known as the linearisation theorem.

Theorem 1. [38, Theorem 1.3.1] *If matrix $\mathbf{A} = \left. \frac{\partial \mathbf{f}(\mathbf{x})}{\partial \mathbf{x}} \right|_{\mathbf{x}=\mathbf{x}_\star}$ has no zero or purely imaginary eigenvalues, that is, $n_c = 0$, then there is a homeomorphism h defined in some neighbourhood U of \mathbf{x}_\star in \mathbb{R}^n locally taking orbits of nonlinear flow (1.4) to those of the linear flow (1.5). The homeomorphism preserves the sense of orbit and can also be chosen to preserve parametrisation by time.*

This theorem shows an important relationship between nonlinear systems and linear systems. In other words, the point \mathbf{x}_\star is a hyperbolic equilibrium of $\dot{\mathbf{x}} = \mathbf{f}(\mathbf{x})$ if the first

order partial derivative of the function $\mathbf{f}(\mathbf{x}_*)$ (Jacobian matrix) does not have zero real part of eigenvalues λ_j

$$\operatorname{Re}(\lambda_j) \neq 0, \quad \forall j \in \mathbb{N}.$$

Then, there is a neighbourhood such that trajectories of the nonlinear flow are mapped to trajectories of the linearised flow of nonlinear systems [68].

As explained in the above subsection, we can understand stable and unstable solutions of ordinary differential equations for autonomous systems using the linearised system. In an analogy to the above, we illustrate the stability analysis for partial differential equations later in the thesis. In the next subsection, we explain stable and unstable periodic solutions.

1.4.2 Stability of Periodic Solutions

In this subsection, we consider periodic solutions of system (1.4) such that the general solution for this system is given by $\mathbf{x}(t) = \varphi(t, \mathbf{x}_0)$. Let us assume now that a solution $\mathbf{x}_*(t)$ of the nonlinear model (1.4) is a periodic orbit, that is there is a $\tau > 0$ such that

$$\mathbf{x}_*(t) = \mathbf{x}_*(t + \tau), \quad \forall t > 0,$$

where $\tau > 0$ is the period and $\mathbf{x}_*(t) \neq \mathbf{x}_*(t + s_1)$ for all $s_1 \in (0, \tau)$. We say that the periodic orbit (curve) $h(\mathbf{x}_0)$ is asymptotically stable for the nonlinear system (1.4) such that h is a subset of points in phase space and \mathbf{x}_0 is an initial point, that is

$$h(\mathbf{x}_0) = \{\varphi(t, \mathbf{x}_0) \mid t \in \mathbb{R}^+\} \subseteq \mathbb{R}^n, \quad n \in \mathbb{N},$$

if it satisfies the following conditions:

1. The curve $h(\mathbf{x}_0)$ is *Liapunov stable*, that is, given any neighbourhood $M(h(\mathbf{x}_0))$, then there is a neighbourhood $N(h(\mathbf{x}_0))$ such that any solution of system (1.4) beginning in neighbourhood $N(h(\mathbf{x}_0))$ stays in $M(h(\mathbf{x}_0))$ for all $t \geq 0$.

2. In addition, it is *asymptotically stable*, that is there exists a neighbourhood $M(h(\mathbf{x}_0))$ such that

$$\lim_{t \rightarrow \infty} d(\varphi(t, \mathbf{x}), h(\mathbf{x}_0)) = 0,$$

for all $\mathbf{x} \in M(h(\mathbf{x}_0))$ [81, p.311]. Note that $d(\mathbf{x}, S) = \inf\{|\mathbf{x} - \mathbf{y}| \mid \mathbf{y} \in S\}$ refers to the distance between the point \mathbf{x} and the set S such that

$$S \subseteq \mathbb{R}^n.$$

Consider a perturbation to $\mathbf{x}_*(t)$ as follows:

$$\mathbf{x}(t) = \mathbf{x}_*(t) + \mathbf{y}(t), \tag{1.11}$$

such that \mathbf{y} is a perturbation. Using a Taylor series expansion we obtain

$$\frac{d\mathbf{x}_*}{dt} + \frac{d\mathbf{y}}{dt} = \mathbf{f}(\mathbf{x}_*) + \frac{\partial \mathbf{f}(\mathbf{x}_*)}{\partial \mathbf{x}_*} \mathbf{y} + \mathcal{O}(|\mathbf{y}|^2),$$

for small $|\mathbf{y}|$. Because

$$\frac{d\mathbf{x}_*}{dt} = \mathbf{f}(\mathbf{x}_*),$$

so this implies

$$\frac{d\mathbf{y}}{dt} = \mathbf{J}(t)\mathbf{y} + \mathcal{O}(|\mathbf{y}|^2), \tag{1.12}$$

where

$$\mathbf{J}(t) = \left. \frac{\partial \mathbf{f}(\mathbf{x})}{\partial \mathbf{x}} \right|_{\mathbf{x}=\mathbf{x}_*(t)}.$$

Note that the Jacobian matrix $\mathbf{J}(t)$ is periodic with minimal period τ . Now, we consider a linearised system (1.12) of the nonlinear equation (1.4). We observe that equation (1.12) is continuous with time and non-autonomous. Moreover, equation (1.12) is a homogeneous system. In order to investigate stability of this system, we need to study the stability

of solutions for system (1.12). By using Floquet theory, we can understand stability of periodic orbits in terms of eigenvalues [29]. Since the matrix $\mathbf{J}(t)$ is a function depending on time t , let $\Phi_1(t), \dots, \Phi_n(t)$ be linearly independent solutions of the system $\dot{\mathbf{y}} = \mathbf{J}(t)\mathbf{y}$ and let $\mathbf{F}(t)$ be the fundamental matrix [81], that is

$$\mathbf{F}(t) = \left[\begin{array}{c|c|c} \Phi_1(t) & \cdots & \Phi_n(t) \end{array} \right], \quad n \in \mathbb{N},$$

where

$$|\mathbf{F}(t)| \neq 0. \quad (1.13)$$

Since each column of matrix $\mathbf{F}(t)$ is a linearly independent solution of system (1.12), the fundamental matrix $\mathbf{F}(t)$ satisfies system (1.12) [47], that is

$$\frac{d\mathbf{F}(t)}{dt} = \mathbf{J}(t)\mathbf{F}(t).$$

This implies the following:

$$\frac{d\mathbf{F}(t+\tau)}{dt} = \mathbf{J}(t)\mathbf{F}(t+\tau).$$

If $\mathbf{F}(t)$ is a fundamental matrix, then $\mathbf{F}(t+\tau)$ is also a fundamental matrix [47]. Let us introduce the monodromy matrix \mathbf{M} that is defined as a fundamental matrix of ordinary differential equations computed at the initial time $t_0 = 0$, that is

$$\mathbf{M} = \mathbf{F}^{-1}(0)\mathbf{F}(\tau).$$

The fundamental theorem of Floquet is:

Theorem 2. [47, Theorem 9.1] *If the monodromy matrix \mathbf{M} has n different Floquet multipliers μ_j , for $j \in \{1, \dots, n\}$, then the linear dynamical system (1.12) has n linearly independent solutions in the following form:*

$$\Phi_j(t) = \mathbf{P}(t)e^{\rho_j t}, \quad j \in \{1, \dots, n\}, \quad (1.14)$$

where ρ_j are constant and $\mathbf{P}(t)$ is a function with period τ and $\Phi_j(t)$ are the column vectors of the fundamental matrix $\mathbf{F}(t)$. Therefore, formula (1.14) can be posed as follows:

$$\mathbf{F}(t) = \mathbf{P}(t)e^{\mathbf{R}t},$$

where \mathbf{R} is a constant matrix (indicator matrix). Moreover, $\mathbf{P}(t)$ is a periodic matrix such that

$$\mathbf{P}(0) = \mathbf{I}, \quad \mathbf{I} = \text{diag}[1, \dots, 1].$$

This leads to the fundamental matrix $\mathbf{F}(0)$ to be the identity matrix \mathbf{I} , so we find that

$$\mathbf{M} = \mathbf{F}(\tau).$$

The Floquet multipliers of a linear system (1.12) are defined as the eigenvalues of the monodromy matrix \mathbf{M} , that is, μ_j such that

$$|\mathbf{M} - \mu_j \mathbf{I}| = 0, \quad j = 1, \dots, n, \quad (1.15)$$

where

$$\mu_j = e^{\rho_j \tau},$$

such that ρ_j is called the Floquet exponent. If all Floquet multipliers lie in the unit circle, that is, $|\mu_j| < 1$, then we say that the periodic linear system (1.12) is stable [81, Corollary 12.3], that is, when

$$|\mu_j| < 1 \quad \forall j \in \{1, \dots, n\}. \quad (1.16)$$

If there exists a Floquet multiplier μ_j for some j such that

$$|\mu_j| > 1, \quad (1.17)$$

we can say that the linear system (1.12) is unstable. Note that if there exists a periodic solution, the modulus of Floquet multiplier is equal to one, that is,

$$|\mu_\star| = 1. \quad (1.18)$$

According to the stable manifold for periodic orbits theorem [81, Theorem 12.8], there is always one Floquet multiplier $\mu_* = 1$.

Following the above, it is now important to relate Floquet multipliers of a periodic linear system (1.12) to the stability of the periodic orbit of the nonlinear model (1.4). Based on this, we suppose that the nonlinear model (1.4) has the following periodic solution:

$$\varphi(t + \tau, \mathbf{x}) = \varphi(t, \mathbf{x}).$$

Define a Poincaré map as follows:

$$\mathbf{p}(\mathbf{x}) = \varphi(t + \tau, \mathbf{x}),$$

such that Poincaré map is discrete and a fixed point (intersection point on surface) $\mathbf{x}(0) = \mathbf{x}_0$ is an initial condition for the Poincaré map, that is

$$\mathbf{p}(\mathbf{x}(0)) = \varphi(\tau, \mathbf{x}(0)) = \mathbf{x}_0.$$

If all eigenvalues (Floquet multipliers) of the Jacobian matrix \mathbf{B} of the Poincaré map are located inside the unit circle such that

$$\mathbf{B} = \left. \frac{\partial \mathbf{p}(\mathbf{x})}{\partial \mathbf{x}} \right|_{\mathbf{x}=\mathbf{x}_0},$$

then we can say that the periodic solution \mathbf{x} of the nonlinear system (1.4) is asymptotically stable. If there exists Floquet multipliers of the Jacobian matrix \mathbf{B} such that the modulus of at least one Floquet multiplier is greater than 1, then the periodic solution \mathbf{x} is unstable [56, 81].

It is useful to introduce the adjoint linear system in ordinary differential equations so that we can compute the left eigenvector. The reason for this is that we can understand the adjoint linear system in partial differential equations, so the following section investigates adjoint linear models.

1.5 Adjoint Linear System for Ordinary Differential Equations

For a linear system of ODEs, the solution can be written in terms of the right eigenvectors of the matrix defining the ODE. We can also find vectors that multiply the matrix to the left termed left eigenvectors. If we transpose equation (1.6), the left eigenvectors and the right eigenvectors are exchanged [70], that is, if λ_j is the eigenvalue for matrix A with right eigenvector \mathbf{v}_j , then

$$\mathbf{v}_j^T \mathbf{A} = \lambda_j \mathbf{v}_j^T, \quad \mathbf{A}^T \mathbf{v}_j = \lambda_j \mathbf{v}_j.$$

If \mathbf{A} is the symmetric matrix, then the left eigenvectors are simply the transpose of the right eigenvectors. The motivation for finding the left and right eigenvectors is that we can calculate the dual form [31]. Now, we consider how we can compute adjoint eigenvectors (left eigenvectors) of autonomous and non-autonomous systems using the linear system (1.5) or (1.12) and transposing the matrix [33], that is,

$$\frac{d\mathbf{z}_1}{dt} = -\mathbf{A}^T \mathbf{z}_1, \tag{1.19a}$$

$$\frac{d\mathbf{z}_2}{dt} = -\mathbf{J}^T(t) \mathbf{z}_2. \tag{1.19b}$$

The adjoint linear system was first defined by Lagrange and Jacobi [41, p. 92]. In 1973, the term *adjoint* was first introduced by Fuchs [41, p. 92]. We observe that the right hand side of equations (1.19a) and (1.19b) is multiplied by a negative sign, so stability of the linear and the adjoint system in some sense are opposite. We observe that the inner product between any solutions of linear system and its adjoint are constant, that is,

$$\langle \mathbf{z}_1(t) | \mathbf{y}(t) \rangle = c,$$

for some $c \in \mathbb{R}$. This is because

$$\begin{aligned}
 \frac{d}{dt} \langle \mathbf{z}_1(t) | \mathbf{y}(t) \rangle &= \left\langle \frac{d\mathbf{z}_1(t)}{dt} | \mathbf{y}(t) \right\rangle + \left\langle \mathbf{z}_1(t) | \frac{d\mathbf{y}(t)}{dt} \right\rangle, \\
 &= \langle -\mathbf{A}^\top \mathbf{z}_1 | \mathbf{y} \rangle + \langle \mathbf{z}_1 | \frac{d\mathbf{y}}{dt} \rangle, \\
 &= -\langle \mathbf{z}_1 | \mathbf{A}\mathbf{y} \rangle + \langle \mathbf{z}_1 | \mathbf{A}\mathbf{y} \rangle, \\
 &= 0.
 \end{aligned}$$

Note that the eigenvalues of matrices \mathbf{B} and \mathbf{B}^T are the same [5]; therefore, if the solution of the linear system (1.5) is stable, the solution of the adjoint linear system (1.19a) is stable backwards in time and vice versa. This leads us to show the following theorem that relates the linear system and adjoint linear systems.

Proposition 1.1. [59] *If the matrix \mathbf{A} has a basis \mathbf{v}_i of right eigenvectors, then there is also a basis \mathbf{w}_j of left eigenvectors of \mathbf{A} such that $i, j \in \mathbb{N}$, and the basis \mathbf{w}_j is dual to basis \mathbf{v}_i .*

Note that basis \mathbf{w}_j and \mathbf{v}_i are dual if

$$\langle \mathbf{w}_i | \mathbf{v}_j \rangle = \delta_{i,j} = \begin{cases} 0 & i \neq j \\ 1 & i = j \end{cases}, \quad (1.20)$$

where $\delta_{i,j}$ is the Kronecker delta. The purpose of finding adjoint autonomous linear system or adjoint non-autonomous linear systems is to compute dual basis. The next section investigates the role of adjoint eigenvectors for nonlinear systems under certain perturbations.

1.6 Perturbed Nonlinear Systems and the Adjoint

Linear System

Following Biktashev [12, 63], we consider the system (1.4) with a small perturbation

$$\frac{d\mathbf{u}(t)}{dt} = \mathbf{f}(\mathbf{u}(t)) + \epsilon \mathbf{h}(\mathbf{u}(t)), \quad (1.21)$$

where $\epsilon \mathbf{h}(\mathbf{u}(t))$ is a perturbation and $\epsilon \ll 1$ and $\mathbf{u} \in \mathbb{R}^n$, $n \in \mathbb{N}$. We assume for $\epsilon = 0$ that the system (1.21) has a manifold of equilibria $\mathbf{U}(\mathbf{a})$, with \mathbf{a} parameterizing equilibria \mathbf{U} , satisfying

$$\mathbf{f}(\mathbf{U}(\mathbf{a})) = 0, \quad (1.22)$$

and

$$\mathbf{a} \in A \subset \mathbb{R}^m, \quad m < n, m \in \mathbb{N}.$$

This means that all solutions $\mathbf{U}(\mathbf{a})$ in phase portrait are equilibria. We assume that all real parts of eigenvalues of the linearised system for the nonlinear system (1.21) are non-positive. If we differentiate equation (1.22) with respect to the variable \mathbf{a} using the chain rule, then we find that

$$\frac{\partial \mathbf{f}(\mathbf{U})}{\partial \mathbf{U}} \frac{\partial \mathbf{U}}{\partial \mathbf{a}} = 0. \quad (1.23)$$

Equation (1.23) can be formulated as components, that is,

$$\sum_{j=1}^m \frac{\partial f_i(\mathbf{U})}{\partial U_j} \frac{\partial U_j}{\partial a_k} = 0, \quad i, k = 1, \dots, m,$$

where $\mathbf{F} = \left[\frac{\partial f_i(\mathbf{U})}{\partial U_j} \right]$ is the Jacobian matrix, such that

$$\mathbf{F}(\mathbf{a}) = \left[\frac{\partial f_i(\mathbf{U}(\mathbf{a}))}{\partial U_j} \right].$$

Moreover, $\frac{\partial \mathbf{U}_j}{\partial \mathbf{a}_k}$ are tangent vectors. Suppose that the column vector is $\mathbf{V}_k(\mathbf{a}) = \frac{\partial \mathbf{U}_j}{\partial \mathbf{a}_k}$. Then

$$\mathbf{F}\mathbf{V}_k = 0 \implies \mathbf{F}\mathbf{V}_k = 0\mathbf{V}_k,$$

where \mathbf{V}_k is a right eigenvector. This means that

$$\lambda_k = 0 \iff \lambda_k(\mathbf{a}) = 0.$$

For

$$\epsilon \neq 0.$$

Following Biktashev's paper [63], we find that there exists an invariant manifold in the neighbourhood of \mathbf{U} with slow dynamics and we can suppose that

$$\mathbf{u} = \mathbf{U}(\mathbf{a}(t)) + \epsilon \mathbf{v}(t). \quad (1.24)$$

Equation (1.24) will be unambiguous if the vector $\mathbf{v}(t)$ is always orthogonal to vector $\mathbf{U}(\mathbf{a}(t))$, that is

$$\langle \mathbf{W}_k(\mathbf{a}) | \mathbf{v} \rangle = 0, \quad k = 1, \dots, m$$

such that \mathbf{W}_k are left eigenvectors that are computed as follows:

$$\mathbf{F}^\top(\mathbf{a})\mathbf{W}_k(\mathbf{a}) = \bar{\lambda}_k \mathbf{W}_k(\mathbf{a}).$$

The biorthogonal vectors $\mathbf{w}_j(\mathbf{a})$ and $\mathbf{V}_{\bar{j}}(\mathbf{a})$ can be written as follows

$$\langle \mathbf{W}_k(\mathbf{a}) | \mathbf{V}_{\bar{k}}(\mathbf{a}) \rangle = \delta_{k\bar{k}}, \quad \bar{k} \in \mathbb{N}.$$

By using equation (1.24) for the functions $\mathbf{f}(\mathbf{u})$ and $\mathbf{h}(\mathbf{u})$ and applying the Taylor series expansion [20],

$$\begin{aligned} \mathbf{f}_k(\mathbf{U} + \epsilon \mathbf{v}) &= \sum_{l=0}^{\infty} \left(\frac{1}{l!} \left(\sum_{g=1}^n \epsilon \mathbf{v}_g \frac{\partial}{\partial \mathbf{U}_g} \right)^l \mathbf{f}_k(\mathbf{U}) \right), \\ \mathbf{h}_k(\mathbf{U} + \epsilon \mathbf{v}) &= \sum_{l=0}^{\infty} \left(\frac{1}{l!} \left(\sum_{g=1}^n \epsilon \mathbf{v}_g \frac{\partial}{\partial \mathbf{U}_g} \right)^l \mathbf{h}_k(\mathbf{U}) \right). \end{aligned}$$

Biktashev [63, p.530] found the differential equation of evolution equations for the variable \mathbf{a} as follows:

$$\frac{d\mathbf{a}_k}{dt} = \epsilon h_k + \epsilon^2 \left(- \sum_{g=m+1}^n \frac{h_{kg} h_g}{\lambda_g} + \sum_{g=m+1}^n \sum_{p=m+1}^n \left(\frac{K_{kpg} h_g h_p}{\lambda_g} + \frac{f_{kpg} h_k h_g}{\lambda_g \lambda_p} \right) \right) + \mathcal{O}(\epsilon^3), \quad (1.25)$$

where

$$K_{kpg} = \left\langle \frac{\partial \mathbf{W}_k(\mathbf{a})}{\partial \mathbf{a}_k} \mid \mathbf{V}_p(\mathbf{a}) \right\rangle = - \left\langle \mathbf{W}_p(\mathbf{a}) \mid \frac{\partial \mathbf{V}_k(\mathbf{a})}{\partial \mathbf{a}_k} \right\rangle.$$

The variables h_{kg} and f_{kpg} are coefficients of the Taylor series expansion for the functions \mathbf{h} and \mathbf{f} such that they can be formulated as follows:

$$h_{kg} = \frac{\partial h_k(\mathbf{U})}{\partial U_g}, h_{kpg} = \frac{\partial h_k(\mathbf{U})}{2 \partial U_g \partial U_p}, f_{kpg} = \frac{\partial f_k(\mathbf{U})}{2 \partial U_g \partial U_p}.$$

1.7 Basic Concepts of the Euclidean Group of Symmetries

Euclidean symmetries have been used to study instabilities of spiral waves [30]. We say a system has symmetries if there is the action of a group (set) S such that properties of the system are preserved by the group action (group orbit). The Euclidean group consists of translations, rotations or reflections of Euclidean space. The idea behind the phenomenon of the drift of spiral waves using symmetries of the system is explained in [9, 55, 60, 95]. We discuss the special Euclidean group $SE(2)$ which is a subgroup of the Euclidean group $E(2)$, that is,

$$SE(2) = \{g \mid g: \mathbb{R}^2 \rightarrow \mathbb{R}^2, g(\mathbf{r}_1) = \mathbf{A}\mathbf{r}_1 + \mathbf{r}_2, \mathbf{A} \in SO(2), \mathbf{r}_1, \mathbf{r}_2 \in \mathbb{R}^2\},$$

where g is a mapping from the group \mathbb{R}^2 to the space \mathbb{R}^2 and

$$SO(2) = \{B \mid B \in \mathbb{R}^{2 \times 2}, \det(B) = 1, B^T = B^{-1}\}.$$

and the Euclidean group is posed as follows:

$$E(2) = \{f: \mathbb{R}^2 \rightarrow \mathbb{R}^2 \mid f(\mathbf{r}_1) = A\mathbf{r}_1 + \mathbf{r}_2, A \in O(2), \mathbf{r}_1, \mathbf{r}_2 \in \mathbb{R}^2\},$$

such that f is a mapping from the group \mathbb{R}^2 to itself and $O(2)$ is the orthogonal matrix of size 2×2 , that is

$$O(2) = \{B \mid B \in \mathbb{R}^{2 \times 2}, B^\top = B^{-1}, \det(B) = \pm 1\}.$$

Each element in the group $SE(2)$ can be defined in terms of rotation and translation, that is,

$$g \in SE(2), \quad g = \{\mathbf{r}, \theta\},$$

such that the variable θ is the angle of rotation of the spiral wave and the vector $\mathbf{r} = (x, y)$ is the translation. In [11], the matrix A has been defined as follows:

$$A = \begin{bmatrix} \cos(\theta) & \sin(\theta) \\ -\sin(\theta) & \cos(\theta) \end{bmatrix}.$$

This section is useful to understand evolution equations (1.25) which describe or approximate the motion (evolution) of a spiral wave tip in Euclidean symmetry as discussed in Section 1.6. In other words, Biktashev wants to find an equation such that the solution of the equation is the tip trajectory of a spiral wave. With regards to the assumption in Section 1.6 as manifold of equilibria $\mathbf{U}(\mathbf{a})$, this leads us to have equilibria of spiral waves. In other words, if we have spiral wave solutions and are also acted by Euclidean symmetry, then we will have other spiral wave solutions. This means that spiral wave solutions do not exist their own as equilibria, but they will be existed as manifold of solutions (spiral wave solutions will be existed as group orbit of spiral wave solutions). Meaning if spiral wave solutions are translated, rotated and reflected, then they are also solutions. Therefore, solution $\mathbf{U}(\mathbf{a})$ is a group orbit of spiral waves. For example, if the solution $\mathbf{U}(\mathbf{a})$ is a periodic orbit and also transformed in a plane, then we will obtain

another periodic orbit. This is because the response functions of the adjoint linear system will work.

In the next section, we show the summary of new materials that we do in terms of control of spiral wave drift for FHN system.

1.8 Summary of the Thesis, Highlighting New Material

First of all, we present the FitzHugh-Nagumo system and solve it numerically using a semi-implicit scheme in Chapter 2. By the automated scan of parameters and using extraction of spiral tip curvature as explained in Appendix A, we recreate Winfree's diagram as shown in Chapter 2. We discuss the FitzHugh-Nagumo system in terms of the dynamical spiral wave solution, response functions and properties of the spiral wave in Chapter 3. Moreover, we also discuss the adjoint linear system for the FHN equation using both, Cartesian and polar coordinate systems in Chapter 3. We also formulate this system in a frame of reference with an angular velocity of the spiral wave in Chapter 3. Therefore, we compute the angular velocity of the spiral wave numerically using *Newton's method* because we can numerically find the eigenvalue from the linear system of the FHN system in a polar coordinate system as discussed in Chapter 3. We investigate how dynamical spiral waves behave in a bounded domain for specific parameters ϵ and β as elaborated in Chapter 3. In Chapter 4, we investigate control of spiral wave tip for the whole (ϵ, β) -parameter space. The localisation of the solutions of the adjoint linear system suggest that the proportional feedback control can be numerically localised and we calculate the time average of this response function in Chapter 5. We can use this localised support to successfully control the drift of the spiral wave tip. We numerically show the spiral wave tip can be controlled using large enough radius of the support

perturbation function such that the function depends on the radius R as given in more detail in Chapter 5. Corresponding to the fixed-localised control action at centre (x_c, y_c) of the spiral core, numerically we also study dynamical spiral wave solution for different values of radius by implementing Lyapunov exponent in Chapter 5. We also discuss the main contributions in my thesis. These can be summarised as follows:

- We verify numerically that the spiral wave can be stabilised using a large enough radius of support control action.
- We find that the size of the spatial localisation of the support control functions using response function of the adjoint linear problem.
- We find that they are comparable.

Finally, we finish with a discussion of results, further work and open questions in Chapter 6.

THE FITZHUGH-NAGUMO SYSTEM AND SPIRAL WAVES

This chapter reviews some properties of the FHN equation and explains the main concepts of spiral wave dynamics. First, spiral waves are presented including their characteristics and most significant features. We explain how to find the initial condition for the FHN system that gives a spiral wave and also demonstrate how to find the tip trajectory of the spiral wave numerically. In this chapter, and throughout the thesis, we shall be conducting the numerical simulations of the FHN system using numerical methods written in MATLAB.

2.1 The FitzHugh-Nagumo Model on the Plane

This section gives some background to the FHN model and spiral wave solutions in two dimensions. We use Neumann boundary condition, which means that there is no flux of system components at the boundaries.

Our mathematical model for the reaction-diffusion system (1.1) is the FHN RD equation. According to [94], the FHN model is a partial differential equation with two

components (u, v) formulated as follows on the plane $(x, y) \in \mathbb{R}^2, t \in \mathbb{R}$:

$$u_t = g(u, v) + \nabla^2 u, \quad (2.1a)$$

$$v_t = h(u, v), \quad (2.1b)$$

where

$$g(u, v) = \frac{1}{\epsilon} \left(u - \frac{u^3}{3} - v \right),$$

$$h(u, v) = \epsilon(u - \alpha v + \beta), \quad u = u(x, y, t), \quad v = v(x, y, t), \quad (2.2a)$$

and there are parameters

$$0 < \alpha < 1, \quad \beta > 0, \quad \epsilon > 0. \quad (2.3)$$

We consider these equations (2.1b) and (2.2a) defined on a square domain

$$(x, y) \in [0, L]^2, \quad L \in \mathbb{R}^+, \quad (2.4)$$

with appropriate initial and boundary conditions. In Section 2.2, we discuss the numerical scheme for the system (2.1) in order to understand the system behaviour of the solutions in two dimensions depending on the parameters with numerical methods and the bifurcation theory.

2.2 Numerical Solutions of the FitzHugh-Nagumo Model

Analytical solutions of a system are not always possible and we observe that no analytical spiral wave solutions for the FHN model have been found explicitly. Before we talk about numerical solutions, we discuss homogeneous solutions of the partial differential

equations (2.1) satisfy ordinary differential equations

$$\begin{aligned}\dot{u} &= \frac{1}{\epsilon} \left(u - \frac{u^3}{3} - v \right) = g(u, v), \\ \dot{v} &= \epsilon (u - \alpha v + \beta) = h(u, v).\end{aligned}\tag{2.5}$$

For parameters $\epsilon = 0.3$, $\alpha = 0.5$, $\beta = 0.75$, Figure 2.1 shows that the only real equilibrium solution of equations (2.5) is

$$(u_*, v_*) = (-1.08, -0.6601),$$

where

$$g(u_*, v_*) = h(u_*, v_*) = 0,$$

so that we find that the global minimum and maximum points of function g are at

$$(u, v) = \left(-1, -\frac{2}{3}\right), \left(1, \frac{2}{3}\right),$$

and we also observe that intersection points on the v axis are at

$$(-\sqrt{3}, 0), (\sqrt{3}, 0).$$

By looking at the non-linear system (2.5), the linearised system of ordinary differential equations (2.5) near equilibrium point (u_*, v_*) is found through the Jacobian matrix of system (2.5), that is,

$$(u, v) = (u_* + \hat{u}, v_* + \hat{v})$$

and

$$\begin{bmatrix} \frac{d\hat{u}}{dt} \\ \frac{d\hat{v}}{dt} \end{bmatrix} = \mathbf{J}(u_*, v_*) \begin{bmatrix} \hat{u} \\ \hat{v} \end{bmatrix} + \mathcal{O}(|\hat{u}|^2, |\hat{v}|^2),$$

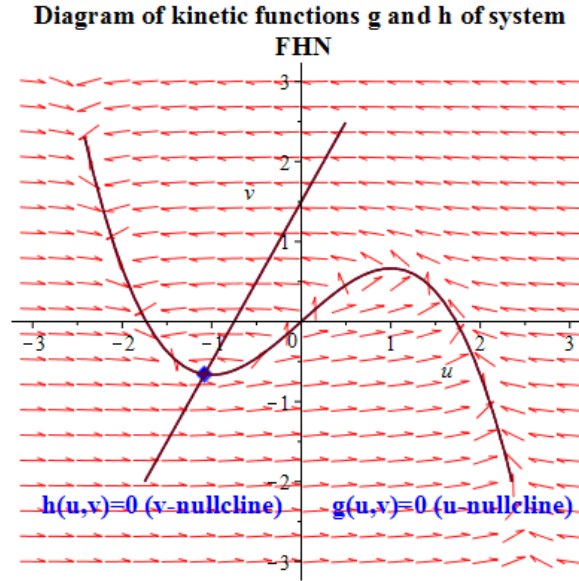


Figure 2.1: Diagram of nullclines for homogeneous FHN model is in the (u, v) phase plane for $\alpha = 0.5$, $\beta = 0.75$ and $\epsilon = 0.3$. The unique equilibrium point (u_*, v_*) corresponds to the homogeneous solution of the ordinary differential equations (2.5). The point $(-u_*, -v_*)$ will be used later in generating the initial condition for spiral waves. The null clines of reaction functions are obtained by Maple.

where

$$\mathbf{J}(u_*, v_*) = \begin{bmatrix} \left. \frac{\partial g(u,v)}{\partial u} \right|_{(u,v)=(u_*,v_*)} & \left. \frac{\partial g(u,v)}{\partial v} \right|_{(u,v)=(u_*,v_*)} \\ \left. \frac{\partial h(u,v)}{\partial u} \right|_{(u,v)=(u_*,v_*)} & \left. \frac{\partial h(u,v)}{\partial v} \right|_{(u,v)=(u_*,v_*)} \end{bmatrix} = \begin{bmatrix} \frac{1}{\epsilon} (1 - u_*^2) & -\frac{1}{\epsilon} \\ \epsilon & -\epsilon \alpha \end{bmatrix}, \quad (2.6)$$

such that $\mathcal{O}(|\hat{u}|^2, |\hat{v}|^2)$ is a truncation error. For the equilibrium point (u_*, v_*) , we have eigenvalues $\lambda_{1,2}$ of matrix (2.6) as follows:

$$|\mathbf{J}(u_*, v_*) - \lambda I_2| = 0 \implies \lambda_{1,2} = -0.3523 \pm 0.9793i,$$

where I_2 is the identity matrix of size 2×2 and i is the unit imaginary number. We observe that eigenvalues $\lambda_{1,2}$ are complex numbers with negative real parts, so the equilibrium point (u_*, v_*) is a stable focus and the spiral trajectories are approaching at the point (u_*, v_*) . We used a phase plane diagram (phase portrait) for equations (2.5) (these points are shown in Figure 2.1). Figure 2.1 shows the homogeneous steady state

at the intersection point (u_*, v_*) between the zero curves of $h(u, v)$ and $g(u, v)$. We also observe that Figure 2.1 has a u -nullcline and the intersection point (u_*, v_*) is on the inner branch of u - nullcline, so the homogeneous equations (2.5) have steady state and unique attractor limit cycles. If the three parameters ϵ, α and β are taken as

$$\epsilon = 0.03, \quad \alpha = 0.5, \quad \beta = 1.2,$$

then the equilibrium point (u_*, v_*) of the homogeneous equation is

$$(u_*, v_*) = (-1.4284, -0.4569),$$

and eigenvalues μ of matrix \mathbf{J} are

$$\mu_1 = -34.6528, \quad \mu_2 = -0.0439.$$

Therefore, we observe that we can have a stable node of homogeneous equation (2.5). The FHN system can be solved numerically, so we can generate an initial condition in terms of components u and v for the homogeneous equation in 2D (the initial condition will be discussed more detail in Section 2.3).

We now explain how we solve the FHN RD equation numerically. We consider the FHN system (2.1b) with (2.2), (2.3), (2.4), initial condition

$$u(x, y, 0) = u_0(x, y), \quad v(x, y, 0) = v_0(x, y), \quad (2.7)$$

and the following (Neumann) boundary condition

$$\begin{aligned} \frac{\partial u(0, y, t)}{\partial x} &= 0, & \frac{\partial u(L, y, t)}{\partial x} &= 0, \\ \frac{\partial u(x, 0, t)}{\partial y} &= 0, & \frac{\partial u(x, L, t)}{\partial y} &= 0. \end{aligned} \quad (2.8)$$

We use the semi-implicit scheme to find approximate solutions of the FHN system (2.1b) such that

$$u_{j,k}^m = u(x_j, y_k, t_m), \quad v_{j,k}^m = v(x_j, y_k, t_m), \quad j, k = 0, 1, \dots, n, \quad m = 0, 1, \dots, n_1, \quad n, n_1 \in \mathbb{N},$$

for space and time steps $\Delta x, \Delta y, \Delta t$ in x, y and t directions. Numerically, space step Δx on the x axis, space step Δy on the y axis and time step Δt are defined as follows

$$x_j = j\Delta x, \quad y_k = k\Delta y, \quad t_m = m\Delta t, \quad \Delta x = \frac{L}{n}, \quad \Delta y = \frac{L}{n}, \quad \Delta t = \frac{\tau}{n_1},$$

where

$$t \in [0, \tau], \quad \tau \in \mathbb{R}^+.$$

In 1969, Robert introduced use of the semi-implicit time stepping method [48]. Thus, the system (2.1) is numerically solved by Forward and Backward Euler methods (FEM and BEM) and Central Finite Difference Method (FDM) (this numerical method is explained in Appendix B) given as follows [8]:

$$\frac{\partial u(x_j, y_k, t_m)}{\partial t} = \frac{u_{j,k}^{m+1} - u_{j,k}^m}{\Delta t} + \mathcal{O}(\Delta t),$$

and

$$\begin{aligned} \frac{\partial^2 u(x_j, y_k, t_{m+1})}{\partial x^2} &= \frac{u_{j+1,k}^{m+1} - 2u_{j,k}^{m+1} + u_{j-1,k}^{m+1}}{(\Delta x)^2} + \mathcal{O}((\Delta x)^2), \\ \frac{\partial^2 u(x_j, y_k, t_{m+1})}{\partial y^2} &= \frac{u_{j,k+1}^{m+1} - 2u_{j,k}^{m+1} + u_{j,k-1}^{m+1}}{(\Delta y)^2} + \mathcal{O}((\Delta y)^2), \end{aligned}$$

such that $\mathcal{O}(\Delta t)$, $\mathcal{O}((\Delta x)^2)$ and $\mathcal{O}((\Delta y)^2)$ are truncation errors. Using the semi-implicit (Crank-Nicholson) scheme involves the fully implicit method related to the diffusion term of equation (2.1a), whereas the fully explicit method is used with the reaction function of equation (2.1), that is

$$u_{j,k}^{m+1} \approx \frac{\Delta t}{\epsilon} \left(u_{j,k}^m - \frac{(u_{j,k}^m)^3}{3} - v_{j,k}^m \right) + \Delta t \frac{u_{j+1,k}^{m+1} - 2u_{j,k}^{m+1} + u_{j-1,k}^{m+1}}{(\Delta x)^2} + \Delta t \frac{u_{j,k+1}^{m+1} - 2u_{j,k}^{m+1} + u_{j,k-1}^{m+1}}{(\Delta y)^2} + u_{j,k}^m. \quad (2.9)$$

For (2.1b), there is no diffusion and so we use a fully explicit scheme, that is

$$v_{j,k}^{m+1} \approx \Delta t \epsilon \left(u_{j,k}^m - \alpha v_{j,k}^m + \beta \right) + v_{j,k}^m. \quad (2.10)$$

The algorithm of the numerical solvers for the FHN system is explained in appendix [B](#).

Note that we can also estimate the approximate solution of FHN system using the fully explicit method instead of the semi implicit method. The problem with the fully explicit method is that the numerical solution is obtained more slowly using Matlab compared with the semi implicit method, which can be found relatively quickly. However, we observe that the numerical solver $u_{j,k}^m$ corresponding with u component needs to be evaluated for each grid points j and k . Regarding the x axis, we observe that the numerical solver $u_{j,k}^m$ is not defined for $j - 1$ and $j + 1$ if we have 0 and n . So, using Neumann boundary condition [\(2.8\)](#), in terms of the x axis, we find

$$j = 0 \implies u_{1,k}^m = u_{-1,k}^m, \quad j = n \implies u_{n+1,k}^m = u_{n-1,k}^m.$$

According to the y axis, we observe that

$$k = 0 \implies u_{j,1}^m = u_{j,-1}^m, \quad k = n \implies u_{j,n+1}^m = u_{j,n-1}^m.$$

We use the initial condition [\(2.7\)](#) as follows

$$u_{j,k}^0 = u_0(j \Delta x, k \Delta y), \quad v_{j,k}^0 = v_0(j \Delta x, k \Delta y).$$

Following the above, we now need to carefully determine the time step Δt and the space step Δx , such that Δt and Δx are small enough numbers so that the approximate solutions are accurate. Note that we have to be careful when choosing the optimal time step Δt and space step Δx in order for the numerical solutions of system [\(2.1\)](#) to be stable. Since the numerical method is semi implicit, the stability condition of the FHN system in 2D can not be derived using Von Neumann stability analysis [\[18\]](#) unlike with the fully explicit method. By numerical observation, we assume that the time step Δt and space steps $\Delta x = \Delta y$ are equal to 0.1 and 0.3 respectively for the numerical solver because the numerical solution of the FHN system is stable.

2.3 Simulation of Spiral Waves

The numerical schemes are important to investigate the initiation problem if there are no analytical solutions. Therefore, we now need to discuss how to generate the initial condition of spiral waves for system (2.1) using Barkley's method [4]. As in Figure 2.1, we have a steady state point (u_*, v_*) for homogeneous equations (2.5). We consider the initial conditions $u_0(x, y)$ and $v_0(x, y)$ of system (2.1) posed as follows

$$\begin{aligned} u_0(x, y) &= \begin{cases} u_* & \text{if } y \geq \frac{L}{2} \\ -u_* & \text{if } y < \frac{L}{2} \end{cases} \\ v_0(x, y) &= \begin{cases} v_* & \text{if } x \geq \frac{L}{2} \\ -v_* & \text{if } x < \frac{L}{2} \end{cases}, \end{aligned} \quad (2.11)$$

on the region $(x, y) \in [0, L]^2$. Note that $u_0(x, y)$ is at the homogeneous steady state only in the subregion $(x, y) \in [0, \frac{L}{2}] \times [0, L]$. As observed by Barkley [4], with such an initial condition solutions rapidly evolves into a spiral wave as shown in Figure 2.2. Barkley's method can be used to generate the initial condition of spiral waves that are approximate solutions for the FHN model such that the spiral wave solutions rotate counterclockwise. In the FHN system, only initial value problems (forwards time) can be solved because of the diffusion terms. Using the initial condition at the final moment of time, as shown in Figure 2.2, a numerical solution of the FHN system is shown in Figure 2.3 such that Winfree chooses $\alpha = 0.5$ [92]. The most basic type of spiral wave motion is called a rigid rotation, as shown in Figure 2.3. The shape remains constant while it rotates rigidly around the centre point of rotation, as its name suggests. One of the characteristics of the spiral wave with a rigid rotation is that it has a constant core radius. This means that the spiral wave rotates around the spiral core with constant radius and angular velocity if we increase time. According to Figure 2.3, we need to remove the initial transient in order for the spiral wave to have a periodic orbit, otherwise the tip trajectory of the spiral wave will not be in a circular orbit [75]. As discussed in [75], the spiral tip for the rigid

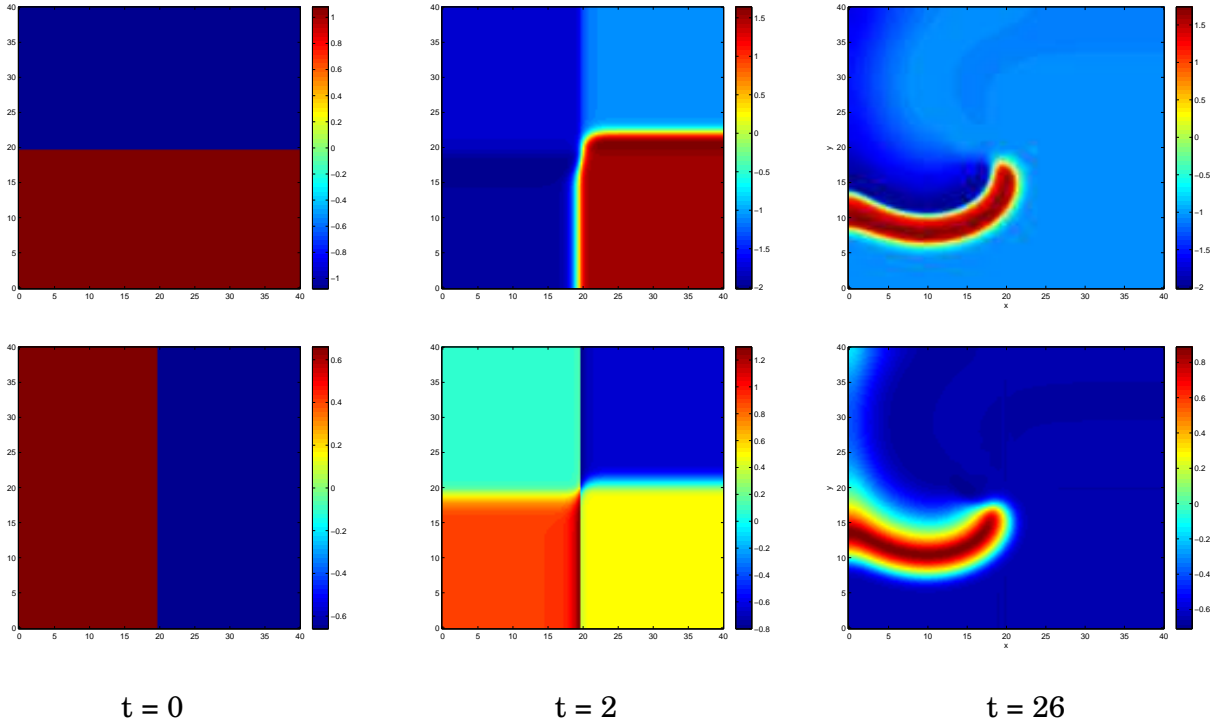


Figure 2.2: Evolution of the initial condition (2.11) showing generation of spiral waves using Barkley's initial condition [4]. The three diagrams in the first row indicate the component u while the three diagrams in the second row indicate the component v at times $t = 0, t = 2$ and $t = 26$. The time step Δt and space steps $\Delta x = \Delta y$ are 0.1 and 0.3 respectively. The parameters ϵ, β and α of the FHN model are 0.3, 0.75 and 0.5 respectively.

rotation is attracted to a circular orbit and has a reference point (centre point). If we decrease the parameter ϵ and also increase the parameter β as follows:

$$\epsilon = 0.2, \quad \beta = 0.85,$$

then the numerical solution of the FHN system shows a spiral tip meander, as in Figure 2.4. The meander is a more complicated type of motion insofar as the tip path of the spiral wave consists of many small loops, so the pattern of the spiral wave location looks like a flower-orbit with loops as shown in Figure 2.4. In other words, there are two types of spiral waves for the meander, one of them is called outward meander and the other type is called the inward meander. These types are named depending on the shape of their tip path motion [74]. In our case Figure 2.4, the spiral tip meander is an outward

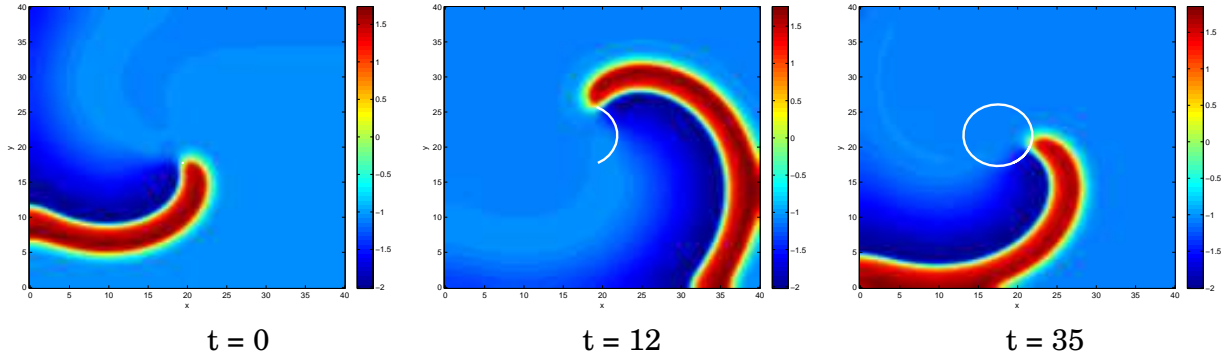


Figure 2.3: Numerical solution of the FHN system for u component with parameters $\alpha = 0.5$, $\beta = 0.75$ and $\epsilon = 0.3$ showing a rigid rotation such that the numerical simulation is found by the semi implicit method. Moreover, the initial condition is the spiral wave from Figure 2.2. The time step Δt is 0.1. Moreover, the space steps Δx and Δy are 0.3.

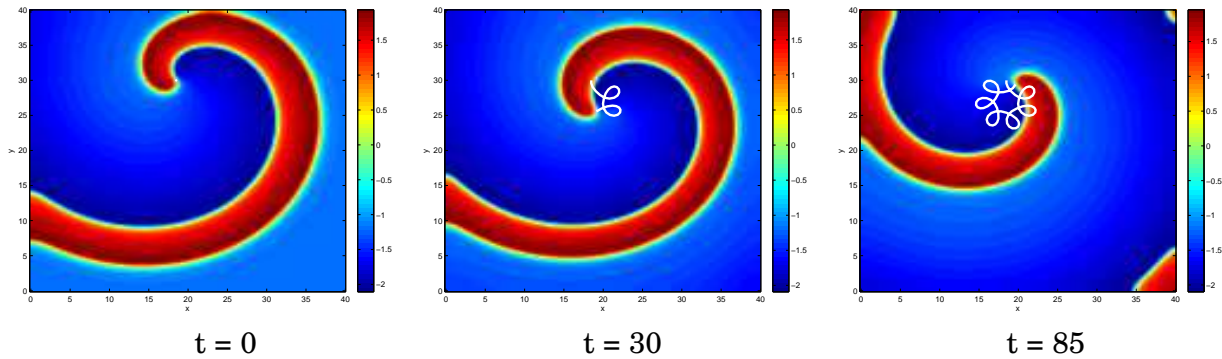


Figure 2.4: Numerical solution of the FHN for u component with parameters $\alpha = 0.5$, $\beta = 0.85$ and $\epsilon = 0.2$ using the semi implicit method from Appendix B. Moreover, the initial condition is the spiral wave from Figure 2.2, while the spiral tip meander is a loop. The pattern is not a rigid rotation limit but shows a meandering spiral tip. The time step Δt is 0.1 while space steps Δx and Δy are 0.3 for the space scale 40.

meander. As shown in Figure 2.4, we need to eliminate the initial transient in order to obtain a meander, otherwise the shape of meander will not be a flower-orbit with loops. Therefore, we can observe that the behaviour of the spiral wave tip for the meander is a quasi-periodic movement instead of a periodic orbit as in the rigid rotation [74, 75]. In a meander regime, if we change the parameters ϵ and β of FHN to be:

$$\beta = 0.77, \epsilon = 0.15,$$

then the tip trajectory of the spiral wave will become triangle-shaped, as shown in Figure 2.5. For parameters ϵ and β given by:

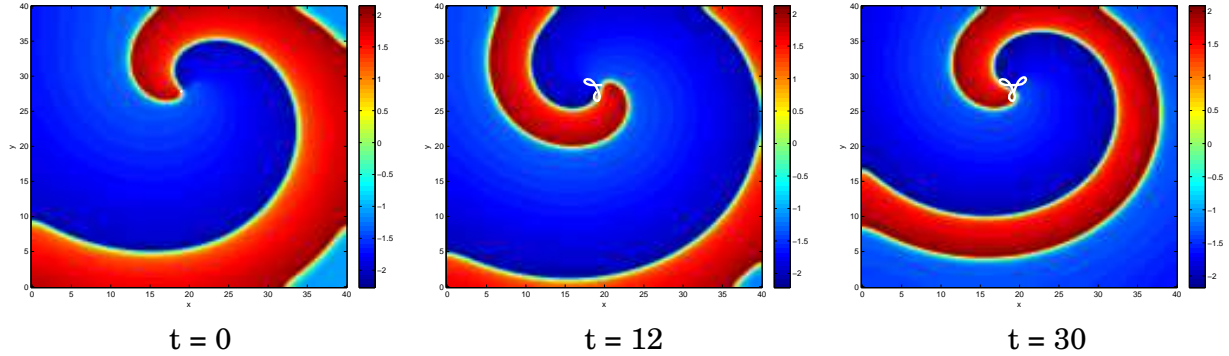


Figure 2.5: A snapshot of the tip path of the spiral wave behaviour for component u with parameters $\epsilon = 0.15$ and $\beta = 0.77$ and time step $\Delta t = 0.1$ and space steps $\Delta y = \Delta x = 0.30$ for the space scale 40. The numerical simulation is found by the semi implicit method. This shows an example of a triangle-shaped meander.

$$\beta = 1.2, \epsilon = 0.02,$$

then we find that the motion of the spiral wave is a hypermeander, as shown in Figure 2.6. As shown in Figure 2.6, the tip of the spiral wave has a hypermeander motion [92] if

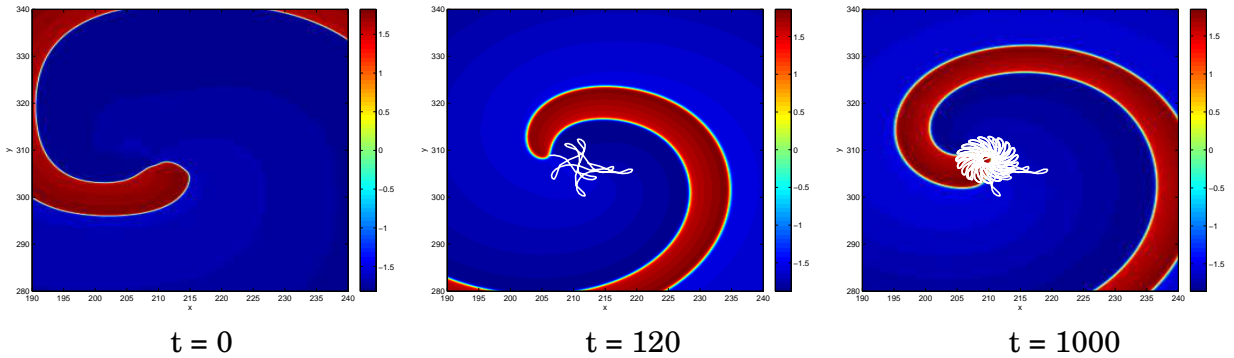


Figure 2.6: The numerical solution u of the non-linear system for the FHN model with parameters $\alpha = 0.5$, $\beta = 1.2$ and $\epsilon = 0.02$ such that the numerical solution is found using the semi implicit method. Moreover, the initial condition is a spiral wave. The time step Δt is equal to 0.005 and space steps Δx on the x axis $[0, 420]$ and Δy on the y axis $[0, 420]$ are $\frac{1}{\sqrt{5}} = 0.1818$. This shows an example of hypermeander.

it has at least three irregular frequencies compared with the meander of the spiral wave that moves regularly.

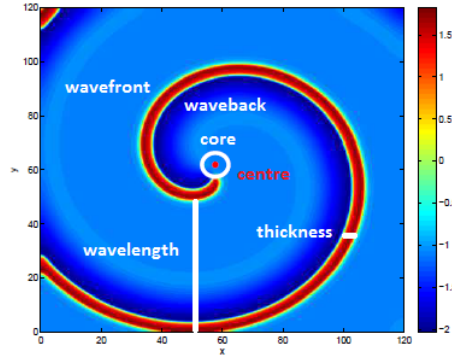


Figure 2.7: A snapshot of a spiral wave for FHN (equation (2.1)) indicates component u where $\epsilon = 0.3$ and $\beta = 0.75$. Details of the numerical method are given in Sections 2.2 – 2.4. The front and back of the spiral wave are shown, along with the thickness and the wavelength of the front. The path of the spiral tip (where the front and back meet) is shown in white. The spiral wave tip is called a core while the red point is the centre of the core.

2.4 Trajectory of the Spiral Wave Tip

The trajectory of the spiral wave tip can be used to understand many properties of the behaviour of spiral waves for the FHN model. Using the initial condition shown in Figure 2.2, spiral waves, which depend on parameters ϵ and β , are shown in Figure 2.7. Spiral waves in a FHN model consist of a wavefront and a waveback that meet at a spiral tip, so we consider the isolines of the numerical spiral wave solutions of FHN system for two components u and v , as shown in Figure 2.8. The intersection of two isolines can be used to characterise a spiral tip (x_{tip}, y_{tip}) [97]. More precisely, given values

$$u_{iso}, v_{iso} \in \mathbb{R},$$

we define the isolines for the u and v components

$$U = \{(x, y) \mid u(x, y, t) = u_{iso}, x, y \in \mathbb{R}, t \geq 0\},$$

$$V = \{(x, y) \mid v(x, y, t) = v_{iso}, x, y \in \mathbb{R}, t \geq 0\},$$

and the intersection point (x_{tip}, y_{tip}) , that is,

$$(x_{tip}, y_{tip}) = U \cap V. \quad (2.12)$$

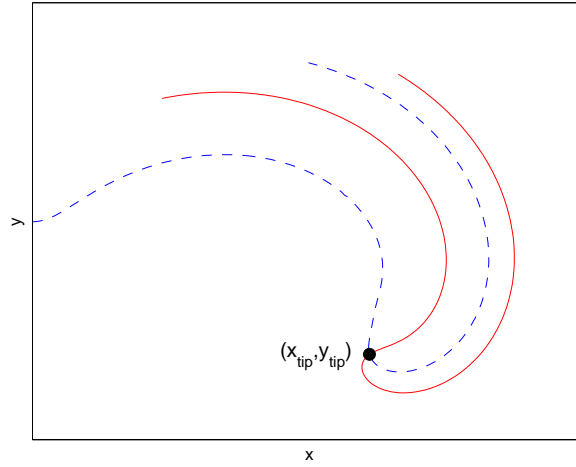


Figure 2.8: Typical isolines for u (solid) and v (dash) for the spiral wave pattern shown in Figure 2.2 at time moment $t = 26$. The location will vary depending on the value of u and v for the isoline, which shows the isolines for $u = 0$ and $v = 0$. The spiral tip (x_{tip}, y_{tip}) is at the intersection of these isolines.

As shown in [24], a good level of isoline for components u and v is zero [24], that is,

$$u_{iso} = v_{iso} = 0. \quad (2.13)$$

An example of isolines of $u_{iso} = v_{iso} = 0$ for spiral wave solutions is shown in Figure 2.8. Numerically, we find the intersection (x_{tip}, y_{tip}) between these isolines and note that the location depends on chosen values of u_{iso} and v_{iso} [25]. By looking at sets U and V , if the numerical approximations for u and v is defined as follows

$$\begin{aligned} \hat{u}(x, y) &\approx u(x, y, t_1), \\ \hat{v}(x, y) &\approx v(x, y, t_1), \quad (x, y) \in [0, L]^2 \end{aligned}$$

where time t_1 is fixed so that

$$\begin{aligned} \hat{u}(x_j, y_k) &= \hat{u}(j \Delta x, k \Delta y), \\ \hat{v}(x_j, y_k) &= \hat{v}(j \Delta x, k \Delta y), \end{aligned} \quad (2.14)$$

then, we find the approximation of the u -isoline such that $(\hat{x}_l, \hat{y}_l) \in U$ and $l \in \mathbb{N}$. For each point (\hat{x}_l, \hat{y}_l) the chosen values (j, k) are as follows:

$$(\hat{x}_l, \hat{y}_l) \in [x_j, x_{j+1}] \times [y_k, y_{k+1}].$$

Then, we use a bilinear interpolation (3.66) [54] of value $\hat{v}_l(\hat{x}_l, \hat{y}_l)$, that is,

$$\hat{v}_l(\hat{x}_l, \hat{y}_l) = r_1 + e_1 \hat{x}_l + f_1 \hat{y}_l + g_1 \hat{x}_l \hat{y}_l = \hat{v}_l(\hat{x}_l, \hat{y}_l), \quad r_1, e_1, f_1, g_1 \in \mathbb{R}, \quad (2.15)$$

such that $\hat{v}_l > 0$ and $\hat{v}_{l+1} < 0$ or $\hat{v}_l < 0$ and $\hat{v}_{l+1} > 0$. By using the linear equation (2.16)

$$v = mx + c, \quad m, c \in \mathbb{R}, \quad (2.16)$$

we can find x_{tip} through some procedures, that is,

$$c = v_l - \left(\frac{v_l - v_{l+1}}{\hat{x}_l - \hat{x}_{l+1}} \right) \hat{x}_l, \quad v_l > v_{l+1}, v_l > 0, v_{l+1} < 0,$$

such that slope m is as follows

$$m = \frac{v_l - v_{l+1}}{\hat{x}_l - \hat{x}_{l+1}}.$$

Since the isoline for the v component is zero, we find that

$$0 = \left(\frac{v_l - v_{l+1}}{\hat{x}_l - \hat{x}_{l+1}} \right) \hat{x}_{tip} + v_l - \left(\frac{v_l - v_{l+1}}{\hat{x}_l - \hat{x}_{l+1}} \right) \hat{x}_l \implies x_{tip} = -v_l \left(\frac{\hat{x}_l - \hat{x}_{l+1}}{v_l - v_{l+1}} \right) + \hat{x}_l,$$

where

$$x_{tip} \in [\hat{x}_l, \hat{x}_{l+1}].$$

Similarly, let us calculate y_{tip} . We find

$$c = v_l - \left(\frac{v_l - v_{l+1}}{\hat{y}_l - \hat{y}_{l+1}} \right) \hat{y}_l, \quad v_l > v_{l+1}, v_l > 0, v_{l+1} < 0,$$

such that

$$m = \frac{v_l - v_{l+1}}{\hat{y}_l - \hat{y}_{l+1}}.$$

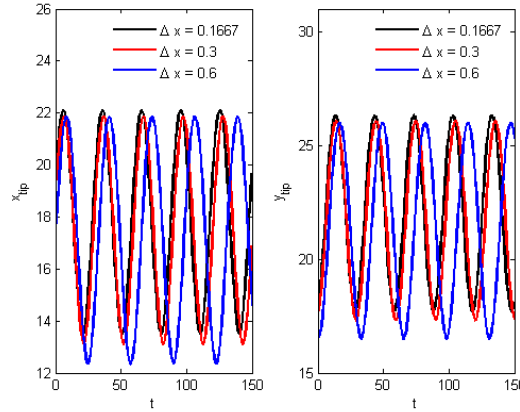


Figure 2.9: The tip location is calculated numerically for parameters $\alpha = 0.5$, $\beta = 0.75$ and $\epsilon = 0.3$ in different space steps such that the time step Δt is equal to 0.1. The size of the bounded domain of the spiral wave in the (x, y) -plane is $[0, 40]^2$.

Since the isoline for the v component is zero, we find that

$$0 = \left(\frac{v_l - v_{l+1}}{\hat{y}_l - \hat{y}_{l+1}} \right) y_{tip} + v_l - \left(\frac{v_l - v_{l+1}}{\hat{y}_{l+1} - \hat{y}_l} \right) \hat{y}_l \implies y_{tip} = -v_l \left(\frac{\hat{y}_l - \hat{y}_{l+1}}{v_l - v_{l+1}} \right) + \hat{y}_l,$$

where

$$y_{tip} \in [y_l, y_{l+1}].$$

We investigate the error in measuring the tip location (x_{tip}, y_{tip}) using the two norm. We observe that a reasonable value of the space step Δx for the semi implicit method is 0.1667 because by numerical observation we have a stable spiral wave solution and also because the simulation using Matlab can be obtained quickly. Therefore, let us assume that we have the optimal numerical tip trajectory for $\Delta x = 0.1667$. If we have two other values of the space step Δx , then the diagram of the tip location is shown in Figure (2.9). This means that if we decrease the space step as much as possible, then the tip trajectory of the spiral wave is more accurate.

Winfree discussed the motion of spiral waves depending on the parameters β and ϵ as shown in Figure 2.10 [92]. The left picture is plotted through studying the signed curvature of the spiral wave tip (plot Winfree's diagram is explained in appendix A). This is because the Matlab code can distinguish between the three main types of motion

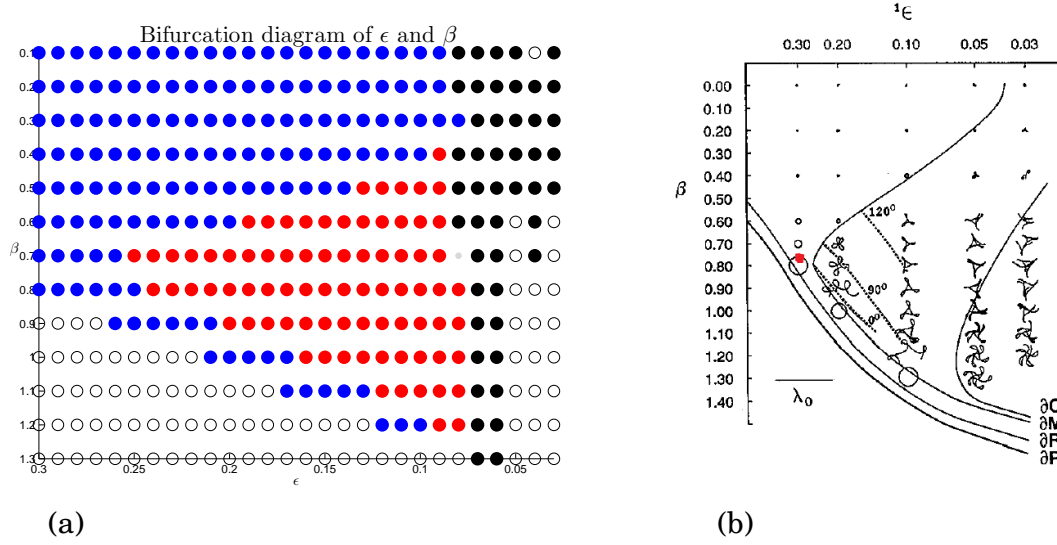


Figure 2.10: The picture (a) shows the filled blue points indicate the rigid region. The filled red points indicate the meander region such that the spatial domain is $[0, 150]^2$. The open black points indicate the spiral wave solution has collided with the boundary domain and disappeared. The filled black points indicate the unstable spiral wave solution which undergoes an alternans instability and breaks up into multiple spiral segments. The picture (b), taken from [92], shows how ϵ , β and $\alpha = 0.5$ change the spiral wave behaviour. ∂P is the boundary of permitted propagation (propagation boundary). ∂R is the rotor boundary (see Figure 2.7). ∂M is the boundary of the meander. ∂C is the hypermeander boundary. The small diagrams show examples of trajectories of the wavytip of spiral waves that exist above the rotor boundary ∂R . The circular loop of the wavytip of the spiral wave gets larger upon approaching the boundary ∂R [96], [36].

of spiral waves to generate the plot, Winfree's diagram. However, we now need to study the spiral wave tip with different domain sizes using the Figure 2.10. Firstly, if the total length of x and y is equal to 100, then the spiral wave behaviour is as illustrated by Figure 2.11. Finally, if the total length of x and y axes is equal to 50, then the wavytip can be described by Figure 2.11. If we consider a small region of Winfree's diagram for specific parameters ϵ and β as follows:

$$\epsilon \in \{0.17, 0.173, \dots, 0.227, 0.23\}, \quad \beta \in \{0.8, 0.815, \dots, 1.085, 1.1\},$$

then the behaviour of the spiral wave for Winfree's diagram is demonstrated by Figure 2.12.

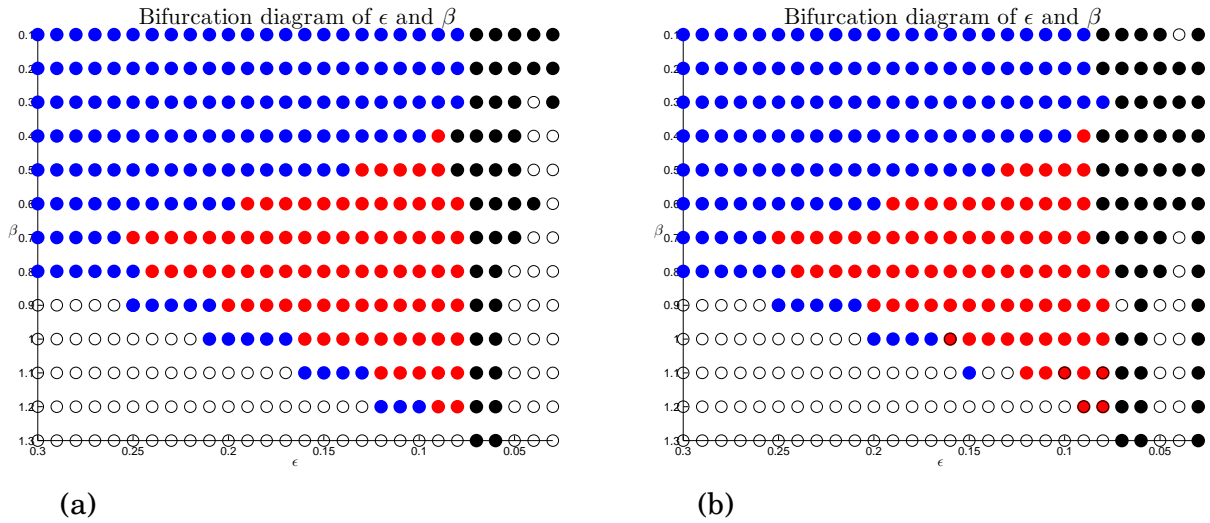


Figure 2.11: The diagram (a) shows how ϵ , β and $\alpha = 0.5$ change the spiral wave behaviour such that the total length of x and y axes is equal to 100, while the diagram (b) explains the spiral wave tip for domain $[0, 50]^2$. All diagrams explain that the filled blue points indicate the rigid region whereas the filled red points indicate a meander region. The open and filled black points indicate no spiral waves such that the open black points indicate the spiral wave solution has collided with the boundary domain and disappeared. Furthermore, the filled black points indicate the unstable spiral wave solution.

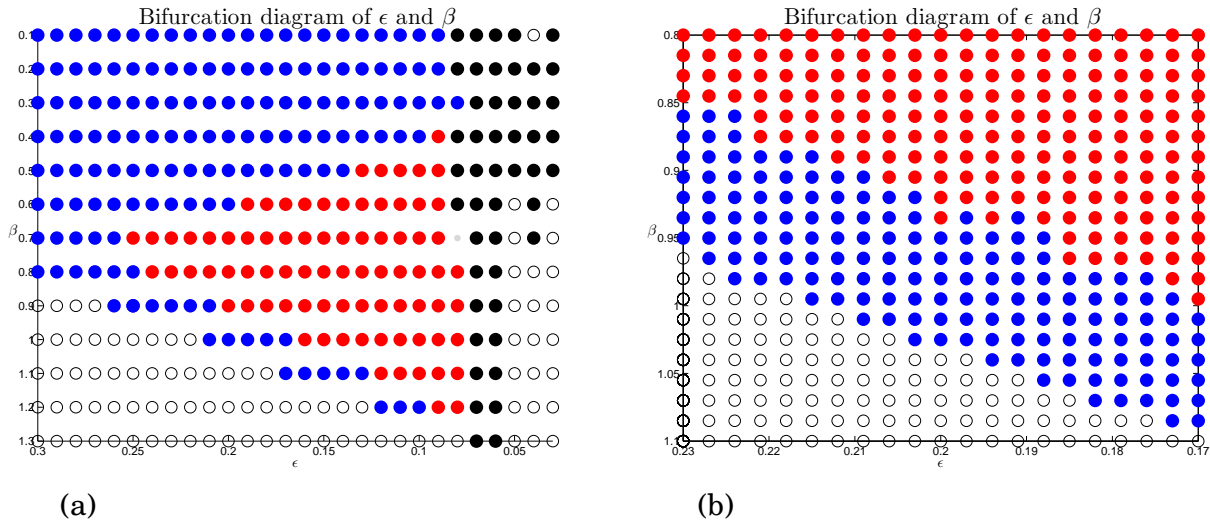


Figure 2.12: The diagram (a) shows how ϵ , β and $\alpha = 0.5$ change the spiral wave behaviour such that the total length of x and y axes is equal to 150 compared with the diagram (b) which explains the spiral wave tip in the small region. All diagrams explain that the filled blue points indicate the rigid region whereas the filled red points indicate a meander region. The open and filled black points indicate no spiral wave such that the open black points indicate the spiral wave solution has collided with the boundary domain and disappeared. Furthermore, the filled black points indicate the unstable spiral wave solution.

STABILITY OF THE SPIRAL WAVE, SYMMETRIES AND RESPONSE FUNCTIONS

In order to investigate and understand the stability of spiral wave solutions for the FHN system, we need to linearize the model about the solution. Based on the linearization, we discuss the response functions (eigenvectors of the adjoint linear system) as these tell us how the system responds to perturbation. In this chapter, we discuss how to numerically solve the linear and adjoint linear systems in Cartesian coordinates. We also analyse how to formulate the FHN model in a corotating frame of reference and polar coordinates.

3.1 Numerical Solutions of the Linearised FitzHugh-Nagumo System and Response Functions

As we know, the purpose of linearising the FHN system is that we seek to study the stability and instability of the spiral wave numerical solution through finding the eigen-

values of the linear system [15, 68, 73]. Moreover, we can compute the dual basis of the left eigenfunctions, as it is discussed in Section 1.5. Nonetheless, we now need to linearise the FHN system following a number of processes. First, the FHN system can be formulated as follows:

$$\mathbf{u}_t = \mathbf{D}(\mathbf{u}_{xx} + \mathbf{u}_{yy}) + \mathbf{f}(\mathbf{u}), \quad (3.1)$$

where

$$\mathbf{u}_t = \begin{bmatrix} u_t \\ v_t \end{bmatrix}, \mathbf{D} = \begin{bmatrix} 1 & 0 \\ 0 & 0 \end{bmatrix}, \mathbf{u}_{xx} = \begin{bmatrix} u_{xx} \\ v_{xx} \end{bmatrix}, \mathbf{u}_{yy} = \begin{bmatrix} u_{yy} \\ v_{yy} \end{bmatrix}, \mathbf{f}(\mathbf{u}) = \begin{bmatrix} g \\ h \end{bmatrix}.$$

Now, the equation (3.1) can be linearised through using the equation (3.2)

$$\mathbf{u} = \mathbf{q} + \mathbf{v}, \quad (3.2)$$

where

$$\mathbf{q} = \mathbf{q}(x, y, t), \mathbf{v} = \mathbf{v}(x, y, t), 0 < x < L, 0 < y < L, L \in \mathbb{R}^+,$$

and

$$\mathbf{q}(x, y, t) = \begin{bmatrix} a(x, y, t) \\ b(x, y, t) \end{bmatrix}, \mathbf{v}(x, y, t) = \begin{bmatrix} c(x, y, t) \\ d(x, y, t) \end{bmatrix}.$$

We can also assume that \mathbf{q} is a solution of the nonlinear system (3.1), whereas \mathbf{v} is the linear part of the equation (3.2). Therefore, if we differentiate the equation (3.2) with respect to the variable t , then we find that

$$\mathbf{u}_t = \mathbf{q}_t + \mathbf{v}_t.$$

If we also differentiate the equation (3.2) with respect to variables x and y twice, then we find that

$$\mathbf{u}_{xx} = \mathbf{q}_{xx} + \mathbf{v}_{xx}$$

$$\mathbf{u}_{yy} = \mathbf{q}_{yy} + \mathbf{v}_{yy}.$$

3.1. NUMERICAL SOLUTIONS OF THE LINEARISED FITZHUGH-NAGUMO SYSTEM AND RESPONSE FUNCTIONS

According to $\mathbf{f}(\mathbf{u})$, by using Taylor series expansion, we find that the function $\mathbf{f}(\mathbf{u})$ of the equation (3.1) is expressed as follows

$$\begin{aligned}\mathbf{f}(\mathbf{q} + \mathbf{v}) &= \mathbf{f}(\mathbf{q}) + \frac{\partial \mathbf{f}(\mathbf{q})}{\partial \mathbf{q}} \mathbf{v} + \mathcal{O}(|\mathbf{v}|^2) \\ &= \mathbf{f}(\mathbf{q}) + \left. \frac{\partial \mathbf{f}(\mathbf{u})}{\partial \mathbf{u}} \right|_{\mathbf{u}=\mathbf{q}} \mathbf{v} + \mathcal{O}(|\mathbf{v}|^2) \\ &\approx \mathbf{f}(\mathbf{q}) + \left. \frac{\partial \mathbf{f}(\mathbf{u})}{\partial \mathbf{u}} \right|_{\mathbf{u}=\mathbf{q}} \mathbf{v} \\ &= \mathbf{f}(\mathbf{q}) + \mathbf{F}(\mathbf{q}) \mathbf{v},\end{aligned}$$

where

$$\mathbf{F}(\mathbf{q}) = \left. \frac{\partial \mathbf{f}(\mathbf{u})}{\partial \mathbf{u}} \right|_{\mathbf{u}=\mathbf{q}}.$$

Therefore, we can write the equation (3.1) as follows

$$\mathbf{q}_t + \mathbf{v}_t \approx \mathbf{D}(\mathbf{q}_{xx} + \mathbf{v}_{xx} + \mathbf{q}_{yy} + \mathbf{v}_{yy}) + \mathbf{f}(\mathbf{q}) + \mathbf{F}(\mathbf{q}) \mathbf{v}. \quad (3.3)$$

We can now split the equation (3.3) into two equations one of which relates to a nonlinear system and the other to a linear model, that is

$$\mathbf{q}_t = \mathbf{D}(\mathbf{q}_{xx} + \mathbf{q}_{yy}) + \mathbf{f}(\mathbf{q}), \quad (3.4)$$

$$\mathbf{v}_t = \mathbf{D}(\mathbf{v}_{xx} + \mathbf{v}_{yy}) + \mathbf{F}(\mathbf{q}) \mathbf{v}. \quad (3.5)$$

We can observe that the partial differential equation (3.4) is a non-linear system because this equation is the same as the original system (3.1). With regard to the equation (3.5), we can see that it is a linear homogeneous equation of the non-linear system (3.1), with an independent time [8]. However, we note that the equation (3.4) can be posed as follows:

$$a_t = a_{xx} + a_{yy} + g(a, b),$$

$$b_t = h(a, b).$$

We also note that the equation (3.5) can be formed as follows:

$$\begin{aligned}c_t &= c_{xx} + c_{yy} + \left. \frac{\partial g(u, v)}{\partial u} \right|_{u=a} c + \left. \frac{\partial g(u, v)}{\partial v} \right|_{v=b} d, \\ d_t &= \left. \frac{\partial h(u, v)}{\partial u} \right|_{u=a} c + \left. \frac{\partial h(u, v)}{\partial v} \right|_{v=b} d,\end{aligned} \quad (3.6)$$

where

$$\begin{aligned}\frac{\partial g(u,v)}{\partial u}\Big|_{u=c} &= \frac{\partial}{\partial u} \left(\frac{1}{\epsilon} \left(u - \frac{u^3}{3} - v \right) \right) \Big|_{u=a} = \frac{1}{\epsilon} (1 - u^2) \Big|_{u=a} = \frac{1}{\epsilon} (1 - a^2) = \frac{1}{\epsilon} (1 - u^2), \\ \frac{\partial g(u,v)}{\partial v}\Big|_{v=b} &= \frac{\partial}{\partial v} \left(\frac{1}{\epsilon} \left(u - \frac{u^3}{3} - v \right) \right) \Big|_{v=b} = \frac{1}{\epsilon} (-1) \Big|_{v=b} = -\frac{1}{\epsilon}, \\ \frac{\partial h(u,v)}{\partial u}\Big|_{u=c} &= \frac{\partial}{\partial u} (\epsilon(u - \alpha v + \beta)) \Big|_{u=a} = \epsilon(1) \Big|_{u=a} = \epsilon, \\ \frac{\partial h(u,v)}{\partial v}\Big|_{v=b} &= \frac{\partial}{\partial v} (\epsilon(u - \alpha v + \beta)) \Big|_{v=b} = \epsilon(-\alpha) \Big|_{v=b} = -\epsilon\alpha.\end{aligned}$$

The reason for switching between two variables $\mathbf{u} = \begin{bmatrix} u \\ v \end{bmatrix}$ and $\mathbf{q} = \begin{bmatrix} a \\ b \end{bmatrix}$ is that the equation (3.1) is same as the equation (3.4). Therefore, the linear system (3.6) can be written explicitly as follows:

$$\begin{aligned}c_t &= c_{xx} + c_{yy} + \frac{1}{\epsilon}(1 - u^2)c - \frac{1}{\epsilon}d, \\ d_t &= \epsilon c - \epsilon\alpha d,\end{aligned}\tag{3.7}$$

where the variable u is known that is calculated numerically in the FHN system.

By looking at the equation (3.5), we can simplify the following linear system in this way

$$\mathbf{v}_t = \mathcal{L} \mathbf{v},\tag{3.8}$$

where

$$\mathcal{L} = \mathbf{D}\nabla^2 + \mathbf{F}(\mathbf{q}(x, y, t)),$$

such that $\mathbf{q}(x, y, t)$ is the solution of the nonlinear system (3.4). We then observe that the linear operator \mathcal{L} depends on time t , so by using numerical methods of finding eigenvalues, as discussed in Chapter 1, the linear system (3.8) is stable if the Floquet multipliers are in unit circle corresponding with [61]. Moreover, if the Floquet multipliers are outside of the unit circle, then the linear system (3.8) will be unstable.

Following the above linear approximation, we now need to show the numerical simulation of the equation (3.7) in different types of spiral wave motions including the rigid rotation and the meander. Each type of motion is related to the approximate solution of the FHN system in the

3.1. NUMERICAL SOLUTIONS OF THE LINEARISED FITZHUGH-NAGUMO SYSTEM AND RESPONSE FUNCTIONS

same time periods. Let us begin with the rigid rotation. For system (3.7), we apply the Neumann boundary conditions and the initial condition of the partial differential equations (3.7) is the white noises that can be generated by choosing random numbers for each value of the numerical solutions of the linear system [8]. By using semi implicit method, we can formulate the equations (3.7) as follows:

$$c_{j,k}^{m+1} = \Delta t \frac{c_{j+1,k}^{m+1} - 2c_{j,k}^{m+1} + c_{j-1,k}^{m+1}}{\Delta x^2} + \Delta t \frac{c_{j,k+1}^{m+1} - 2c_{j,k}^{m+1} + c_{j,k-1}^{m+1}}{\Delta y^2} + \frac{\Delta t}{\epsilon} \left(1 - (u_{j,k}^m)^2 \right) c_{j,k}^m - \frac{\Delta t}{\epsilon} d_{j,k}^m + c_{j,k}^m,$$

$$d_{j,k}^{m+1} = \Delta t \left(\epsilon c_{j,k}^m - \epsilon \alpha d_{j,k}^m \right) + d_{j,k}^m, \quad j, k = 0, 1, \dots, n, \quad m = 0, 1, \dots, n_1, \quad n, n_1 \in \mathbb{N},$$

such that the fully implicit method is used for the diffusion part of the linear system, whereas the fully explicit method is applied for the reaction functions. The numerical solution of the linear system (3.7) can be obtained, as shown in Figure 3.1. If we use the parameters ϵ and β related to

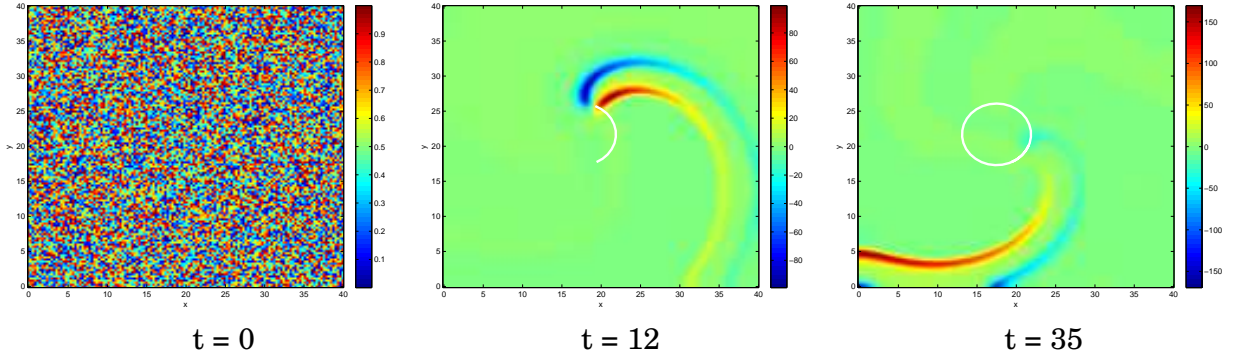


Figure 3.1: The numerical solution c of the linear system for FHN model with parameters $\alpha = 0.5$, $\beta = 0.75$ and $\epsilon = 0.3$ such that the numerical solution is found by semi implicit method. We choose a random initial condition at $t = 0$ such that $\Delta t = 0.1$ and $\Delta x = \Delta y = 0.3$.

the Figure 2.4, then the numerical solution of the right linear problem (3.7) can be demonstrated, as shown in Figure (3.2)

We now compute the response functions (RFs) of the spiral wave solutions that are also called left eigenfunctions of the adjoint linear system. The aim of doing this is that if the FHN system is perturbed, then this perturbation part will impact the spatial position of the spiral waves for the rotation core centre and the frequency (drift) subject to the parameters ϵ and β . Therefore, the eigenfunctions of the adjoint linear system is useful to describe the spiral waves's sensitivity

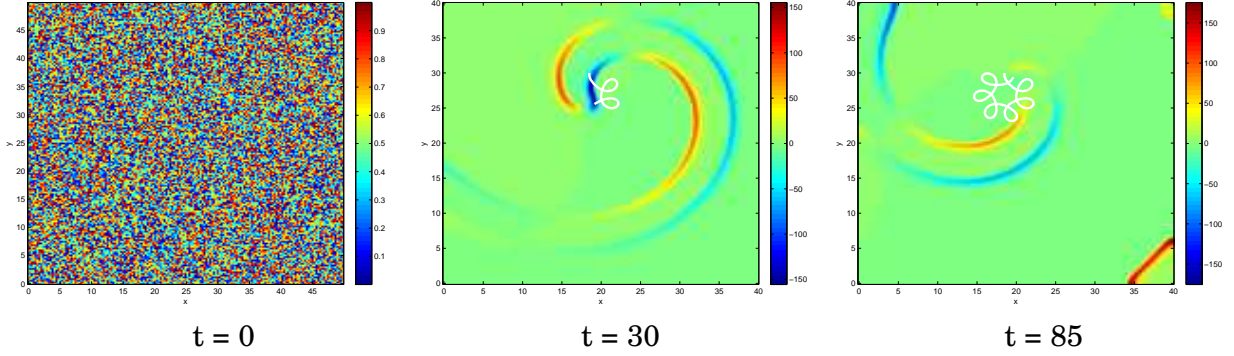


Figure 3.2: Numerical solution c of the linear system for the FHN model with parameters $\alpha = 0.5$, $\beta = 0.85$ and $\epsilon = 0.2$ such that the approximate solution is found by semi implicit method. We choose a random initial condition at $t = 0$ such that $\Delta t = 0.1$ and $\Delta x = \Delta y = 0.3$.

with a small perturbation. Note that, if the RFs are converging to zero, then this means that the spiral waves solution will be insensitive [14]. Furthermore, we now need to find the adjoint linear system. To do this, let us suppose that we have a solution of adjoint linear system given as follows:

$$\mathbf{w} = \mathbf{w}(x, y, t) = \begin{bmatrix} k(x, y, t) \\ s(x, y, t) \end{bmatrix}.$$

From Biktashev's study [8], using the linearised system (3.8) and using the definition of the adjoint linear operator, we can conclude that the (left) adjoint linear system of the equation (3.5) in 2D can be formulated as follows:

$$\partial_t \mathbf{w} = \mathcal{L}^+ \mathbf{w}, \quad (3.9)$$

where

$$\mathcal{L}^+ := \mathbf{D}^\top \nabla^2 + \mathbf{F}^\top(\mathbf{q}),$$

and the initial condition of the adjoint linear system (3.9) will be $\mathbf{w}(x, y, \tau)$, so the adjoint linear system (3.9) is posed as follows [8]:

$$\begin{aligned} k_t &= k_{xx} + k_{yy} + \frac{1}{\epsilon}(1 - \tilde{u}^2)k + \epsilon s, \\ s_t &= -\frac{1}{\epsilon}k - \epsilon a s, \end{aligned} \quad (3.10)$$

3.1. NUMERICAL SOLUTIONS OF THE LINEARISED FITZHUGH-NAGUMO SYSTEM AND RESPONSE FUNCTIONS

where

$$k = k(x, y, t), \quad s = s(x, y, t), \quad 0 < x < L, \quad 0 < y < L,$$

and

$$\tilde{u} = u(x, y, \tau - t), \quad t \in [0, \tau], \quad \tau \in \mathbb{R}^+. \quad (3.11)$$

By looking at the formula (3.11), the time of the component u in the system (3.10) should move backward, otherwise the dynamical numerical spiral wave solutions are unstable. The boundary condition of the system (3.10) is also Neumann and the initial condition of the partial differential equations (3.10) is random. By using the semi implicit method, the equations (3.10) can be solved numerically such that the fully implicit method is used for the diffusion part of the adjoint linear system, whereas the fully explicit method is applied for the reaction functions. Therefore, the numerical solution of the adjoint linear system (3.10) using in a Cartesian coordinate system that is related to the parameters ϵ and β as written in Figure 2.3 is obtained, as shown in Figure 3.3. We observe that the resulting response function is close to zero except in some neighbourhood of

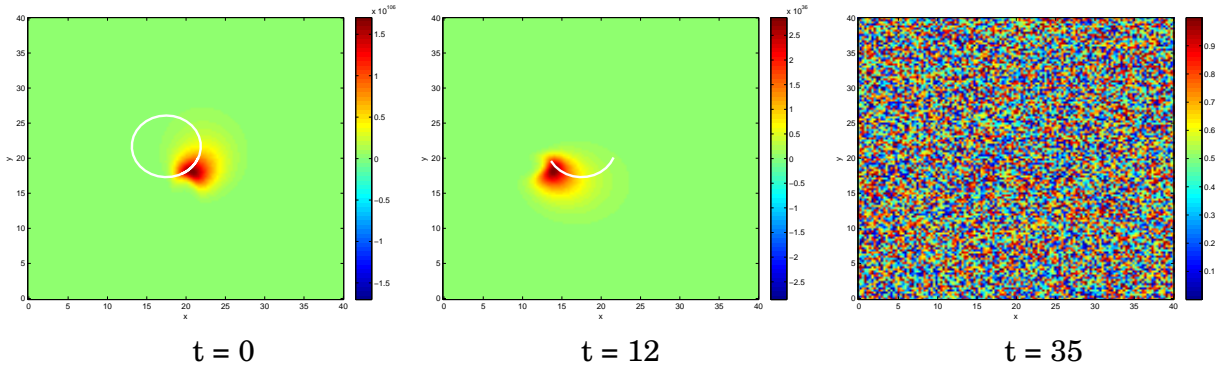


Figure 3.3: The numerical solution k of the adjoint linear system for FHN model with parameters $\alpha = 0.5$, $\beta = 0.75$ and $\epsilon = 0.3$. The numerical solution is found by the semi implicit method integrating back from the final condition. We choose a random initial condition at $t = 35$ such that $\Delta t = 0.1$ and $\Delta x = \Delta y = 0.3$.

the spiral tip. According to parameters ϵ and β in Figure 2.4, the numerical solution of the left linear system is obtained, as shown in Figure 3.4.

In the next section, we discuss a rigid rotating spiral wave can be transformed from a periodic orbit into a steady solution by looking in a comoving reference frame. Hence, the FHN system will be formulated in the reference frame moving with an angular velocity of the spiral wave.

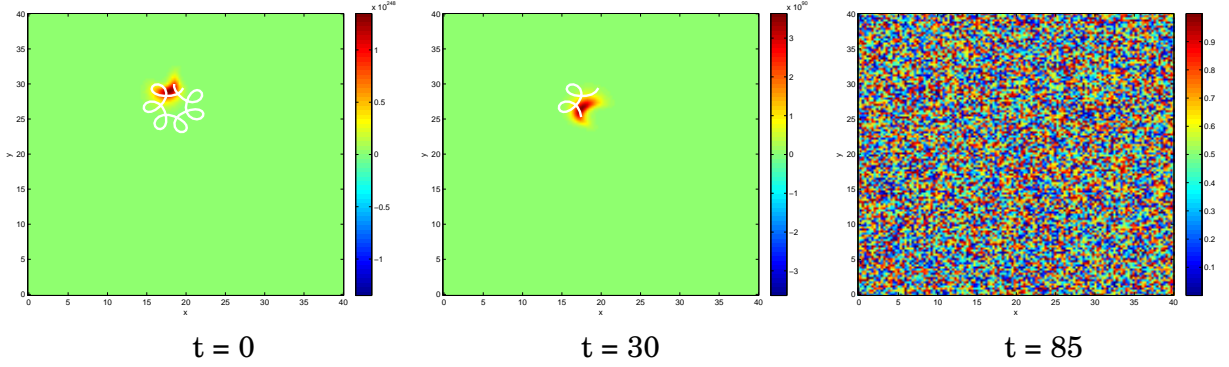


Figure 3.4: The numerical solution k of the adjoint linear system for FHN model with parameters $\alpha = 0.5$, $\beta = 0.85$ and $\epsilon = 0.2$ such that the numerical stimulation is found by semi implicit method integrating back from the final condition. We choose a random initial condition at $t = 85$ such that $\Delta t = 0.1$ and $\Delta x = \Delta y = 0.3$.

3.2 Symmetries and Drift of the Spiral Waves

We transform the FHN system into a rotating frame of reference with constant angular velocity such that the spiral wave solution rotates around a point in the plane. In this comoving frame of reference, the rigid rotating spiral wave solution of the FHN system becomes stationary. The problem is that we need to compute the speed of the spiral wave numerically. Let us assume that the spiral rotates around the origin and rewrite the FHN system in an infinite plane using (r, θ) polar coordinates with origin at the centre of the spiral core by writing (3.12) [16]

$$\mathbf{u}(x, y, t) = \check{\mathbf{u}}(r, \theta, t), \quad (3.12)$$

where

$$x = x(r, \theta) = r \cos(\theta), \quad (3.13a)$$

$$y = y(r, \theta) = r \sin(\theta), \quad (3.13b)$$

Using the standard method, the system (1.1) in polar coordinates becomes:

$$\begin{aligned} \check{\mathbf{u}}_t &= \mathbf{D} \left(\check{\mathbf{u}}_{rr} + \frac{1}{r^2} \check{\mathbf{u}}_{\theta\theta} + \frac{1}{r} \check{\mathbf{u}}_r \right) + \mathbf{f}(\check{\mathbf{u}}) \\ &= \mathbf{D} \nabla^2 \check{\mathbf{u}} + \mathbf{f}(\check{\mathbf{u}}), \end{aligned} \quad (3.14)$$

where

$$\check{\mathbf{u}} = \begin{bmatrix} \check{u}(r, \theta, t) \\ \check{v}(r, \theta, t) \end{bmatrix}, \quad \mathbf{f}(\check{\mathbf{u}}) = \begin{bmatrix} g(\check{u}, \check{v}) \\ h(\check{u}, \check{v}) \end{bmatrix} = \begin{bmatrix} \frac{1}{\epsilon} \left(\check{u} - \frac{\check{u}^3}{3} - \check{v} \right) \\ \epsilon (\check{u} - \alpha \check{v} + \beta) \end{bmatrix},$$

and

$$\nabla^2 = \frac{\partial^2}{\partial x^2} + \frac{\partial^2}{\partial y^2} = \frac{\partial^2}{\partial r^2} + \frac{1}{r^2} \frac{\partial^2}{\partial \theta^2} + \frac{1}{r} \frac{\partial}{\partial r}. \quad (3.15)$$

Now, let us reformulate the partial differential equation (3.14) in a frame of reference moving with speed c in order to have a rigid rotation of the spiral wave around the origin, so that $\check{\mathbf{u}}(r, \theta, t) = \check{\mathbf{z}}(r, \Theta, t)$ is defined in the movement of the frame [16] such that

$$\Theta = \theta - ct, \quad (3.16)$$

where Θ is a polar angle in the rigid rotating frame of reference with an angular velocity c of the spiral wave, while variables r and θ are polar coordinates in the original non rotating frame of reference [15]. By using the chain rule and the partial derivative for $\check{\mathbf{u}}(r, \theta, t) = \check{\mathbf{z}}(r, \Theta, t)$, the system (3.14) becomes:

$$\begin{aligned} \check{\mathbf{z}}_t &= \mathbf{D} \left(\check{\mathbf{z}}_{rr} + \frac{1}{r^2} \check{\mathbf{z}}_{\Theta\Theta} + \frac{1}{r} \check{\mathbf{z}}_r \right) + \mathbf{f}(\check{\mathbf{z}}) + c \check{\mathbf{z}}_{\Theta}, \\ &= \mathbf{D} \nabla^2 \check{\mathbf{z}} + \mathbf{f}(\check{\mathbf{z}}) + c \check{\mathbf{z}}_{\Theta}, \end{aligned} \quad (3.17)$$

where

$$\check{\mathbf{z}} = \begin{bmatrix} \check{\chi}(r, \Theta, t) \\ \check{\zeta}(r, \Theta, t) \end{bmatrix}, \quad \mathbf{f}(\check{\mathbf{z}}) = \begin{bmatrix} g(\check{\chi}, \check{\zeta}) \\ h(\check{\chi}, \check{\zeta}) \end{bmatrix} = \begin{bmatrix} \frac{1}{\epsilon} \left(\check{\chi} - \frac{\check{\chi}^3}{3} - \check{\zeta} \right) \\ \epsilon (\check{\chi} - \alpha \check{\zeta} + \beta) \end{bmatrix}.$$

The solution of the dynamical system (3.17) is not stationary because the t is not invariant. If we are looking for a stationary solution for the system (3.14), that is, with the time t fixed, we need to formulate the variable $\check{\mathbf{u}}$ as follows:

$$\check{\mathbf{u}}(r, \theta, t) = \mathbf{z}(r, \Theta). \quad (3.18)$$

CHAPTER 3. STABILITY OF THE SPIRAL WAVE, SYMMETRIES AND RESPONSE FUNCTIONS

Thus, the system (3.17) will be transformed as follows:

$$0 = \mathbf{D}\nabla^2 \mathbf{z} + \mathbf{f}(\mathbf{z}) + c \mathbf{z}_\Theta, \quad (3.19)$$

where

$$\mathbf{z} = \begin{bmatrix} \chi(r, \Theta) \\ \zeta(r, \Theta) \end{bmatrix}, \quad \mathbf{f}(\mathbf{z}) = \begin{bmatrix} g(\chi, \zeta) \\ h(\chi, \zeta) \end{bmatrix} = \begin{bmatrix} \frac{1}{\epsilon} \left(\chi - \frac{\chi^3}{3} - \zeta \right) \\ \epsilon(\chi - \alpha\zeta + \beta) \end{bmatrix}.$$

This equation (3.19) transforms the rotating spiral wave solutions of the original equation (1.1) into the stationary solutions (equilibrium solutions).

Now, let us linearise the reaction-diffusion system (3.14) in the comoving frame of reference around the critical solution $\mathbf{z}(r, \theta)$ where the time is independent through the equation (3.20)

$$\check{\mathbf{u}}(r, \theta, t) = \mathbf{z}(r, \theta) + \check{\mathbf{v}}(r, \theta, t), \quad (3.20)$$

where $\check{\mathbf{v}}$ is the linear solution (perturbation solution) [16]. Therefore, by also taking differentiating equation (3.20) with respect t , we find that

$$\frac{\partial \check{\mathbf{u}}}{\partial t} = \frac{\partial \mathbf{z}}{\partial t} + \frac{\partial \check{\mathbf{v}}}{\partial \theta} \frac{\partial \theta}{\partial t} + \frac{\partial \check{\mathbf{v}}}{\partial t}.$$

Furthermore, we find that

$$\check{\mathbf{u}}_{rr} = \mathbf{z}_{rr} + \check{\mathbf{v}}_{rr},$$

$$\check{\mathbf{u}}_{\theta\theta} = \mathbf{z}_{\theta\theta} + \check{\mathbf{v}}_{\theta\theta}.$$

Corresponding with the function \mathbf{f} in equation (3.14), by using Taylor series expansion, we find that

$$\begin{aligned} \mathbf{f}(\mathbf{z} + \check{\mathbf{v}}) &= \mathbf{f}(\mathbf{z}) + \frac{\partial \mathbf{f}(\mathbf{z})}{\partial \mathbf{z}} \check{\mathbf{v}} + \mathcal{O}(|\check{\mathbf{v}}|^2), \\ &= \mathbf{f}(\mathbf{z}) + \left. \frac{\partial \mathbf{f}(\check{\mathbf{u}})}{\partial \check{\mathbf{u}}} \right|_{\check{\mathbf{u}}=\mathbf{z}} \check{\mathbf{v}} + \mathcal{O}(|\check{\mathbf{v}}|^2), \\ &\approx \mathbf{f}(\mathbf{z}) + \mathbf{F}(\mathbf{z}) \check{\mathbf{v}}, \end{aligned}$$

where

$$\mathbf{F}(\mathbf{z}) = \left. \frac{\partial \mathbf{f}(\check{\mathbf{u}})}{\partial \check{\mathbf{u}}} \right|_{\check{\mathbf{u}}=\mathbf{z}},$$

is the Jacobian matrix of the reaction function. Therefore, the equation (3.14) can be approximated as follows

$$\mathbf{D} \left(\mathbf{z}_{\theta\theta} + \frac{1}{r^2} \mathbf{z}_{\theta\theta} + \frac{1}{r} \mathbf{z}_\theta \right) + c \mathbf{z}_\theta + \mathbf{f}(\mathbf{z}) \approx 0,$$

and

$$\check{\mathbf{v}}_t = \mathbf{D} \check{\mathbf{v}}_{rr} + \mathbf{D} \frac{1}{r^2} \check{\mathbf{v}}_{\theta\theta} + \mathbf{D} \frac{1}{r} \check{\mathbf{v}}_r + c \check{\mathbf{v}}_\theta + \mathbf{F}(\mathbf{z}) \check{\mathbf{v}}, \quad (3.21)$$

such that the linearised operator can be defined as follows

$$\check{\mathcal{L}} := \mathbf{D} \frac{\partial^2}{\partial r^2} + \mathbf{D} \frac{1}{r^2} \frac{\partial^2}{\partial \theta^2} + \mathbf{D} \frac{1}{r} \frac{\partial}{\partial r} + c \frac{\partial}{\partial \theta} + \mathbf{F}(\mathbf{z}) = \mathbf{D} \nabla^2 + c \partial_\theta + \mathbf{F}(\mathbf{z}(r, \theta)).$$

Moreover, by looking at the equation (3.21), we can simplify the linear system (3.21) as follows

$$\check{\mathbf{v}}_t = \check{\mathcal{L}} \check{\mathbf{v}}. \quad (3.22)$$

We observe that the linear operator $\check{\mathcal{L}}$ does not depend on time t , so by using numerical methods we can find the eigenvalues of the linear system. According to paper [14], the linear stability spectrum for the equation (3.22) can be formulated as follows:

$$\check{\mathcal{L}} \hat{\mathbf{v}} = \hat{\lambda} \hat{\mathbf{v}}, \quad (3.23)$$

where

$$\hat{\mathbf{v}} = \hat{\mathbf{v}}(r, \theta).$$

Based on the linear system (3.23) and paper [9], the adjoint linear system in the polar coordinate can be formulated as follows:

$$\check{\mathcal{L}}^+ \hat{\mathbf{w}} = \hat{\mu} \hat{\mathbf{w}}, \quad (3.24)$$

where

$$\check{\mathcal{L}}^+ = \mathbf{D}^\top \nabla^2 - c \partial_\theta + \mathbf{F}^\top(\mathbf{z}(r, \theta)), \quad \hat{\mathbf{w}} = \hat{\mathbf{w}}(r, \theta).$$

CHAPTER 3. STABILITY OF THE SPIRAL WAVE, SYMMETRIES AND RESPONSE FUNCTIONS

In addition, we now need to find the left eigenfunction $\check{\mathbf{w}}$ in the comoving frame of reference, which can be done through equation (3.21). Therefore, we have

$$\check{\mathbf{w}}_t = \check{\mathcal{L}}^+ \check{\mathbf{w}}, \quad (3.25)$$

where

$$\check{\mathbf{w}} = \check{\mathbf{w}}(r, \theta, t),$$

and

$$\check{\mathcal{L}}^+ := \mathbf{D}^\top \frac{\partial^2}{\partial r^2} + \mathbf{D}^\top \frac{1}{r^2} \frac{\partial^2}{\partial \theta^2} + \mathbf{D}^\top \frac{1}{r} \frac{\partial}{\partial r} - c \frac{\partial}{\partial \theta} + \mathbf{F}^\top(\mathbf{z}).$$

We observe that the vector $\check{\mathbf{w}}$ is named the response function of the spiral wave [15].

With regards to the Euclidean group of symmetries, there is a useful theorem that is needed to be discussed about spiral wave solution a finite domain and an infinite domain. Biktashev and Holden imply but do not explicitly state or prove a result in their paper that the solutions of the system (1.1) on the infinite domain are also the solution of the equation (1.1) when acted by symmetries of transition into a finite space [9]. Therefore, we explicitly state this theorem as follows.

Theorem 3. [9] *If we have the homogeneous reaction diffusion equation formulated in the following form*

$$\partial_t \mathbf{u} = \mathbf{f}(\mathbf{u}) + \mathbf{D} \nabla^2 \mathbf{u}, \quad (3.26)$$

such that the vector $\mathbf{u} = \mathbf{u}(\mathbf{r}, t)$ is the solution of the equation (3.26) and

$$\mathbf{r} = (x, y) \in \mathbb{R}^2,$$

then the shifted solution $\mathbf{U}(\mathbf{r}, t) = \mathbf{u}(\mathbf{r} - \delta \mathbf{r}, t - \delta t)$ is also the solution of the nonlinear system (3.26) for the arbitrary $\delta \mathbf{r}$ and δt constants when the time t is infinite such that the boundary conditions are periodic, that is

$$\mathbf{U}(x+L, y, t) = \mathbf{U}(x, y, t), \mathbf{U}(x, y+L, t) = \mathbf{U}(x, y, t), \quad L \in \mathbb{R}^+,$$

and the initial condition is spiral waves.

Proof. Since \mathbf{u} is the solution of the system (3.26) in 2D, we need to show that the solution $\mathbf{U}(\mathbf{r}, t)$ is also the solution of the equation (3.26). If we differentiate the function $\mathbf{U}(\mathbf{r}, t) = \mathbf{u}(\mathbf{r} - \delta \mathbf{r}, t - \delta t)$ with respect to t, x and y , then we find that

$$\begin{aligned}\mathbf{U}_t(\mathbf{r}, t) &= \mathbf{u}_t(\mathbf{r} - \delta \mathbf{r}, t - \delta t) \\ \mathbf{U}_x(\mathbf{r}, t) &= \mathbf{u}_x(\mathbf{r} - \delta \mathbf{r}, t - \delta t)\end{aligned}\tag{3.27}$$

$$\mathbf{U}_y(\mathbf{r}, t) = \mathbf{u}_y(\mathbf{r} - \delta \mathbf{r}, t - \delta t).\tag{3.28}$$

In addition, if we take the derivative of the equations (3.27) and (3.28) with respect to x and y again, then we find that

$$\mathbf{U}_{xx}(\mathbf{r}, t) = \mathbf{u}_{xx}(\mathbf{r} - \delta \mathbf{r}, t - \delta t)$$

$$\mathbf{U}_{yy}(\mathbf{r}, t) = \mathbf{u}_{yy}(\mathbf{r} - \delta \mathbf{r}, t - \delta t).$$

Therefore, if we substitute the variable \mathbf{U} instead of the variable \mathbf{u} into the equation (1.1), then we find that

$$\mathbf{U}_t = \mathbf{D}(\mathbf{U}_{xx} + \mathbf{U}_{yy}) + \mathbf{f}(\mathbf{U}),\tag{3.29}$$

so \mathbf{U} is also the solution of the system (3.26). ■

The reason for studying the shifted solution of the reaction-diffusion is that this describes the influences of drifting spiral wave in terms of spiral wave core location. We will discuss the property of spiral wave solution of the linear system for the reaction-diffusion equation that is shown in Chapter 2, so there is an important theorem for a linear system of partial differential equations, which is called *the principle of superposition*.

Theorem 4. [23, p.121] *If u_1, \dots, u_n such that $n \in \mathbb{N}$ are solutions of the homogeneous linear partial differential equations, then their linear combination is also the solution of the same homogeneous system of the linear partial differential equations.*

However, we need to discuss how to minimise two norms in order to find the global minimum. This method was also called the *generalised minimum residuals* (GMRES) in 1986 [71]. Therefore,

CHAPTER 3. STABILITY OF THE SPIRAL WAVE, SYMMETRIES AND RESPONSE FUNCTIONS

we can use this method to demonstrate the characteristics of linear system of reaction diffusion equation that is not applicable in a finite domain, whereas it can be applied in an infinite domain with the Euclidean group of symmetries. The linearised system for the unshifted nonlinear system (3.26) is as follows

$$\mathbf{v}_t = D\nabla^2 \mathbf{v} + \mathbf{F}(\mathbf{u})\mathbf{v}, \quad (3.30)$$

where $\mathbf{F}(\mathbf{u}) = \frac{\partial \mathbf{f}(\mathbf{u})}{\partial \mathbf{u}}$ is the matrix of the first order of the partial derivatives for the reaction function $\mathbf{f}(\mathbf{u})$ with respect to \mathbf{u} . Note that three vectors $\mathbf{v}_1 = \frac{\partial \mathbf{u}}{\partial x}$, $\mathbf{v}_2 = \frac{\partial \mathbf{u}}{\partial y}$ and $\mathbf{v}_3 = \frac{\partial \mathbf{u}}{\partial t}$ are the solutions of the unshifted linearised system (3.30) such that $\mathbf{v}_1, \mathbf{v}_2$ and \mathbf{v}_3 are periodic solutions. If we assume that, other than these neutral modes, \mathbf{U} is a stable rigidly rotating spiral, then there is non decaying solution of the linear system (3.30) that can be written as a linear combination of the three functions $\mathbf{v}_1(t), \mathbf{v}_2(t)$ and $\mathbf{v}_3(t)$ when the time goes infinity, that is, there is choice of functions $\alpha_1(t), \alpha_2(t)$ and $\alpha_3(t)$ such that

$$\|\mathbf{v} - \alpha_1 \mathbf{v}_1 - \alpha_2 \mathbf{v}_2 - \alpha_3 \mathbf{v}_3\|^2 \rightarrow 0 \text{ as } t \rightarrow \infty, \quad \alpha_1, \alpha_2, \alpha_3 \in \mathbb{R}. \quad (3.31)$$

By looking at the equation (3.26), if we take the derivative related to time t , then we find that

$$\frac{\partial}{\partial t} \mathbf{u}_t = D \frac{\partial}{\partial t} (\mathbf{u}_{xx} + \mathbf{u}_{yy}) + \frac{\partial}{\partial t} \mathbf{f}(\mathbf{u}). \quad (3.32)$$

Regarding the term $\frac{\partial}{\partial t} \mathbf{f}(\mathbf{u})$ of the equation (3.32), by using the chain rule, we find that

$$\frac{\partial}{\partial t} \mathbf{f}(\mathbf{u}) = \frac{\partial \mathbf{f}(\mathbf{u})}{\partial \mathbf{u}} \mathbf{u}_t = \mathbf{f}'(\mathbf{u}) \mathbf{u}_t.$$

Therefore, the equation (3.32) becomes as follows

$$\frac{\partial}{\partial t} \mathbf{u}_t = D \left(\frac{\partial^2}{\partial x^2} \mathbf{u}_t + \frac{\partial^2}{\partial y^2} \mathbf{u}_t \right) + \mathbf{f}'(\mathbf{u}) \mathbf{u}_t. \quad (3.33)$$

If we take the derivative of the equation (3.26) in relation to x , then we have

$$\frac{\partial}{\partial x} \mathbf{u}_t = D \frac{\partial}{\partial x} (\mathbf{u}_{xx} + \mathbf{u}_{yy}) + \frac{\partial}{\partial x} \mathbf{f}(\mathbf{u}). \quad (3.34)$$

According to the part $\frac{\partial}{\partial x} \mathbf{f}(\mathbf{u})$ of the equation (3.34), by using the chain rule again, we find that

$$\frac{\partial}{\partial x} \mathbf{f}(\mathbf{u}) = \frac{\partial \mathbf{f}(\mathbf{u})}{\partial \mathbf{u}} \mathbf{u}_x = \mathbf{f}'(\mathbf{u}) \mathbf{u}_x.$$

Therefore, we have

$$\frac{\partial}{\partial t} \mathbf{u}_x = \mathbf{D} \left(\frac{\partial^2}{\partial x^2} \mathbf{u}_x + \frac{\partial^2}{\partial y^2} \mathbf{u}_x \right) + \mathbf{f}'(\mathbf{u}) \mathbf{u}_x. \quad (3.35)$$

If we take the derivative of the equation (3.26) with respect to y , then we find that

$$\frac{\partial}{\partial y} \mathbf{u}_t = \mathbf{D} \frac{\partial}{\partial y} (\mathbf{u}_{xx} + \mathbf{u}_{yy}) + \frac{\partial}{\partial y} \mathbf{f}(\mathbf{u}). \quad (3.36)$$

With regards the part $\frac{\partial}{\partial y} \mathbf{f}(\mathbf{u})$ of the equation (3.36), by using the chain rule, we find that

$$\frac{\partial}{\partial y} \mathbf{f}(\mathbf{u}) = \frac{\partial \mathbf{f}(\mathbf{u})}{\partial \mathbf{u}} \mathbf{u}_y = \mathbf{f}'(\mathbf{u}) \mathbf{u}_y. \quad (3.37)$$

Therefore, the equation (3.36) leads to the equation (3.38), that is

$$\frac{\partial}{\partial t} \mathbf{u}_y = \mathbf{D} \left(\frac{\partial^2}{\partial x^2} \mathbf{u}_y + \frac{\partial^2}{\partial y^2} \mathbf{u}_y \right) + \mathbf{f}'(\mathbf{u}) \mathbf{u}_y. \quad (3.38)$$

Since, the equation (3.30) is the linearised system of the nonlinear system (3.26), so comparing the equations (3.33), (3.35), (3.38) with equation (3.30), we find that \mathbf{u}_t , \mathbf{u}_x and \mathbf{u}_y are the solutions of the linear system (3.30). By using the principle of superposition, the linear combination of solutions \mathbf{u}_t , \mathbf{u}_x and \mathbf{u}_y is also the solution of the linear system (3.30), that is,

$$\mathbf{v} = \alpha_1 \mathbf{u}_x + \alpha_2 \mathbf{u}_y + \alpha_3 \mathbf{u}_t, \quad \alpha_1, \alpha_2, \alpha_3 \in \mathbb{R}. \quad (3.39)$$

Furthermore, note that the previous discussions for the reaction diffusion system (3.26) is defined on the whole plane. So let us now consider what happens, instead, on a bounded domain, that is, when the reaction diffusion equation (3.26) is posed on

$$0 < x < L, 0 < y < L, L \in \mathbb{R}^+.$$

In this case, we transfer the solution of nonlinear and linear problem from infinite domain to finite domain, so let us rewrite theorem 3 in finite domain.

Theorem 5. *Suppose that the function $\mathbf{u} = \mathbf{u}(\mathbf{r}, t)$ is the solution of the nonlinear equation (3.26) with Neumann boundary conditions (2.8) on the domain $[0, L]^2$, then, the function $\mathbf{U}(\mathbf{r}, t) = \mathbf{u}(\mathbf{r} - \delta \mathbf{r}, t - \delta t)$ is also the solution of the system (3.26) on $[-\delta x, L - \delta x] \times [-\delta y, L - \delta y]$ with Neumann boundary conditions.*

Proof. Since the solution $\mathbf{u}(x, y, t)$ is defined in the domain $[0, L]^2$ such that the Neumann boundary condition is satisfied for $\mathbf{u}(x, y, t)$, we know that the function $\mathbf{U}(x, y, t)$ can be posed as follows

$$\mathbf{U}(x, y, t) = \mathbf{u}(\mathbf{r} - \delta \mathbf{r}, t - \delta t) = \mathbf{u}(x - \delta x, y - \delta y, t - \delta t).$$

So we need to show that the Neumann boundary condition is satisfied for the function $\mathbf{U}(\mathbf{r}, t)$ on the domain $[-\delta x, L - \delta x] \times [-\delta y, L - \delta y]$. Since the function $\mathbf{U}(x, y, t)$ is defined as follows:

$$\mathbf{U}(x, y, t) = \mathbf{u}(x - \delta x, y - \delta y, t - \delta t), \quad (3.40)$$

it is also the solution of the nonlinear system (3.26) because the function $\mathbf{U} = \mathbf{U}(x, y, t)$ satisfies the solution of the following nonlinear system (3.41)

$$\partial_t \mathbf{U} = \mathbf{f}(\mathbf{U}) + D \nabla^2 \mathbf{U}. \quad (3.41)$$

In addition, the function $\mathbf{u}(x, y, t)$ is the solution of the nonlinear system (3.41) because the function $\mathbf{u} = \mathbf{u}(x, y, t)$ satisfies the solution of the non linear system (3.42)

$$\partial_t \mathbf{u} = \mathbf{f}(\mathbf{u}) + D \nabla^2 \mathbf{u}. \quad (3.42)$$

■

We can observe that the nonlinear system (3.42) represents the drift of the spiral wave for the equation (3.41) with respect to the shift in space and time. In particular, this theorem notes that the translated solution is only a solution on the translated domain. But in the linear system (3.30), the solution \mathbf{v} does not need to be formulated as a linear combination of three independent solutions $\mathbf{v}_1, \mathbf{v}_2$ and \mathbf{v}_3 with the Neumann condition on the domain $[0, L]^2$

$$\left. \frac{\partial}{\partial x} \mathbf{v}(x, y, t) \right|_{x=0} = \left. \frac{\partial}{\partial x} \mathbf{v}(x, y, t) \right|_{x=L} = 0$$

$$\left. \frac{\partial}{\partial y} \mathbf{v}(x, y, t) \right|_{y=0} = \left. \frac{\partial}{\partial y} \mathbf{v}(x, y, t) \right|_{y=L} = 0.$$

We are now going to show that the solution \mathbf{v} of the linear system (3.30) cannot be written as the linear combination of $\frac{\partial \mathbf{U}}{\partial t}$, $\frac{\partial \mathbf{U}}{\partial x}$ and $\frac{\partial \mathbf{U}}{\partial y}$ through applying the numerical method and also using

the two norm (also called the Euclidean norm) and the infinity norm. Let us define the two norm using the solution \mathbf{v} and the linear combination of \mathbf{v}_1 , \mathbf{v}_2 and \mathbf{v}_3 through the following equation

(3.43) [80]:

$$\|\mathbf{v}^m - \sum_{i=1}^3 \alpha_i \mathbf{v}_i^m\|_2 = \sqrt{\Delta y \Delta x} \times \sqrt{\sum_{j=1}^n \sum_{i=1}^n \left(\left[\tilde{c}(x_i, y_j) - \check{c}(x_i, y_j) \right]^2 + \left[\tilde{d}(x_i, y_j) - \check{d}(x_i, y_j) \right]^2 \right)}, \quad m, n \in \mathbb{N}, \quad (3.43)$$

where

$$\mathbf{v} = \begin{bmatrix} \tilde{c}(x, y) \\ \tilde{d}(x, y) \end{bmatrix} = \begin{bmatrix} c(x, y, t_m) \\ d(x, y, t_m) \end{bmatrix}, \quad \sum_{i=1}^3 \alpha_i \mathbf{v}_i^m = \begin{bmatrix} \check{c}(x, y) \\ \check{d}(x, y) \end{bmatrix}, \quad (3.44)$$

and

$$\mathbf{v}_1^m = \begin{bmatrix} \frac{\partial u(x, y, t)}{\partial x} \\ \frac{\partial v(x, y, t)}{\partial x} \end{bmatrix}, \quad \mathbf{v}_2^m = \begin{bmatrix} \frac{\partial u(x, y, t)}{\partial y} \\ \frac{\partial v(x, y, t)}{\partial y} \end{bmatrix}, \quad \mathbf{v}_3^m = \begin{bmatrix} \frac{\partial u(x, y, t)}{\partial t} \\ \frac{\partial v(x, y, t)}{\partial t} \end{bmatrix}. \quad (3.45)$$

The variable m refers to index of time. Moreover, the infinity norm for the forward linear solution \mathbf{v}^m and the linear combination $\sum_{i=1}^3 \alpha_i \mathbf{v}_i^m$ can be posed as follows [80]:

$$\|\mathbf{v}^m - \sum_{i=1}^3 \alpha_i \mathbf{v}_i^m\|_\infty = \left\| \begin{bmatrix} \tilde{c}(x, y) - \check{c}(x, y) \\ \tilde{d}(x, y) - \check{d}(x, y) \end{bmatrix} \right\|_\infty = \|\mathcal{V}_{s,d}\|_\infty, \quad s = 1, \dots, 2n, \quad d = 1, \dots, n,$$

where

$$\|\mathbf{v}^m - \sum_{i=1}^3 \alpha_i \mathbf{v}_i^m\|_\infty = \max_{1 \leq s \leq 2n} \max_{1 \leq d \leq n} |\mathcal{V}_{s,d}|. \quad (3.46)$$

The reason for using the two norm and the infinity norm is that we can calculate the error between the solution \mathbf{v} of the linear system and the linear combination of three solutions \mathbf{v}_1 , \mathbf{v}_2 and \mathbf{v}_3 .

Therefore, we now need to normalise the Euclidean and infinity norms of the approximation errors (3.43) and (3.46) through using the equation (3.47)

$$e_{k_1} = \frac{\|\mathbf{v}^m - \sum_{i=1}^3 \alpha_i \mathbf{v}_i^m\|_{k_1}}{\|\mathbf{v}^m\|_{k_1}}, \quad (3.47)$$

where

$$|e_{k_1}| \leq 1, \quad k_1 = 2, \infty.$$

CHAPTER 3. STABILITY OF THE SPIRAL WAVE, SYMMETRIES AND RESPONSE FUNCTIONS

This is because the error e_{k_1} can be observed more clearly. Before showing that the second part of the Theorem 3 is not true on the boundary domain $[0, L]^2$, we need to compute the coefficients α_1, α_2 and α_3 following a certain process. Since \mathbf{v} is the linear combination of vectors $\mathbf{v}_1, \mathbf{v}_2$ and \mathbf{v}_3 , this means that the vectors $\mathbf{v}_1, \mathbf{v}_2$ and \mathbf{v}_3 are linearly independent. As a result, using the Euclidean norm, we can minimise the equation (3.31) by squaring, that is, we choose α_i such that

$$\|\mathbf{v} - \alpha_1 \mathbf{v}_1 - \alpha_2 \mathbf{v}_2 - \alpha_3 \mathbf{v}_3\|_2^2 \quad (3.48)$$

is minimized. In other words, the Euclidean norm is minimal. Let define that

$$\tilde{f}(\alpha_1, \alpha_2, \alpha_3) = \|\mathbf{v} - \alpha_1 \mathbf{v}_1 - \alpha_2 \mathbf{v}_2 - \alpha_3 \mathbf{v}_3\|_2^2. \quad (3.49)$$

After calculating and simplifying the equation (3.49), we can derive that the function $\tilde{f}(\alpha_1, \alpha_2, \alpha_3)$ consists of a quadratic form (quadratic equation) and a constant (more detail can be found in appendix C). In order to compute the values α_1, α_2 and α_3 , we use the following result.

Theorem 6. [43, Theorem 7.17] *If the function $f(x_1, \dots, x_k)$ has the equation of quadratic form $q(x_1, \dots, x_k)$ plus a constant c_* such that the function $f(x_1, \dots, x_k)$ is positive for all values of x_1, x_{k-1} and x_k , that is*

$$\forall \mathbf{x}, \quad f(\mathbf{x}) = \mathbf{x}^\top A \mathbf{x} + c_* \geq 0,$$

where

$$\mathbf{x} = \begin{bmatrix} x_1 \\ x_2 \\ \vdots \\ x_{k-1} \\ x_k \end{bmatrix} \in \mathbb{R}^k, q(\mathbf{x}) = \mathbf{x}^\top A \mathbf{x}, A \in \mathbb{R}^{k \times k}, A^\top = A, c_* \geq 0, \quad i \in \{1, \dots, k\}, k \in \mathbb{N},$$

then the quadratic form $q(x_1, \dots, x_k)$ is positive and semi-definite, that is

$$\forall x_i, \quad q(x_1, \dots, x_k) \geq 0 \iff \forall \mathbf{x}, \quad q(\mathbf{x}) \geq 0.$$

Let us to introduce the proposition that can be also used for the second part of the Theorem 3. In other words, we will attempt to show that the second part of this theorem does not work in a bounded domain but works in infinite domains.

Proposition 1. [79] *If B is a symmetric, positive definite matrix, then the quadratic function $f(\mathbf{x})$ has a unique minimiser, also called global minimum, such that the minimum value of the function $f(\mathbf{x})$ is equal to the following expression:*

$$f(\mathbf{x}) = \frac{1}{2} \mathbf{x}^\top B \mathbf{x} + \mathbf{x}^\top \mathbf{c} + \tilde{c},$$

where

$$\mathbf{c} = \begin{bmatrix} c_1 \\ c_2 \\ \vdots \\ c_{k-1} \\ c_k \end{bmatrix}, \quad \mathbf{x} = \begin{bmatrix} x_1 \\ x_2 \\ \vdots \\ x_{k-1} \\ x_k \end{bmatrix} \in \mathbb{R}^k, \quad B \in \mathbb{R}^{k \times k}, \quad \tilde{c} \in \mathbb{R}, \quad k \in \mathbb{N}.$$

In addition, if we focus on equation (3.49) and also use a complete square in order to find the minimal, we can derive the minimal value of the function $\tilde{f}(\alpha_1, \alpha_2, \alpha_3)$ through using Cramer's rule such that $(\alpha_1, \alpha_2, \alpha_3)$ is the critical point, also known as the stationary point. A detailed of how to compute the minimal value ϵ of function \tilde{f} that has been demonstrated generally in the appendix C. Therefore, it is important to show the minimal values α_1, α_2 and α_3 such that the parameters and scalars are given as follows:

$$\Delta t = 0.1, \quad \Delta x = \Delta y = 0.3, \quad \alpha = 0.5, \quad \beta = 0.75, \quad \epsilon = 0.3, \quad t \in [0, 82],$$

so, the the minimal values α_1, α_2 and α_3 are demonstrated in the Figure 3.5. By looking at the figure 3.5, the neither two nor infinity norms go to zero. Therefore, the solution \mathbf{v}^m in a finite domain cannot be written as the linear combination of three independent solutions $\mathbf{v}_1^m, \mathbf{v}_2^m$ and \mathbf{v}_3^m that are not decaying on time such that vectors $\mathbf{v}^m, \alpha_1 \mathbf{v}_1^m, \alpha_2 \mathbf{v}_2^m$ and $\alpha_3 \mathbf{v}_3^m$. Therefore, the diagram of $c(x, y, t), \alpha_1 \frac{\partial u(x, y, t)}{\partial x}, \alpha_2 \frac{\partial u(x, y, t)}{\partial y}$ and $\alpha_3 \frac{\partial u(x, y, t)}{\partial t}$ are shown in a specific moment in time, as shown in Figures 3.6 and 3.7. Moreover, we also find that other diagrams are shown in Figures 3.8, and 3.9. If the error in the Figure 3.5 goes close to zero, then the solution of the linear system in the finite domain can be written as a linear combination of three independent solutions. We have to be aware that the spiral wave solution of the nonlinear system rotates rigidly for very long time, then it may move along domain. Furthermore, if the spiral wave rotates close enough to

CHAPTER 3. STABILITY OF THE SPIRAL WAVE, SYMMETRIES AND RESPONSE FUNCTIONS

the boundary, then it may interact with the boundary. In current years, the boundary domain has been used as the perturbation equation in order for the spiral wave dynamics to be understood [58].

In the next section, we focus on how to compute the eigenvalues of the linear system numerically and also investigate the stable or unstable solutions of the FHN system.

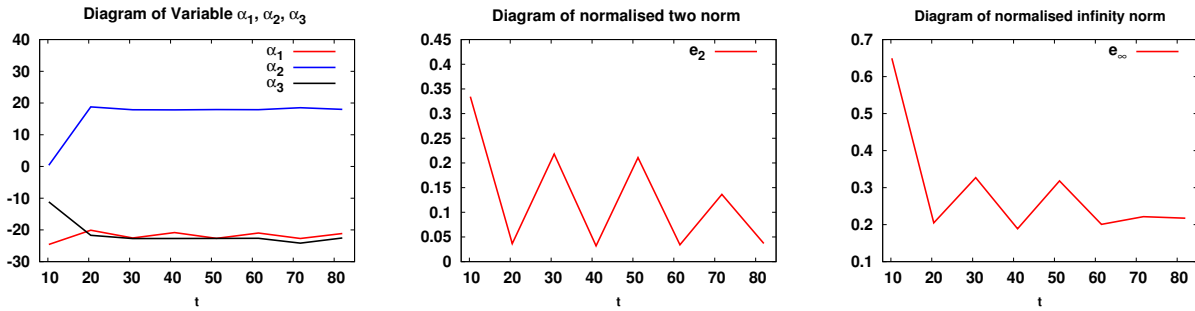


Figure 3.5: The numerical solution of linear system for FHN model with parameters $\alpha = 0.5$, $\beta = 0.75$ and $\epsilon = 0.3$ is found by central difference and forward Euler method. The time step Δt is equal to 0.1 for the period of time $[0, 82]$ as well as space steps Δx and Δy are 0.3 for space scale 40×40 . Scalars α_1 , α_2 and α_3 are found by minimizing the expression (3.49). The normalised two norm e_2 of approximation error are found through using the equation (3.47) and infinity norm e_∞ of approximation error are also found through using the equation (3.47).

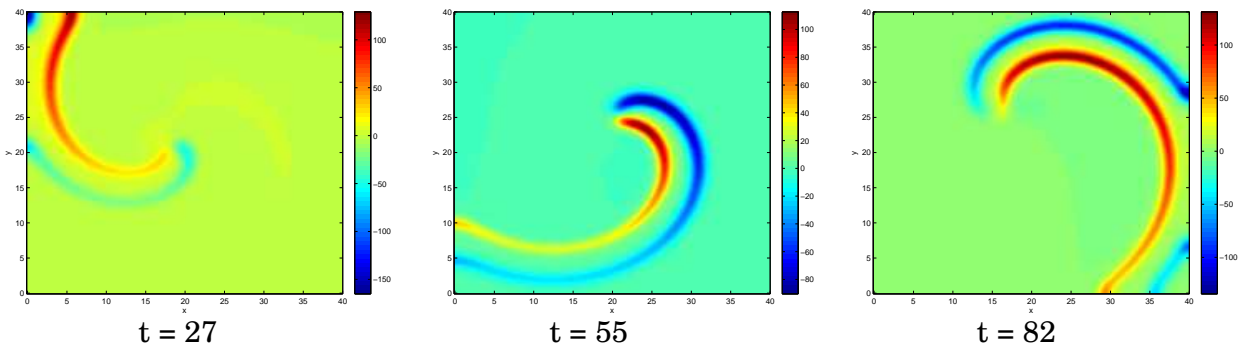


Figure 3.6: The numerical solution of linear system for FHN model with parameters $\alpha = 0.5$, $\beta = 0.75$ and $\epsilon = 0.3$ is found by using central difference and forward Euler method such that this diagram indicates the component $c(x, y, t)$ of formula (3.44). The time step Δt is equal to 0.1 for the period of time $[0, 82]$ as well as space steps Δx and Δy are 0.3 for space scale 40×40 .

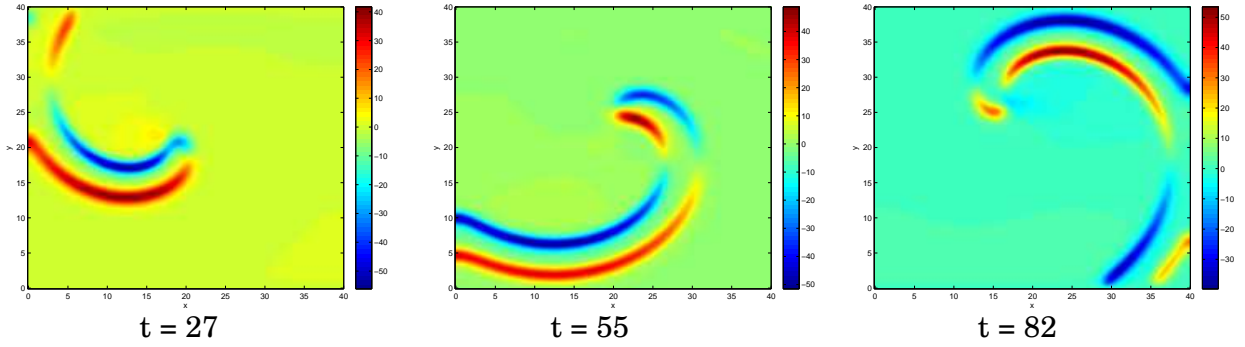


Figure 3.7: The numerical solution of linear system for FHN model with parameters $\alpha = 0.5$, $\beta = 0.75$ and $\epsilon = 0.3$ is found by using central difference and forward Euler method. This diagram indicates $\alpha_1 \frac{\partial u}{\partial x}$ such that $\frac{\partial u}{\partial x}$ of formula (3.45) is found through differentiating forward nonlinear solution u of FHN in 2D with respect to variable t . The time step Δt is equal to 0.1 for the period of time $[0, 82]$ as well as space steps Δx and Δy are 0.3 for space scale 40×40 .

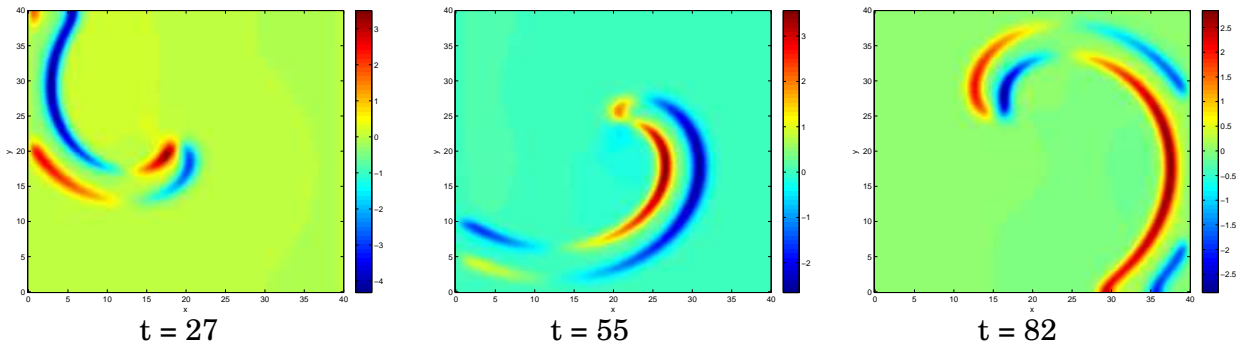


Figure 3.8: The numerical solution of linear system for FHN model with parameters $\alpha = 0.5$, $\beta = 0.75$ and $\epsilon = 0.3$ is found by using central difference and forward Euler method. This diagram indicates $\alpha_2 \frac{\partial u}{\partial y}$ such that $\frac{\partial u}{\partial y}$ of formula (3.45) is found through differentiating forward nonlinear solution u of FHN in 2D with respect to variable x . The time step Δt is equal to 0.1 for the period of time $[0, 82]$ as well as space steps Δx and Δy are 0.3 for space scale 40×40 .

3.3 Linear stability of the Spiral Wave

By looking at paper [61], we numerically study Floquet multipliers λ of FHN system in order to understand that spiral wave solutions of nonlinear system (2.1) is stable or unstable. As we know that computers does not have enough memory in order to compute all eigenvalues λ from Jacobian matrix \mathbf{J} especially FHN system in 2D. To avoid this issue, we will use alternative method to calculate Floquet multipliers λ . Using linear system (3.7) of FHN, forward Euler

CHAPTER 3. STABILITY OF THE SPIRAL WAVE, SYMMETRIES AND RESPONSE FUNCTIONS

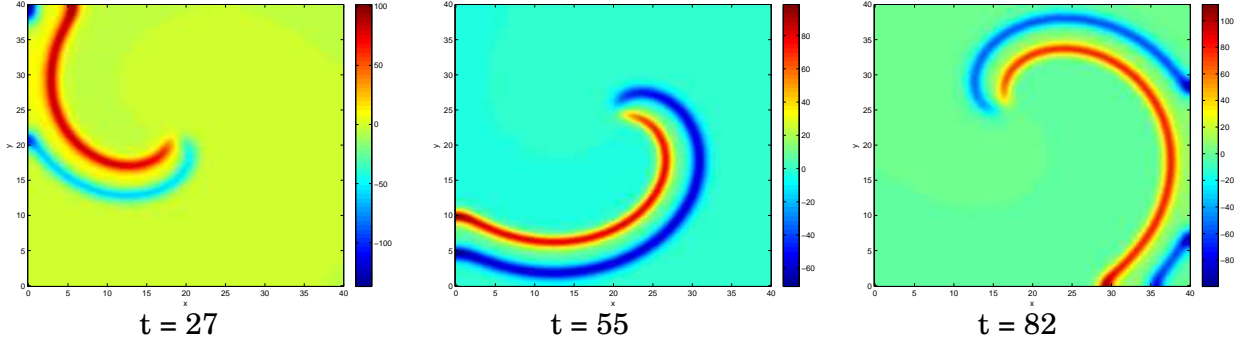


Figure 3.9: The numerical solution of the linear system for the FHN model with parameters $\alpha = 0.5$, $\beta = 0.75$ and $\epsilon = 0.3$ is found by using central difference and forward Euler method. This diagram indicates $\alpha_3 \frac{\partial u}{\partial t}$ such that $\frac{\partial u}{\partial t}$ of formula (3.45) is found through differentiating forward nonlinear solution u of FHN system in 2D with respect to variable y . The time step Δt is equal to 0.1 for the period of time $[0, 82]$ as well as space steps Δx and Δy are 0.3 for space scale 40×40 .

method, backward Euler method and also central difference method, that is,

$$\frac{c_{j,k}^{m+\frac{1}{2}} - c_{j,k}^m}{\Delta t} = \frac{c_{j+1,k}^{m+\frac{1}{2}} - 2c_{j,k}^{m+\frac{1}{2}} + c_{j-1,k}^{m+\frac{1}{2}}}{\Delta x^2} + \frac{c_{j,k+1}^{m+\frac{1}{2}} - 2c_{j,k}^{m+\frac{1}{2}} + c_{j,k-1}^{m+\frac{1}{2}}}{\Delta x^2}, \quad (3.50)$$

$$\frac{c_{j,k}^{m+1} - c_{j,k}^{m+\frac{1}{2}}}{\Delta t} = \frac{1}{\epsilon} \left(1 - (u_{j,k}^{m+\frac{1}{2}})^2 \right) c_{j,k}^{m+\frac{1}{2}} - \frac{1}{\epsilon} d_{j,k}^m, \quad (3.51)$$

$$\frac{d_{j,k}^{m+1} - d_{j,k}^m}{\Delta t} = \epsilon c_{j,k}^m - \epsilon \alpha d_{j,k}^m, \quad (3.52)$$

where

$$j, k = 1, \dots, n, \quad m = 1, \dots, n_1, \quad n, n_1 \in \mathbb{N},$$

and $\Delta x = \Delta y$ is space step, while Δt is time step. Let us consider about the equations (3.50), so the numerical solver (3.50) can be posed as follows:

$$c_{j,k}^m = \delta_1 c_{j,k}^{m+\frac{1}{2}} - \delta_2 c_{j+1,k}^{m+\frac{1}{2}} - \delta_2 c_{j-1,k}^{m+\frac{1}{2}} - \delta_2 c_{j,k+1}^{m+\frac{1}{2}} - \delta_2 c_{j,k-1}^{m+\frac{1}{2}},$$

where

$$\delta_1 = 1 + \frac{4\Delta t}{\Delta x^2}, \quad \delta_2 = \frac{\Delta t}{\Delta x^2}.$$

By using Neumann boundary condition and reshaping the matrix as vector, we have:

$$\mathbf{c}_{j,k}^{m+\frac{1}{2}} = \mathbf{S}_1^{-1} \mathbf{c}_{j,k}^m,$$

where

$$S = \begin{pmatrix} \delta_1 & -2\delta_2 & 0 & 0 & \cdots & 0 & -2\delta_2 & 0 & 0 & \cdots & 0 & 0 & 0 & 0 & 0 & 0 & 0 & 0 & 0 & 0 & 0 & 0 \\ -\delta_2 & \delta_1 & -\delta_2 & 0 & \cdots & 0 & 0 & -2\delta_2 & 0 & \cdots & 0 & 0 & 0 & 0 & 0 & 0 & 0 & 0 & 0 & 0 & 0 & 0 \\ 0 & -\delta_2 & \delta_1 & -\delta_2 & \cdots & 0 & 0 & 0 & -2\delta_2 & \cdots & 0 & 0 & 0 & 0 & 0 & 0 & 0 & 0 & 0 & 0 & 0 & 0 \\ 0 & 0 & -\delta_2 & \delta_1 & \cdots & 0 & 0 & 0 & 0 & \cdots & 0 & 0 & 0 & 0 & 0 & 0 & 0 & 0 & 0 & 0 & 0 & 0 \\ \vdots & \vdots & \vdots & \ddots & \ddots & \vdots & \vdots & \vdots & \vdots & \vdots & \ddots & \vdots & \vdots & \vdots & \vdots & \vdots & \vdots & \vdots & \vdots & \vdots & \vdots & \vdots \\ 0 & 0 & \cdots & 0 & -2\delta_2 & \delta_1 & 0 & 0 & 0 & \cdots & 0 & -2\delta_2 & 0 & 0 & 0 & 0 & 0 & 0 & 0 & 0 & 0 & 0 \\ -\delta_2 & 0 & 0 & 0 & \cdots & 0 & \delta_1 & -2\delta_2 & 0 & \cdots & 0 & 0 & -\delta_2 & 0 & 0 & 0 & 0 & 0 & 0 & 0 & 0 & 0 \\ 0 & -\delta_2 & 0 & 0 & \cdots & 0 & -\delta_2 & \delta_1 & -\delta_2 & \cdots & 0 & 0 & 0 & 0 & -\delta_2 & 0 & 0 & 0 & 0 & 0 & 0 & 0 \\ \vdots & \vdots & \ddots & \vdots & \cdots & \vdots & \vdots & \ddots & \vdots & \vdots & \vdots & \vdots & \ddots & \vdots & \vdots & \vdots & \ddots & \vdots & \vdots & \vdots & \vdots & \vdots \\ 0 & 0 & 0 & -\delta_2 & \cdots & 0 & 0 & -2\delta_2 & \delta_1 & \cdots & 0 & 0 & 0 & 0 & 0 & -\delta_2 & 0 & 0 & 0 & 0 & 0 & 0 \\ \vdots & \vdots & \vdots & \vdots & \ddots & \vdots & \vdots & \vdots & \vdots & \vdots & \ddots & \vdots & \vdots & \vdots & \vdots & \vdots & \ddots & \vdots & \vdots & \vdots & \vdots & \vdots \\ 0 & 0 & 0 & 0 & \cdots & -\delta_2 & 0 & 0 & 0 & \cdots & 0 & \delta_1 & -\delta_2 & 0 & 0 & 0 & 0 & -\delta_2 & 0 & 0 & 0 & 0 \\ 0 & 0 & 0 & 0 & \cdots & 0 & -\delta_2 & 0 & 0 & \cdots & 0 & -\delta_2 & \delta_1 & -\delta_2 & 0 & 0 & 0 & 0 & -\delta_2 & 0 & 0 & 0 \\ \vdots & \vdots & \vdots & \vdots & \cdots & \vdots & \vdots & \ddots & \vdots & \cdots & \vdots & \ddots & \vdots & \ddots & \vdots & \vdots & \vdots & \vdots & \ddots & \vdots & \vdots & \vdots \\ 0 & 0 & 0 & 0 & \cdots & 0 & 0 & 0 & -\delta_2 & \cdots & 0 & 0 & 0 & -\delta_2 & \delta_1 & -\delta_2 & 0 & 0 & 0 & 0 & -\delta_2 & 0 \\ 0 & 0 & 0 & 0 & \cdots & 0 & 0 & 0 & 0 & \ddots & 0 & 0 & 0 & 0 & -\delta_2 & \delta_1 & -\delta_2 & 0 & 0 & 0 & 0 & -\delta_2 \\ 0 & 0 & 0 & 0 & \cdots & 0 & 0 & 0 & 0 & \cdots & -\delta_2 & 0 & 0 & 0 & 0 & -2\delta_2 & \delta_1 & 0 & 0 & 0 & 0 & -\delta_2 \\ 0 & 0 & 0 & 0 & \cdots & 0 & 0 & 0 & 0 & \cdots & 0 & -2\delta_2 & 0 & 0 & 0 & 0 & \delta_1 & -2\delta_2 & 0 & 0 & 0 & 0 \\ 0 & 0 & 0 & 0 & \cdots & 0 & 0 & 0 & 0 & \cdots & 0 & 0 & 0 & 0 & 0 & -\delta_2 & \delta_1 & -\delta_2 & 0 & 0 & 0 & 0 \\ 0 & 0 & 0 & 0 & \cdots & 0 & 0 & 0 & 0 & 0 & 0 & -2\delta_2 & 0 & 0 & 0 & 0 & -\delta_2 & \delta_1 & -\delta_2 & 0 & 0 & 0 \\ 0 & 0 & 0 & 0 & \cdots & 0 & 0 & 0 & 0 & 0 & 0 & 0 & -2\delta_2 & 0 & 0 & 0 & -\delta_2 & \delta_1 & -\delta_2 & 0 & 0 & 0 \\ \vdots & \vdots & \vdots & \vdots & \cdots & \vdots & \vdots & \vdots & \vdots & \vdots & \vdots & \vdots & \ddots & \vdots & \vdots & \vdots & \vdots & \vdots & \vdots & \ddots & \vdots & \vdots \\ 0 & 0 & 0 & 0 & \cdots & 0 & 0 & 0 & 0 & \cdots & 0 & 0 & 0 & 0 & 0 & -2\delta_2 & 0 & 0 & 0 & 0 & -2\delta_2 & \delta_1 \end{pmatrix}_{n^2 \times n^2},$$

and

$$\begin{aligned} \left(\mathbf{c}_{j,k}^m \right)^\top &= \left[c_{11}^m \quad \cdots \quad c_{1n}^m \quad c_{21}^m \quad \cdots \quad c_{2n}^m \quad \cdots \quad c_{n1}^m \quad \cdots \quad c_{nn}^m \right]_{1 \times n^2}, \\ \left(\mathbf{c}_{j,k}^{m+\frac{1}{2}} \right)^\top &= \left[c_{11}^{m+\frac{1}{2}} \quad \cdots \quad c_{1n}^{m+\frac{1}{2}} \quad c_{21}^{m+\frac{1}{2}} \quad \cdots \quad c_{2n}^{m+\frac{1}{2}} \quad \cdots \quad c_{n1}^{m+\frac{1}{2}} \quad \cdots \quad c_{nn}^{m+\frac{1}{2}} \right]_{1 \times n^2}. \end{aligned}$$

Since, S_1 is a sparse matrix, we will use a sparse matrix solver in Matlab to find the variable $\mathbf{c}_{j,k}^{m+\frac{1}{2}}$. By looking at the equation (3.51), we will have

$$c_{j,k}^{m+1} = \left(\frac{\Delta t}{\epsilon} \left(1 - \left(u_{j,k}^{m+\frac{1}{2}} \right)^2 \right) + 1 \right) c_{j,k}^{m+\frac{1}{2}} - \frac{\Delta t}{\epsilon} d_{j,k}^m.$$

The second equation of system (3.7), we will use fully explicit method, that is

$$\frac{d_{j,k}^{m+1} - d_{j,k}^m}{\Delta t} = \epsilon c_{j,k}^{m+\frac{1}{2}} - \epsilon \alpha d_{j,k}^m \implies d_{j,k}^{m+1} = \Delta t \epsilon c_{j,k}^{m+\frac{1}{2}} + (1 - \Delta t \epsilon \alpha) d_{j,k}^m.$$

In order to use the power iteration method, we need to formulate the linear system (3.7) as follows:

$$\begin{bmatrix} \mathbf{c}_{j,k}^{m+1} \\ \mathbf{d}_{j,k}^{m+1} \end{bmatrix} = \begin{bmatrix} B_1 & B_2 \\ B_3 & B_4 \end{bmatrix} \begin{bmatrix} \mathbf{c}_{j,k}^{m+\frac{1}{2}} \\ \mathbf{d}_{j,k}^m \end{bmatrix},$$

where the submatrices B_1 is a diagonal matrix with entries

$$p_{jk}^m = \frac{\Delta t}{\epsilon} \left(1 - \left(u_{j,k}^{m+\frac{1}{2}} \right)^2 \right) + 1,$$

Moreover, we find that submatrices B_2, B_3 , and B_4 is diagonal with entries

$$c_1 = -\frac{\Delta t}{\epsilon}, \quad a_2 = \Delta t \epsilon, \quad c_2 = 1 - \Delta t \epsilon \alpha.$$

Moreover, we observe that the size of matrix B is $2n^2 \times 2n^2$, so for large n it may be impossible to calculate all the eigenvalues. In the partial differential equations, we can numerically calculate some eigenvalues and eigenvectors through using the common method of estimating eigenvalue called the power iteration method (this method also named Von Mises iteration) [22, 86]. In 1965, this method was explained by Wilkinson how to find principal vectors [88]. The property of power iteration is calculated the best approximated principal eigenvalue (largest eigenvalue) for giving diagonalisable matrix $A \in \mathbb{C}^{n \times n}$ such that $n \in \mathbb{N}$ and we can also program the algorithm of the power iteration easily compared with other methods such as Arnoldi iteration method. The matrix A is called diagonalisable if it satisfies the condition (3.53) [62]:

$$V^{-1} A V = \Lambda, \tag{3.53}$$

where the columns of V form a basis of right eigenvectors and Λ is diagonal matrix with diagonal entries of the eigenvalues $\lambda_1, \dots, \lambda_n$. Moreover, estimated largest eigenvalue is defined as follows:

$$|\lambda_1| > |\lambda_i|, \quad i = 2, \dots, n, \quad n \in \mathbb{N}.$$

so the power iteration can be formulated as follows:

$$\mathbf{v}^{m+1} = A \mathbf{v}^m = A^{m+1} \mathbf{v}^0, \quad m \in \mathbb{N},$$

such that the principal eigenvector \mathbf{v}^{m+1} is converge if it satisfies the formula (3.54)

$$\left| \frac{\lambda_i}{\lambda_1} \right| < 1. \tag{3.54}$$

By using Rayleigh quotient iteration, the principal eigenvalue λ_{m+1} is formed as follows [57]:

$$\lambda_{m+1} = \frac{\langle A \mathbf{v}^{m+1} | \mathbf{v}^{m+1} \rangle}{\langle \mathbf{v}^{m+1} | \mathbf{v}^{m+1} \rangle}.$$

According to stability of analysis eigenvalues, we can recognise stable or instable spiral wave solutions through study the principal eigenvalue λ_{m+1} . The method has good advantage because

we do not need to investigate all rest of Floquet multipliers if we study the large eigenvalue λ_{m+1} . The most main advantage of using this method is a fast convergence, whereas main disadvantage of this method is only computed one estimated principal eigenvector with single largest eigenvalue. By looking at the linear system (3.7), we will find principle eigenvector \mathbf{v} through using power iteration method, that is

$$\begin{aligned}\mathbf{v}_{j,k}^1 &= \mathbf{B}\mathbf{v}_{j,k}^0 \\ \mathbf{v}_{j,k}^2 &= \mathbf{B}\mathbf{v}_{j,k}^1 \\ &\vdots \\ \mathbf{v}_{j,k}^m &= \mathbf{B}\mathbf{v}_{j,k}^{m-1} \\ \mathbf{v}_{j,k}^{m+1} &= \mathbf{B}\mathbf{v}_{j,k}^m.\end{aligned}\tag{3.55a}$$

By using Rayleigh quotient iteration, the principle eigenvalue λ_{m+1} is found as follows:

$$\lambda_{m+1} = \frac{\langle \mathbf{B}\mathbf{v}_{j,k}^{m+1} | \mathbf{v}_{j,k}^{m+1} \rangle}{\langle \mathbf{v}_{j,k}^{m+1} | \mathbf{v}_{j,k}^{m+1} \rangle}.\tag{3.56}$$

By looking at the equation (3.56), we need to compute the term $\mathbf{B}\mathbf{v}_{j,k}^{m+1}$ through increasing one more step of iteration, that is

$$\mathbf{v}_{j,k}^{m+2} = \mathbf{B}\mathbf{v}_{j,k}^{m+1},$$

so principle eigenvalue λ_{m+1} is as follows

$$\lambda_{m+1} = \frac{\mathbf{v}_{j,k}^{m+2} \cdot \mathbf{v}_{j,k}^{m+1}}{\mathbf{v}_{j,k}^{m+1} \cdot \mathbf{v}_{j,k}^{m+1}}.$$

By looking at equation (3.23), we observe that the solution $\hat{\mathbf{v}}$ is stationary solution, so we find that

$$\check{\mathcal{L}}\hat{\mathbf{v}} = 0 \implies \hat{\lambda}\hat{\mathbf{v}} = 0\tag{3.57a}$$

$$\implies \hat{\lambda} = 0.\tag{3.57b}$$

By using power iteration method and matlab software, the greatest eigenvalue λ_{m+1} is as follows:

$$\lambda_{m+1} = 0.9699,$$

such that the time t belongs to time interval $[0, 35]$. According to the condition (1.16), the dynamical solution of the linear system (3.22) in cartesian coordinate is stable.

In the next section, we need to discuss how to compute the angular velocity of the spiral wave's drift numerically and this result of the calculation will also be used to find the wavelength of spiral wave (see Figure 2.7).

3.4 Angular Velocity and Wavelength of the Spiral Wave

The equation (3.19) is useful to calculate the angular velocity of the spiral wave. The angular velocity of the spiral wave c is computed numerically through using *Newton-Raphson method*. Using this method in addition to beginning with an initial guess helps us find a good approximation of the value c . The idea behind using this method is that we need to have the numbers of iterations to obtain an approximate value c . We can know that this value is a good approximation if the approximated value c is iterated. We demonstrate Newton-Raphson method through calculating the angular velocity c . By looking at the equation (3.19), we observe that the spiral wave solution is in stationary rotation. We need to find a stationary rotating spiral wave in order for the angular velocity c to be computed numerically. By looking at a paper by Biktasheva et al. [14], the formula (3.19) can be formulated as follows:

$$\mathbf{F}(\mathbf{z}) = 0, \quad (3.58)$$

where

$$\mathbf{F}(\mathbf{z}) = \mathbf{D} \left(\mathbf{z}_{rr} + \frac{1}{r^2} \mathbf{z}_{\theta\theta} + \frac{1}{r} \mathbf{z}_r \right) + c \mathbf{z}_\theta + \mathbf{f}(\mathbf{z}). \quad (3.59)$$

This lead us to write the equation (3.59) as follows:

$$\begin{bmatrix} F_1(\chi, \zeta) \\ F_2(\chi, \zeta) \end{bmatrix} = \begin{bmatrix} 1 & 0 \\ 0 & 0 \end{bmatrix} \left(\begin{bmatrix} \chi_{rr} \\ \zeta_{rr} \end{bmatrix} + \frac{1}{r^2} \begin{bmatrix} \chi_{\theta\theta} \\ \zeta_{\theta\theta} \end{bmatrix} + \frac{1}{r} \begin{bmatrix} \chi_r \\ \zeta_r \end{bmatrix} \right) + c \begin{bmatrix} \chi_\theta \\ \zeta_\theta \end{bmatrix} + \begin{bmatrix} g(\chi, \zeta) \\ h(\chi, \zeta) \end{bmatrix}, \quad (3.60)$$

where

$$\mathbf{F}(\mathbf{z}) = \begin{bmatrix} F_1(\chi, \zeta) \\ F_2(\chi, \zeta) \end{bmatrix}, \mathbf{z} = \begin{bmatrix} \chi(r, \Theta) \\ \zeta(r, \Theta) \end{bmatrix}, \mathbf{f}(\mathbf{z}) = \begin{bmatrix} g(\chi, \zeta) \\ h(\chi, \zeta) \end{bmatrix} = \begin{bmatrix} \frac{1}{\epsilon} \left(\chi - \frac{\chi^3}{3} - \zeta \right) \\ \epsilon(\chi - \alpha\zeta + \beta) \end{bmatrix}.$$

The components χ and ζ are explained in the beginning. Numerically, we can compute the angular velocity c through using Newton's method as follows:

$$\mathbf{x}^{m+1} = \mathbf{x}^m - (\mathbf{F}'(\mathbf{x}^m))^{-1} \mathbf{F}(\mathbf{x}^m), \quad (3.61)$$

where

$$\mathbf{x} = \begin{bmatrix} \mathbf{z} \\ c \end{bmatrix}, \quad \mathbf{F}(\mathbf{x}) = \begin{bmatrix} F_1(\chi, \zeta, c) \\ F_2(\chi, \zeta, c) \\ F_3(\chi, \zeta, c) \end{bmatrix}, \quad m \in \mathbb{N},$$

such that c refers to angular velocity of spiral wave. We now observe that the equation (3.59) can be posed as follows

$$\begin{bmatrix} F_1(\chi, \zeta, c) \\ F_2(\chi, \zeta, c) \\ F_3(\chi, \zeta, c) \end{bmatrix} = \begin{bmatrix} 1 & 0 & 0 \\ 0 & 0 & 0 \\ 0 & 0 & 0 \end{bmatrix} \left(\begin{bmatrix} \chi_{rr} \\ \zeta_{rr} \\ 0 \end{bmatrix} + \frac{1}{r^2} \begin{bmatrix} \chi_{\Theta\Theta} \\ \zeta_{\Theta\Theta} \\ 0 \end{bmatrix} + \frac{1}{r} \begin{bmatrix} \chi_r \\ \zeta_r \\ 0 \end{bmatrix} \right) + c \begin{bmatrix} \chi_\Theta \\ \zeta_\Theta \\ 0 \end{bmatrix} + \begin{bmatrix} g(\chi, \zeta) \\ h(\chi, \zeta) \\ z(\chi, \zeta) \end{bmatrix}. \quad (3.62)$$

Based on the formula (3.62), we can derive that

$$F_1(\chi, \zeta, c) = \chi_{rr} + \frac{1}{r^2} \chi_{\Theta\Theta} + \frac{1}{r} \chi_r + c \chi_\Theta + g(\chi, \zeta), \quad (3.63a)$$

$$F_2(\chi, \zeta, c) = c \zeta_\Theta + h(\chi, \zeta), \quad (3.63b)$$

$$F_3(\chi, \zeta, c) = z(\chi, \zeta). \quad (3.63c)$$

By using the Euler forward and central difference methods, the equations (3.63a), (3.63b) and (3.63c) will be written as follows:

$$F_1(\chi_{j,k}, \zeta_{j,k}, c) \approx \frac{c}{2\Delta\Theta} (\chi_{j,k+1} - \chi_{j,k-1}) + \frac{1}{\epsilon} \left(\chi_{j,k} - \frac{(\chi_{j,k})^3}{3} - \zeta_{j,k} \right) + \frac{1}{(\Delta r)^2} (\chi_{j+1,k} - 2\chi_{j,k} + \chi_{j-1,k}) + \frac{1}{r_j^2} \frac{1}{(\Delta\Theta)^2} (\chi_{j,k+1} - 2\chi_{j,k} + \chi_{j,k-1}) + \frac{1}{r_j 2\Delta r} (\chi_{j+1,k} - \chi_{j-1,k}) \quad (3.64a)$$

$$F_2(\chi_{j,k}, \zeta_{j,k}, c) \approx \frac{c}{2\Delta\Theta} (\zeta_{j,k+1} - \zeta_{j,k-1}) + \epsilon (\chi_{j,k} - \alpha\zeta_{j,k} + \beta) \quad (3.64b)$$

$$F_3(\chi_{j_\star, k_\star}, \zeta_{j_\star, k_\star}, c) = z(\chi_{j_\star, k_\star}, \zeta_{j_\star, k_\star}), \quad (3.64c)$$

CHAPTER 3. STABILITY OF THE SPIRAL WAVE, SYMMETRIES AND RESPONSE FUNCTIONS

where

$$r_j = 0.01 + (j-1)\Delta r, \Theta_k = (k-1)\Delta\Theta, \quad \Delta r = \frac{20-0.01}{N_r-1}, \quad \Delta\Theta = \frac{2\pi}{N_\theta-1}, \quad j = 1, \dots, N_r, k = 1, \dots, N_\theta, \quad N_r, N_\theta \in \mathbb{N},$$

and

$$j_\star, k_\star \in \mathbb{N}.$$

According to the number of indexes j and k , the vector \mathbf{x} can be derived as follows:

$$\mathbf{x}_{j,k} = \begin{bmatrix} \left[\chi(r_j, \Theta_k) \right]_{N_r N_\theta \times 1} \\ \left[\zeta(r_j, \Theta_k) \right]_{N_r N_\theta \times 1} \\ \left[c \right]_{1 \times 1} \end{bmatrix}_{(2N_r N_\theta + 1) \times 1} = \begin{bmatrix} \left[\chi_{j,k} \right]_{N_r N_\theta \times 1} \\ \left[\zeta_{j,k} \right]_{N_r N_\theta \times 1} \\ \left[c \right]_{1 \times 1} \end{bmatrix}_{(2N_r N_\theta + 1) \times 1}.$$

This means that the function $\mathbf{F}(\mathbf{z})$ can be also formulated as follows:

$$\mathbf{F}(\mathbf{x}_{j,k}) = \begin{bmatrix} \left[F_1(\chi_{j,k}, \zeta_{j,k}, c) \right]_{N_r N_\theta \times 1} \\ \left[F_2(\chi_{j,k}, \zeta_{j,k}, c) \right]_{N_r N_\theta \times 1} \\ \left[F_3(\chi_{j_\star, k_\star}, \zeta_{j_\star, k_\star}, c) \right]_{1 \times 1} \end{bmatrix}_{(2N_r N_\theta + 1) \times 1}.$$

By using the Neumann boundary condition and through finding the values of the functions F_1 , F_2 and F_3 corresponding with indexes j and k , the differentiation of function $\mathbf{F}(\mathbf{x})$ with respect to \mathbf{x} can be given as follows:

$$\mathbf{F}'(\mathbf{x}_{j,k}) = \begin{bmatrix} \mathbf{A}_1 & \mathbf{A}_2 & \mathbf{c}_1 \\ \mathbf{A}_3 & \mathbf{A}_4 & \\ \mathbf{r}_1 & & e_1 \end{bmatrix}_{(2N_r N_\theta + 1) \times (2N_r N_\theta + 1)},$$

because the size of the function $\mathbf{F}(\mathbf{x}_{j,k})$ is $(2N_r N_\theta + 1) \times 1$ in order for the formula (3.61) to be calculated. We also observe that the block matrix \mathbf{A}_1 can be found through multiple calculations

which can be simplified and formalised as follows:

$$\mathbf{A}_1 = \begin{pmatrix}
 a_{11} & a_1 & 0 & 0 & \cdots & 0 & \frac{2}{\Delta r^2} & 0 & 0 & \cdots & 0 & 0 & 0 & 0 & 0 & 0 & 0 & 0 & 0 & 0 \\
 b_1 & a_{12} & c_1 & 0 & \cdots & 0 & 0 & \frac{2}{\Delta r^2} & 0 & \cdots & 0 & 0 & 0 & 0 & 0 & 0 & 0 & 0 & 0 & 0 \\
 0 & b_1 & a_{13} & c_1 & \cdots & 0 & 0 & 0 & \frac{2}{\Delta r^2} & \cdots & 0 & 0 & 0 & 0 & 0 & 0 & 0 & 0 & 0 & 0 \\
 0 & 0 & b_1 & a_{14} & \cdots & 0 & 0 & 0 & 0 & \cdots & 0 & 0 & 0 & 0 & 0 & 0 & 0 & 0 & 0 & 0 \\
 \vdots & \vdots & \vdots & \ddots & \ddots & \vdots & \vdots & \vdots & \vdots & \ddots & \vdots & \vdots & \vdots & \vdots & \vdots & \vdots & \vdots & \vdots & \vdots \\
 0 & 0 & \cdots & 0 & a_1 & a_{1N_\theta} & 0 & 0 & 0 & \cdots & 0 & \frac{2}{\Delta r^2} & 0 & 0 & 0 & 0 & 0 & 0 & 0 & 0 \\
 d_2 & 0 & 0 & 0 & \cdots & 0 & a_{21} & a_2 & 0 & \cdots & 0 & 0 & e_2 & 0 & 0 & 0 & 0 & 0 & 0 & 0 \\
 0 & d_2 & 0 & 0 & \cdots & 0 & b_2 & a_{22} & c_2 & \cdots & 0 & 0 & 0 & e_2 & 0 & 0 & 0 & 0 & 0 & 0 \\
 \vdots & \vdots & \ddots & \vdots & \cdots & \vdots & \vdots & \ddots & \ddots & \vdots & \vdots & \vdots & \vdots & \vdots & \ddots & \vdots & \vdots & \vdots & \vdots & \vdots \\
 0 & 0 & 0 & d_2 & \cdots & 0 & 0 & 0 & a_2 & a_{2N_\theta} & \cdots & 0 & 0 & 0 & e_2 & 0 & 0 & 0 & 0 & 0 \\
 \vdots & \vdots & \vdots & \vdots & \ddots & \vdots & \vdots & \vdots & \vdots & \vdots & \ddots & \vdots & \vdots & \vdots & \vdots & \ddots & \vdots & \vdots & \vdots & \vdots \\
 0 & 0 & 0 & 0 & \cdots & d_j & 0 & 0 & 0 & 0 & \cdots & a_{jk} & c_j & 0 & 0 & 0 & 0 & e_j & 0 & 0 & 0 \\
 0 & 0 & 0 & 0 & \cdots & 0 & d_{j+1} & 0 & 0 & 0 & \cdots & b_{j+1} & a_{(j+1)(k+1)} & c_{j+1} & 0 & 0 & 0 & 0 & e_{j+1} & 0 & 0 \\
 \vdots & \vdots & \vdots & \vdots & \cdots & \vdots & \vdots & \ddots & \ddots & \vdots & \vdots & \vdots & \vdots & \vdots & \vdots & \vdots & \vdots & \vdots & \vdots & \ddots & \vdots \\
 0 & 0 & 0 & 0 & \cdots & 0 & 0 & 0 & d_{N_r-1} & 0 & \cdots & 0 & a_{N_r-1} & a_{(N_r-1)(N_\theta-1)} & 0 & 0 & 0 & 0 & 0 & 0 & e_{N_r-1} \\
 0 & 0 & 0 & 0 & \cdots & 0 & 0 & 0 & 0 & \frac{2}{\Delta r^2} & \cdots & 0 & 0 & a_{N_r,1} & a_{N_r} & 0 & 0 & 0 & 0 & 0 & 0 \\
 0 & 0 & 0 & 0 & \cdots & 0 & 0 & 0 & 0 & 0 & \ddots & 0 & 0 & b_{N_r} & a_{N_r,2} & c_{N_r} & 0 & 0 & 0 & 0 & 0 \\
 0 & 0 & 0 & 0 & \cdots & 0 & 0 & 0 & 0 & 0 & \cdots & \frac{2}{\Delta r^2} & 0 & 0 & b_{N_r} & a_{N_r,3} & c_{N_r} & 0 & 0 & 0 & 0 \\
 0 & 0 & 0 & 0 & \cdots & 0 & 0 & 0 & 0 & 0 & \cdots & 0 & \frac{2}{\Delta r^2} & 0 & 0 & b_{N_r} & a_{N_r,4} & c_{N_r} & 0 & 0 & 0 \\
 0 & 0 & 0 & 0 & \cdots & 0 & 0 & 0 & 0 & 0 & \cdots & 0 & 0 & 0 & 0 & b_{N_r} & a_{N_r,5} & c_{N_r} & 0 & 0 & 0 \\
 0 & 0 & 0 & 0 & \cdots & 0 & 0 & 0 & 0 & 0 & \cdots & 0 & 0 & \frac{2}{\Delta r^2} & 0 & 0 & 0 & b_{N_r} & a_{N_r,6} & c_{N_r} & 0 \\
 \vdots & \vdots & \vdots & \vdots & \cdots & \vdots & \vdots & \vdots & \vdots & \vdots & \cdots & \vdots & \vdots & \vdots & \ddots & \vdots & \vdots & \vdots & \ddots & \ddots & \vdots \\
 0 & 0 & 0 & 0 & \cdots & 0 & 0 & 0 & 0 & 0 & \cdots & 0 & 0 & 0 & 0 & \frac{2}{\Delta r^2} & 0 & 0 & 0 & a_{N_r} & a_{N_r, N_\theta}
 \end{pmatrix},$$

where the variables in the block matrix \mathbf{A}_1 can be defined as follows:

$$\begin{aligned}
 a_{jk} &= \frac{1}{\epsilon} - \frac{2}{\Delta r^2} - \frac{2}{r_j^2 \Delta \theta} - \frac{\chi_{jk}^2}{\epsilon}, & a_j &= \frac{2}{r_j^2 \Delta \theta^2}, & b_j &= \frac{1}{r_j^2 \Delta \theta^2} - \frac{c}{2 \Delta \theta}, \\
 c_j &= \frac{1}{r_j^2 \Delta \theta^2} + \frac{c}{2 \Delta \theta}, & d_j &= \frac{1}{\Delta r^2} - \frac{1}{2 r_j^2 \Delta r}, & e_j &= \frac{1}{\Delta r^2} + \frac{1}{2 r_j^2 \Delta r}.
 \end{aligned}$$

Moreover, other block matrices \mathbf{A}_2 and \mathbf{A}_3 are a diagonal with entries $-\frac{1}{\epsilon}$ and ϵ respectively. The block matrix \mathbf{A}_4 are formed as follows:

$$\mathbf{A}_4 = \begin{pmatrix}
 -\epsilon \alpha & 0 & 0 & \cdots & 0 & 0 & 0 \\
 -\frac{c}{2 \Delta \theta} & -\epsilon \alpha & \frac{c}{2 \Delta \theta} & \cdots & 0 & 0 & 0 \\
 0 & -\frac{c}{2 \Delta \theta} & -\epsilon \alpha & \cdots & 0 & 0 & 0 \\
 \vdots & \vdots & \vdots & \ddots & \vdots & \vdots & \vdots \\
 0 & 0 & 0 & \cdots & -\epsilon \alpha & \frac{c}{2 \Delta \theta} & 0 \\
 0 & 0 & 0 & \cdots & -\frac{c}{2 \Delta \theta} & -\epsilon \alpha & \frac{c}{2 \Delta \theta} \\
 0 & 0 & 0 & \cdots & 0 & 0 & -\epsilon \alpha
 \end{pmatrix}_{N_r N_\theta \times N_r N_\theta}.$$

CHAPTER 3. STABILITY OF THE SPIRAL WAVE, SYMMETRIES AND RESPONSE FUNCTIONS

With regard to the matrix $\mathbf{F}'(\mathbf{x}_{j,k})$, the vectors \mathbf{c}_1 , \mathbf{r}_1 and the one element e_1 are posed as follows:

$$\mathbf{c}_1^\top = \left[0 \quad -\frac{\chi_{11}}{2\Delta\Theta} + \frac{\chi_{13}}{2\Delta\Theta} \quad -\frac{\chi_{12}}{2\Delta\Theta} + \frac{\chi_{14}}{2\Delta\Theta} \quad \dots \quad -\frac{\chi_{1(N_\Theta-2)}}{2\Delta\Theta} + \frac{\chi_{1N_\Theta}}{2\Delta\Theta} \quad 0 \quad \dots \quad 0 \quad -\frac{\zeta_{21}}{2\Delta\Theta} + \frac{\zeta_{23}}{2\Delta\Theta} \quad \dots \quad -\frac{\zeta_{j(k-2)}}{2\Delta\Theta} + \frac{\zeta_{jk}}{2\Delta\Theta} \quad \dots \quad -\frac{\zeta_{N_r(N_\Theta-2)}}{2\Delta\Theta} + \frac{\zeta_{N_r N_\Theta}}{2\Delta\Theta} \quad 0 \right]_{1 \times 2N_r N_\Theta} \quad (3.65a)$$

$$\mathbf{r}_1 = \left[\frac{\partial F_3}{\partial \chi_{11}} \quad \frac{\partial F_3}{\partial \chi_{12}} \quad \frac{\partial F_3}{\partial \chi_{13}} \quad \dots \quad \frac{\partial F_3}{\partial \chi_{1N_\Theta}} \quad \frac{\partial F_3}{\partial \chi_{21}} \quad \dots \quad \frac{\partial F_3}{\partial \chi_{2(N_\Theta-1)}} \quad \frac{\partial F_3}{\partial \chi_{2N_\Theta}} \quad \frac{\partial F_3}{\partial \chi_{31}} \quad \dots \quad \frac{\partial F_3}{\partial \zeta_{11}} \quad \dots \quad \frac{\partial F_3}{\partial \zeta_{jk}} \quad \dots \quad \frac{\partial F_3}{\partial \zeta_{N_r,1}} \quad \dots \quad \frac{\partial F_3}{\partial \zeta_{N_r, N_\Theta}} \right]_{1 \times 2N_r N_\Theta} \quad (3.65b)$$

$$e_1 = \left[\frac{\partial F_3}{\partial c} \right]_{1 \times 1} = \left[0 \right]_{1 \times 1}. \quad (3.65c)$$

In order for the vector $\mathbf{x}_{j,k}$ to be computed through the Newton's method, the matrix $\mathbf{F}'(\mathbf{x}_{j,k})$ should not be singular, that is, $(|\mathbf{F}'(\mathbf{x}_{j,k})| \neq 0)$. Therefore, by looking at the row vector \mathbf{r}_1 in the equation (3.65b), each element in the vector \mathbf{r}_1 becomes equal to zero. In linear Algebra, by using the properties of the determinants of matrices and if we have a square matrix with a row vector where every element is zero, or a column vector where each entry is zero, then the determinant of square matrix is equal to zero [5]. To avoid this problem, we can review how this was successfully done in a paper by Biktasheva et al. [14] using a pinning condition. Therefore, we need to define the function z as follows:

$$z(\chi_{j_\star, k_\star}, \zeta_{j_\star, k_\star}) = \zeta_{j_\star, k_\star},$$

where

$$\zeta(r_j, \Theta_k) = \zeta(0.01 + (j-1)\Delta r, (k-1)\Delta\Theta).$$

So we derive that

$$\zeta_{j_\star, k_\star} \equiv \zeta(0.01 + (j_\star - 1)\Delta r, (k_\star - 1)\Delta\Theta), \quad (3.66)$$

which means that we need to select any arbitrary value from the second component ζ . Therefore, let us suppose that

$$j_\star = N_r, k_\star = N_\Theta,$$

so we find that

$$\mathbf{r}_1 = \left[0 \ 0 \ \dots \ 0 \ 0 \ \dots \ 0 \ 0 \ 0 \ \dots \ 0 \ \dots \ 0 \ \dots \ 1 \right].$$

We know that

$$\frac{\partial \chi(r_j, \Theta_k)}{\partial \Theta} = \frac{\chi_{j,k+1} - \chi_{j,k-1}}{2\Delta\Theta} + \mathcal{O}((\Delta\Theta)^2), \quad (3.67a)$$

$$\frac{\partial \zeta(r_j, \Theta_k)}{\partial \Theta} = \frac{\zeta_{j,k+1} - \zeta_{j,k-1}}{2\Delta\Theta} + \mathcal{O}((\Delta\Theta)^2), \quad (3.67b)$$

where

$$r \in [0.01, 20], \quad \Theta \in [0, 2\pi].$$

In order for the approximate solution \mathbf{x}^{m+1} of the equation (3.61) to be found for each iteration, we need to define the equation (3.59) in the disk instead of the square boundary domain using the formulas (3.13) as shown in the panel (b) of Figure 3.10. The reason for doing this is that we can compute the angular velocity c of the spiral wave solution in the polar coordinate system. By using the initial condition of FHN system shown in Figure 2.2, we need to transfer the initial spiral wave for component u to the disk through using an approximate function such as the bilinear or the bicubic interpolation functions. By using the bilinear interpolation function, the diagram of the initial spiral wave as shown in Figure 2.2 has been transferred in the disk as highlighted in Figure 3.10. Therefore, simulations of the equation (3.59) in polar coordinate (r, Θ) can be performed on a domain $[0, L_r] \times [0, 2\pi]$ consisting of $N_r \times N_\Theta$ grid points such that the radius $L_r \in \mathbb{R}^+$ [42]. By using the numerical solver (3.61), the angular velocity c will be found for each iteration m , as shown in the Table 3.1. With regards to the stationary partial differential equation (3.19), we can numerically find the critical solution, which is stationary in the moving frame using the Central Finite Difference method. Hence, equation (3.19) can be formulated as follows:

$$0 = \chi_{rr} + \frac{1}{r^2} \chi_{\Theta\Theta} + \frac{1}{r} \chi_r + c \chi_\Theta + \frac{1}{\epsilon} \left(\chi - \frac{\chi^3}{3} - \zeta \right), \quad (3.68a)$$

$$0 = c \zeta_\Theta + \epsilon (\chi - \alpha \zeta + \beta), \quad (3.68b)$$

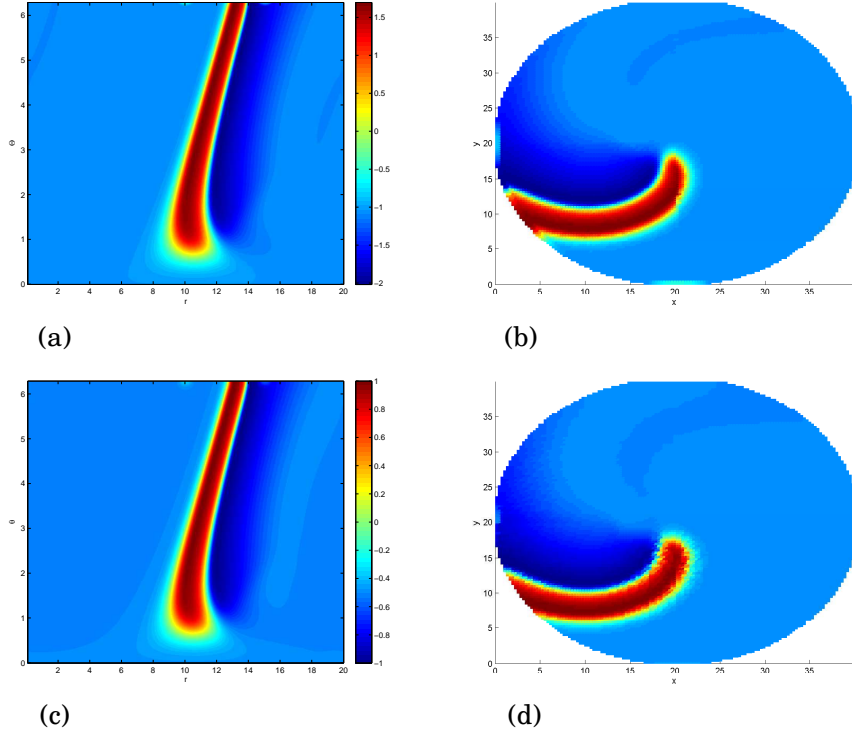


Figure 3.10: The panels (a) and (b) indicate the initial approximation of the spiral wave pattern for component χ for the stationary partial differential equation (3.19). The diagram (a) indicates the initial approximation of the spiral wave in the polar coordinate system (r, Θ) using the bilinear interpolation function such that $N_r = 550$ and $N_\Theta = 550$, while diagram (b) indicates the initial approximation of the spiral wave in the disk using the functions $x(r, \Theta)$ and $y(r, \Theta)$. The parameters ϵ , β and α of equation (3.19) are 0.3, 0.75 and 0.5 respectively. The panels (c) and (d) point out the numerical stationary critical solution for components χ such that diagram (c) shows the stationary solution of the spiral wave in the polar coordinate system (r, Θ) . While diagram (d) indicates the stationary solution in the disk. The total length of the circle radius L_r is 20 such that the space step Δr for the radius is 0.0362. The total measure of the circle angle θ is 2π such that the space step $\Delta \Theta$ for the circle angle is equal to 0.0114.

By using the Central Finite Difference method, the numerical solver for the stationary partial differential equations (3.68a) and (3.68b) can be written as follows:

$$\chi_{j,k} \approx H^{-1} \left(\frac{\chi_{j+1,k} + \chi_{j-1,k}}{\Delta r^2} + \frac{1}{r_j^2} \frac{\chi_{j,k+1} + \chi_{j,k-1}}{\Delta \Theta^2} + \frac{1}{r_j} \frac{\chi_{j+1,k} + \chi_{j-1,k}}{2\Delta r} + c \frac{\chi_{j,k+1} + \chi_{j,k-1}}{2\Delta \Theta} - \frac{1}{\epsilon} \frac{(\chi_{j,k})^3}{3} - \frac{1}{\epsilon} \zeta_{j,k} \right),$$

$$\zeta_{j,k} \approx \frac{c}{\epsilon \alpha} \frac{\zeta_{j,k+1} + \zeta_{j,k-1}}{2\Delta \Theta} + \frac{1}{\alpha} \chi_{j,k} + \frac{\beta}{\alpha}, \quad j, k = 0, 1, \dots, n, \quad n \in \mathbb{N},$$

where H is a diagonal matrix with entries $h_j = \frac{2}{\Delta r^2} + \frac{1}{r_j^2} \frac{2}{\Delta \Theta^2} - \frac{1}{\epsilon}$. By applying Neumann boundary conditions, the numerical stationary critical solution is shown in panels (c) and (d) of Figure 3.10.

Iteration numbers m	Angular velocity estimate c^m
1	$c^1 = 0.0111$
2	$c^2 = 0.62015$
3	$c^3 = 0.62015$

Table 3.1: This table shows the approximate angular velocity c^m for the FitzHugh-Nagumo model through using the Newton's iteration method. The parameters for FHN are $\epsilon = 0.3$, $\alpha = 0.5$ and $\beta = 0.75$ such that the initial guess for the angular velocity c is 0.0111.

Let us now consider the wavelength of the spiral that was explained in Section 2.4 by using the angular velocity c of the spiral wave if a periodic time is known. In a paper [53], we found that the wavelength l can be formed as follows:

$$l = c \times \tau, \quad (3.69)$$

such that the variable τ is the periodic rotation of the spiral wave and c is the angular velocity. Now, we will numerically find the periodic time τ if the variables x and y are fixed for the function $u(x, y, t)$ that is the solution of the nonlinear system (1.1). Therefore, we find that

$$\mathbf{f}(t) = \mathbf{u}(x_*, y_*, t). \quad (3.70)$$

We can now calculate numerically the periodic time τ . So let us assume that the variables x_* and y_* are equal to zero; according to the u component, we find that

$$\mathbf{f}(t) = \mathbf{u}(0, 0, t). \quad (3.71)$$

The diagram of the function (3.71) is shown in Figure 3.11. Consequently, the periodic time τ is equal to 22.05. By using the equation (3.69), the approximated wavelength l of the spiral wave of the rigid rotation shown in Figure 2.7 is 13.674.

CHAPTER 3. STABILITY OF THE SPIRAL WAVE, SYMMETRIES AND RESPONSE FUNCTIONS

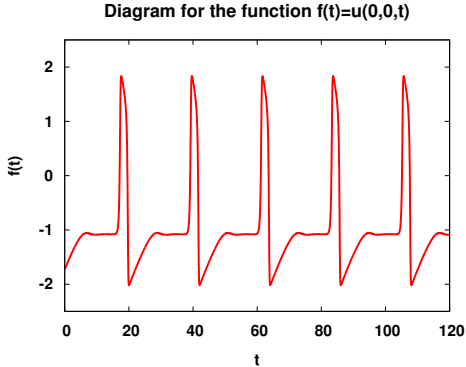


Figure 3.11: The parameters are $\alpha = 0.5$, $\beta = 0.75$ and $\epsilon = 0.3$. The solution of the non-linear system is found by the central difference and the forward Euler methods. This diagram is plotted using the function $\mathbf{f}(t)$ of the equation (3.71). The time step Δt is equal to 0.1 and space steps Δx and Δy are equal to 0.3.

CONTROL OF SPIRAL WAVES USING PROPORTIONAL FEEDBACK CONTROL

As briefly discussed in Chapter 1, the study of spiral waves has implications for sciences in general and medicine in particular. Indeed, the spiral wave pattern can be observed in cardiac muscle tissues [42] and are associated with cardiac arrhythmias. The typical example of this is ventricular fibrillation, where the electrical activity in cardiac arrhythmias indicates the presence of spiral waves. We start with Schlesner et al.'s method [75] where the drift of the spiral wave tip is subjected to proportional feedback control (PFC). This method involves homogeneous perturbations. The problem of using is that most of the cardiac cells will be damaged as elaborated in more detail in Section 4.1. Instead of perturbing the whole domain of the heart, we will consider a localised perturbations in order for the majority of the cardiac muscle cells not to die. Therefore, one motivation for conducting this study is that we hope to overcome this problem using local control action.

4.1 Proportional Feedback Control for the FitzHugh-Nagumo Model

One significant challenge is related to how to control the spiral wave tip for the FHN model, especially if the spiral wave solution of the FHN system (2.1) undergoes a meander or hypermeander. Several methods exist to control the spiral wave tip such as an external periodic force, which is able to remove the spiral wave by a periodic parameter modulation. Moreover, the spiral wave tip can be forced with a frequency larger than its intrinsic frequency [72, 85, 95]. Another method of controlling the spiral tip is Schlesner et al.'s method, namely proportional feedback control. This scheme is based on the tip location of the spiral wave and can be successfully applied to stabilise the motion of the spiral wave around a certain centre point in the domain [75]. The difference between the external periodic force and proportional feedback control is control objectives. In other words, we use a specific method based on our target. Therefore, we will focus on Schlesner et al.'s method because we want to make localised perturbations and control is first step to removal. Moreover, the proportional feedback control method will be investigated using a response function. This method will be discussed in more detail in this chapter. Hence, we study the ideas and tools of the control of the motion of the spiral wave for the FHN model using the control method of Schlesner et al. in this section. The FHN system (2.1) can be investigated in excitable media given by the following equations:

$$u_t = \frac{1}{\epsilon} \left(u - \frac{u^3}{3} - v - \tilde{f}(t) \varphi_*(x, y) \right) + \nabla^2 u, \quad (4.1a)$$

$$v_t = \epsilon(u - \alpha v + \beta), \quad (4.1b)$$

where the function $\tilde{f}(t)$ is a proportional feedback control with a control action $\varphi_*(x, y)$. As [75], we choose

$$\tilde{f}(t) = a_1 \left(r_0(t) - r(t) \right), \quad (4.2)$$

where the constant a_1 is called the *feedback strength* and as in [75] we assume this is small, that is,

$$a_1 \ll 1.$$

Moreover, Schlesner et al. [75] use r as the distance of the spiral wave tip from the desired centre, that is

$$r(t) = \| (x_c, y_c) - (x_{ip}(t), y_{ip}(t)) \|_2, \quad (4.3)$$

while the variable r_0 represents a radius of the circular orbit. The point (x_c, y_c) is the desired centre of the circle of the tip trajectory. The centre can be determined in any place within in the bounded domain. Note that Schlesner et al. only consider the case of the homogeneous control action, that is

$$\varphi_*(x, y) = 1, \quad \forall x, y,$$

while we consider cases where φ_* is localised near the desired centre of the spiral wave (see Subsections 4.7.1, 4.7.2 and also in Chapter 5). We aim to find the size of the spatial localisation, which the spiral wave tip can be successfully stabilised in a small perturbation. Proportional feedback control means that the radius r_0 is determined through the following equation (4.4)

$$\frac{dr_0(t)}{dt} = \frac{1}{a_2} (r(t) - r_0(t)), \quad (4.4)$$

where [75]

$$a_2 \gg \tau,$$

such that τ is the periodic rotation of the spiral wave. In contrast to [75], we also find good control when a_2 is much smaller (for more details, see in Section 4.3). Numerically, the controller dynamics (4.4) can be solved using the Euler forward method in order for the radius r_0 to be a good approximation. The reason for using the Euler forward method is that it more efficient as well as the FHN system (2.1) is numerically solved by semi-implicit scheme. Therefore, we observe that

$$\lim_{t \rightarrow \infty} r(t) = r_0, \quad (4.5)$$

which means that the reference point $r(t)$ of the spiral wave tip will be attracted to a core radius r_0 . In other words, when the spiral wave tip is controlled and also stabilised around the centre point (x_c, y_c) , then the function $r(t)$ will be equal to the core radius r_0 (see Figure 4.3). This leads us to have the stabilised regime. The homogeneous control of Schlesner et al. can be formulated as follows:

$$\mathbf{u}_t = \mathbf{f}(\mathbf{u}) + \mathbf{D}\nabla^2\mathbf{u} + \mathbf{h}(t), \quad (4.6)$$

where

$$\mathbf{h}(t) = \begin{bmatrix} -\frac{1}{\epsilon}\tilde{f}(t) \\ 0 \end{bmatrix}.$$

The term $\mathbf{h}(t)$ is called the *perturbation*. In the next section, we will discuss how Schlesner et al. controlled the spiral tip for the FHN equation by adding a perturbation part $\mathbf{h}(t)$.

4.2 Examples of Spiral Wave Behaviour under Proportional Feedback Control

Schlesinger et al. successfully controlled the behaviour of the spiral wave for the periodic, meander and hypermeander regimes [75]. They assumed that a_2 is equal to 200 in order to control the spiral wave tip and also stabilise the spiral wave movement of the tip trajectory around the centre point (x_c, y_c) . With regards to control parameters x_c and y_c , we can assume these values x_c and y_c such that the spiral wave tip moves around the core centre (x_c, y_c) . Moreover, the drift of the spiral wave also moves along a circle as shown in Figure 2.3. This leads us to say that we have successful control. According to the spiral core as shown in Figure 2.3, we can find the centre point (x_c, y_c) numerically. In order for the core center (x_c, y_c) of the spiral wave to be found numerically, we need to find the values of the functions $x_{tip}(t)$ and $y_{tip}(t)$. According to the spiral wave tip as shown in Figure 2.3, by removing the initial transient of the spiral wave, we find that the functions $x_{tip}(t)$ and $y_{tip}(t)$ are bounded between the biggest and smallest values as shown in Figure 4.1. Therefore, the centre (x_c, y_c) of the spiral wave core can generally be found as follows:

4.2. EXAMPLES OF SPIRAL WAVE BEHAVIOUR UNDER PROPORTIONAL FEEDBACK CONTROL

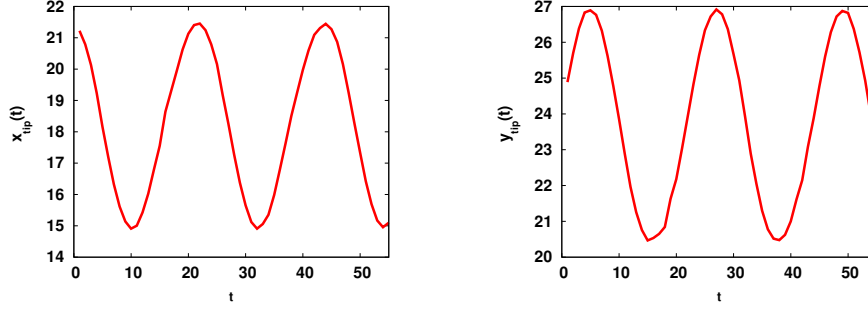


Figure 4.1: Numerical tip trajectory for functions $x_{tip}(t)$ and $y_{tip}(t)$ with parameters $\alpha = 0.5$, $\beta = 0.75$ and $\epsilon = 0.3$.

$$x_c = \frac{\max_{0 \leq t \leq t_1} (x_{tip}(t)) + \min_{0 \leq t \leq t_1} (x_{tip}(t))}{2},$$

$$y_c = \frac{\max_{0 \leq t \leq t_1} (y_{tip}(t)) + \min_{0 \leq t \leq t_1} (y_{tip}(t))}{2}, \quad t_1 \in \mathbb{R}^+.$$

As illustrated by Figure 4.1, the centre point (x_c, y_c) is found as follows:

$$x_c = \frac{\max_{0 \leq t \leq 55} (x_{tip}(t)) + \min_{0 \leq t \leq 55} (x_{tip}(t))}{2} = \frac{22.6653 + 13.8710}{2} = 18.2682, \quad (4.7a)$$

$$y_c = \frac{\max_{0 \leq t \leq 55} (y_{tip}(t)) + \min_{0 \leq t \leq 55} (y_{tip}(t))}{2} = \frac{28.1384 + 19.3466}{2} = 23.7425. \quad (4.7b)$$

With respect to the desired radius r_0 of the spiral core, as shown in Figure 2.3, we can determine the core radius r_0 numerically using the 1D controller dynamics of the equation (4.4) with a given initial guess. The easiest method to calculate the core radius r_0 is by using the formula (4.8):

$$r_0 = \sqrt{(x_{tip} - x_c)^2 + (y_{tip} - y_c)^2}, \quad (4.8)$$

so the desired radius of the circular orbit is as follows:

$$r_0 = 4.3950.$$

Now, we proceed to control the spiral wave solution of the FHN system (4.6) showing how we successfully controlled the behaviour of the spiral wave, as conducted by Schlesinger et al.. Therefore, by using fixed values of the control parameters $\alpha_1 = 0.01$ and $\alpha_2 = 200$ which are given by Schlesinger et al. [75], and by using the fixed centre point (x_c, y_c) as explained by equations (4.7a) and (4.7b) and using the model parameters $\epsilon = 0.25$, $\beta = 0.85$ in the periodic regime, the

CHAPTER 4. CONTROL OF SPIRAL WAVES USING PROPORTIONAL FEEDBACK CONTROL

drift of the spiral wave becomes a rigid rotation around a chosen spiral core centre, as shown in the panel (a) of Figure 4.2. We observe that if the desired centre point (x_{c_*}, y_{c_*}) such that

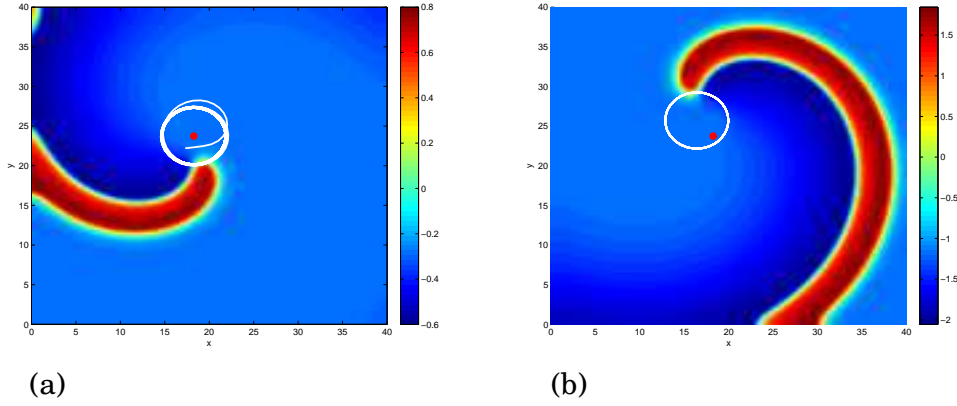


Figure 4.2: The panel (a) indicates successful control of the behaviour of a subjected spiral wave using the control method through the function $\tilde{f}(t)$, such that variables a_1 and a_2 are assumed as 0.01 and 200 respectively with the parameters $\beta = 0.85$ and $\epsilon = 0.25$ for the FHN. The initial guess for r_0 is 4.3950 with the centre core of the rotating spiral wave $(x_c, y_c) = (18.2682, 23.7425)$. The isoconcentration lines (isolines) for u and v components are equal to zero. The snapshot of the spiral wave is 3500 moment of time while the time step Δt is 0.1. Moreover, the space steps Δx and Δy are 0.3. The panel (b) indicates the behaviour of the spiral wave without proportional feedback control using the same model parameters.

$x_{c_*}, y_{c_*} \in \mathbb{R}^+$ is near tip trajectory as shown by a red point in Figure 4.2, then the spiral tip easily becomes attracted to a circular orbit of radius r_0 centred at point $(18.2682, 23.7425)$. This means that the proportional feedback control $\tilde{f}(t)$ can force the drift of the spiral wave tip to move towards the centre and also rotate stably. This example is called *local control*. As illustrated by Figure 4.2, the tip path of the spiral wave does not move in a non-stationary rotation. The drift of the spiral wave tip rotates regularly and the pattern of the tip trajectory becomes a rigid rotation. Therefore, the proportional feedback control $\tilde{f}(t)$ goes to zero at a specific moment in time and the values of functions $r_0(t)$ and $r(t)$ are equal to each other as shown in Figure 4.3. In other words, the control force $\tilde{f}(t)$ vanishes as shown in Figure 4.3. This is because the function $r(t)$ will be equal to the desired core radius r_0 . Hence, this satisfies the formula (4.5) through observing between the panels (a) and (b) of Figure 4.3. The initial transient of the spiral wave, as shown in Figure 4.2, is not removed and the drift of the tip trajectory moves to the left of the y

4.2. EXAMPLES OF SPIRAL WAVE BEHAVIOUR UNDER PROPORTIONAL FEEDBACK CONTROL

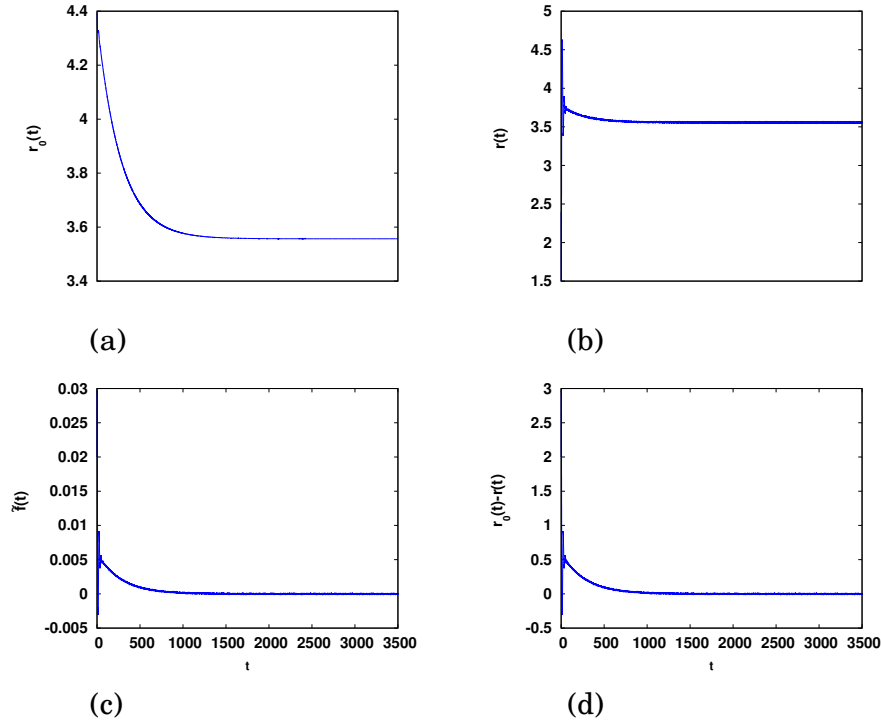


Figure 4.3: Numerical values for functions $r_0(t)$, $r(t)$ and $\tilde{f}(t)$ with parameters $\alpha = 0.5$, $\beta = 0.85$ and $\epsilon = 0.25$. The initial guess for r_0 is 4.3950 with parameters $a_1 = 0.01$, $a_2 = 200$ and $(x_c, y_c) = (18.2682, 23.7425)$. Moreover, the numerical method for the ordinary differential equation (4.4) is the forward Euler method such that the time step Δt is 0.1.

axis because the Cartesian coordinates of the centre circle are $(18.1817, 23.6923)$. If we change the position of the centre (x_{c_*}, y_{c_*}) of the spiral wave location or start plotting the spiral wave tip from the end of the initial transient, then the initial transient of the tip path will not appear and the behaviour of the spiral wave will immediately become a rigid rotation. We have to be aware that the centre core (x_c, y_c) of spiral wave converges to the target location (x_{c_*}, y_{c_*}) if the spiral wave tip is controlled successfully rounded the centre core. If the drift of the spiral wave is not stabilised round centre point (x_c, y_c) as periodic orbit, then the target and centre points will be totally different. Let us suppose that the centre core (x_c, y_c) is $(30, 15)$, so the drift of the tip of the spiral wave moves into the centre in a rigid rotation, as shown in Figure 4.4. We observe that the initial transient in Figure 4.2 is smaller than tip trajectory of initial transient as Figure 4.4 because the location of the centre (x_{c_*}, y_{c_*}) is far from the pattern of the spiral wave. Since, the behaviour of the spiral wave is suppressed, consequently this example is termed *global*

CHAPTER 4. CONTROL OF SPIRAL WAVES USING PROPORTIONAL FEEDBACK CONTROL

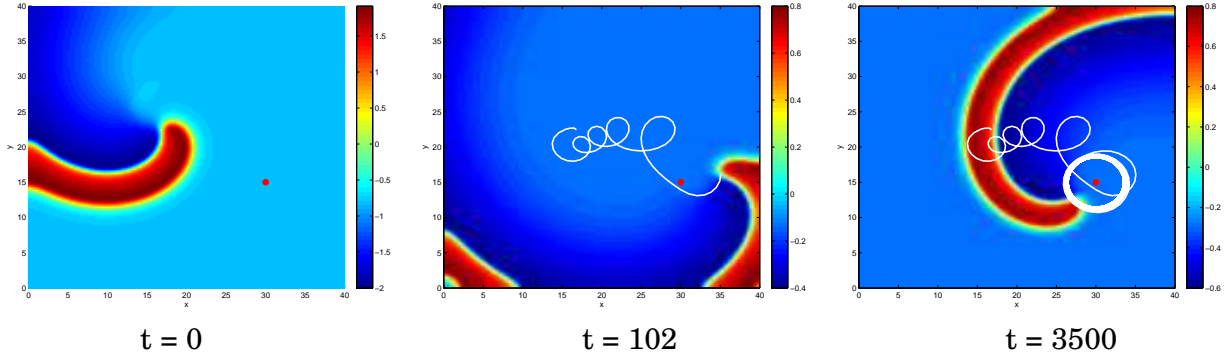


Figure 4.4: Numerical solution of FHN model with parameters $\alpha = 0.5$, $\beta = 0.85$ and $\epsilon = 0.25$ showing the successful transition of the rigid rotation to the centre $(x_c, y_c) = (30, 15)$ indicated by the red point. The initial guess for r_0 is 4.3950 with parameters $a_1 = 0.01, a_2 = 200$. The time step Δt is 0.1 while the space steps Δx and Δy are 0.3.

control. However, the above is an example of a successful control of the rigid rotation, so we now focus on the meander regime. If we have the following parameters:

$$\epsilon = 0.292, \beta = 0.8,$$

then the behaviour of the spiral wave is a meander, as shown in Figure 4.5. Moreover, we observe

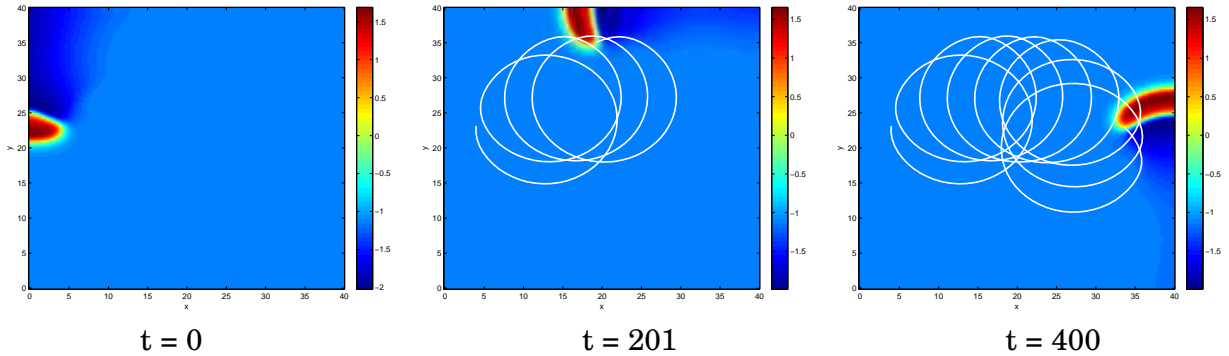


Figure 4.5: Numerical solution of the FHN system with parameters $\alpha = 0.5$, $\beta = 0.8$ and $\epsilon = 0.292$ showing the meander of the spiral wave. The time step Δt is equal to 0.1 while the space steps Δx and Δy are equal to 0.3.

that the drift of the spiral wave solution rotates as a meander around the bounded square. If we extend the time of the rotating spiral wave, then the drift of the spiral wave tip also moves around the bounded domain. As illustrated by Figure 4.5, we can control the tip path of the spiral wave meander using the proportional feedback control $\tilde{f}(t)$. Therefore, the spiral wave

tip trajectory in a meander regime is stabilised to a rigid rotation, as demonstrated in Figure 4.6. The the proportional feedback control $\tilde{f}(t)$ is not always successful to stabilise rigid rotation

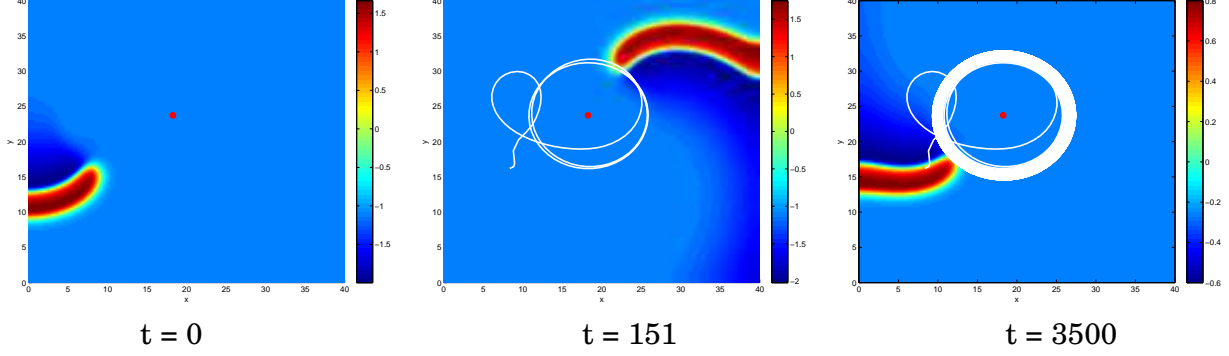


Figure 4.6: Numerical solution of the FHN system with parameters $\alpha = 0.5$, $\beta = 0.8$ and $\epsilon = 0.292$ showing the transition from the meander to rigid rotation. The drift of the spiral wave tip moves towards the centre $(x_c, y_c) = (18.2682, 23.7425)$ successfully. The initial guess for r_0 is 4.3950 with parameters $a_1 = 0.01$, $a_2 = 200$. The time step Δt is equal to 0.1 while the space steps Δx and Δy are equal to 0.3.

in the periodic or meandering regimes. Therefore, we will also discuss the list factors of main influences on controlling the spiral wave tip in Section 4.6. Concerning the control parameters a_1 and a_2 , Schlesner et al. provide the condition for the values of these parameters. They claim that the parameter a_2 should be much larger than the periodic time τ as mentioned in Section 4.1. Thus, the next section investigates the bounded region of the values a_1 and a_2 through numerical simulation.

4.3 Control Parameter Regions for Successful

Control

Following the above successful control of the spiral behaviour, we will now investigate the parameters a_1 and a_2 when the desired radius r_0 and the model parameters of the FHN system are fixed. By varying the control parameters a_1 and a_2 , we can do successful control of spiral wave tip in some range. For instance, if we assume a small parameter such as a_2 , that is

$$a_2 < \tau,$$

such that τ is the periodic rotation of the spiral wave, then we can also manage to control the behaviour of the spiral wave, but we will use Schlesinger et al's assumption for a_2 . We need to pay enough attention to the choice of the level of the isolines for component u -the field and component v -the field in order to extract the spiral tip using a method which is similar to the one explained in Section 2.4. Schlesinger et al. chose values of the isolines as $u_{iso} = 0.2$ and $v_{iso} = -0.12$ [75]. Therefore, these isolines for the components u and v do not help to find the tip path of the spiral wave through numerical observations. This is because of selecting the parameters a_1 and a_2 of the proportional feedback control impact the values of isolines. The best level of the isolines for the components u and v is zero in a periodic regime, which will also work successfully in meander and hypermeander regimes. However, in the perturbed system (4.1) of the FHN model, we will numerically estimate the region of control parameters a_1 and a_2 using the function $\tilde{f}(t)$ in the regime of the rigid rotation, so that the spiral wave tip moves in a stable rotation. By numerical observation, different values a_1 and a_2 can be determined in a bounded domain and used for the proportional feedback control, so that the rigid rotation of the spiral wave solution is a stable movement. Therefore, the bounded region of these parameters for the fixed centre point $(x_c, y_c) = (30, 15)$ and the core radius $r_0 = 4.3950$ with fixed model parameters are restricted between specified limits, as shown in Figure 4.7. Note that the region of the values a_1 and a_2 in the periodic regime is found through using stable spiral wave. By looking at Figure 4.7, choosing values of control parameters a_1 and a_2 have effects on the characteristics of existing spiral waves or controlling spiral wave tip. We consider in a small domain for specific control parameters a_1 and a_2 as shown following:

$$a_1 \in A_1 = \{\beta_1 : \beta_1 = e^{\omega_1}, \omega_1 = -5 + 0.1 \times (n - 1), 1 \leq n \leq 51, n \in \mathbb{N}\},$$

$$a_2 \in A_2 = \{\beta_2 : \beta_2 = 2.1 + 2 \times (n - 1), 1 \leq n \leq 100, n \in \mathbb{N}\},$$

where

$$\ln a_1 \in A_3 = \{\omega_1 : \omega_1 = \ln \beta_1, \beta_1 \in A_1\}$$

This shows that fixed model parameters β and ϵ are example in the periodic regime, that is

$$\beta = 0.75, \quad \epsilon = 0.3.$$

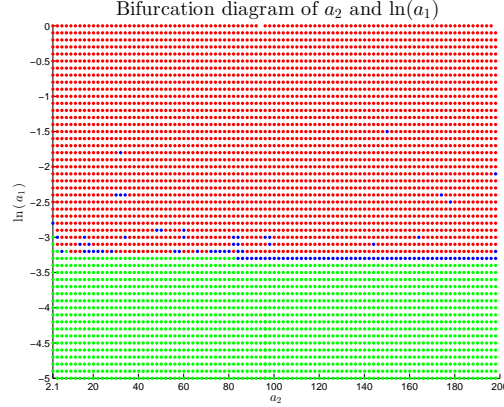


Figure 4.7: The red, green and blue points of the varying control parameters a_1 and a_2 are found by using the perturbed system (4.6) of the FHN model with fixed model parameters $\beta = 0.75$ and $\epsilon = 0.3$. The red points indicate unstable spiral wave, whereas the green points indicate existing spiral waves which can be controlled successfully such that a tolerance Tol is equal to 0.5. The blue points indicate existing spiral waves which cannot be controlled successfully. The initial condition for the perturbed system (4.6) are the spiral waves for fixed bounded domain $[0, 40]^2$ which are taken from Figure 2.2. The space steps Δx and Δy are equal to 0.3 while the time step Δt is equal to 0.1 for time period $t \in [0, 1500]$. Moreover, the initial guess for r_0 is 4.3950 with the fixed target core of the rotating spiral wave $(x_c, y_c) = (30, 15)$.

It is worth noting here that if we change the centre of the spiral wave core or the parameters β and ϵ of FHN system, the bounded region of green points of control parameters a_1 and a_2 for specific parameters in the periodic regime will have a different shape. By choosing any values for a_1 and a_2 in the bounded region of green points, the proportional feedback control function $\tilde{f}(t)$ shows that the tip trajectory is stabilised, which means that we can control the motion of the spiral wave. By numerical observation we note that if we extend the a_2 axis, as shown in Figure 4.7, then the bounded region of green points shrinks. Also, if we choose any values for a_1 and a_2 outside this domain, the rigid rotation will not be stabilised or the spiral wave solutions of the FHN model will disappear with boundary domain. Therefore, the tip path cannot be found because the isolines for the two components u and v of FHN model are equal to zero. By numerical observation, we also note that if the parameters a_1 and a_2 are very close to the frame of axes, we need more time in order for the rigid rotation of the spiral wave to be stabilised. Compared with points (a_1, a_2) in the middle of the green bounded region, the tip path of the rotating spiral wave solutions is stabilised quickly. Note that we cannot sometimes control the

behaviour of the tip path of the spiral wave easily for some parameters in a rigid rotation regime as we will give an example of unsuccessful control in Section 4.6.

Now, it is important to study the bounded region of the control parameters a_1 and a_2 for specific model parameters in the meander regime through fixing the parameters $\epsilon, \beta, \alpha, r_0$ and the centre core (x_c, y_c) . Therefore, if we choose the parameters ϵ and β as follows:

$$\epsilon = 0.292, \beta = 0.8,$$

where these parameters are in the meander regime and the drift of the spiral wave tip rotates rigidly with these parameters through using the function $\tilde{f}(t)$ as shown in Figure 4.6. We also consider in a small domain for specific control parameters a_1 and a_2 as shown following:

$$a_1 \in \mathbf{A}_1, \quad a_2 \in \mathbf{A}_2,$$

then diagram of parameters a_1 and a_2 is shown in Figure 4.8. The region of the values a_1 and

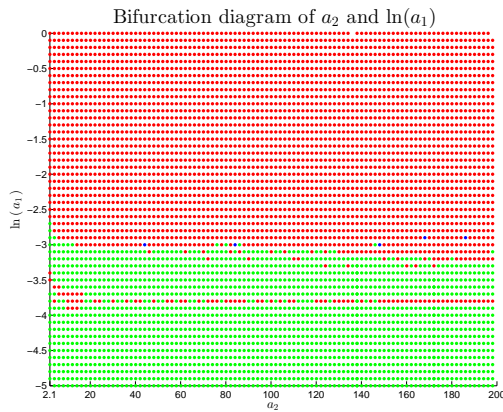


Figure 4.8: The red, green and blue points of the varying control parameters a_1 and a_2 are found by using the perturbed system (4.6) of the FHN model with fixed model parameters $\beta = 0.8$ and $\epsilon = 0.292$. The red points indicate unstable spiral wave, whereas the green points indicate existing spiral waves which can be controlled successfully such that a tolerance Tol is equal to 0.5. The blue points point out existing spiral waves which cannot be controlled successfully. The initial condition for the perturbed system (4.6) are the spiral waves for fixed bounded domain $[0, 40]^2$. The space steps Δx and Δy are equal to 0.3 while the time step Δt is equal to 0.1 for time period $t \in [0, 1500]$. Moreover, the initial guess for r_0 is 4.3950 with the fixed target core of the rotating spiral wave $(x_c, y_c) = (18, 24)$.

a_2 in the meander regime is found through using stable spiral wave as shown in Figure 4.5. By

numerical observations, if the value a_1 is big enough, then the drift of the tip trajectory of the spiral wave will be controlled quickly into the centre. In other words, if the parameter a_1 is very small and if the parameter a_2 is very large, then the spiral wave tip will be controlled very slowly. Through numerical observation, we observe that if we extend the a_2 axis, as shown in Figure 4.8, then the top line of the green bounded region will go down. However, we have to be aware that if we change any parameters ϵ and β of the FHN system and also the position of the target core (x_{c_*}, y_{c_*}) , or the core radius r_0 , then the shape of the bounded domain of the parameters a_1 and a_2 for the the meander regime will be also different. By looking at the Figure 4.8, there is a line of extra red points, which show unstable spiral wave, in the region of green points because the total length of axes x and y is not big enough. Therefore, if we increase the size of the bounded domain and also time period or if we change the position of the target core, then the line of extra red points will become green points. This is because the spiral wave will be stable as shown in the panel (a) of Figure 4.9, so this leads us to control the spiral wave tip.

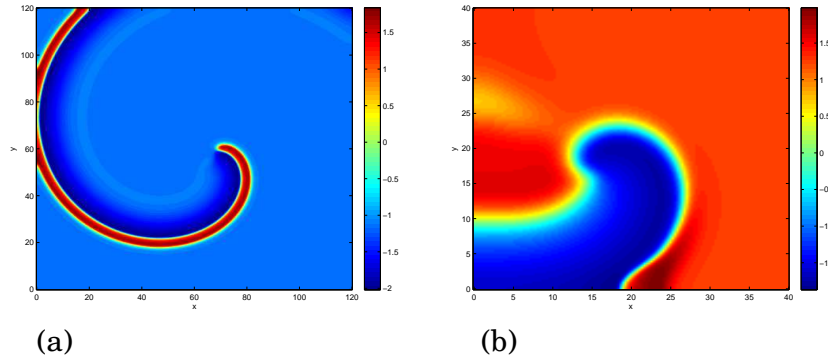


Figure 4.9: Diagram shows numerical simulations for same values of parameter and different domain sizes in panels (a) and (b). The case (a) shows that the numerical simulation converges to stable spiral wave solution such that the total length of x and y is equal to 120. The case (b) shows the transient of spiral wave and no stable spiral wave solution starting from the initial condition such that the total length of x and y is equal to 40. The parameters of the FHN system with controller model are $\alpha = 0.5$, $\beta = 0.80$ and $\epsilon = 0.292$. The control parameters are chosen as $a_1 = 0.0224$, $a_2 = 40.1$ such that $\ln(a_1) = -3.8$. Moreover, the centre core (x_c, y_c) is equal to $(60, 60)$. With regard to the case (b), the centre core (x_c, y_c) is equal to $(18, 24)$.

With respect to this section, we have found the range of the control parameters, which shows a successful control. In other words, we have discussed the properties of the perturbation function

for the perturbed system of the FHN model, which is related to the machine of heart defibrillator. We need to determine the region of successful and unsuccessful control for model parameters ϵ and β for the FHN system. These parameters are related to the properties of the heart. Therefore, we will discuss criteria of successful and unsuccessful control of the spiral wave tip in the next section.

4.4 Criteria for Successful Control

However, as highlighted in Figure 2.10, we will investigate the successful and unsuccessful control behaviour of the spiral wave for parameter space (ϵ, β) related to local and global control. This means that if the tip path of the spiral wave starts to become close to the desired location (the target location or the centre point of the circular orbit) and if we can successfully govern the behaviour of the spiral wave using proportional feedback control method, then this is called local control as discussed briefly in Section 4.2. Moreover, we state that the control is global if any initial condition is not close to the target location. The difference between local and global control is just the initial condition. In order to investigate the successful and unsuccessful control of the tip trajectory, we need to formulate systematic criteria to automate the parameter space study. Thus, we say that the spiral wave is successfully controlled if

$$|r(t) - r_0(t)| \leq \text{Tol},$$

for the appropriate set of time t . Figure 4.4 is an example of successful control. Also, we can see that the formula $-0.1 \leq r_0(t) - r(t) \leq 0.1$ is realised for this time interval according to the panel (d) of Figure 4.3. In contrast, if we have the following formula:

$$r_0(t) - r(t) > 0.1,$$

then we say unsuccessful control where over this range of time. Therefore, we can choose a tolerance Tol equal to 0.1 with the time test window T_{test} equal to 20. In order to determine whether the control method of the tip path is successful, we need to consider a time $T > 0$ such

that $T > T_{\text{test}}$ and also a maximum time $T_{\text{max}} > 0$. By looking at Figures 4.3, we assume that

$$T_{\text{max}} = 2000.$$

We can say that the control of the spiral wave tip is successful if there is a $T < T_{\text{max}}$ such that inequality holds for all t from $T - T_{\text{test}}$ to T and is also less than or equal to the tolerance Tol, that is

$$|r(t) - r_0(t)| \leq 0.1, \quad \forall t \in [T - T_{\text{test}}, T]. \quad (4.9)$$

Moreover, the control of the tip trajectory is unsuccessful if the converse inequality holds for some t from $T - T_{\text{test}}$ to T and is also greater than the tolerance Tol, that is

$$|r(t) - r_0(t)| > 0.1, \quad \exists t \in [T - T_{\text{test}}, T]. \quad (4.10)$$

Since we have two cases of controlled spiral wave tips, successful and unsuccessful control should be recognised for both situations more precisely. The first case is that if the target core (x_{c_*}, y_{c_*}) is close enough to the pattern of the initial spiral wave (local control), then we can say that the control method is successful if the condition (4.9) is achieved for the test window. Since the initial condition for the successful and unsuccessful control is shown in Figure 2.2 for component u , we can suppose that the centre core (x_c, y_c) is equal to $(19.5, 18)$. However, if we assume that

$$T = 1800,$$

and that the condition (4.9) satisfies for all the time test window T_{test} , then we can control the spiral wave tip successfully. If we have the condition (4.10) in the time test window T_{test} , then we can say that the control method is unsuccessful.

With regard to the second case, that is, if the the desired location (x_{c_*}, y_{c_*}) is away from the pattern of the initial spiral wave (global control), we can say that the control method is successful if the condition (4.9) is achieved. The initial condition for the global control is also shown in the panel (c) of Figure 4.10 for component u . So, the centre core (x_c, y_c) is supposed to be $(19.5, 18)$ such that $T = 1800$ and also the value of the test window T_{test} in this situation is also equal to 20 units. In contrast, if we have the formula (4.10), then the proportional feedback control $\tilde{f}(t)$ will not control the motion of the spiral tip.

It is worth bearing in mind the total length for both x and y in order to find the spiral wave because if the total length for both x and y is not large enough, then the spiral wave for parameters ϵ and β will crash and also disappear with the bounded domain and the tip trajectory, as a result, will not be found. In the next section, we will discuss the region of model parameters ϵ and β for the FHN system using criteria of the studying successful and unsuccessful control of the tip trajectory.

4.5 Region of Successful Control for Model

Parameters

As we discussed criteria of successful and unsuccessful control of the spiral wave tip in Section 4.4, we can write an automatic Matlab code to find the (ϵ, β) -parameter space in terms of successful and unsuccessful control. Let us begin with the global and local control for the bounded domain $[0, 40]^2$. By numerical observation, we find the successful control for the whole parameters ϵ and β , as shown in Figure 4.10. We have found the bounded regions for the local and global control using the initial condition, as shown in the panels (c) and (g) of Figure (4.10). According to the global control, the spiral wave solution is not controlled easily even the bounded domain is bigger because the centre point (x_c, y_c) is not close to spiral wave. By looking at local successful control method, we will have more points of local successful control as the reason was previously explained.

However, we note that we study the spiral wave tip by using the proportional feedback control $\tilde{f}(t)$. Thus, this function does not depend on the spatial localisation in $x-y$ plane, so we will define the function $\tilde{f}(t)$ as depending on two variables x and y through using target location (x_{c_*}, y_{c_*}) or (x_{tip}, y_{tip}) as discussed in more detail in Subsections 4.7.1, 4.7.2 and Chapter 5. This is because we want to know that how large enough of the spatial localisation for the function $\tilde{f}(t)$ that controls spiral wave tip. In the next section, we will discuss that the proportional feedback control $\tilde{f}(t)$ does not control the spiral wave dynamics for some parameters ϵ and β because there are the main influences which affect stabilising the spiral tip. Therefore, more detail will

4.6. EXAMPLES OF UNSUCCESSFUL CONTROL OF THE SPIRAL WAVE BEHAVIOUR

be shown in Section 4.6.

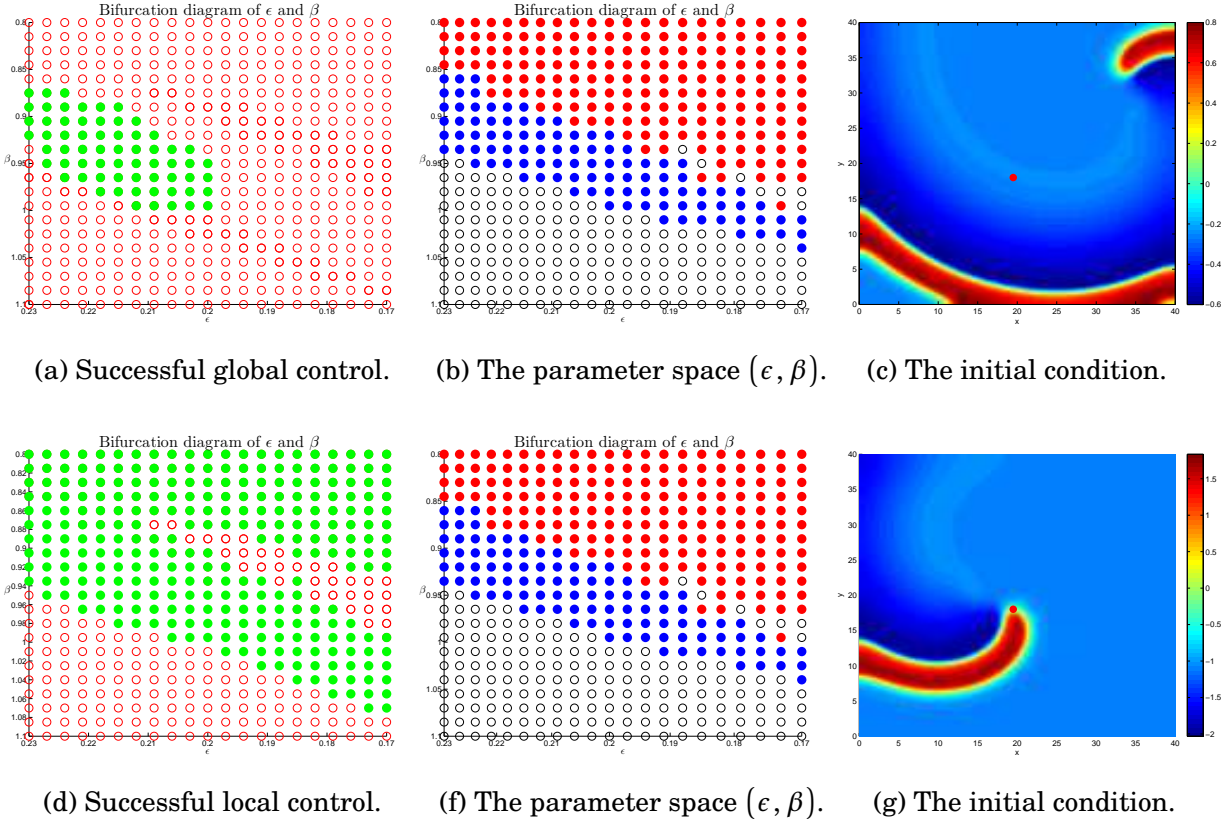


Figure 4.10: The panels (a) and (d) point out the successful control region using the proportional feedback control for space scale 40×40 such that the filled green points indicate the successful control whereas the open red points indicate the unsuccessful control. The panels (b) and (f) indicate regions of the periodic and meander regimes without using the proportional feedback control such that the filled blue points show the rigid rotation of the spiral wave whereas the filled red points show meander of the spiral wave. The open black points in the panels (b) and (f) point out no spiral wave. The centre point (x_c, y_c) for both cases as shown in the panels (c) and (g) is $(19.5, 18)$ with the values $a_1 = 0.01$ and $a_2 = 0.25$. The tolerance Tol is equal to 0.2 and the time test window T_{test} is equal to 20.

4.6 Examples of Unsuccessful Control of the Spiral Wave Behaviour

It is possible to control the behaviour of the spiral wave through adding the perturbation term in FHN system. If we choose certain parameters for the function $\tilde{f}(t)$ and the position of the

CHAPTER 4. CONTROL OF SPIRAL WAVES USING PROPORTIONAL FEEDBACK CONTROL

centre of the circular core, the proportional feedback control will overcome the motion of the spiral wave in meander or periodic regimes and become a stable rigid rotation. However, the control of the behaviour of the spiral wave solution is not always successful. There are different types of unsuccessful control. The first type is that the spiral wave tip sometimes moves towards the centre and does not rotate stably. This case can be controlled but in a weak way. The second type is that the spiral wave tip does move towards the centre. The third type is that if the spiral tip rotate very close the boundary, then it may cross the boundary domain which is the worst case. This is because there are many factors which influence the drift of the spiral tip. The first factor is certain parametric system (model parameters) of FHN model. For example, if we start with model parameters ϵ and β for the meander regime as follows:

$$\epsilon = 0.2, \beta = 0.85,$$

then the proportional feedback control $\tilde{f}(t)$ will not suppress the motion of tip and stabilise the periodic orbit, as shown in Figure 4.11. As explained by Figure 4.11, the average of location of

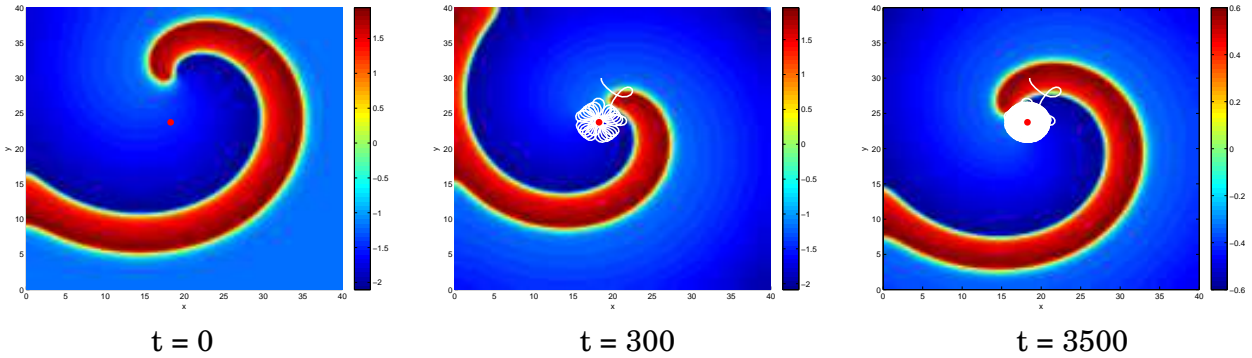


Figure 4.11: A snapshot of unsuccessful control of the tip path of the spiral wave behaviour for component u such that parameters ϵ and β are 0.2 and 0.85 respectively with time step Δt equal to 0.1 and space steps Δx and Δy equal to 0.3 for the scale space 40. The initial guess for r_0 is 4.3950 with parameters $a_1 = 0.01$, $a_2 = 200$ and $(x_c, y_c) = (18.2682, 23.7425)$. The behaviour of the spiral wave in the meander regime is not a stable rigid rotation and the drift of the spiral tip moves to the centre, but the spiral wave tip does not rotate rigidly.

spiral wave tip is going around centre target and does not rotate stably. We also observe that the diagram of the functions $r_0(t)$ and $r(t)$ are shown in Figure 4.12.

4.6. EXAMPLES OF UNSUCCESSFUL CONTROL OF THE SPIRAL WAVE BEHAVIOUR

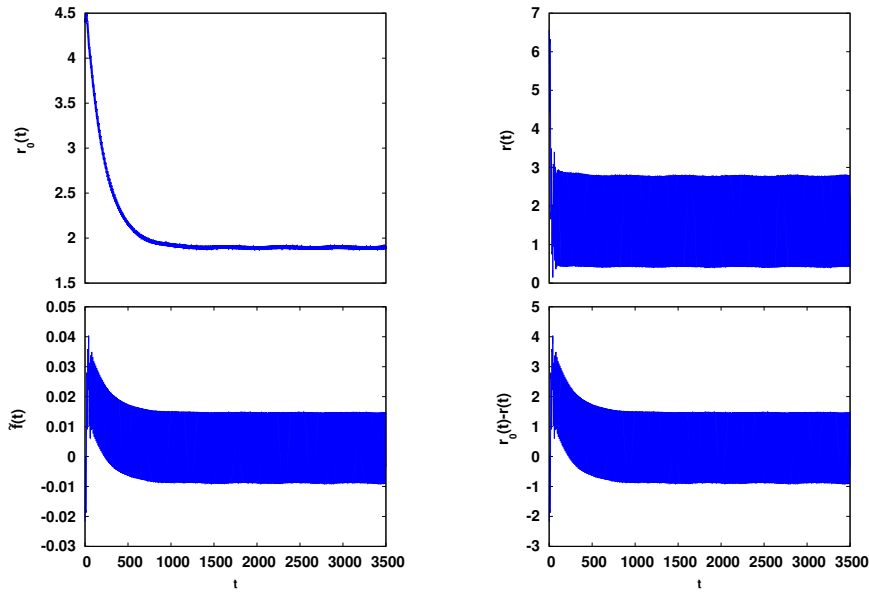


Figure 4.12: Numerical values for functions $r_0(t)$, $r(t)$ and $\tilde{f}(t)$ with parameters $\alpha = 0.5$, $\beta = 0.85$ and $\epsilon = 0.2$. The initial guess for r_0 is 4.3950 with parameters $a_1 = 0.01$, $a_2 = 200$ and $(x_c, y_c) = (18.2682, 23.7425)$. Moreover, the numerical method used for the ordinary differential equation (4.4) is the forward Euler method with the time step Δt equal to 0.1.

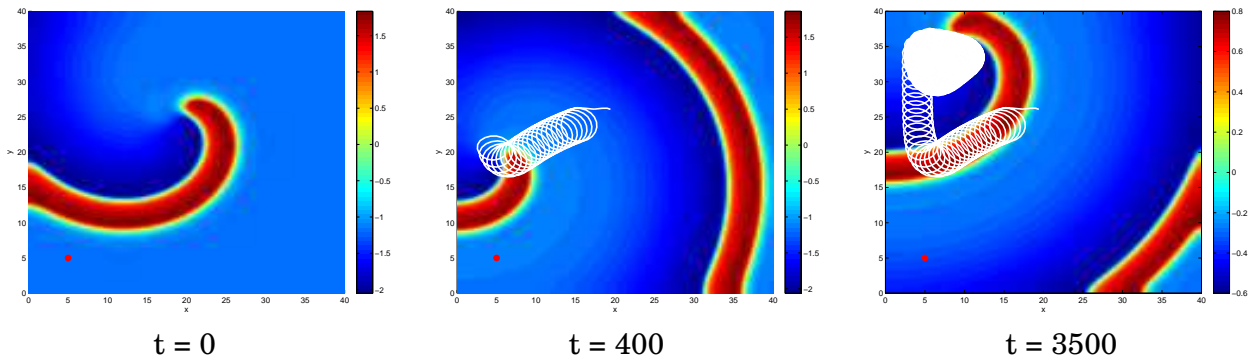


Figure 4.13: A snapshot of the unsuccessful control of the tip path of the spiral wave behaviour for component u such that parameters ϵ and β are 0.25 and 0.8288 respectively with the time step Δt equal to 0.1 and space steps Δx and Δy equal to 0.3 for the scale space 40. The initial guess for r_0 is 4.3950 with parameters $a_1 = 0.01$, $a_2 = 0.5$ and $(x_c, y_c) = (5, 5)$. The behaviour of the spiral wave in the periodic regime is not a stable rigid rotation around the centre core.

We note that we cannot move the spiral wave tip into the desired point $(18.2682, 23.7425)$ or control the motion of the spiral wave as a stationary rotation. This is because the initial condition for the spiral wave solutions, especially for this pattern, does not help the proportional feedback

control $\tilde{f}(t)$ to control the tip motion even though we chose the good value of feedback strength a_1 and the good value of parameters a_2 . These cases will affect the control of the spiral motion using the proportional feedback control. Using the parameters highlighted in Figure 4.11, Figure 4.12 representing functions $r_0(t)$, $r(t)$ and $\tilde{f}(t)$ suggests that the tip path, that undergoes the proportional feedback control, cannot be stabilised because the tip trajectory of the spiral wave moves around the neighbourhood of the reference radius function r_0 , in contrast with Figure 4.3 where oscillations cannot be observed. If we do not pay enough attention to the choice of the centre of rotation of the spiral wave, then the the proportional feedback control does not perform a periodic motion. We provide an additional example of unsuccessful stabilisation for this case. If we choose the centre core as follows:

$$(x_c, y_c) = (5, 5),$$

then the stationary rotation of the spiral wave is not stabilised around the target location, as shown in Figure 4.13. In other words, this function cannot be used to displace the spiral core region through moving the drift of the spiral wave tip around the red point as as indicated in Figure 4.13. This is because the desired location is quite far from the spiral tip. With regards to the difficulties of controlling the spiral tip, we find that the size of the bounded domain also affects successful control of spiral tip. The example of effects of the bounded domain is that if we expand the bounded domain, as in Figure 4.5, to $[80, 80]$ instead of $[40, 40]$, then the spiral wave solution of the original system (1.1) for FHN model rotates rigidly instead of a spiral wave meander, as shown Figure 4.14. According to Biktashev et al. [10], the behaviour of the spiral wave will be affected by boundaries. This means that the boundary affects the spiral wave behaviour in different ways; hence, Biktashev and Holden investigated the perturbation of the boundary through computing the response function when the spiral wave solutions are close to the finite domain because the response function is not affected by the boundary domain. Finally, the numerical scheme and step size will also impact the transition from the meandering or hypermeandering spiral wave tip to the rigid rotation using the function $\tilde{f}(t)$.

4.7. PROPORTIONAL FEEDBACK CONTROL WITH LOCALISED CONTROL ACTION

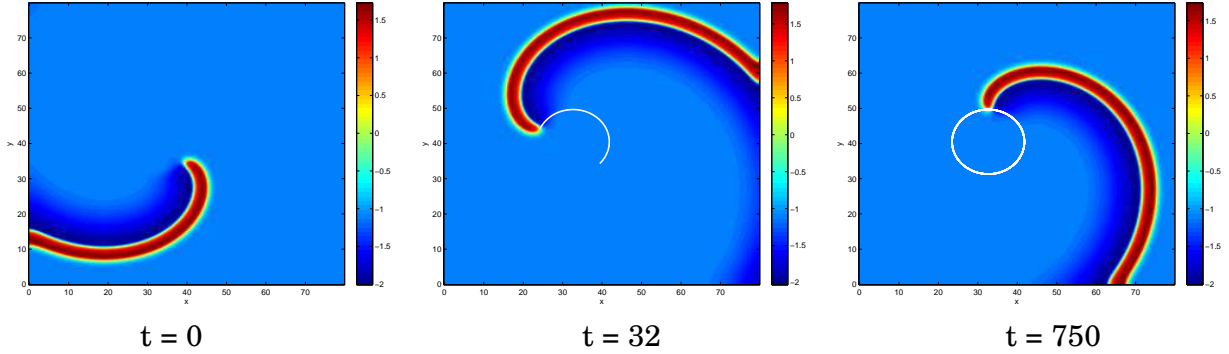


Figure 4.14: Numerical solution of the FHN with parameters $\alpha = 0.5$, $\beta = 0.8$ and $\epsilon = 0.292$ showing the transition from the meander to the rigid rotation without using the proportional feedback control. The time step Δt is equal to 0.1 while the space steps Δx and Δy are equal to 0.3.

Based on this, in the next section, we will also discuss the proportional feedback control $\tilde{f}(t)$ with localised control action $\varphi_*(x, y)$. As explained previously that Schlesinger et al only consider the homogeneous control action in the FHN system, which means that the proportional feedback control function $\tilde{f}(t)$ is homogeneous on x and y .

4.7 Proportional Feedback Control with Localised Control Action

In the previous sections, we discussed Schlesner et al.'s method using proportional feedback control $\tilde{f}(t)$ which does not depend on the spatial variables and only depends on time t . This means that proportional feedback control is able to stabilise the spiral wave tip around a centre point (x_c, y_c) in the excitable medium. Therefore, we may obtain better performance for a small perturbation by assuming localised control action. Now, we consider control of spiral wave using these possible control actions. It makes sense to consider whether a localised control action can also suppress the motion of a spiral wave, that is only supported near the desired centre (x_c, y_c) . Therefore, there exist two possible cases to localise the spiral tip using control action. The first one of these cases is called fixed-localised action and the second case is tip-localised action. By employing these cases of control action for the FHN model, we will study the successful and

unsuccessful control behaviour of the spiral wave for model parameters.

4.7.1 Control Using a Fixed-Localised Control Action

We now investigate the control of the spiral wave through looking at the target location (x_c, y_c) of the bounded domain for the control function $\tilde{f}(t)$ with a function $\varphi_*(x, y)$ that is defined as follows:

$$\varphi_*(x, y) = \begin{cases} 1 & \text{if } |(x, y) - (x_c, y_c)| < r_1 \\ 0 & \text{if otherwise} \end{cases}.$$

The function $\varphi_*(x, y)$ is termed as fixed-localised control action, so the perturbed system (4.6), which Schlesner et al considered the case where depends on time t , becomes as follows:

$$\mathbf{u}_t = \mathbf{f}(\mathbf{u}) + \mathbf{D}\nabla^2\mathbf{u} + \mathbf{h}_1(t, x, y), \quad (4.11)$$

where

$$\mathbf{h}_1(t, x, y) = \begin{bmatrix} -\frac{1}{\epsilon}\tilde{f}(t)\varphi_*(x, y) \\ 0 \end{bmatrix},$$

such that point (x, y) is the spatial location in the plane that supports the control function and r_1 is the radius of the circle. Note that the system (4.11) is general feedback control which depends on the spatial spaces and the time. The value of the constant r_1 should be recognised to show us the control of the spiral wave tip. Thus, the radius r_1 can be assumed as 10. In this case, the tolerance Tol to study the successful and unsuccessful control of the spiral wave tip is given as follows:

$$\text{Tol} = 0.1.$$

Now, we consider what happens if we focus on fixed-localised action, which depends on x and y , instead of the homogenous function. Therefore, we study the successful control method of the tip trajectory of the spiral wave using the fixed support function $\mathbf{h}_1(t, x, y)$, as shown in the panel (a) of Figure 4.15.

4.7. PROPORTIONAL FEEDBACK CONTROL WITH LOCALISED CONTROL ACTION

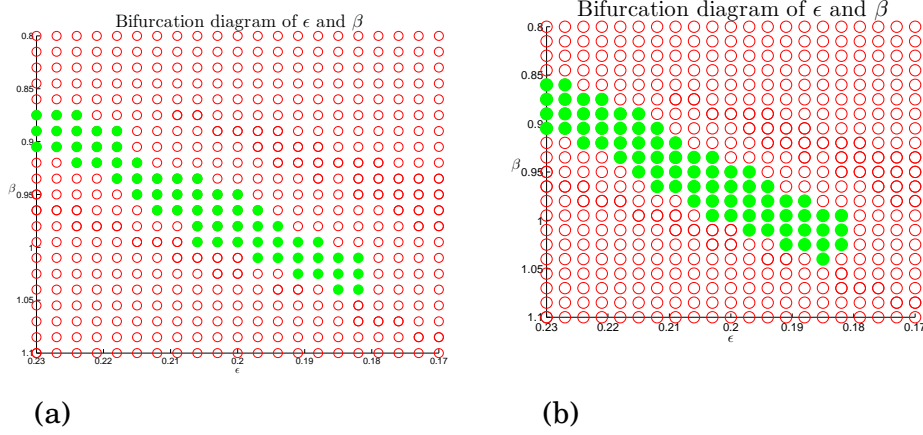


Figure 4.15: The panel (a) points out the successful control region using the fixed-localised control action such that the filled green points indicates the successful control region whereas the open red points indicates the unsuccessful control. The centre core (x_c, y_c) for the fixed-localised control action is $(19.5, 18)$. The panel (b) points out the successful control region using the tip-localised control action such that the filled green points indicate the successful control region whereas the open red points indicate the unsuccessful control. The centre point (x_c, y_c) for the tip-localised control action is $(10, 10)$. The radius r_1 for both cases is equal to 10 and the initial condition for the perturbation system (4.11) is shown in Figure 2.2. The tolerance Tol is equal to 0.2 and the time test window T_{test} is equal to 20. The space scale is 40×40 .

4.7.2 Control Using a Tip-Localised Control Action

An alternative localised control action is to follow the tip path, that is use a control action of the form $\varphi_\circ(x, y, t)$ where we follow the tip location $(x_{tip}(t), y_{tip}(t))$:

$$\varphi_\circ(x, y, t) = \begin{cases} 1 & \text{if } |(x, y) - (x_{tip}(t), y_{tip}(t))| < r_1 \\ 0 & \text{if otherwise} \end{cases}.$$

We call the function $\varphi_\circ(x, y, t)$ is called the tip-localised control action and that depends on (u, v) .

For this, the perturbed system (4.6) becomes as follows:

$$\mathbf{u}_t = \mathbf{f}(\mathbf{u}) + \mathbf{D}\nabla^2 \mathbf{u} + \mathbf{h}_2(x, y, u, v),$$

where

$$\mathbf{h}_2(x, y, u, v) = \begin{bmatrix} -\frac{1}{\epsilon} \tilde{f}(t) \varphi_\circ(x, y, t) \\ 0 \end{bmatrix}.$$

In order for the spiral wave to be controlled for parameters ϵ and β successfully, the radius r_1 should not be smaller than 10. By using the function \mathbf{h}_2 instead of the parametric forcing function and the fixed support function, the successful and unsuccessful controls of the spiral wave tip are investigated for all parameters ϵ and β such that $(x_c, y_c) = (10, 10)$ as shown in the panel (b) of Figure 4.15. The tolerance Tol in this case is given as follows:

$$\text{Tol} = 0.2.$$

We observe that using a control action localised at the tip path $(x_{tip}(t), y_{tip}(t))$ for controlling the behaviour of the spiral wave can be much better than the target location (x_c, y_c) through comparison between the panels (a) and (b) of Figure 4.15.

The proportional feedback control cannot always control the tip motion of the spiral wave. Therefore, it is useful to investigate the FitzHugh-Nagumo equation (4.1) with the 1D controller dynamics (4.4) appended. This allows us to study successful control of the spiral motion through computing the eigenvalues of this extended system. This will be discussed in the Chapter 5.

STABILITY OF SPIRAL WAVES WITH LOCALISED CONTROL ACTION

As we elaborated in Chapter 4, the spiral wave tip can be controlled using the homogeneous function $\tilde{f}(t)$ with different types of control action. This leads us to have the different regions of successful control for (ϵ, β) -parameter space. With regards proportional feedback control, we will investigate how big perturbation of the function $\tilde{f}(t)$, which can suppress the drift of spiral wave tip using the response function of the adjoint linear system for the FHN system with the 1D controller dynamics and also stability of control method as a function of the radius R . Therefore, we can understand the size of the spatial localisation of the support control function.

5.1 Study the Dynamical Stability Spiral Wave

Solution for Different Values of Radius

Let us define the perturbation function $\mathbf{h}(t)$ of equation (4.6) using the local support perturbation function $\mathbf{h}_R(t, x, y)$, that is

$$\mathbf{h}_R(t, x, y) = \begin{bmatrix} -\frac{1}{\epsilon} \tilde{f}(t) \varphi_R(x, y) \\ 0 \end{bmatrix},$$

where the control action $\varphi_R(x, y)$ is defined as follows:

$$\varphi_R(x, y) = \begin{cases} 1 & \text{if } (x - x_c)^2 + (y - y_c)^2 < R^2 \\ 0 & \text{if otherwise} \end{cases},$$

such that R is radius and the point (x_c, y_c) is centre core of spiral wave. Now, we will investigate the dynamical stability solution of the FHN model (4.1) with the controller equation if the values of radius R are different through computing the largest eigenvalues. Let us begin with the unsuccessful control in meander regime from Figure 4.15 to be as follows:

$$\epsilon = 0.20, \quad \beta = 0.93,$$

so the relation between the different values of of radius R and the largest eigenvalues γ is shown in Figure 5.1. Looking at Figure 5.1, we observe that the critical radius, R_c , at which the controlled spiral wave tip is first stabilised is

$$R_c \approx 10.$$

The reason for choosing $R_c \approx 10$ is that the red horizontal line, located at $\lambda = 0$, shows stable and unstable movements of the spiral wave tip due to the stability condition of using power iteration method which has been illustrated in more detail in Section 3.3. This means that if the radius R belongs to the interval $(0, 10)$ approximately, then the local support perturbation function $\mathbf{h}_R(t, x, y)$ of the FHN model (4.1) cannot control the behaviour of the spiral wave tip because the principle eigenvalue γ is greater than one. Therefore, the spiral wave tip of the FHN model

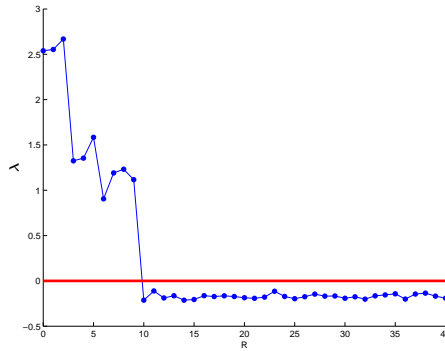


Figure 5.1: The parameters of the FHN system with controller model (4.1) is $\alpha = 0.5$, $\beta = 0.93$ and $\epsilon = 0.20$ such that these parameters ϵ and β are taken from unsuccessful control region as shown in the Figure 4.15. The blue line indicates lyapunov exponent for the largest eigenvalues using formula $\lambda = \frac{\ln|\gamma_{\Delta t}|}{\Delta t}$ such that the time step Δt is equal to 0.1, so the critical radius R_c , at which the controlled spiral wave tip is first located at lyapunov exponent $\lambda = 0$, is equal to 10 approximately. The centre core (x_c, y_c) is equal to (19.5, 18). The parameters of the proportional feedback control \mathbf{h}_R are $a_1 = 0.01$, $a_2 = 200$ such that the initial guess for r_0 is 4.3950 for time period $[0, 2000]$. The total length of the radius R is equal to 40 such that the space step ΔR is equal to 1. The principle eigenvalues are found numerically using power iteration method.

(4.1) can be controlled using the local support perturbation function $\mathbf{h}_R(t, x, y)$ if it satisfies the following formula:

$$R \in (10, 40).$$

This is because the principle eigenvalue γ is less than one.

In the next section, we will discuss how to calculate the average of response functions numerically. Moreover, we will also investigate the size of the spatial localisation of the support of the control action numerically using the average of response functions. In other words, we will find the minimum radius to stabilise the spiral wave tip.

5.2 Computing Response Function in the Small Perturbation

As explained in Chapter 4, the perturbed function $\mathbf{h}(t)$ is defined in the whole bounded domain. Therefore, controlling or removing the spiral wave is an important issue with several implications

and applications, notable in the medical field. Hence, in mathematical terms, the perturbed function $\mathbf{h}(t)$ can be defined in the $x - y$ plane and also depending on time t through calculating the average of the numerical solution of the adjoint linear system and using the *Trapezoidal rule* [26]. This is because the response function of the adjoint linear system gives information about the sensitivity of the spiral wave to a perturbation. Therefore, we suggest that a good strategy for controlling the spiral wave in a more optimal manner is to consider spatially localized perturbations. If we consider the adjoint linear system (3.10) for the FHN equation without the 1D controller dynamics, then the average in Cartesian coordinates is formed as follows:

$$\rho_1(x, y) = \frac{1}{\tau} \int_0^\tau k(x, y, t) dt \approx \frac{1}{\tau} \left(\sum_{m=0}^{(n_1-1)} \frac{\Delta t}{2} \left(k(x_i, y_j, t_m) + k(x_i, y_j, t_{m+1}) \right) \right), \quad (5.1a)$$

$$\rho_2(x, y) = \frac{1}{\tau} \int_0^\tau s(x, y, t) dt \approx \frac{1}{\tau} \left(\sum_{m=0}^{(n_1-1)} \frac{\Delta t}{2} \left(s(x_i, y_j, t_m) + s(x_i, y_j, t_{m+1}) \right) \right), \quad (5.1b)$$

where

$$k(x_i, y_j, t_m) = k_{i,j}^m, \quad s(x_i, y_j, t_m) = s_{i,j}^m, \quad i, j = 0, 1, \dots, n, \quad m = 0, 1, \dots, n_1, n, n_1 \in \mathbb{N}, t \in [0, \tau], \tau \in \mathbb{R}^+,$$

and variables $k(x, y, t)$ and $s(x, y, t)$ are components of the adjoint linear system (3.10). Since, the FHN system (2.1) consists of two components, it is useful to apply the length of the vector $(\rho_1(x, y), \rho_2(x, y))$ of the average solutions of response functions, that is

$$A_R = \sqrt{(\rho_1(x, y))^2 + (\rho_2(x, y))^2},$$

where A_R is the length of the vector $(\rho_1(x, y), \rho_2(x, y))$ and variables $\rho_1(x, y)$ and $\rho_2(x, y)$ are the average solutions of response functions. The reason for computing the length of the vector $(\rho_1(x, y), \rho_2(x, y))$ is that the average solutions of response functions are more accurate. Therefore, the average solutions $\rho_1(x, y)$ and $\rho_2(x, y)$ of the adjoint linear system (3.10) for the time period $[0, 93]$ are shown in Figure 5.2. By using bilinear interpolation, we can find an approximate function for $\varphi(x_i, y_j)$ using the average solution A_R , as shown in Figure 5.2. We know that perturbed spiral tip can be controlled through using the control function $\tilde{f}(t)$. Instead of Schlesinger et al.'s method, we will explain how to suppress the spiral dynamics in a small perturbation using response functions. By looking at the perturbation function $\mathbf{h}(t)$ of the

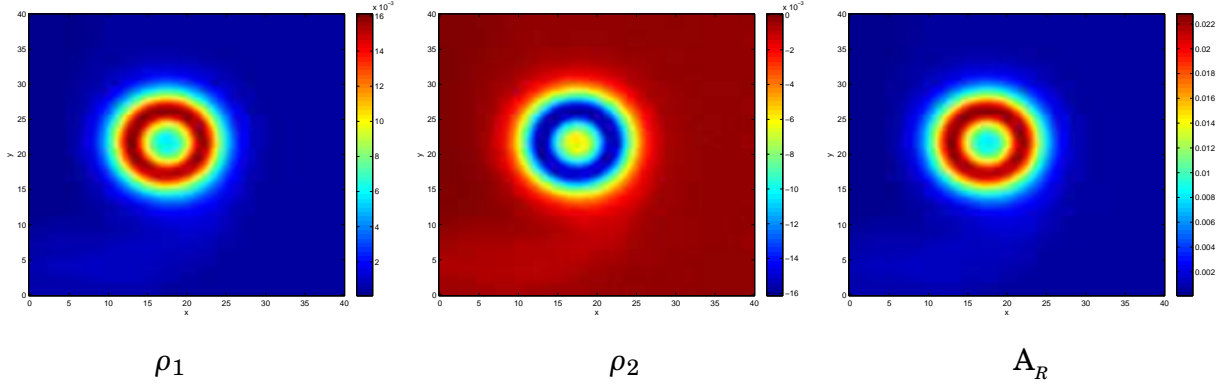


Figure 5.2: The variable ρ_1 is the average of the numerical solution $k(x, y, t)$ of the adjoint linear system (3.10) and the variable ρ_2 is the average of the numerical solution $s(x, y, t)$ of the adjoint linear system (3.10) using the Trapezoidal rule for the periodic time $[0, 93]$. The numerical solutions are for the two components $k(x, y, t)$ and $s(x, y, t)$ of the adjoint linear system for the FHN model with parameters $\beta = 0.75$ and $\epsilon = 0.3$. The response functions k and s is normalized.

FHN model (4.6), we observe that the perturbation function $\mathbf{h}(t)$ does not depend on the spatial variables x and y . This means that the spiral wave tip is not localised. By using the average of the response function k of the adjoint linear system, as shown in Figure 5.2, we can reformulate the perturbation function $\mathbf{h}(t)$ through the interpolation function $\varphi(x_i, y_j)$ for the average solution $\rho_1(x_i, y_j)$ as follows:

$$\mathbf{h}_3(t, x, y) = \begin{bmatrix} -\frac{1}{\epsilon} \tilde{f}(t) \varphi(x, y) \\ 0 \end{bmatrix}.$$

Thus, the equation (4.6) becomes as follows:

$$\mathbf{u}_t = \mathbf{f}(\mathbf{u}) + \mathbf{D}\nabla^2 \mathbf{u} + \mathbf{h}_3(t, x, y).$$

Let us now define the interpolation function φ as follows:

$$\varphi = \varphi(x_{tip} - (x_a + x_c), y_{tip} - (y_a + y_c)),$$

where the point (x_a, y_a) is the centre of the circles, as shown in Figure 5.2, the point (x_{tip}, y_{tip}) is the Cartesian coordinate system of the spiral wave tip and point (x_c, y_c) is the centre core. As illustrated by Figure 4.4, we can localise the tip trajectory of the spiral wave using the perturbed function $\mathbf{h}_3(t, x, y)$ instead of the function $\mathbf{h}(t)$. Let us apply the function \mathbf{h}_3 for the parameters

of the FHN system and the temporal and spatial steps, as shown in Figure 4.4. Thus, we cannot control the behaviour of the spiral wave for the parameters $\epsilon = 0.25$ and $\beta = 0.85$ successfully because the total length of the radius r is not big enough to suppress the spiral wave tip. In other word, if we look at the circles of the approximate averages ρ_1, ρ_1 and the average solution \hat{A}_R in the Cartesian plane, then we note that the radius r of the circles in the bounded domain $[0, 40]^2$, as shown in Figure 5.2, does not help to control the spiral wave tip using the response functions. Therefore, we need to increase the radius r of circle through computing the average of adjoint eigenfunctions $k(x, y, t)$ and $s(x, y, t)$ in polar coordinates by the following formulas:

$$\hat{\rho}_1(x, y, t) = \frac{1}{2k_1\pi} \int_0^{2k_1\pi} k(\mathbf{R}_{\theta_{m_1}}(x, y), t) d\theta \approx \frac{1}{2k_1\pi} \left(\sum_{m_1=0}^{(n_2-1)} \frac{\Delta\theta}{2} \left(k(\mathbf{R}_{\theta_{m_1}}(x_i, y_j), t_m) + k(\mathbf{R}_{\theta_{m_1+1}}(x_i, y_j), t_m) \right) \right), \quad (5.2a)$$

$$\hat{\rho}_2(x, y, t) = \frac{1}{2k_1\pi} \int_0^{2k_1\pi} s(\mathbf{R}_{\theta_{m_1}}(x, y), t) d\theta \approx \frac{1}{2k_1\pi} \left(\sum_{m_1=0}^{(n_2-1)} \frac{\Delta\theta}{2} \left(s(\mathbf{R}_{\theta_{m_1}}(x_i, y_j), t_m) + s(\mathbf{R}_{\theta_{m_1+1}}(x_i, y_j), t_m) \right) \right), \quad (5.2b)$$

where

$$\begin{aligned} \mathbf{R}_{\theta_{m_1}} \begin{bmatrix} x_i \\ y_j \end{bmatrix} &= \begin{bmatrix} \cos\theta_{m_1} & \sin\theta_{m_1} \\ -\sin\theta_{m_1} & \cos\theta_{m_1} \end{bmatrix} \begin{bmatrix} x_i - x_a \\ y_j - y_a \end{bmatrix} + \begin{bmatrix} x_a \\ y_a \end{bmatrix}, \\ &= \begin{bmatrix} \cos\theta_{m_1}(x_i - x_a) + \sin\theta_{m_1}(y_j - y_a) + x_a \\ -\sin\theta_{m_1}(x_i - x_a) + \cos\theta_{m_1}(y_j - y_a) + y_a \end{bmatrix}. \end{aligned}$$

and

$$\theta_{m_1} = m_1 \Delta\theta, \quad \Delta\theta = \frac{2k_1\pi}{n_2}, \quad m_1 = 0, 1, \dots, n_2, \quad k_1, n_2 \in \mathbb{N}.$$

Moreover, we can also find the length of the vector $(\hat{\rho}_1(x, y, t), \hat{\rho}_2(x, y, t))$, that is

$$\hat{A}_R = \sqrt{(\hat{\rho}_1(x, y, t))^2 + (\hat{\rho}_2(x, y, t))^2}. \quad (5.3)$$

Corresponding to parameters $\epsilon = 0.3$ and $\beta = 0.75$, we find that the average solutions $\hat{\rho}_1$ and $\hat{\rho}_2$ of the adjoint linear system (3.10) is shown in Figure 5.3.

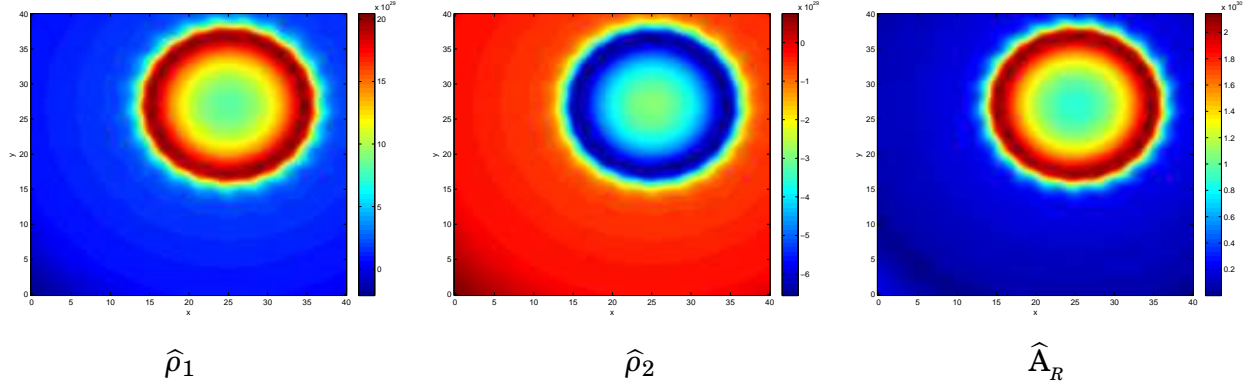


Figure 5.3: The variable $\hat{\rho}_1$ is the average for the numerical solution $k(x, y, t)$ of the adjoint linear system and the variable $\hat{\rho}_2$ is the average for the numerical solution $s(x, y, t)$ of the adjoint linear system using the Trapezoidal rule for $\theta \in [0, 16\pi]$. The numerical solutions for the two components $k(x, y, t)$ and $s(x, y, t)$ of the adjoint linear system are for the FHN model with parameters $\beta = 0.75$ and $\epsilon = 0.3$. The variable k_1 is equal to 8 such that the centre point (x_a, y_a) is equal to $(27, 25)$. These solutions, k and s , of the adjoint linear problem are not normalized.

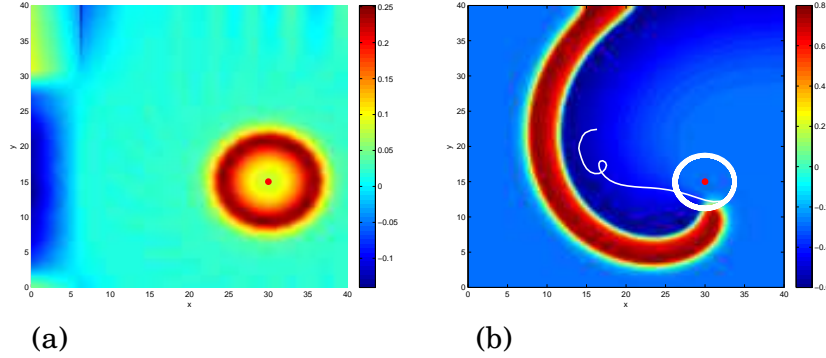


Figure 5.4: The parameters of the FHN system is $\alpha = 0.5$, $\beta = 0.8288$ and $\epsilon = 0.25$ such that the average of adjoint eigenfunctions k and s are computed by using the Trapezoidal rule of equations (5.2a) and (5.2b) for $\theta \in [0, 16\pi]$. The panel (a) shows the interpolation function φ using the average of adjoint eigenfunctions k , while the panel (b) demonstrates successful control in small perturbation for component u using response function. The centre core (x_c, y_c) and centre point (x_a, y_a) are equal to $(30, 15)$. The parameters of the proportional feedback control \mathbf{h}_3 are $\alpha_1 = 0.01$, $\alpha_2 = 200$ such that the initial guess for r_0 is 4.3950. The solutions k and s of the adjoint linear problem are not normalized for the time period is $[0, 1500]$.

Let us apply the the perturbed function \mathbf{h}_3 for the controlled tip motion as shown in Figure 4.4 again through deducing interpolation function φ using the equations (5.2a) and (5.2b). Therefore, the behavior of the spiral wave can also be controlled using small perturbations of response

functions instead of using the larger perturbations as shown in Figure 5.4.

However, let us now investigate the size of the spatial localisation of the local support perturbation function $\mathbf{h}_R(t, x, y)$ using response functions for FHN model with the controller system. By looking at the adjoint linear system of FHN with controller model in cartesian coordinate system and also using the parameters $\epsilon = 0.20$ and $\beta = 0.93$ with the radius $R = 40$, the left eigenfunction of the adjoint linear system of FHN with controller model can be demonstrated, as shown in Figure (5.5). We can now compute the average of the response function. With regards the Trapezoidal rule and by using the equations (5.2a), (5.2b) and (5.3), we can compute that the average solutions $\hat{\rho}_1$ and $\hat{\rho}_2$ of the adjoint linear system of FHN with controller model as shown in Figure 5.6. In order for the minimum radius of the average solutions $\hat{\rho}_1$ and $\hat{\rho}_2$ of the adjoint linear system of FHN with controller model as shown in Figure 5.6 to be computed numerically, we need to use the formula (5.3) such that the variable x is fixed or the variable y is fixed. This is because we can see the minimum radius for response functions using stable controlling spiral wave tip for different values of radius as shown in Figure 5.1. The diagram of amplitude of length \hat{A}_R with fixed variable x is shown in Figure 5.7.

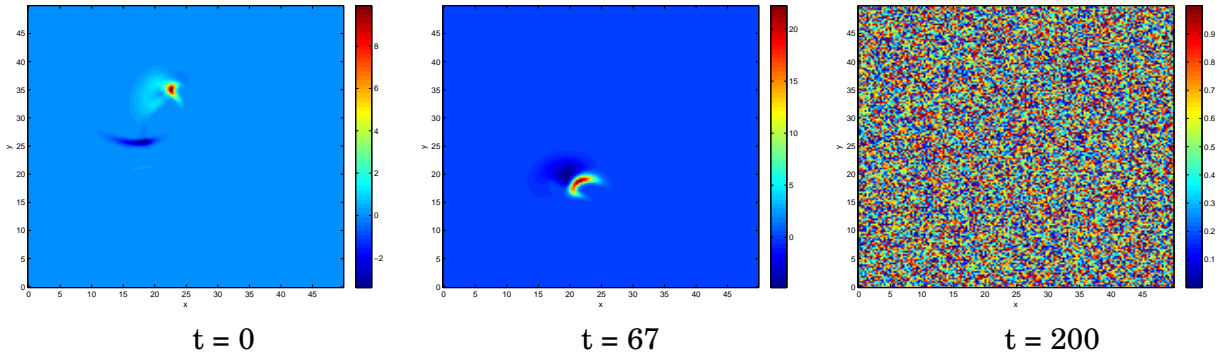


Figure 5.5: The left eigenfunction of the adjoint linear system of FHN system with controller equation is in cartesian coordinate such that parameters $\alpha, \beta =$ and ϵ are equal to 0.5, 0.93 and 0.20 respectively. The left eigenfunction is found numerically using semi-implicit method such that we choose a random initial condition at $t = 200$. The centre core (x_c, y_c) is equal to $(19.5, 18)$ while the parameters of the proportional feedback control \mathbf{h}_R are $a_1 = 0.01, a_2 = 200$ and $R = 40$. The time step Δt is equal to 0.1 and space steps Δx on x axis $[0, 50]$ and Δy on y axis $[0, 50]$ are equal to 0.3.

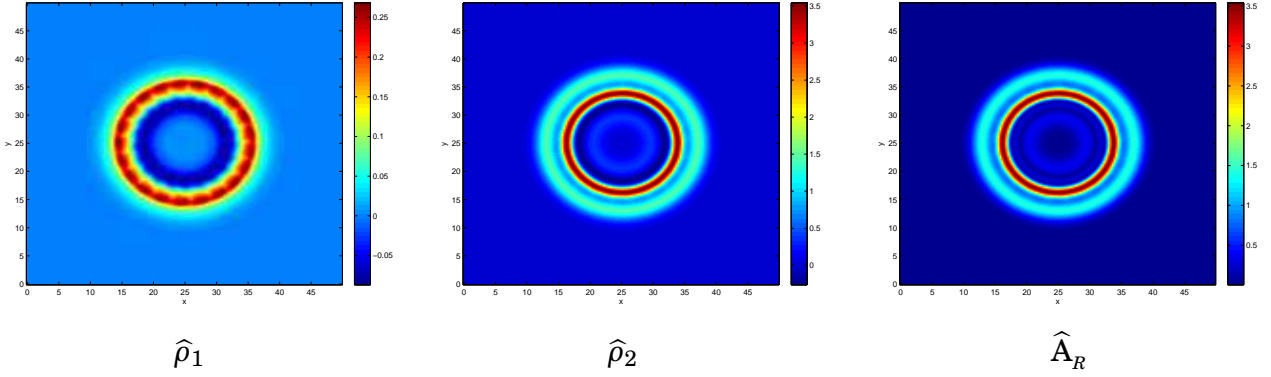


Figure 5.6: The variables $\hat{\rho}_1$ and $\hat{\rho}_2$ are the average for the numerical solutions of the adjoint linear system of FHN system with controller equation using the Trapezoidal rule for $\theta \in [0, 32\pi]$ with parameters $\alpha = 0.5$, $\beta = 0.93$ and $\epsilon = 0.20$. The variable k_1 is equal to 16 such that the centre point (x_a, y_a) is equal to $(25, 25)$. The solutions of the adjoint linear problem are not normalized. The centre core (x_c, y_c) is equal to $(19.5, 18)$ while the parameters of the local support perturbation function \mathbf{h}_R are $a_1 = 0.01$, $a_2 = 200$ and $R = 40$. The time step Δt is equal to 0.1 and space steps Δx on x and Δy are equal to 0.3.

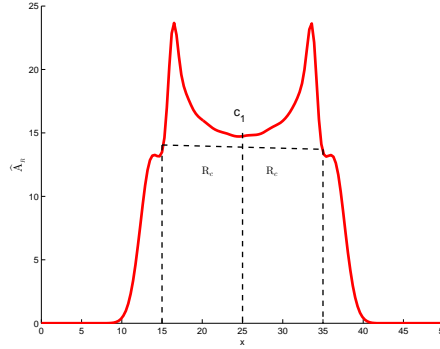


Figure 5.7: Diagram indicates comparison of the amplitude \hat{A}_R of the average of the response function and the size of the smallest radius R_c such that the local support function $\mathbf{h}_R(t, x, y)$ stabilise the spiral wave. The amplitude of length \hat{A}_R is calculated by using the average solutions $\hat{\rho}_1$ and $\hat{\rho}_2$ of the adjoint linear system of FHN with controller model. The parameters of the FHN system with controller model are $\alpha = 0.5$, $\beta = 0.93$ and $\epsilon = 0.20$ and the parameters of local support perturbation function \mathbf{h}_R are chosen as $a_1 = 0.01$, $a_2 = 200$. The centre core (x_c, y_c) is equal to $(19.5, 18)$. The critical radius R_c is standard for the minimum radius of the circle as shown in Figure 5.6, while the variable c_1 refers to the centre of the circle as shown in Figure 5.6. By comparing between amplitude \hat{A}_R of response function and the size of the smallest radius R_c for the local support perturbation function $\mathbf{h}_R(t, x, y)$, the spiral wave can be numerically stabilised such that the radius R_c is approximately equal to 10 through looking at Figure 5.1. The radius R_c for the local support perturbation function $\mathbf{h}_R(t, x, y)$ and the proportional feedback control function $\tilde{f}(t)$ is comparable.

As illustrated by Figure 5.7, we observe that the centre of the circles as shown in Figure 5.6 is $(25, 25)$. In addition, the minimum radius R is equal to 10 approximately as shown in Figure 5.6. Thus, we deduce that we can successfully stabilise the rotation of the spiral wave using the small perturbation as long as the support of the control action covers the region where the response function is non-negligible. In particular, we show that the method of Schlesner et al. works even for localised control action. In practical terms, this may be a better way of controlling spiral waves in the heart tissue because only localised perturbation is required.

CONCLUSION

In this last chapter, we shall summarise the results that have been obtained in this thesis and conclude with an outline of further work.

6.1 Summary of the Results

In this thesis, we examine several aspects of the dynamics of spiral waves using the semi-implicit method. In order to study spiral waves, we write Matlab codes to do numerical simulations of the FitzHugh-Nagumo system without using the 1D controller dynamics and also with the 1D controller equation. Moreover, we locate the spiral wave tip numerically and we are able to understand the different behaviours of the spiral wave tip, as discussed in Chapter 2. In Chapters 1 and 3, we review some material in Euclidean symmetry and consider the relationship between the spiral waves in bounded and infinite domains [9]. As a result, we show that the non-decaying numerical solutions of the linear system are approximated by a linear combination of three independent non-decaying solutions of the linear system. Moreover, we numerically compute Floquet multipliers and verify that the numerical solutions of the spiral wave are apparently asymptotically stable as discussed in Chapter 3. We calculate the numerical angular

velocity of the spiral wave in the rotating frame of reference related to FitzHugh-Nagumo system without using the 1D controller dynamics in Chapter 3. This allows us to find the approximate wavelength of the spiral wave. Numerically, we also calculate the angular velocity of the spiral wave for the FitzHugh-Nagumo system using the 1D controller equation in Chapter ???. We implement proportional feedback control [75] to stabilise the rigid rotation of the spiral wave and meandering spiral wave as elaborated in Chapter 4. We also examine some examples of unsuccessful control. Moreover, we quantify a region of the feedback parameters a_1 and a_2 of the proportional feedback control that gives successful control. Based on this study, we also investigate successful and unsuccessful control of the spiral wave around tip trajectory point or target point using tip-localised control action and fixed-localised control action. In Chapter 5 the response functions of the adjoint linear problem for the FitzHugh- Nagumo equation with 1D controller dynamics related to fixed-localised control action at the centre are computed. Therefore, we verify numerically that the spiral wave can be stabilised using a large enough radius of support control action and also found the size of the spatial localisation of the support control functions. This leads us to derive that the stabilising spiral wave tip using a large enough radius of the support control action and also, the size of the spatial localisation of the support control function, using the response function of the adjoint linear problem are identical.

6.2 Further Work and Open Questions

As explained in chapter 4, rigidly rotating spiral waves can be stabilised using proportional feedback control $\tilde{f}(t)$ applied in whole spatial domain. In order to optimise the control of spiral waves, for instance in the cardiac tissue, it is worth trying to find local perturbation of function $\mathbf{h}(t)$ in order for the spiral wave to be controlled in a small perturbation. We note that the adjoint linear system of the FHN model with the controller dynamics gives information about the sensitivity of the spiral wave to a perturbation. Therefore, it is a good strategy for controlling the spiral wave tip in a more optimal manner which considers spatially localized perturbation using the response function. However, there are several interested types of research that remain:

1. It would be interesting to work with a more realistic physically-based model such as the Hodgkin-Huxley equations, the Karma model or Bueno-Orovio-Cherry-Fenton model instead of the FHN system [17, 44, 49, 50]. A reason to study the complex model is that we can obtain results that are more relevant understanding to cardiac arrhythmias. The challenge would be to understand similar control spiral waves in the Hodgkin-Huxley equations, the Karma system or Bueno-Orovio-Cherry-Fenton model. These models are typically stiff differential equations, so they are more challenging to solve numerically. For investigating the numerical simulation of these models, we would need to use a more powerful numerical code, for example BeatBox [3] which is written in C language and runs much faster than Matlab. We can also use BeatBox to solve the realistic models numerically.
2. It would be interesting to work with a simple model such as the Barkley system which is less realistic than the FHN system. The main advantage of the Barkley system instead of the FitzHugh-Nagumo system is that we would be able more rapidly perform simulations, and so for example perform higher resolution scans or longer simulations. Using the response function, we could investigate stabilization via various control methods.
3. Related to Schlesner et al.'s [75] method in Chapter 4, we apply this method to control rigidly rotating spiral waves and meandering spirals for certain parameter values but not for all parameter values. Further research is needed to understand why this control method seems to fail for some control parameters through using stable rigid rotation. Moreover, in meander case, there are the bounded regions of control parameters which show successful and unsuccessful controls. Therefore, it would be interesting to find the bifurcation analysis through computing eigenvalues numerically. In other words, the successful and unsuccessful control regions should be determined for both rigid and meander regimes by calculating eigenvalues numerically.
4. Schlesner et al. studied the control of a spiral wave tip in a hypermeander regime [75], so it would be worth investigating the behaviour of the spiral wave using the support of the

control action in this regime as well.

5. It would be interesting to calculate the rest of the spectrum of Floquet multipliers of FitzHugh-Nagumo equation without the controller system and FitzHugh-Nagumo equation with the controller system numerically, for example using a numerical method such as Arnoldi iteration.



COMPUTING WINFREE'S DIAGRAM

Here, we present the algorithm used to generate the plot illustrated in Figure 2.10 with different parameters ϵ and β in order to understand the behaviour of the spiral wave tip. We use a systematic Matlab code for different parameter points (ϵ, β) with a fully developed spiral initial condition for specific parameters $\epsilon = 0.30$ and $\beta = 0.75$ using Barkley initial condition. Therefore, before computing the spiral wave tip, we need to remove the initial transient through a computation of the numerical solution of the FHN model for the time period $[0, 300]$ and the spatial domain $[0, 150]^2$. The appropriate value of the time step Δt is equal to 0.1 and the appropriate value of the space step $\Delta x = \Delta y$ is equal to 0.30 such that the maximum time T_{\max} is equal to 350. Since the initial condition is found using specific parameters $\epsilon = 0.30$ and $\beta = 0.75$, which generate the rigid rotation, the time period $[0, 300]$ is long enough to remove the initial transient for all locations on the regular grid through numerical observation. The different parameter points (ϵ, β) are as a uniform grid such that

$$\epsilon \in \{0.03, 0.04, \dots, 0.29, 0.3\}, \quad \beta \in \{0.1, 0.2, \dots, 1.2, 1.3\}.$$

Although the same initial condition is used for all parameters to save time, we should also be aware that the initial condition might be quite far from the attractor in some cases. Since the systematic Matlab code is written for different parameters ϵ and β which generate a rigid

rotation, meandering or hypermeandering spiral waves, the Matlab algorithm code should be defined for any any possible cases such as when the spiral wave tip approaches the boundary domain or when the spiral wave solution is unstable because the total length of the x and y axes is not good enough to generate the spiral wave solution. We look at these cases to prevent the Matlab code from stopping the computation of the tip path of the spiral wave. If the spiral wave tip (x_{tip}^m, y_{tip}^m) such that $m \in \mathbb{N}$ satisfies the following formula:

$$d_1 = \sqrt{(x_{tip}^m - x)^2 + (y_{tip}^m - y)^2} < 2, \quad m \in \mathbb{N},$$

where the point (x, y) is a Cartesian coordinate of the bounded domain, then the Matlab code will stop calculating the spiral wave tip and also use different parameters. According to the unstable spiral wave solution, if the numerical simulation of the FHN model has the $v_{\min} < 0, v_{\max} < 0$ or $v_{\min} > 0, v_{\max} > 0$ such that the variable v_{\min} is the minimum value of v component whereas the variable v_{\max} is the maximum value of the component v , then the Matlab code will stop calculating the spiral wave tip and also use different parameters ϵ and β . We also apply these procedures for the component u . Moreover, if we have

$$u_{\max} > 10^5, u_{\min} < -10^5, v_{\max} > 10^5, v_{\min} < -10^5,$$

then the Matlab code will also stop calculating the spiral wave tip and use different parameters ϵ and β . This means that there is no spiral wave. Since the systematic Matlab code is running for $T_{\max} = 350$, this code may produce the full spiral wave tip earlier than the time 350, as shown in the example of the rigid rotation in the Figure 2.3 or the meander in the Figure 2.4. We need to have a strong condition to stop calculating the spiral wave tip for different parameters. As we know that the spiral wave rotates in a bounded domain, when the Matlab code removes the initial transient, then the code will compute the centre point $(x_c(t_m), y_c(t_m))$ for each time, as demonstrated in Section 4.2, and also the tip point $(x_{tip}(t_m), y_{tip}(t_m))$, likewise explained in Section 2.4. In order for the systematic Matlab code to identify which spiral wave tip is rigidly rotating or meandering, it needs to calculate a signed curvature K of the spiral wave tip (x_{tip}^m, y_{tip}^m)

in a Cartesian coordinate system [34], that is

$$\mathbf{K} = \frac{\frac{dx_{tip}}{dt} \frac{d^2 y_{tip}}{dt^2} - \frac{dy_{tip}}{dt} \frac{d^2 x_{tip}}{dt^2}}{\left(\left(\frac{dx_{tip}}{dt} \right)^2 + \left(\frac{dy_{tip}}{dt} \right)^2 \right)^{\frac{3}{2}}} = \frac{\dot{x}_{tip} \ddot{y}_{tip} - \dot{y}_{tip} \ddot{x}_{tip}}{(\dot{x}^2 + \dot{y}^2)^{\frac{3}{2}}}, \quad (\text{A.1})$$

where

$$x_{tip} = x_{tip}(t), y_{tip} = y_{tip}(t).$$

The signed curvature \mathbf{K} is found numerically through using central difference method, that is

$$\frac{dx_{tip}^m}{dt} = \frac{x_{tip}^{m+1} - x_{tip}^{m-1}}{2\Delta t} + \mathcal{O}(\Delta t) \approx \frac{x_{tip}^{m+1} - x_{tip}^{m-1}}{2\Delta t}, \quad (\text{A.2a})$$

$$\frac{\partial^2 x_{tip}^m}{\partial t^2} = \frac{x_{tip}^{m+1} - 2x_{tip}^m + x_{tip}^{m-1}}{(\Delta t)^2} + \mathcal{O}((\Delta t)^2) \approx \frac{x_{tip}^{m+1} - 2x_{tip}^m + x_{tip}^{m-1}}{(\Delta t)^2}, \quad (\text{A.2b})$$

$$\frac{dy_{tip}^m}{dt} = \frac{y_{tip}^{m+1} - y_{tip}^{m-1}}{2\Delta t} + \mathcal{O}(\Delta t) \approx \frac{y_{tip}^{m+1} - y_{tip}^{m-1}}{2\Delta t}, \quad (\text{A.2c})$$

$$\frac{\partial^2 y_{tip}^m}{\partial t^2} = \frac{y_{tip}^{m+1} - 2y_{tip}^m + y_{tip}^{m-1}}{(\Delta t)^2} + \mathcal{O}((\Delta t)^2) \approx \frac{y_{tip}^{m+1} - 2y_{tip}^m + y_{tip}^{m-1}}{(\Delta t)^2}, \quad (\text{A.2d})$$

such that $\mathcal{O}(\Delta t)$ and $\mathcal{O}((\Delta t)^2)$ are truncation errors. The curvature \mathbf{K} should be computed in the different time moment in order for the curvature to be more accurate such as different time moment between the curvatures is approximately 2. By using the equations (A.2a), (A.2b), (A.2c) and (A.2d), the curvature \mathbf{K} can be written as follows:

$$\begin{aligned} \mathbf{K} &\approx \frac{\left(\frac{x_{tip}^{m+1} - x_{tip}^{m-1}}{2\Delta t} \right) \left(\frac{y_{tip}^{m+1} - 2y_{tip}^m + y_{tip}^{m-1}}{(\Delta t)^2} \right) - \left(\frac{y_{tip}^{m+1} - y_{tip}^{m-1}}{2\Delta t} \right) \left(\frac{x_{tip}^{m+1} - 2x_{tip}^m + x_{tip}^{m-1}}{(\Delta t)^2} \right)}{\left(\left(\frac{x_{tip}^{m+1} - x_{tip}^{m-1}}{2\Delta t} \right)^2 + \left(\frac{y_{tip}^{m+1} - y_{tip}^{m-1}}{2\Delta t} \right)^2 \right)^{\frac{3}{2}}}, \\ &= \frac{8 \left(x_{tip}^{m-1} y_{tip}^m - x_{tip}^{m-1} y_{tip}^{m+1} - x_{tip}^{m+1} y_{tip}^m + x_{tip}^{m+1} y_{tip}^{m-1} - x_{tip}^m y_{tip}^{m-1} + x_{tip}^m y_{tip}^{m+1} \right)}{\left((x_{tip}^{m+1} - x_{tip}^{m-1})^2 + (y_{tip}^{m+1} - y_{tip}^{m-1})^2 \right)^{\frac{3}{2}}}. \end{aligned}$$

If the difference between the maximum and minimum values of the curvature \mathbf{K} is less than a tolerance Tol for a suitable choice of the time test window \mathbf{T}_{test} , then the spiral wave tip is rigidly rotating for a maximum time $\mathbf{T}_{\text{max}} > 0$, that is

$$\frac{\max_{(T-\mathbf{T}_{\text{test}}) \leq t \leq T} (\mathbf{K}(t)) - \min_{(T-\mathbf{T}_{\text{test}}) \leq t \leq T} (\mathbf{K}(t))}{\min_{(T-\mathbf{T}_{\text{test}}) \leq t \leq T} (\mathbf{K}(t))} \leq \text{Tol}, \quad \forall t \in [T - \mathbf{T}_{\text{test}}, T],$$

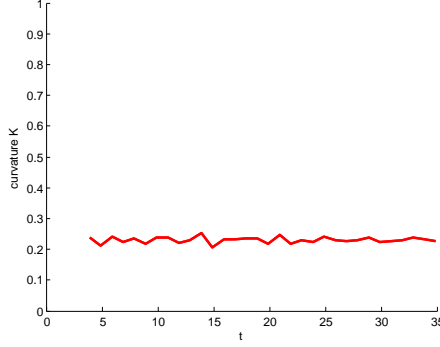


Figure A.1: The curvature $K(t)$ is calculated using the equation (A.1) for the periodic regime as shown in Figure 2.3. The parameters of the FHN model are $\alpha = 0.5$, $\beta = 0.75$ and $\epsilon = 0.3$.

such that $T_{\max} > T > T_{\text{test}} > 0$. According to Figure 2.3 in the periodic regime, the curvature K is numerically estimated as follows:

$$\min_{0 \leq t \leq 35} (K(t)) \leq K(t) \leq \max_{0 \leq t \leq 35} (K(t)) \iff 0.2064 \leq K(t) \leq 0.2522, \quad \forall t \in [0, 35],$$

such that the diagram of the curvature $K(t)$ is shown in Figure A.1. We observe that

$$\frac{\max_{0 \leq t \leq 35} (K(t)) - \min_{0 \leq t \leq 35} (K(t))}{\min_{0 \leq t \leq 35} (K(t))} = 0.2219,$$

so the spiral wave tip is in rigid rotation if it satisfies the following condition:

$$\frac{\max_{(T-T_{\text{test}}) \leq t \leq T} (K(t)) - \min_{(T-T_{\text{test}}) \leq t \leq T} (K(t))}{\min_{(T-T_{\text{test}}) \leq t \leq T} (K(t))} \leq \text{Tol} = 3,$$

where

$$T_{\max} = 350, T_{\text{test}} = 15, T = 16.$$

In contrast, if the systematic Matlab code satisfies the following condition:

$$\frac{\max_{(T-T_{\text{test}}) \leq t \leq T} (K(t)) - \min_{(T-T_{\text{test}}) \leq t \leq T} (K(t))}{\min_{(T-T_{\text{test}}) \leq t \leq T} (K(t))} > \text{Tol} = 3, \quad \exists t \in [T - T_{\text{test}}, T], \quad (\text{A.3})$$

then the spiral wave tip is meandering. Regarding Figures 2.4 and 2.5 in a meander regime, the curvature K is estimated as follows:

$$\min_{0 \leq t \leq 85} (K(t)) \leq K(t) \leq \max_{0 \leq t \leq 85} (K(t)) \iff 0.2158 \leq K(t) \leq 1.8018, \quad \forall t \in [0, 85],$$

$$\min_{0 \leq t \leq 30} (K(t)) \leq K(t) \leq \max_{0 \leq t \leq 30} (K(t)) \iff 0.0617 \leq K(t) \leq 4.8911, \quad \forall t \in [0, 30],$$

such that the diagram of the curvature $K(t)$ is shown in Figure A.2. We find that

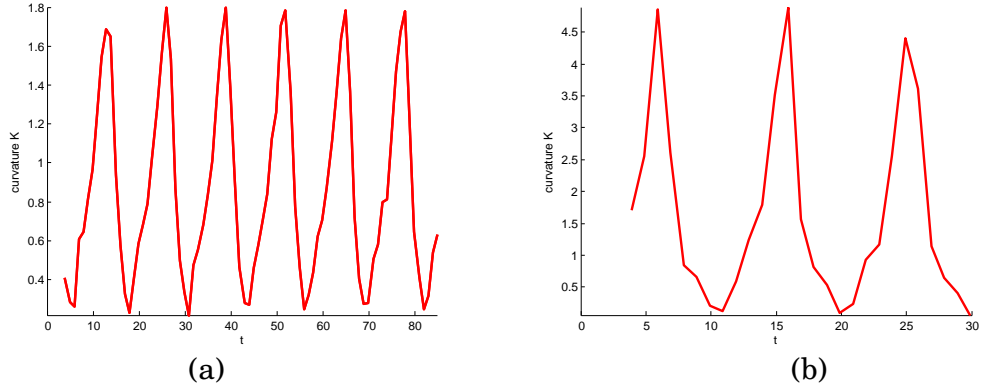


Figure A.2: The curvature $K(t)$ is calculated using the equation (A.1) for the meander regime such that $t \in [0, 85]$ and $t \in [0, 30]$. Diagram (a) shows the the curvature of Figure 2.4, while the diagram (b) shows the the curvature of Figure 2.5. The parameters of the FHN model are $\alpha = 0.5$, $\beta = 0.85, 0.77$ and $\epsilon = 0.20, 0.15$.

$$\frac{\max_{0 \leq t \leq 85} (K(t)) - \min_{0 \leq t \leq 85} (K(t))}{\min_{0 \leq t \leq 85} (K(t))} = 7.3494,$$

$$\frac{\max_{0 \leq t \leq 30} (K(t)) - \min_{0 \leq t \leq 30} (K(t))}{\min_{0 \leq t \leq 30} (K(t))} = 78.2723,$$

so the spiral wave tip is meandering if it satisfies the condition (A.3).

When the Matlab algorithm code can distinguish between the rigid rotation and the meander, then it will plot the diagram of the spiral wave tip and the data of the tip trajectory will also be saved. Moreover, when the Matlab code finishes computing the spiral wave tip for all the parameters, then the loop of the Matlab code will be broken. The Matlab code will plot the rigid rotation and meander as grid points such that the filled blue colour points show the periodic regime while the filled red colour points demonstrate the meander regime as shown in Figure A.3. In order to clarify the previous explanation, the Matlab algorithm code is shown as follows:

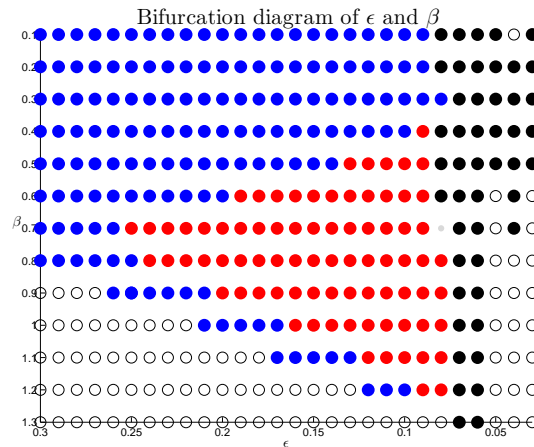


Figure A.3: The filled blue points show the rigid region whereas the filled red points show meander region. The filled black points indicate unstable whereas the open black points show the spiral wave solution has collided with the boundary domain. The initial condition for both cases is shown in Figure 2.2. The tolerance Tol is equal to 0.5 and the time test window T_{test} is equal to 15. Moreover, the maximum time T_{max} is equal to 350 such that the spatial domain $[0, 150]^2$.

```

1 % Winfree_diagram_epsilon_beta
2 % Plots behaviour in parameter space
3 % Oct 2018
4 % Saad Almuaddi
5 %%
6 close
7 clear
8 clc
9 %% range to scan parameters
10 beta_values=0.1:0.1:1.3;
11 epsilon_values=0.03:0.01:0.3;
12 %% fixed parameters
13 alpha=0.5;
14 %% params to find initial condition
15 epsilon=0.30;

```

```

16 beta=0.75;
17 %% numerical parameters
18 timestep =0.1; %time step
19 spacestepx =0.3; % space step for x axis
20 totallengthx=150; % total length of x axis
21 totallengthy=totallengthx; % total length of y axis
22 value_unstable=1e+5; % the condition for unstable dynamical solution
23 finaltime_intial =100; % the time for generating the initial condition
24 T_max_time=200; % the time for numerical simulation of FHN system
25 T_test=1; % time test window
26 T=16; % maximum time for test window
27 T_T_test=T-T_test; % the begining of time test window
28 number_grid_points=length(T_test:timestep:T);% number grid points for
    test window
29 number_curvature=floor(number_grid_points/8); %the number of computing
    the curvature of tip path
30 time_of_initial_trans=100; % the time for removing the initial transient
31 %% set up various arrays
32 L_epsilon=length(epsilon_values); % the number of parameters for epsilon
33 L_beta=length(beta_values);
34 vector_epsilon_beta=[]; % the number of parameters for epsilon and beta
35 spacestepy =spacestepx; % space step for y axis
36 gridx =0:spacestepx:totallengthx;
37 gridy =0:spacestepy:totallengthy;
38 threshold_b=2; % threshold for boundary domain
39 Nx=length(gridx)+2; % the number of grid points for x axis
40 Ny=length(gridy)+2; % the number of grid points for y axis
41 timegrid = 0:timestep:T_max_time;

```

APPENDIX A. COMPUTING WINFREE'S DIAGRAM

```
42 M=length(timegrid); % the biggest index for time
43 isoline_level_u=0; % isoline for u component
44 isoline_level_v=0; % isoline for v component
45 tolerance_curvature=0.5; % tolerance for curvature of rigid rotation and
    meander
46 intersection_x_y=[]; % vector for spiral wave tip of u and v components
47 %% set up results storage
48 number_plot=floor(M/T_max_time); % the number of plot for spiral wave
    solutions
49 x_points=[gridx(1),gridx(end)]; % the points on begining and end on x
    axis
50 y_points=[gridy(1),gridy(end)]; % the points on begining and end on y
    axis
51 length_x_points=length(x_points); % the number of points on x axis
52 length_y_points=length(y_points); % the number of points on y axis
53 points_x_bounded_domain=zeros(2*(Nx-2),length_y_points); % vector of
    points on x axis
54 points_y_bounded_domain=zeros(2*(Ny-2),length_y_points);% vector of
    points on y axis
55 index_j=0; % index j for y axis in order to compute all points around
    bounded domain
56 index_i=0; % index i for x axis in order to compute all points around
    bounded domain
57 for i=1:length_y_points
58     y=y_points(i);
59     for j=1:(Nx-2)
60         x=gridx(j);
61         points_y_bounded_domain(j+index_i,:) =[x,y];
```

```

62     end
63     index_i=Nx-2;
64 end
65 for i=1:length_x_points
66     x=x_points(i);
67     for j=1:(Ny-2)
68         y=gridy(j);
69         points_x_bounded_domain(j+index_j,:)=[x,y ];
70     end
71     index_j=Ny-2;
72 end
73 points_x_y_bounded_domain=[points_y_bounded_domain;
        points_x_bounded_domain]; % all points around bounded domain
74 length_points_x_y=length(points_x_y_bounded_domain);
75 %% find initial condition for spiral
76 matrix_no_spiral_wave_epsilon_beta=zeros(M,3); % numerical solver does
        not produce spiral wave tip
77 matrix_unstable_solution_epsilon_beta=zeros(M,3); % numerical solution of
        spiral wave is unstable
78 matrix_crash_with_bounded_domain_epsilon_beta=zeros(M,3); % numerical
        solution of spiral wave crash with bounded domain
79 index_no_spiral_wave=0; % the first value of index
80 index_unstable_solution=0;
81 index_crashed_solution=0;
82 [ initial_conditionu1 ,initial_conditionv1 ] =...
83     INITIAL_CONDITION_EPSILON_BETA_IMPLICIT_CORRECTED_1( alpha ,...
84     epsilon ,beta ,timestep ,spacestepx ,totallengthx ,finaltime_intial); %
        The function generate the initial condition using parameters

```

epsilon = 0.30 and beta beta =0.75

```
85 load( 'initial_conditionu1.dat' );
86 load( 'initial_conditionv1.dat' );
87 all_points_rigid_rotation=zeros(M,2); % the matrix shows spiral wave tip
   for rigid rotation
88 accountor_rigid=1; % the number of iteration
89 all_points_meander=zeros(M,2); % the matrix shows spiral wave tip for
   meander
90 accountor_meander=1; % the number of iteration
91 tic
92 %% loop on epsilon
93 for i=1:L_epsilon
94     epsilon =epsilon_values(i);% choosing parameter epsilon for each
       iteration
95     %% loop on beta
96     for j=1:L_beta
97         distance_boundary=10;
98         beta = beta_values(j); % choosing parameter beta for each
           iteration
99         u=initial_conditionu1; % the initial condition for u component
100        v=initial_conditionv1; % the initial condition for u component
101        index_removing_end=0; % the last index for removing initial
           transient
102        index_removed_end=0; % the first index
103        counter=1; %the number of indexes satisfying the condition of
           time test window
104        index_removing=1; % the number of indexes for removing initial
           transient
```

```

105     index_removed=1; % the number of indexes without initial
        transient
106     index_curvature=1; % the number of indexes for curvature
107     index_curvature_1=1; % the number of indexes for curvature using
        central difference method
108     all_distance_x_y=zeros(length_points_x_y,1); % set up results
        storage for values of distance
109     numerical_intersection_remove=zeros(M,2); % set up storage of
        spiral wave tip for removing initial transient
110     numerical_intersection=zeros(M,2); % set up storage of spiral
        wave tip after removing initial transient
111     time_numerical_intersection=zeros(M,3); % set up storage of
        spiral wave tip after removing initial transient including t,
        x and y
112     vector_time_curvature=zeros(M,2); % set up storage of curvature K
113     index_i=1;
114     for m=1:M-1
115         t=timegrid(m+1); % time of numerical solution
116         time=t-time_of_initial_trans; % the time with removing
            initial transient
117         [u,v,intersection ,intersection_x_y]=...
118             THE_NUMERICAL_SOLVER_1(alpha ,epsilon ,beta ,u,v,...
119             isoline_level_u ,totallengthx ,spacestepx ,timestep); %
            the numerical solver for FHN system using implicit
            scheme
120         if(t <=time_of_initial_trans ) % the condition for for
            removing initial transient
121             index_removing_end = 2+index_removing_end; % the number

```

```

    of last index
122     index_removing_begin=2*(index_removing-1)+1; % the number
        of first index
123     numerical_intersection_remove(index_removing_begin:
        index_removing_end,:) = intersection; % matrix of spiral
        wave tip for removing initial transient
124     index_removing=index_removing+1; % the next row for
        spiral wave tip numerical_intersection_remove
125     max_value_u=max(max(u));
126     min_value_u=min(min(u));
127     max_value_v=max(max(v));
128     min_value_v=min(min(v));
129     %% check if non-oscillatory
130     if( ((max_value_u>value_unstable )&&(min_value_u<-
        value_unstable )) || ...
131         ( (max_value_v>value_unstable )&&(min_value_v<-
        value_unstable ) ) )
132         index_no_spiral_wave=index_no_spiral_wave+1;
133         matrix_no_spiral_wave_epsilon_beta(
            index_no_spiral_wave,:) = [t, epsilon, beta];
134         index_unstable_solution=index_unstable_solution+1;
135         matrix_unstable_solution_epsilon_beta(
            index_unstable_solution,:) = [t, epsilon, beta];
136         break
137     elseif(((max_value_u>0 )&&(min_value_u>0 )) || ...
138         ((max_value_u<0 )&&(min_value_u<0 )) ) || ...
139         ( (max_value_v>0 )&&(min_value_v>0 ) ) || ...
140         ( (max_value_v<0 )&&(min_value_v<0 ) ) )

```

```

141         index_no_spiral_wave=index_no_spiral_wave+1;
142         matrix_no_spiral_wave_epsilon_beta(
            index_no_spiral_wave ,:)= [t , epsilon , beta ];
143         index_unstable_solution=index_unstable_solution+1;
144         matrix_unstable_solution_epsilon_beta(
            index_unstable_solution ,:)= [t , epsilon , beta ];
145         break
146     elseif (((max_value_u>0 )&&(min_value_u<-value_unstable )
            ) || ...
147         ((max_value_u>value_unstable )&&(min_value_u<0 )
            ) || ...
148         ( (max_value_v>0 )&&(min_value_v<-value_unstable
            ) ) || ...
149         ( (max_value_v>value_unstable )&&(min_value_v<0
            ) ) )
150         index_no_spiral_wave=index_no_spiral_wave+1;
151         matrix_no_spiral_wave_epsilon_beta(
            index_no_spiral_wave ,:)= [t , epsilon , beta ];
152         index_unstable_solution=index_unstable_solution+1;
153         matrix_unstable_solution_epsilon_beta(
            index_unstable_solution ,:)= [t , epsilon , beta ];
154         break
155     end
156     %% plot numerical solution for u component
157     h2=figure(2);
158     imagesc(gridx , gridy , u)
159     line(numerical_intersection_remove(1:index_removing_end
            ,1) , numerical_intersection_remove(1:index_removing_end

```

```
        ,2), 'Color', 'w', 'LineWidth', 2);
160    set(gca, 'YDir', 'normal');
161    title(sprintf(' The removing initial transient of spiral
        wave in two dimesions for u, t=%g', t));
162    shading interp
163    xlabel('x')
164    ylabel('y')
165    colorbar
166    drawnow
167    %% check if too close to boundary
168    x_tip=intersection(1,1);
169    y_tip=intersection(1,2);
170    for k=1:length_points_x_y
171        bounded_x= points_x_y_bounded_domain(k,1);
172        bounded_y= points_x_y_bounded_domain(k,2);
173        distance_x_y_tip =sqrt(( bounded_x - x_tip)^2+(
        bounded_y - y_tip  )^2);
174        all_distance_x_y(k,1)=distance_x_y_tip;
175    end
176    distance_boundary=min(all_distance_x_y);
177    if(distance_boundary<threshold_b)
178        index_no_spiral_wave=index_no_spiral_wave+1;
179        matrix_no_spiral_wave_epsilon_beta(
        index_no_spiral_wave,:)=[t, epsilon, beta];
180        index_crashed_solution=index_crashed_solution+1;
181        matrix_crash_with_bounded_domain_epsilon_beta(
        index_crashed_solution,:)=[t, epsilon, beta];
182    break
```

```

183         end
184
185     elseif (t>time_of_initial_trans)
186         index_removed_end = 2+index_removed_end; % the number of
           last index
187         index_removed_begin=2*(index_removed-1)+1; % the number
           of first index
188         %% find tip location and record in numerical_intersection
189         numerical_intersection(index_removed_begin:
           index_removed_end,:)=intersection; % set up storage of
           spiral wave tip without initial transient
190         time_numerical_intersection(index_removed,:)= [time,
           intersection_x_y];
191         index_removed=index_removed+1;
192         max_value_u=max(max(u)); % maximum value of u component
193         min_value_u=min(min(u)); % minimum value of u component
194         max_value_v=max(max(v)); % maximum value of v component
195         min_value_v=min(min(v)); % minimum value of v component
196         %% check if non-oscillatory
197         if( (max_value_u>value_unstable) || (min_value_u<-
           value_unstable) || ...
198             (max_value_v>value_unstable) || (min_value_v<-
           value_unstable) )
199             index_no_spiral_wave=index_no_spiral_wave+1;
200             matrix_no_spiral_wave_epsilon_beta(
           index_no_spiral_wave,:)=[t,epsilon,beta];
201             index_unstable_solution=index_unstable_solution+1;
202             matrix_unstable_solution_epsilon_beta(

```

```
        index_unstable_solution,:)=[t,epsilon,beta];
203     break
204     %% check if non-oscillatory
205     elseif((max_value_u>0)&&(min_value_u>0))||...
206         ((max_value_u<0)&&(min_value_u<0))||...
207         ((max_value_v>0)&&(min_value_v>0))||...
208         ((max_value_v<0)&&(min_value_v<0))
209     index_no_spiral_wave=index_no_spiral_wave+1;
210     matrix_no_spiral_wave_epsilon_beta(
        index_no_spiral_wave,:)=[t,epsilon,beta];
211     index_unstable_solution=index_unstable_solution+1;
212     matrix_unstable_solution_epsilon_beta(
        index_unstable_solution,:)=[t,epsilon,beta];
213     break
214     end
215     %% record tip trajectory
216     x_tip=intersection(1,1);
217     y_tip=intersection(1,2);
218     for g=1:length_points_x_y
219         bounded_x= points_x_y_bounded_domain(g,1);
220         bounded_y= points_x_y_bounded_domain(g,2);
221         distance_x_y_tip =sqrt((bounded_x - x_tip)^2+(
                bounded_y - y_tip )^2);
222         all_distance_x_y(g,1)=distance_x_y_tip;
223     end
224     distance_boundary=min(all_distance_x_y);
225     %% check if too close to boundary
226     if(distance_boundary<threshold_b)
```

```

227         index_no_spiral_wave=index_no_spiral_wave+1;
228         matrix_no_spiral_wave_epsilon_beta(
                index_no_spiral_wave ,:)= [t, epsilon , beta ];
229         index_crashed_solution=index_crashed_solution+1;
230         matrix_crash_with_bounded_domain_epsilon_beta(
                index_crashed_solution ,:)= [t, epsilon , beta ];
231         break
232     end
233     %% plot figure for u component
234     t_figure = PLOTTING_DIAGRAM_SPIRAL_WAVE_1( ...
235             gridx , gridy , u , numerical_intersection , time ,
                index_removed_end );
236     %% calculating the signed curvature K for u component
237     if ((time>=T_test)&&(time<=T))
238         counter=counter+1;
239         if ((mod(counter , number_curvature)==0))
240             n_index_removed=index_removed-1;
241             curvature_K = CURVATURE_FUNCTION_3(
                time_numerical_intersection , n_index_removed );
242             vector_time_curvature(index_curvature ,:)= [time ,
                curvature_K];
243             index_curvature=index_curvature+1;
244
245         end
246     elseif (time> T )
247         max_value_curvature_K=max(vector_time_curvature(1:
                index_curvature-1,2)); % maximum value of
                curvature K(t)

```

```
248     min_value_curvature_K=min(vector_time_curvature(1:
        index_curvature-1,2)); % minimum value of
        curvature K(t)
249     difference_max_min=max_value_curvature_K-
        min_value_curvature_K; %the difference between the
        maximum and minimum values of the curvature K(t)
250     if(difference_max_min<=tolerance_curvature)
251         all_points_rigid_rotation(accountor_rigid ,:)=[
            epsilon ,beta ];
252         accountor_rigid=accountor_rigid+1;
253         %the Matlab code will plot the diagram of the
            spiral wave tip and the data of the tip
            trajectory will also be saved
254         [ h3,h4 ] = PRINTING_FIG_SAVEING_DATA_2(...
255             time_numerical_intersection ,u, epsilon ,beta ,
                gridx ,gridy ,n_index_removed);
256         break
257     elseif(difference_max_min>tolerance_curvature)
258         all_points_meander(accountor_meander ,:)=[epsilon ,
            beta ];
259         accountor_meander=accountor_meander+1;
260         %the Matlab code will plot the diagram of the
            spiral wave tip and the data of the tip
            trajectory will also be saved
261         [ h3,h4 ] = PRINTING_FIG_SAVEING_DATA_2(...
262             time_numerical_intersection ,u, epsilon ,beta ,
                gridx ,gridy ,n_index_removed);
263         break
```

```

264             end
265         end
266     end
267 end
268 end
269     if ((epsilon==epsilon_values(end))&&(beta==beta_values(end)))
270         break
271     end
272 end
273 toc
274 VECTOR_TIME_CURVATURE =vector_time_curvature(1:index_curvature-1,:);
275 MATRIX_NO_SPIRAL_WAVE=matrix_no_spiral_wave_epsilon_beta(1:
    index_no_spiral_wave-1,:);
276 ALL_POINTS_RIGID_ROTATION= all_points_rigid_rotation(1:accountor_rigid
    -1,:);
277 ALL_POINTS_MEANDER= all_points_meander(1:accountor_meander-1,:);
278 All_POINTS_UNSTABLE_SOLUTION=matrix_unstable_solution_epsilon_beta(1:
    index_unstable_solution-1,:);
279 ALL_POINTS_CRASHED_SOLUTION =
    matrix_crash_with_bounded_domain_epsilon_beta(1:index_crashed_solution
    -1,:);
280 save( 'MATRIX_NO_SPIRAL_WAVE.dat', 'MATRIX_NO_SPIRAL_WAVE', '-ascii')%
    saving data for no spiral wave
281 save( 'ALL_POINTS_RIGID_ROTATION.dat', 'ALL_POINTS_RIGID_ROTATION', '-ascii'
    ) % saving data for rigid
282 save( 'ALL_POINTS_MEANDER.dat', 'ALL_POINTS_MEANDER', '-ascii') % saving
    data for meander
283 save( 'All_POINTS_UNSTABLE_SOLUTION.dat', 'All_POINTS_UNSTABLE_SOLUTION', '-

```

```
        ascii')
284 save('ALL_POINTS_CRASHED_SOLUTION.dat', 'ALL_POINTS_CRASHED_SOLUTION', '-
        ascii')
285 max_epsilon=max(epsilon_values);
286 min_epsilon=min(epsilon_values);
287 max_beta=max(beta_values);
288 min_beta=min(beta_values);
289 h5=figure(5);
290 axis([min_epsilon max_epsilon min_beta max_beta]);% defining the total
        length of the points for epsilon and beta
291 hold on;
292 plot(ALL_POINTS_RIGID_ROTATION(:,1), ALL_POINTS_RIGID_ROTATION(:,2), '.g', '
        MarkerSize', 15)
293 plot(ALL_POINTS_MEANDER(:,1), ALL_POINTS_MEANDER(:,2), '.b', 'MarkerSize'
        ,15)
294 plot(MATRIX_NO_SPIRAL_WAVE(:,2), MATRIX_NO_SPIRAL_WAVE(:,3), '.r', '
        MarkerSize', 15)
295 set(gca, 'XTick', min(epsilon_values):0.05:max(epsilon_values), 'YTick',
        min(beta_values):0.1:max(beta_values));
296 set(gca, 'XScale', 'log');
297 set(gca, 'XAxisLocation', 'bottom', 'xdir', 'reverse', 'YAxisLocation', 'left',
        'ydir', 'reverse');
298 xlabel('$\epsilon$', 'Interpreter', 'Latex', 'fontsize', 13)
299 ylabel('$\beta$', 'Interpreter', 'Latex', 'fontsize', 13, 'Rotation', 360)
300 title(' Bifurcation diagram of $\epsilon$ and $\beta$', 'Interpreter', '
        Latex', 'fontsize', 20)
301 grid on
302 name5=sprintf('Bifurcation_diagram_of_epsilon_and_beta_grid_points');
```

```

303 print(h5, '-dpdf', name5);
304 hold off
305 h6=figure(6);
306 axis([min_epsilon max_epsilon min_beta max_beta]);% defining the total
      length of the points for epsilon and beta
307 hold on;
308 plot(ALL_POINTS_RIGID_ROTATION(:,1), ALL_POINTS_RIGID_ROTATION(:,2), '.g', '
      MarkerSize', 15)
309 plot(ALL_POINTS_MEANDER(:,1), ALL_POINTS_MEANDER(:,2), '.b', 'MarkerSize'
      ,15)
310 plot(All_POINTS_UNSTABLE_SOLUTION(:,2), All_POINTS_UNSTABLE_SOLUTION(:,3),
      '.r', 'MarkerSize', 15)
311 plot(ALL_POINTS_CRASHED_SOLUTION(:,2), ALL_POINTS_CRASHED_SOLUTION(:,3), '.
      k', 'MarkerSize', 15)
312 set(gca, 'XTick', min(epsilon_values):0.05:max(epsilon_values), 'YTick',
      min(beta_values):0.1:max(beta_values));
313 set(gca, 'XScale', 'log');
314 set(gca, 'XAxisLocation', 'bottom', 'xdir', 'reverse', 'YAxisLocation', 'left',
      'ydir', 'reverse');
315 xlabel(' $\epsilon$', 'Interpreter', 'Latex', 'fontsize', 13)
316 ylabel(' $\beta$', 'Interpreter', 'Latex', 'fontsize', 13, 'Rotation', 360)
317 title(' Bifurcation diagram of $\epsilon$ and $\beta$', 'Interpreter', '
      Latex', 'fontsize', 20)
318 grid on
319 name6=sprintf('
      Bifurcation_diagram_of_epsilon_and_beta_grid_points_crashed_solution_with_boundary
      ');
320 print(h6, '-dpdf', name6);

```

```
321 hold off

1 function [ initial_conditionu1 ,initial_conditionv1 ] =
    INITIAL_CONDITION_EPSILON_BETA_IMPLICIT_CORRECTED_1( alpha ,epsilon ,
    beta ,timestep ,spacestepx ,totallengthx ,finaltime_intial)

2 %% numerical parameters
3 spacestepy =spacestepx; % space step for y axis
4 totallengthy=totallengthx; % total length of y axis
5 gridx =0:spacestepx:totallengthx;
6 gridy =0:spacestepy:totallengthy;
7 Nx=length(gridx)+2; % the number of grid points for x axis
8 Ny=length(gridy)+2; % the number of grid points for y axis
9 imin=2; % the smallest index on x axis
10 imax=Nx-1; % the biggest index on x axis
11 jmin=2; % the smallest index on y axis
12 jmax=Ny-1; % the biggest index on y axis
13 timegrid = 0:timestep:finaltime_intial;
14 M=length(timegrid); % the biggest index for time
15 %% equilibrium point
16 delta = (3/alpha)-3;
17 rho=(3*beta)/alpha;
18 k1=-rho/2;
19 k2=((rho^(2)/4)+(delta^(3)/27))^(1/2);
20 k3=rho/2;
21 k1sk2=k1+k2;
22 k3sk2=k3+k2;
23 constantu=(k1sk2)^(1/3)-(k3sk2)^(1/3);
24 constantv=(constantu+beta)/alpha;
25 %% set up results storage
```

```

26 u = zeros(Nx,Ny);
27 v = zeros(Nx,Ny);
28 %% Barkley initial condition
29 for i=imin:imax
30     for j=jmin:jmax
31         if((i<=(imax/2)))
32             u(i,j)=-constantu;
33         else
34             u(i,j)=constantu;
35         end
36         if ((j<=jmax/2))
37             v(i,j)=-constantv;
38         else
39             v(i,j)=constantv;
40         end
41     end
42 end
43
44 number_plot=floor(M/ finaltime_intial);
45 %% Calculating sparse coefficient matrix of diffusion by implicit scheme
46 coefficient_matrix_i=sparse(2:Nx-2,1:Nx-3,1,Nx-2,Nx-2);
47 matrix_i=coefficient_matrix_i+coefficient_matrix_i'-2*speye(Nx-2);
48 matrix_i(1,1)=-1;
49 matrix_i(Nx-2,Nx-2)=-1;
50 coefficient_matrix_j=sparse(2:Ny-2,1:Nx-3,1,Ny-2,Ny-2);
51 matrix_j=coefficient_matrix_j+coefficient_matrix_j'-2*speye(Ny-2);
52 matrix_j(1,1)=-1;
53 matrix_j(Ny-2,Ny-2)=-1;

```

```
54 A=kron(matrix_i/spacestepx^2,speye(Nx-2))+kron(speye(Ny-2),matrix_j/  
    spacestepy^2);  
55 % S matrix must be inverted to timestep the diffusion problem  
56 S=speye((Nx-2)*(Ny-2))-timestep*A;  
57 u(:,1)=[];u(:,end)=[];u(1,:)=[];u(end,:)=[];  
58 v(:,1)=[];v(:,end)=[];v(1,:)=[];v(end,:)=[];  
59 %% numerical solver  
60 for m=1:M-1  
61     % convert into column vector  
62     u=reshape(u,[],1);  
63     % solve the linear problem  
64     u=S\u;  
65     u=reshape(u,Nx-2,Ny-2);  
66     % add back on edges  
67     u(1:Nx-2,1:Ny-2)=u;  
68     % Reaction function  
69     fu=(u-u.^3/3-v)/epsilon;  
70     fv=epsilon*(u-alpha*v+beta*ones(size(u)));  
71     % Explicit Euler update  
72     u=u+timestep*fu;  
73     v=v+timestep*fv;  
74     if (mod(m+1,number_plot)==0)  
75         figure(1);  
76         time=timegrid(m+1);  
77         imagesc(gridx,gridy,u)  
78         set(gca, 'YDir', 'normal');  
79         title(sprintf(' The initial spiral wave in two dimesions for u, t  
            =%g',time));
```

```

80     shading interp
81     xlabel('x')
82     ylabel('y')
83     colorbar
84     drawnow
85     end
86 end
87 initial_conditionu1=u;
88 initial_conditionv1=v;
89 save('initial_conditionu1.dat','initial_conditionu1','-ascii')
90 save('initial_conditionv1.dat','initial_conditionv1','-ascii')
91 end

1 function [u,v,intersection ,intersection_x_y]= THE_NUMERICAL_SOLVER_1(
    alpha ,epsilon ,beta , u,v, isoline_level_u ,totallengthx ,spacestepx ,
    timestep)
2 spacestepy =spacestepx;
3 totallengthy=totallengthx;
4 gridx =0:spacestepx:totallengthx;
5 gridy =0:spacestepy:totallengthy;
6 Nx=length(gridx)+2;
7 Ny=length(gridy)+2;
8 %Calculating sparse coefficient matrix of diffusion by implicit scheme
9 coefficient_matrix_i=sparse(2:Nx-2,1:Nx-3,1,Nx-2,Nx-2);
10 matrix_i=coefficient_matrix_i+coefficient_matrix_i'-2*speye(Nx-2);
11 matrix_i(1,1)=-1;
12 matrix_i(Nx-2,Nx-2)=-1;
13 coefficient_matrix_j=sparse(2:Ny-2,1:Nx-3,1,Ny-2,Ny-2);
14 matrix_j=coefficient_matrix_j+coefficient_matrix_j'-2*speye(Ny-2);

```

```
15 matrix_j(1,1)=-1;
16 matrix_j(Ny-2,Ny-2)=-1;
17 A=kron(matrix_i/spacstepx^2,speye(Nx-2))+kron(speye(Ny-2),matrix_j/
    spacstepy^2);
18 % S matrix must be inverted to timestep the diffusion problem
19 S=speye((Nx-2)*(Ny-2))-timestep*A;
20 % convert into column vector
21 u=reshape(u,[],1);
22 % solve the linear problem
23 u=S\u;
24 u=reshape(u,Nx-2,Ny-2);
25 % add back on edges
26 u(1:Nx-2,1:Ny-2)=u;
27 % Reaction function
28 fu=(u-u.^3/3-v)/epsilon;
29 fv=epsilon*(u-alpha*v+beta*ones(size(u))));
30 % Explicit Euler update
31 u=u+timestep*fu;
32 v=v+timestep*fv;
33 [matrix_isoline_zero_u,h_u]=contour(gridx,gridy,u,[isoline_level_u,
    isoline_level_u]); % finding Cartesian coordinates (x,y) of u
    component for isoline zero
34 trans_matrix_isoline_zero_u=matrix_isoline_zero_u'; % transpose
    matrix_isoline_zero_u as column vector
35 set(h_u,'EdgeColor','none');
36 matrix_trans_matrix_isoline_zero_u=zeros(length(matrix_isoline_zero_u
    (:,1)),2);
37 index_removing=1; % the number of indexes for isoline of v compnent
```

```

38 for i=1:length(matrix_isoline_zero_u(1,:))
39     if(( (trans_matrix_isoline_zero_u(i,1)~=0 )&&(
        trans_matrix_isoline_zero_u(i,2)~=0 ) ))
40         matrix_trans_matrix_isoline_zero_u(index_removing,:)=
            trans_matrix_isoline_zero_u(i,:); % finding all values of v
            component for all isolines except zero isoline
41         index_removing=index_removing+1; % the index for next row for
            matrix matrix_isoline_zero_v
42     end
43 end
44 matrix_trans_matrix_isoline_zero_u(index_removing:end,:)=[];
45
46
47 [all_v , h_v_all]=contour(gridx , gridy , v); % finding Cartesian coordinates (
        x,y) of v component
48 %clabel(all_v , h_v_all)
49 set(h_v_all , 'EdgeColor' , 'none');
50 size_all_v = size(all_v , 2);
51 initial_i_v = 1;
52 initial_j_v = 1;
53 s_v = struct('v' , 'x' , 'y' , ...
54     {zeros(size_all_v , 1)}); % the structure for matrix s_v
55 while initial_i_v < size_all_v      % While we haven't exhausted the
        array
56     n = all_v(2, initial_i_v);      % How many points in this contour?
57     s_v(initial_j_v).v = all_v(1, initial_i_v);      % Value of the
        contour
58     s_v(initial_j_v).x = all_v(1, initial_i_v+1:initial_i_v+n); % X

```

```
        coordinates
59     s_v(initial_j_v).y = all_v(2,initial_i_v+1:initial_i_v+n); % Y
        coordinates
60     value_x_y_v(initial_i_v:initial_i_v+n,1)=all_v(1,initial_i_v:
        initial_i_v+n);
61     value_x_y_v(initial_i_v:initial_i_v+n,2)=all_v(2,initial_i_v:
        initial_i_v+n);
62     value_x_y_v(initial_i_v:initial_i_v+n,3)=s_v(initial_j_v).v;
63     initial_i_v = initial_i_v + n+1 ;           % Skip ahead to next
        contour line
64     initial_j_v = initial_j_v +1;           % Increment number of
        contours
65 end
66 matrix_points_value_v=zeros(size_all_v,9); % storage for all values of v
        component corresponding to isoline of u component
67 index_removing=1; % the number of indexes for isoline of v component
68 %% finding value of v component corresponding to isoline of u component
69 for i=2:length(matrix_trans_matrix_isoline_zero_u(:,1))-3
70     x_value_u=matrix_trans_matrix_isoline_zero_u(i,1);
71     y_value_u=matrix_trans_matrix_isoline_zero_u(i,2);
72     for j=2:(Nx-3);
73         if((gridx(j-1)<x_value_u )&&(x_value_u<gridx(j+1) ))
74             for k=2:(Ny-3)
75                 if ((gridy(k-1)<y_value_u )&&(y_value_u<gridy(k+1) ))
76                     matrix_points_value_v(index_removing,:)=[gridx(j-1),
77                         x_value_u,gridx(j+1),k, gridy(k-1),y_value_u,gridy
78                         (k+1),j ,v(k,j) ];
79                     index_removing=index_removing+1;
```

```

78         end
79     end
80 end
81 end
82 end
83 matrix_points_value_v(index_removing:end,:)=[]; % removing all zero
      values in matrix
84 %% ordering all all values of v component
85 [value_v,index_v]=sort( matrix_points_value_v(:,9));
86 order_matrix_points_value_u=matrix_points_value_v(index_v,:);
87 %% finding different sign of value of v component
88 for i=1:(length(value_v)-1)
89     v_value=order_matrix_points_value_u(i,9);
90     v_value_f=order_matrix_points_value_u(i+1,9);
91     if((v_value<0)&&(v_value_f>0))
92         value_v_points=[order_matrix_points_value_u(i-2:i,:);
93             order_matrix_points_value_u(i+1:i+3,:)];
94     end
95
96 end
97 %% checking the previous value of x or y is not equal to next value of x
      or y
98 for i=1:length(value_v_points)-3
99     index_b=3-(i-1);
100    index_f=4+(i-1);
101    b_x_u=value_v_points(index_b,2); % previous value x on isoline for u
      component

```

```
102     b_y_u=value_v_points(index_b,6); % previous value y on isoline for u
        component
103     f_x_u=value_v_points(index_f,2); % next value x on isoline for u
        component
104     f_y_u=value_v_points(index_f,6); % next value y on isoline for u
        component
105     if((b_x_u~=f_x_u)&&(b_y_u~=f_y_u))
106         value_v_points=[value_v_points(index_b,:);value_v_points(index_f
            ,:)] ;
107         break
108     end
109
110 end
111 b_x_u=value_v_points(1,2); % previous value x on isoline for u component
112 b_y_u=value_v_points(1,6); % previous value y on isoline for u component
113 f_x_u=value_v_points(2,2); % next value x on isoline for u component
114 f_y_u=value_v_points(2,6); % next value y on isoline for u component
115 interpolation_function_v = scatteredInterpolant(value_x_y_v(:,1),
        value_x_y_v(:,2),value_x_y_v(:,3),'linear'); % the interpolation
        function for v component
116 value_v_b=interpolation_function_v(b_x_u,b_y_u); % value of v component
        for previous point ( b_x_u,b_y_u)
117 value_v_f=interpolation_function_v(f_x_u,f_y_u); % value of v component
        for previous point ( b_x_u,b_y_u)
118 x_tip=-value_v_f*(( f_x_u-b_x_u )/( value_v_f-value_v_b ) )+f_x_u; %
        spiral wave tip for x
119 y_tip=-value_v_f*(( f_y_u-b_y_u )/( value_v_f-value_v_b ) )+f_y_u; %
        spiral wave tip for y
```

```

120 intersection=[x_tip , y_tip ; x_tip , y_tip ]; % matrix of spiral wave tip (
        x_tip , y_tip )
121 intersection_x_y=[x_tip , y_tip ]; % matrix of spiral wave tip ( x_tip , y_tip )
122
123 end

1 function t_figure = PLOTTING_DIAGRAM_SPIRAL_WAVE_1( gridx , gridy , u,
        numerical_intersection , time , index_removed_end )
2 %% plot figure for u component
3 figure(3);
4 imagesc(gridx , gridy , u)
5 line(numerical_intersection(1:index_removed_end , 1) , numerical_intersection
        (1:index_removed_end , 2) , 'Color' , 'w' , 'LineWidth' , 2);
6 set(gca , 'YDir' , 'normal');
7 title(sprintf(' The spiral wave solution for u component, t=%g' , time));
8 shading interp
9 xlabel('x')
10 ylabel('y')
11 colorbar
12 drawnow
13 t_figure=time;
14 end

1 function curvature_K = CURVATURE_FUNCTION_3( time_numerical_intersection ,
        n_index_removed )
2 rows_intersec = length(time_numerical_intersection(1:n_index_removed , :));
3 %% using central difference method
4 matrix_t_intersection=zeros(rows_intersec , 3);
5 accountor=1; % the number of iteration

```

```
6 for i=rows_intersec:-1:2
7     time_1=floor(time_numerical_intersection(i,1));
8     time_2=floor(time_numerical_intersection(i+1,1));
9     if(time_1~=time_2)
10         matrix_t_intersection(accountor,:)= time_numerical_intersection(i
            ,:);
11         accountor=accountor+1;
12     end
13     if(accountor>=4)% condition for stop points for tip trajectory of
        spiral wave
14         break
15     end
16 end
17 x_tip_b = matrix_t_intersection(3,2);
18 x_tip_m =matrix_t_intersection(2,2);
19 x_tip_f = matrix_t_intersection(1,2);
20 y_tip_b = matrix_t_intersection(3,3);
21 y_tip_m = matrix_t_intersection(2,3);
22 y_tip_f = matrix_t_intersection(1,3);
23 numerator=8*(x_tip_b*y_tip_m-x_tip_b*y_tip_f-x_tip_f*y_tip_m...
24     +x_tip_f*y_tip_b-x_tip_m*y_tip_b+x_tip_m*y_tip_f);
25 denominator=( ( x_tip_f-x_tip_b
                    )^2+( y_tip_f-y_tip_b
                    )^2
                )^(3/2);
26 %% the value of signed curvature K
27 curvature_K=numerator/ denominator;
28
29 end

1 function [ h3,h4 ] = PRINTING_FIG_SAVEING_DATA_2(
```

```

        time_numerical_intersection , u, epsilon , beta , gridx , gridy , n_index_removed
    )
2 %% plot spiral wave solution with tip trajectory
3 h3=figure(3);
4 imagesc(gridx , gridy , u)
5 line(time_numerical_intersection(1:n_index_removed , 2) ,
        time_numerical_intersection(1:n_index_removed , 3) , 'Color' , 'w' , '
        LineWidth' , 2);
6 set(gca , 'YDir' , 'normal');
7 %title(sprintf(' spiral wave in two dimesions with tip path , t=%g' , time))
    ;
8 xlabel( 'x' )
9 ylabel( 'y' )
10 colorbar
11 drawnow
12 name3=[ 'non_linear_sysem_implicit_epsilon_' num2str(epsilon) '_beta_'
        num2str(beta) ];
13 print(h3 , '-dpdf' , name3);
14 close all
15 %% plot spiral wave tip
16 h4=figure(4);
17 line(time_numerical_intersection(1:n_index_removed , 2) ,
        time_numerical_intersection(1:n_index_removed , 3) , 'Color' , 'black' , '
        LineStyle' , '-' , 'LineWidth' , 20)
18 set(gca , 'YDir' , 'normal');
19 set(gca , 'xcolor' , 'w' , 'ycolor' , 'w' , 'xtick' , [] , 'ytick' , []);
20 get(gca , 'children');
21 set(gcf , 'color' , 'w');

```

```
22 xlabel('x')
23 ylabel('y')
24 drawnow
25 name4=[ 'diagarm_of_tip_trajectory_epsilon_' num2str(epsilon) '_beta_'
          num2str(beta) ];
26 print(h4, '-dpdf', name4);
27 save([name4, '.dat'], 'time_numerical_intersection', '-ascii');
28 end
```

ALGORITHM OF SEMI-IMPLICIT METHOD FOR THE FITZHUGH-NAGUMO MODEL

In this section, we present the loop (Algorithm) to solve the FHN system (2.1) numerically using the semi-implicit method. By looking at the equation (2.1), we can apply the fully implicit method (backward Euler method) for the diffusion term using the sparse matrix that only contains nonzero elements, whereas we use the fully explicit method (forward Euler method) for the kinetic function, that is

$$\mathbf{U}^{m+1} = \mathbf{U}^m + \Delta t g(\mathbf{U}^m, \mathbf{V}^m) + \Delta t \mathbf{S} \mathbf{U}^{m+1}, \quad (\text{B.1})$$

$$\mathbf{V}^{m+1} = \mathbf{V}^m + \Delta t h(\mathbf{U}^m, \mathbf{V}^m), \quad (\text{B.2})$$

where $\mathbf{U}, \mathbf{V} \in \mathbb{R}^{n^2}$, $\mathbf{S} \in \mathbb{R}^{n^2 \times n^2}$ such that $n \in \mathbb{N}$ and Δt is time step. By arranging (B.1), we derive that

$$\mathbf{U}^{m+1} = (\mathbf{I} - \Delta t \mathbf{S})^{-1} \left(\mathbf{U}^m + \Delta t g(\mathbf{U}^m, \mathbf{V}^m) \right), \quad (\text{B.3})$$

where \mathbf{I} is identity matrix of size $n^2 \times n^2$. Since $\mathbf{I} - \Delta t \mathbf{S}$ is a sparse matrix, we will use a sparse matrix solver in Matlab to solve the equation (B.3). By reshaping the vector \mathbf{U}^{m+1} and \mathbf{V}^{m+1} as matrix, we can find the numerical solution for components u and v . In order to understand

APPENDIX B. ALGORITHM OF SEMI-IMPLICIT METHOD FOR THE FITZHUGH-NAGUMO MODEL

the explanation of the algorithm of the solution for the FHN system (2.1b), the Matlab code is provided below:

```
1 close all
2 clear all;
3 clc;
4 tic;
5 epsilon=0.30;
6 alpha=0.5;
7 beta=0.75;
8 timestep =0.1;
9 spacestepx = 0.30;
10 spacestepy =spacestepx;
11 totallengthx=40.0;
12 totallengthy=40.0;
13 gridx =0:spacestepx:totallengthx;
14 gridy =0:spacestepy:totallengthy;
15 Nx=length(gridx)+2;
16 Ny=length(gridy)+2;
17 imin=2;
18 imax=Nx-1;
19 ii=imin:imax;
20 jmin=2;
21 jmax=Ny-1;
22 jj=jmin:jmax;
23 finaltime=26;
24 timegrid = 0:timestep:finaltime;;
25 M=length(timegrid);
26 delta = (3/alpha)-3;
```

```

27 rho=(3*beta)/alpha;
28 k1=-rho/2;
29 k2=((rho^(2)/4)+(delta^(3)/27))^(1/2);
30 k3=rho/2;
31 k1sk2=k1+k2;
32 k3sk2=k3+k2;
33 %equilibrium point
34 constantu=(k1sk2)^(1/3)-(k3sk2)^(1/3);
35 constantv=(constantu+beta)/alpha;
36 methodimplicit=true; % true for implicit, false for explicit
37 u = zeros(Nx,Ny);
38 v = zeros(Nx,Ny);
39 fu = zeros(Nx,Ny);
40 fv = zeros(Nx,Ny);
41 for i=imin:imax
42     for j=jmin:jmax
43         if((i<=(imax./2)))
44             u(i,j)=-constantu;
45         else
46             u(i,j)=constantu;
47         end
48         if((j<=jmax./2))
49             v(i,j)=-constantv;
50         else
51             v(i,j)=constantv;
52         end
53     end
54 end

```

APPENDIX B. ALGORITHM OF SEMI-IMPLICIT METHOD FOR THE
FITZHUGH-NAGUMO MODEL

```

55 %Calculating sparse coefficient matrix of diffusion by implicit scheme
56 coefficient_matrix_i=sparse(2:Nx-2,1:Nx-3,1,Nx-2,Nx-2);
57 matrix_i=coefficient_matrix_i+coefficient_matrix_i'-2*speye(Nx-2);
58 matrix_i(1,1)=-1;
59 matrix_i(Nx-2,Nx-2)=-1;
60 coefficient_matrix_j=sparse(2:Ny-2,1:Nx-3,1,Ny-2,Ny-2);
61 matrix_j=coefficient_matrix_j+coefficient_matrix_j'-2*speye(Ny-2);
62 matrix_j(1,1)=-1;
63 matrix_j(Ny-2,Ny-2)=-1;
64 A=kron(matrix_i/spacstepx^2,speye(Nx-2))+kron(speye(Ny-2),matrix_j/
        spacstepy^2);
65 % S matrix must be inverted to timestep the diffusion problem
66 S=speye((Nx-2)*(Ny-2))-timestep*A;
67 number_plot=floor(M/7);
68 for m=1:M-1
69     m
70     U=u(ii , jj);
71     % convert into column vector
72     U=reshape(U,[],1);
73     % solve the linear problem
74     U=S\U;
75     U=reshape(U,Nx-2,Ny-2);
76     % add back on edges
77     u(2:Nx-1,2:Ny-1)=U;
78     % Reaction function
79     fu(ii , jj)=(u(ii , jj)-u(ii , jj).^3/3-v(ii , jj))/epsilon;
80     fv(ii , jj)=epsilon*(u(ii , jj)-alpha*v(ii , jj)+beta*ones(size(u(ii , jj))))
        ;

```

```

81  % Explicit Euler update
82  u(ii , jj)=u(ii , jj)+timestep*fu(ii , jj);
83  v(ii , jj)=v(ii , jj)+timestep*fv(ii , jj);
84  if (mod(m+1,number_plot)==0)
85      h1=figure(1);
86      time=timegrid(m+1);
87      imagesc(gridx , gridy , u(ii , jj))
88      %          shading interp
89      set(gca , 'YDir' , 'normal');
90      %set(gca , 'YDir' , 'reverse')
91      %    set(gca , 'YTickLabel' , []);
92      %    set(gca , 'XTickLabel' , []);
93      title(sprintf(' The initial spiral wave in two dimesions for u, t
          =%g' , time));
94      shading interp
95      xlabel('x')
96      ylabel('y')
97      colorbar
98      drawnow
99      %    name1=sprintf('non_linear_sysem_%d' , m);
100     %    print(h1 , '-dpdf' , name1);
101     end
102 end
103 toc;
104 initialnonlinearuv=[u(ii , jj) , v(ii , jj)];
105 save('initialnonlinearuv.dat' , 'initialnonlinearuv' , '-ascii')
106 initial_conditionu1=u(ii , jj);
107 initial_conditionv1=v(ii , jj);

```

APPENDIX B. ALGORITHM OF SEMI-IMPLICIT METHOD FOR THE
FITZHUGH-NAGUMO MODEL

```
108 save( 'initial_conditionu1.dat', 'initial_conditionu1', '-ascii' )
109 save( 'initial_conditionv1.dat', 'initial_conditionv1', '-ascii' )
110 save( 'initialnonlinearuv.mat', 'initial_conditionu1', 'initial_conditionv1'
        );

1 close all
2 clear;
3 clc;
4 epsilon=0.30;
5 alpha=0.5;
6 beta=0.75;
7 timestep =0.1;
8 spacestepx =0.30;
9 spacestepy =spacestepx;
10 totallengthx=40.0;
11 totallengthy=totallengthx;
12 gridx =0:spacestepx:totallengthx;
13 gridy =0:spacestepy:totallengthy;
14 Nx=length(gridx)+2;
15 Ny=length(gridy)+2;
16 imin=2;
17 imax=Nx-1;
18 ii=imin:imax;
19 jmin=2;
20 jmax=Ny-1;
21 jj=jmin:jmax;
22 finaltime=25;
23 timegrid = 0:timestep:finaltime;;
24 M=length(timegrid);
```

```

25 isoline_level_u=0;
26 isoline_level_v=0;
27 intersection_x_y=[];
28 u = zeros(Nx,Ny);
29 v = zeros(Nx,Ny);
30 fu = zeros(Nx,Ny);
31 fv = zeros(Nx,Ny);
32 numerical_intersection=[];
33 time_numerical_intersection=[];
34 load('initial_conditionu1.dat');
35 load('initial_conditionv1.dat');
36 u(ii ,jj)=initial_conditionu1;
37 v(ii ,jj)=initial_conditionv1;
38 contour(gridx ,gridy ,u(ii ,jj))
39 %Calculating sparse coefficient matrix of diffusion by implicit scheme
40 coefficient_matrix_i=sparse(2:Nx-2,1:Nx-3,1,Nx-2,Nx-2);
41 matrix_i=coefficient_matrix_i+coefficient_matrix_i'-2*speye(Nx-2);
42 matrix_i(1,1)=-1;
43 matrix_i(Nx-2,Nx-2)=-1;
44 coefficient_matrix_j=sparse(2:Ny-2,1:Nx-3,1,Ny-2,Ny-2);
45 matrix_j=coefficient_matrix_j+coefficient_matrix_j'-2*speye(Ny-2);
46 matrix_j(1,1)=-1;
47 matrix_j(Ny-2,Ny-2)=-1;
48 A=kron(matrix_i/spacestepx^2,speye(Nx-2))+kron(speye(Ny-2),matrix_j/
    spacestepy^2);
49 % S matrix must be inverted to timestep the diffusion problem
50 S=speye((Nx-2)*(Ny-2))-timestep*A;
51 number_plot=floor(M/50);

```

APPENDIX B. ALGORITHM OF SEMI-IMPLICIT METHOD FOR THE
FITZHUGH-NAGUMO MODEL

```

52 iterat_m=0;
53 for m=1:M-1
54     m
55     U=u(ii , jj);
56     % convert into column vector
57     U=reshape(U,[],1);
58     % solve the linear problem
59     U=S\U;
60     U=reshape(U,Nx-2,Ny-2);
61     % add back on edges
62     u(ii , jj)=U;
63     % Reaction function
64     fu(ii , jj)=(u(ii , jj)-u(ii , jj).^3/3-v(ii , jj))/epsilon;
65     fv(ii , jj)=epsilon*(u(ii , jj)-alpha*v(ii , jj)+beta*ones(size(u(ii , jj))))
        ;
66     % Explicit Euler
67     u(ii , jj)=u(ii , jj)+timestep*fu(ii , jj);
68     v(ii , jj)=v(ii , jj)+timestep*fv(ii , jj);
69     if (mod(m+1,number_plot)==0);
70         ml=m
71         t=timegrid(m+1);
72         [matrix_isoline_zero_u , h_u]=contour(gridx , gridy , u(ii , jj) , [
            isoline_level_u , isoline_level_u]);
73         trans_matrix_isoline_zero_u=matrix_isoline_zero_u';
74         clabel(trans_matrix_isoline_zero_u , h_u)
75         set(h_u , 'EdgeColor' , 'none');
76         [all_v , h_v_all]=contour(gridx , gridy , v(ii , jj));
77         clabel(all_v , h_v_all)

```

```

78     set(h_v_all, 'EdgeColor', 'none');
79     intersection = FUNCTION_MORE_ACCURATE_TIP_1(
           trans_matrix_isoline_zero_u, all_v );
80     numerical_intersection=[numerical_intersection; intersection];
81     iterat_m = 2+iterat_m;
82     h1=figure(1);
83     time=timegrid(m+1);
84     imagesc(gridx, gridy, u(ii, jj))
85     line(numerical_intersection(1:iterat_m, 1), numerical_intersection
           (1:iterat_m, 2), 'Color', 'w', 'LineWidth', 2);
86     shading interp
87     set(gca, 'YDir', 'normal');
88     %set(gca, 'YDir', 'reverse')
89     % set(gca, 'YTickLabel', []);
90     % set(gca, 'XTickLabel', []);
91     % title(sprintf(' spiral wave in two dimesions for u, t=%g',
           time));
92     xlabel('x')
93     ylabel('y')
94     colorbar
95     drawnow
96     name1=sprintf(' non_linear_sysem_%d', m);
97     print(h1, '-dpdf', name1);
98     end
99 end
100 % save('numerical_intersection030075.dat', 'numerical_intersection', '-
       ascii')

```

APPENDIX B. ALGORITHM OF SEMI-IMPLICIT METHOD FOR THE
FITZHUGH-NAGUMO MODEL

```

1 function intersection = FUNCTION_MORE_ACCURATE_TIP_1(
    trans_matrix_isoline_zero_u , all_v )
2 size_all_v = size(all_v ,2);
3 initial_i_v = 1;
4 initial_j_v = 1;
5 while initial_i_v < size_all_v      % While we haven't exhausted the
    array
6     n = all_v(2,initial_i_v);      % How many points in this contour?
7     s_v(initial_j_v).v = all_v(1,initial_i_v);      % Value of the
    contour
8     s_v(initial_j_v).x = all_v(1,initial_i_v+1:initial_i_v+n); % X
    coordinates
9     s_v(initial_j_v).y = all_v(2,initial_i_v+1:initial_i_v+n); % Y
    coordinates
10    value_x_y_v(initial_i_v:initial_i_v+n,1)=all_v(1,initial_i_v:
    initial_i_v+n);
11    value_x_y_v(initial_i_v:initial_i_v+n,2)=all_v(2,initial_i_v:
    initial_i_v+n);
12    value_x_y_v(initial_i_v:initial_i_v+n,3)=s_v(initial_j_v).v;
13    initial_i_v = initial_i_v + n+1 ;      % Skip ahead to next
    contour line
14    initial_j_v = initial_j_v +1;      % Increment number of
    contours
15 end
16 matrix_isoline_zero_v=[];
17 for i=1:size_all_v
18     if((value_x_y_v(i,3)==0)&( (value_x_y_v(i,1)~=0 )&(value_x_y_v(i,2)
    ~=0 ) ))

```

```

19         matrix_isoline_zero_v=[matrix_isoline_zero_v;value_x_y_v(i,:)];
20     end
21 end
22 row_u=length(trans_matrix_isoline_zero_u(:,1));
23 row_v=length(matrix_isoline_zero_v(:,1)');
24 min_distance =sqrt((matrix_isoline_zero_v(floor(row_v),1) -
        trans_matrix_isoline_zero_u(floor(row_u/2),1))^2+(
        matrix_isoline_zero_v(floor(row_v/2),2) - trans_matrix_isoline_zero_u(
        floor(row_u),2))^2);
25 for i=1:row_u
26     for j=1:row_v
27         if( ((trans_matrix_isoline_zero_u(i,1)~=0)&(
                trans_matrix_isoline_zero_u(i,2)~=0)) &( (
                matrix_isoline_zero_v(j,1)~=0) &(matrix_isoline_zero_v(j,2)
                ~=0) ) )
28             distance =sqrt((matrix_isoline_zero_v(j,1) -
                trans_matrix_isoline_zero_u(i,1))^2+(matrix_isoline_zero_v
                (j,2) - trans_matrix_isoline_zero_u(i,2))^2);
29             if(distance<min_distance)
30                 index_i=i;
31                 index_j=j;
32                 min_distance= distance;
33                 matrix_u_v_x_y=[index_i ,trans_matrix_isoline_zero_u(i
                    ,1:2) ,index_j ,matrix_isoline_zero_v(j,1:2) ,
                    min_distance];
34             end
35         end
36     end

```

APPENDIX B. ALGORITHM OF SEMI-IMPLICIT METHOD FOR THE
FITZHUGH-NAGUMO MODEL

```
37 end
38 b_x_u=trans_matrix_isoline_zero_u(index_i-1,1);
39 b_y_u=trans_matrix_isoline_zero_u(index_i-1,2);
40 x_u=matrix_u_v_x_y(1,2);
41 y_u= matrix_u_v_x_y(1,3);
42 f_x_u=trans_matrix_isoline_zero_u(index_i+1,1);
43 f_y_u=trans_matrix_isoline_zero_u(index_i+1,2);
44 x_v=matrix_u_v_x_y(1,5);
45 y_v=matrix_u_v_x_y(1,6);
46 interpolation_function_v = scatteredInterpolant(value_x_y_v(:,1),
         value_x_y_v(:,2),value_x_y_v(:,3), 'linear');
47 value_v_b=interpolation_function_v(b_x_u,b_y_u);
48 value_v_f=interpolation_function_v(f_x_u,f_y_u);
49 x_tip=-value_v_f*(( f_x_u-b_x_u )/( value_v_f-value_v_b ) )+f_x_u;
50 y_tip=-value_v_f*(( f_y_u-b_y_u )/( value_v_f-value_v_b ) )+f_y_u;
51 intersection=[x_tip , y_tip ; x_tip , y_tip ];
52 end
```


FINDING THE MINIMUM DISTANCE TO THE HYPERPLANE

In this appendix, we show how to compute the coefficients α_k of formula (3.49) in general case of k vectors such that $k \in \mathbb{N}$. Assume that we have a vector space \mathbb{R}^n such that $n \in \mathbb{N}$, so suppose that we have set S of vectors in \mathbb{R}^n , that is

$$S = \{\mathbf{v}_1, \dots, \mathbf{v}_k\} \subset \mathbb{R}^n, \quad k \in \mathbb{N}, k < n$$

where

$$\mathbf{v}_1 = \begin{bmatrix} v_1^1 \\ v_2^1 \\ v_3^1 \\ \vdots \\ v_{n-2}^1 \\ v_{n-1}^1 \\ v_n^1 \end{bmatrix}, \dots, \mathbf{v}_k = \begin{bmatrix} v_1^k \\ v_2^k \\ v_3^k \\ \vdots \\ v_{n-2}^k \\ v_{n-1}^k \\ v_n^k \end{bmatrix},$$

so these vectors $\mathbf{v}_1, \dots, \mathbf{v}_k$ can be linearly independent if vectors $\mathbf{v}_1, \dots, \mathbf{v}_k$ are formulated as follows

$$\alpha_1 \mathbf{v}_1 + \dots + \alpha_k \mathbf{v}_k = \mathbf{0}, \quad \alpha_1, \dots, \alpha_k \in \mathbb{R},$$

such that $\alpha_1 \mathbf{v}_1 + \dots + \alpha_k \mathbf{v}_k$ is called the linear combination, then

$$\alpha_1 = \dots = \alpha_k = 0.$$

Moreover, suppose that we have the vector \mathbf{x} , that is,

$$\mathbf{x} = \begin{bmatrix} x_1 \\ x_2 \\ x_3 \\ \vdots \\ x_{n-2} \\ x_{n-1} \\ x_n \end{bmatrix}, \quad x_i \in \mathbb{R}, \forall i \in \{1, \dots, n\}.$$

We can find the error or distance between the vectors \mathbf{x} and $\alpha_1 \mathbf{v}_1 + \dots + \alpha_k \mathbf{v}_k$ through using the Euclidean norm in \mathbb{R}^n , that is,

$$\begin{aligned} \|\mathbf{x} - (\alpha_1 \mathbf{v}_1 + \dots + \alpha_k \mathbf{v}_k)\|_2 &= \|\mathbf{x} - \alpha_1 \mathbf{v}_1 - \dots - \alpha_k \mathbf{v}_k\|_2 \\ &= \sqrt{\langle \mathbf{x} - \alpha_1 \mathbf{v}_1 - \dots - \alpha_k \mathbf{v}_k, \mathbf{x} - \alpha_1 \mathbf{v}_1 - \dots - \alpha_k \mathbf{v}_k \rangle}. \end{aligned} \quad (\text{C.1})$$

By using the square of the equation (C.1), we find that

$$\begin{aligned} \|\mathbf{x} - (\alpha_1 \mathbf{v}_1 + \dots + \alpha_k \mathbf{v}_k)\|_2^2 &= \langle \mathbf{x} - \alpha_1 \mathbf{v}_1 - \dots - \alpha_k \mathbf{v}_k, \mathbf{x} - \alpha_1 \mathbf{v}_1 - \dots - \alpha_k \mathbf{v}_k \rangle \\ &= \left(\mathbf{x} - \alpha_1 \mathbf{v}_1 - \dots - \alpha_k \mathbf{v}_k \right) \cdot \left(\mathbf{x} - \alpha_1 \mathbf{v}_1 - \dots - \alpha_k \mathbf{v}_k \right). \end{aligned} \quad (\text{C.2})$$

By using the property of dot product, we find that the equation (C.2) becomes as follows

$$\begin{aligned}
\|\mathbf{x} - (\alpha_1 \mathbf{v}_1 + \dots + \alpha_k \mathbf{v}_k)\|_2^2 &= (\mathbf{x} - \alpha_1 \mathbf{v}_1 - \dots - \alpha_{k-1} \mathbf{v}_{k-1} - \alpha_k \mathbf{v}_k) \cdot (\mathbf{x} - \alpha_1 \mathbf{v}_1 - \dots - \alpha_{k-1} \mathbf{v}_{k-1} - \alpha_k \mathbf{v}_k) \\
&= \mathbf{x} \cdot \mathbf{x} - 2\alpha_1 \mathbf{x} \cdot \mathbf{v}_1 - \dots - 2\alpha_{k-1} \mathbf{x} \cdot \mathbf{v}_{k-1} - 2\alpha_k \mathbf{x} \cdot \mathbf{v}_k \\
&\quad + \alpha_1^2 \mathbf{v}_1 \cdot \mathbf{v}_1 + 2\alpha_1 \alpha_2 \mathbf{v}_1 \cdot \mathbf{v}_2 + \dots + 2\alpha_1 \alpha_{k-1} \mathbf{v}_1 \cdot \mathbf{v}_{k-1} + 2\alpha_1 \alpha_k \mathbf{v}_1 \cdot \mathbf{v}_k \\
&\quad \vdots \\
&\quad + (\alpha_{k-1})^2 \mathbf{v}_{k-1} \cdot \mathbf{v}_{k-1} + 2\alpha_{k-1} \alpha_k \mathbf{v}_{k-1} \cdot \mathbf{v}_k \\
&\quad + (\alpha_k)^2 \mathbf{v}_k \cdot \mathbf{v}_k.
\end{aligned} \tag{C.3}$$

We observe that the Euclidean norm (C.3) is the function of independent variables $\alpha_1, \dots, \alpha_{k-1}$ and α_k . So suppose that

$$\|\mathbf{x} - (\alpha_1 \mathbf{v}_1 + \dots + \alpha_k \mathbf{v}_k)\|_2^2 = f(\alpha_1, \dots, \alpha_k),$$

where

$$\begin{aligned}
f(\alpha_1, \dots, \alpha_k) &= \langle \mathbf{x}, \mathbf{x} \rangle - 2\alpha_1 \langle \mathbf{x}, \mathbf{v}_1 \rangle - \dots - 2\alpha_{k-1} \langle \mathbf{x}, \mathbf{v}_{k-1} \rangle - 2\alpha_k \langle \mathbf{x}, \mathbf{v}_k \rangle \\
&\quad + \alpha_1^2 \langle \mathbf{v}_1, \mathbf{v}_1 \rangle + 2\alpha_1 \alpha_2 \langle \mathbf{v}_1, \mathbf{v}_2 \rangle + \dots + 2\alpha_1 \alpha_{k-1} \langle \mathbf{v}_1, \mathbf{v}_{k-1} \rangle + 2\alpha_1 \alpha_k \langle \mathbf{v}_1, \mathbf{v}_k \rangle \\
&\quad \vdots \\
&\quad + (\alpha_{k-1})^2 \langle \mathbf{v}_{k-1}, \mathbf{v}_{k-1} \rangle + 2\alpha_{k-1} \alpha_k \langle \mathbf{v}_{k-1}, \mathbf{v}_k \rangle \\
&\quad + (\alpha_k)^2 \langle \mathbf{v}_k, \mathbf{v}_k \rangle.
\end{aligned} \tag{C.4}$$

Assume that these vectors $\mathbf{x}, \mathbf{v}_1, \dots, \mathbf{v}_{k-1}$ and \mathbf{v}_k given, we aim to minimise the function $f(\alpha_1, \dots, \alpha_k)$.

Let us now study the function $f(\alpha_1, \dots, \alpha_k)$ that has a local minimum corresponding with variables $\alpha_1, \alpha_2, \dots, \alpha_{k-1}$ and α_k . By looking at the function f of equation (C.4), suppose that

$$\begin{aligned}
c_{0,0} &= \langle \mathbf{x}, \mathbf{x} \rangle, \quad c_{0,1} = \langle \mathbf{x}, \mathbf{v}_1 \rangle, \dots, c_{0,k-1} = \langle \mathbf{x}, \mathbf{v}_{k-1} \rangle, \quad c_{0,k} = \langle \mathbf{x}, \mathbf{v}_k \rangle \\
c_{1,1} &= \langle \mathbf{v}_1, \mathbf{v}_1 \rangle, \quad c_{1,2} = \langle \mathbf{v}_1, \mathbf{v}_2 \rangle, \dots, \quad c_{1,k-1} = \langle \mathbf{v}_1, \mathbf{v}_{k-1} \rangle, \quad c_{1,k} = \langle \mathbf{v}_1, \mathbf{v}_k \rangle \\
&\quad \vdots \\
c_{k-1,k-1} &= \langle \mathbf{v}_{k-1}, \mathbf{v}_{k-1} \rangle, \quad c_{k-1,k} = \langle \mathbf{v}_{k-1}, \mathbf{v}_k \rangle \\
c_{k,k} &= \langle \mathbf{v}_k, \mathbf{v}_k \rangle,
\end{aligned}$$

so the function f of equation (C.4) can be formulated as follows

$$\begin{aligned}
 f(\alpha_1, \dots, \alpha_k) &= c_{0,0} - 2c_{0,1}\alpha_1 - \dots - 2c_{0,k-1}\alpha_{k-1} - 2c_{0,k}\alpha_k \\
 &\quad + c_{1,1}\alpha_1^2 + 2c_{1,2}\alpha_1\alpha_2 + \dots + 2c_{1,k-1}\alpha_1\alpha_{k-1} + 2c_{1,k}\alpha_1\alpha_k \\
 &\quad \vdots \\
 &\quad + c_{k-1,k-1}\alpha_{k-1}^2 + 2c_{k-1,1}\alpha_{k-1}\alpha_k \\
 &\quad + c_{k,k}\alpha_k^2.
 \end{aligned}$$

By using the complete square method, we assume that

$$\alpha_1 = \beta_1 + \rho_1, \alpha_2 = \beta_2 + \rho_2, \dots, \alpha_{k-1} = \beta_{k-1} + \rho_{k-1}, \alpha_k = \beta_k + \rho_k, \quad (\text{C.5})$$

such that β_i are arbitrary variables, whereas ρ_i are constant such that i is defined as follows

$$i \in \{1, \dots, k\}.$$

By using the equations (C.5), the function $f(\alpha_1, \dots, \alpha_k)$ becomes as follows

$$\begin{aligned}
 \tilde{f}(\beta_1, \dots, \beta_k) &= c_{0,0} - 2c_{0,1}(\beta_1 + \rho_1) - \dots - 2c_{0,k-1}(\beta_{k-1} + \rho_{k-1}) - 2c_{0,k}(\beta_k + \rho_k) \\
 &\quad + c_{1,1}(\beta_1 + \rho_1)^2 + 2c_{1,2}(\beta_1 + \rho_1)(\beta_2 + \rho_2) \\
 &\quad \vdots \\
 &\quad + 2c_{1,k-1}(\beta_1 + \rho_1)(\beta_{k-1} + \rho_{k-1}) + 2c_{1,k}(\beta_1 + \rho_1)(\beta_k + \rho_k) \\
 &\quad \vdots \\
 &\quad + c_{k-1,k-1}(\beta_{k-1} + \rho_{k-1})^2 + 2c_{k-1,1}(\beta_{k-1} + \rho_{k-1})(\beta_k + \rho_k) \\
 &\quad + c_{k,k}(\beta_k + \rho_k)^2.
 \end{aligned} \quad (\text{C.6})$$

If we continue the calculations of the equation (C.6) and also simplify this equation, then we will derive the equation (C.7)

$$\begin{aligned}
\tilde{f}(\beta_1, \dots, \beta_k) &= c_{1,1} \beta_1^2 + (2c_{1,1} \rho_1 + 2c_{1,2} \rho_2 + \dots + 2c_{1,k-1} \rho_{k-1} + 2c_{1,k} \rho_k - 2c_{1,0}) \beta_1 \\
&\quad + c_{2,2} \beta_2^2 + (2c_{2,1} \rho_1 + 2c_{2,2} \rho_2 + \dots + 2c_{2,k-1} \rho_{k-1} + 2c_{2,k} \rho_k - 2c_{2,0}) \beta_2 \\
&\quad \vdots \\
&\quad + c_{k-1,k-1} \beta_{k-1}^2 + (2c_{k-1,1} \rho_1 + 2c_{k-1,2} \rho_2 + \dots + 2c_{k-1,k-1} \rho_{k-1} + 2c_{k-1,k} \rho_k - 2c_{k-1,0}) \beta_{k-1} \\
&\quad + c_{k,k} \beta_k^2 + (2c_{k,1} \rho_1 + 2c_{k,2} \rho_2 + \dots + 2c_{k,k-1} \rho_{k-1} + 2c_{k,k} \rho_k - 2c_{k,0}) \beta_k \\
&\quad + c_{0,0} - 2c_{0,1} \rho_1 - \dots - 2c_{0,k-1} \rho_{k-1} - 2c_{0,k} \rho_k.
\end{aligned} \tag{C.7}$$

As we know, the complete square of the equation (C.7) does not have the linear term, so suppose that

$$\begin{aligned}
2c_{1,1} \rho_1 + 2c_{1,2} \rho_2 + \dots + 2c_{1,k-1} \rho_{k-1} + 2c_{1,k} \rho_k - 2c_{1,0} &= 0 \\
2c_{2,1} \rho_1 + 2c_{2,2} \rho_2 + \dots + 2c_{2,k-1} \rho_{k-1} + 2c_{2,k} \rho_k - 2c_{2,0} &= 0 \\
&\vdots \\
2c_{k-1,1} \rho_1 + 2c_{k-1,2} \rho_2 + \dots + 2c_{k-1,k-1} \rho_{k-1} + 2c_{k-1,k} \rho_k - 2c_{k-1,0} &= 0 \\
2c_{k,1} \rho_1 + 2c_{k,2} \rho_2 + \dots + 2c_{k,k-1} \rho_{k-1} + 2c_{k,k} \rho_k - 2c_{k,0} &= 0.
\end{aligned}$$

This implies the following

$$\begin{aligned}
c_{1,1} \rho_1 + c_{1,2} \rho_2 + \dots + c_{1,k-1} \rho_{k-1} + c_{1,k} \rho_k &= c_{1,0} \\
c_{2,1} \rho_1 + c_{2,2} \rho_2 + \dots + c_{2,k-1} \rho_{k-1} + c_{2,k} \rho_k &= c_{2,0} \\
&\vdots \\
c_{k-1,1} \rho_1 + c_{k-1,2} \rho_2 + \dots + c_{k-1,k-1} \rho_{k-1} + c_{k-1,k} \rho_k &= c_{k-1,0} \\
c_{k,1} \rho_1 + c_{k,2} \rho_2 + \dots + c_{k,k-1} \rho_{k-1} + c_{k,k} \rho_k &= c_{k,0}.
\end{aligned} \tag{C.8}$$

We observe that the equations (C.8) are called nonhomogeneous system of linear equations, so we formulate this system as vector and matrix, that is,

$$\begin{bmatrix} c_{1,1} & c_{1,2} & \cdots & c_{1,k-1} & c_{1,k} \\ c_{2,1} & c_{2,2} & \cdots & c_{2,k-1} & c_{2,k} \\ \vdots & \vdots & \cdots & \vdots & \vdots \\ c_{k-1,1} & c_{k-1,2} & \cdots & c_{k-1,k-1} & c_{k-1,k} \\ c_{k,1} & c_{k,2} & \cdots & c_{k,k-1} & c_{k,k} \end{bmatrix} \begin{bmatrix} \rho_1 \\ \rho_2 \\ \vdots \\ \rho_{k-1} \\ \rho_k \end{bmatrix} = \begin{bmatrix} c_{1,0} \\ c_{2,0} \\ \vdots \\ c_{k-1,0} \\ c_{k,0} \end{bmatrix},$$

where

$$\begin{bmatrix} c_{1,1} & c_{1,2} & \cdots & c_{1,k-1} & c_{1,k} \\ c_{2,1} & c_{2,2} & \cdots & c_{2,k-1} & c_{2,k} \\ \vdots & \vdots & \cdots & \vdots & \vdots \\ c_{k-1,1} & c_{k-1,2} & \cdots & c_{k-1,k-1} & c_{k-1,k} \\ c_{k,1} & c_{k,2} & \cdots & c_{k,k-1} & c_{k,k} \end{bmatrix} = \begin{bmatrix} \langle \mathbf{v}_1, \mathbf{v}_1 \rangle & \langle \mathbf{v}_1, \mathbf{v}_2 \rangle & \cdots & \langle \mathbf{v}_1, \mathbf{v}_{k-1} \rangle & \langle \mathbf{v}_1, \mathbf{v}_k \rangle \\ \langle \mathbf{v}_2, \mathbf{v}_1 \rangle & \langle \mathbf{v}_2, \mathbf{v}_2 \rangle & \cdots & \langle \mathbf{v}_2, \mathbf{v}_{k-1} \rangle & \langle \mathbf{v}_2, \mathbf{v}_k \rangle \\ \vdots & \vdots & \cdots & \vdots & \vdots \\ \langle \mathbf{v}_{k-1}, \mathbf{v}_1 \rangle & \langle \mathbf{v}_{k-1}, \mathbf{v}_2 \rangle & \cdots & \langle \mathbf{v}_{k-1}, \mathbf{v}_{k-1} \rangle & \langle \mathbf{v}_{k-1}, \mathbf{v}_k \rangle \\ \langle \mathbf{v}_k, \mathbf{v}_1 \rangle & \langle \mathbf{v}_k, \mathbf{v}_2 \rangle & \cdots & \langle \mathbf{v}_k, \mathbf{v}_{k-1} \rangle & \langle \mathbf{v}_k, \mathbf{v}_k \rangle \end{bmatrix},$$

and

$$\begin{bmatrix} c_{1,0} \\ c_{2,0} \\ \vdots \\ c_{k-1,0} \\ c_{k,0} \end{bmatrix} = \begin{bmatrix} \langle \mathbf{v}_1, \mathbf{x} \rangle \\ \langle \mathbf{v}_2, \mathbf{x} \rangle \\ \vdots \\ \langle \mathbf{v}_{k-1}, \mathbf{x} \rangle \\ \langle \mathbf{v}_k, \mathbf{x} \rangle \end{bmatrix}.$$

Suppose that

$$C = \begin{bmatrix} c_{1,1} & c_{1,2} & \cdots & c_{1,k-1} & c_{1,k} \\ c_{2,1} & c_{2,2} & \cdots & c_{2,k-1} & c_{2,k} \\ \vdots & \vdots & \cdots & \vdots & \vdots \\ c_{k-1,1} & c_{k-1,2} & \cdots & c_{k-1,k-1} & c_{k-1,k} \\ c_{k,1} & c_{k,2} & \cdots & c_{k,k-1} & c_{k,k} \end{bmatrix}, \mathbf{a} = \begin{bmatrix} \rho_1 \\ \rho_2 \\ \vdots \\ \rho_{k-1} \\ \rho_k \end{bmatrix}, \mathbf{c} = \begin{bmatrix} c_{1,0} \\ c_{2,0} \\ \vdots \\ c_{k-1,0} \\ c_{k,0} \end{bmatrix},$$

so we can formulate the system (C.8) as follows

$$C \mathbf{a} = \mathbf{c}. \quad (\text{C.9})$$

The function \tilde{f} has a global minimum because all coefficients $c_{i,i}$ of the function \tilde{f} are positive, which means that we need to solve the linear system of equations (C.9) using Cramer's rule, that is, finding the variables $\rho_1, \rho_2, \dots, \rho_{k-1}$ and ρ_k . Therefore, we find that

$$\rho_1 = \frac{|C_1|}{|C|}, \dots, \rho_k = \frac{|C_k|}{|C|},$$

where

$$|C| = \begin{vmatrix} c_{1,1} & c_{1,2} & \cdots & c_{1,k-1} & c_{1,k} \\ c_{2,1} & c_{2,2} & \cdots & c_{2,k-1} & c_{2,k} \\ \vdots & \vdots & \cdots & \vdots & \vdots \\ c_{k-1,1} & c_{k-1,2} & \cdots & c_{k-1,k-1} & c_{k-1,k} \\ c_{k,1} & c_{k,2} & \cdots & c_{k,k-1} & c_{k,k} \end{vmatrix} \neq 0,$$

and

$$|C_1| = \begin{vmatrix} c_{1,0} & c_{1,2} & \cdots & c_{1,k-1} & c_{1,k} \\ c_{2,0} & c_{2,2} & \cdots & c_{2,k-1} & c_{2,k} \\ \vdots & \vdots & \cdots & \vdots & \vdots \\ c_{k-1,0} & c_{k-1,2} & \cdots & c_{k-1,k-1} & c_{k-1,k} \\ c_{k,0} & c_{k,2} & \cdots & c_{k,k-1} & c_{k,k} \end{vmatrix}, \dots, |C_k| = \begin{vmatrix} c_{1,1} & c_{1,2} & \cdots & c_{1,k-1} & c_{1,0} \\ c_{2,1} & c_{2,2} & \cdots & c_{2,k-1} & c_{2,0} \\ \vdots & \vdots & \cdots & \vdots & \vdots \\ c_{k-1,1} & c_{k-1,2} & \cdots & c_{k-1,k-1} & c_{k-1,0} \\ c_{k,1} & c_{k,2} & \cdots & c_{k,k-1} & c_{k,0} \end{vmatrix}$$

Therefore, the critical point (stationary point) can be posed as follows

$$\mathbf{r} = (\rho_1, \rho_2, \dots, \rho_{k-1}, \rho_k)$$

This leads to the minimal value of function $\tilde{f}(\alpha_1, \dots, \alpha_k)$ to be written as follows

$$\tilde{f}(\rho_1, \dots, \rho_k) = \tilde{f}(\mathbf{r}),$$

so we find that the minimisation of the Euclidean norm (C.4) is as follows

$$\|\mathbf{x} - \rho_1 \mathbf{v}_1 - \dots - \rho_k \mathbf{v}_k\|_2^2 = \tilde{f}(\mathbf{r}). \tag{C.10}$$

BIBLIOGRAPHY

- [1] K. AGLADZE AND O. STEINBOCK, *Waves and vortices of rust on the surface of corroding steel*, The Journal of Physical Chemistry A, 104 (2000), pp. 9816–9819.
- [2] M. A. ALLESSIE, F. I. BONKE, AND F. J. SCHOPMAN, *Circus movement in rabbit atrial muscle as a mechanism of tachycardia*, Circulation research, 33 (1973), pp. 54–62.
- [3] M. ANTONIOLETTI, V. N. BIKTASHEV, A. JACKSON, S. R. KHARCHE, T. STARY, AND I. V. BIKTASHEVA, *Beatbox, Äihpc simulation environment for biophysically and anatomically realistic cardiac electrophysiology*, PloS one, 12 (2017), p. e0172292.
- [4] D. BARKLEY, *A model for fast computer simulation of waves in excitable media*, Physica D: Nonlinear Phenomena, 49 (1991), pp. 61–70.
- [5] R. A. BEEZER, *A first course in linear algebra*, Beezer, 2008.
- [6] A. J. BERNOFF, *Spiral wave solutions for reaction-diffusion equations in a fast reaction / slow diffusion limit*, Physica D: Nonlinear Phenomena, 53 (1991), pp. 125–150.
- [7] O. BERNUS, H. VERSCHELDE, AND A. PANFILOV, *Spiral wave stability in cardiac tissue with biphasic restitution*, Physical Review E, 68 (2003), p. 021917.
- [8] V. BIKTASHEV, *Causodynamics of autowave patterns*, Physical review letters, 95 (2005), p. 084501.
- [9] V. BIKTASHEV AND A. HOLDEN, *Resonant drift of autowave vortices in two dimensions and the effects of boundaries and inhomogeneities*, Chaos, Solitons & Fractals, 5 (1995), pp. 575 – 622.

BIBLIOGRAPHY

- [10] V. BIKTASHEV AND A. HOLDEN, *Resonant drift of autowave vortices in two dimensions and the effects of boundaries and inhomogeneities*, *Chaos, Solitons & Fractals*, 5 (1995), pp. 575–622.
- [11] V. BIKTASHEV, A. HOLDEN, AND E. NIKOLAEV, *Spiral wave meander and symmetry of the plane*, *International Journal of Bifurcation and Chaos*, 6 (1996), pp. 2433–2440.
- [12] V. N. BIKTASHEV, *Envelope equations for modulated non-conservative waves*, in *IUTAM Symposium on Asymptotics, Singularities and Homogenisation in Problems of Mechanics*, Springer, 2003, pp. 525–535.
- [13] V. N. BIKTASHEV, I. V. BIKTASHEVA, AND N. A. SARVAZYAN, *Evolution of spiral and scroll waves of excitation in a mathematical model of ischaemic border zone*, *PLoS One*, 6 (2011), p. e24388.
- [14] I. BIKTASHEVA, D. BARKLEY, V. BIKTASHEV, G. BORDYUGOV, AND A. FOULKES, *Computation of the response functions of spiral waves in active media*, *Physical Review E*, 79 (2009), p. 056702.
- [15] I. V. BIKTASHEVA, *Dynamics of Spiral Waves in Perturbed Excitable Media.*, PhD thesis, The University of Leeds, 2001.
- [16] I. V. BIKTASHEVA, A. V. HOLDEN, AND V. N. BIKTASHEV, *Localization of response functions of spiral waves in the fitzhugh–nagumo system*, *International Journal of Bifurcation and Chaos*, 16 (2006), pp. 1547–1555.
- [17] A. BUENO-OROVIO, E. M. CHERRY, AND F. H. FENTON, *Minimal model for human ventricular action potentials in tissue*, *Journal of theoretical biology*, 253 (2008), pp. 544–560.
- [18] D. CAUSON AND C. MINGHAM, *Introductory finite difference methods for PDEs*, Bookboon, 2010.
- [19] E. M. CHERRY AND F. H. FENTON, *Visualization of spiral and scroll waves in simulated and experimental cardiac tissue*, *New Journal of Physics*, 10 (2008), p. 125016.

- [20] B. COX AND W. COX, *Vector Calculus*, Butterworth-Heinemann, 1998.
- [21] J. CRONIN, *Mathematical aspects of Hodgkin-Huxley neural theory*, vol. 7, Cambridge University Press, 1987.
- [22] W. DUCH, J. KACPRZYK, E. OJA, AND S. ZADROŻNY, *Artificial Neural Networks: Formal Models and Their Applications. ICANN 2005*, Springer Berlin/Heidelberg., 2005.
- [23] D. G. DUFFY, *Advanced engineering mathematics with MATLAB*, CRC Press, 2016.
- [24] F. FENTON AND A. KARMA, *Vortex dynamics in three-dimensional continuous myocardium with fiber rotation: filament instability and fibrillation*, *Chaos: An Interdisciplinary Journal of Nonlinear Science*, 8 (1998), pp. 20–47.
- [25] F. H. FENTON, E. M. CHERRY, H. M. HASTINGS, AND S. J. EVANS, *Multiple mechanisms of spiral wave breakup in a model of cardiac electrical activity*, *Chaos: An Interdisciplinary Journal of Nonlinear Science*, 12 (2002), pp. 852–892.
- [26] C. P. FERREIRA AND W. A. GODOY, *Ecological modelling applied to entomology*, Springer, 2014.
- [27] R. FITZHUGH, *Thresholds and plateaus in the hodgkin-huxley nerve equations*, *The Journal of general physiology*, 43 (1960), pp. 867–896.
- [28] R. FITZHUGH, *Impulses and physiological states in theoretical models of nerve membrane*, *Biophysical journal*, 1 (1961), pp. 445–466.
- [29] G. FLOQUET, *Sur les equations differentielles lineaires*, *Ann. ENS [2]*, 12 (1883), pp. 47–88.
- [30] A. J. FOULKES, *Drift and meander of spiral waves*, arXiv preprint arXiv:0912.4247, (2009).
- [31] M. B. GILES AND N. A. PIERCE, *An introduction to the adjoint approach to design*, *Flow, turbulence and combustion*, 65 (2000), pp. 393–415.
- [32] L. GLASS AND M. E. JOSEPHSON, *Resetting and annihilation of reentrant abnormally rapid heartbeat*, *Physical review letters*, 75 (1995), p. 2059.

BIBLIOGRAPHY

- [33] P. GLENDINNING, *Stability, instability and chaos: an introduction to the theory of nonlinear differential equations*, vol. 11, Cambridge university press, 1994.
- [34] R. GOLDMAN, *Curvature formulas for implicit curves and surfaces*, *Computer Aided Geometric Design*, 22 (2005), pp. 632–658.
- [35] N. GORELOVA AND J. BUREŠ, *Spiral waves of spreading depression in the isolated chicken retina*, *Journal of neurobiology*, 14 (1983), pp. 353–363.
- [36] G. GOTTWALD, A. PUMIR, AND V. KRINSKY, *Spiral wave drift induced by stimulating wave trains*, *Chaos: An Interdisciplinary Journal of Nonlinear Science*, 11 (2001), pp. 487–494.
- [37] R. A. GRAY, J. JALIFE, A. PANFILOV, W. T. BAXTER, C. CABO, J. M. DAVIDENKO, AND A. M. PERTSOV, *Nonstationary vortexlike reentrant activity as a mechanism of polymorphic ventricular tachycardia in the isolated rabbit heart*, *Circulation*, 91 (1995), pp. 2454–2469.
- [38] J. GUCKENHEIMER AND P. J. HOLMES, *Nonlinear oscillations, dynamical systems, and bifurcations of vector fields*, vol. 42, Springer Science & Business Media, 2013.
- [39] Y. GUO, Y. ZHAO, S. BILLINGS, D. COCA, R. RISTIC, AND L. DEMATOS, *Identification of excitable media using a scalar coupled map lattice model*, *International Journal of Bifurcation and Chaos*, 20 (2010), pp. 2137–2150.
- [40] I. HARGITTAI AND C. A. PICKOVER, *Spiral symmetry*, World Scientific, 1992.
- [41] P. HARTMAN, *Ordinary differential equations*, American Mathematical Society Providence, 1964.
- [42] S. HERMANN AND G. A. GOTTWALD, *The large core limit of spiral waves in excitable media: A numerical approach*, *SIAM Journal on Applied Dynamical Systems*, 9 (2010), pp. 536–567.
- [43] J.-B. HIRIART-URRUTY AND A. SEEGER, *A variational approach to copositive matrices*, *SIAM review*, 52 (2010), pp. 593–629.

- [44] A. L. HODGKIN AND A. F. HUXLEY, *A quantitative description of membrane current and its application to conduction and excitation in nerve*, The Journal of physiology, 117 (1952), pp. 500–544.
- [45] E. M. IZHIKEVICH, *Dynamical systems in neuroscience*, MIT press, 2007.
- [46] S. JAKUBITH, H. ROTERMUND, W. ENGEL, A. VON OERTZEN, AND G. ERTL, *Spatiotemporal concentration patterns in a surface reaction: Propagating and standing waves, rotating spirals, and turbulence*, Physical Review Letters, 65 (1990), p. 3013.
- [47] D. W. JORDAN AND P. SMITH, *Nonlinear ordinary differential equations: an introduction to dynamical systems*, vol. 2, Oxford University Press, USA, 1999.
- [48] E. KALNAY, *Atmospheric modeling, data assimilation and predictability*, Cambridge university press, 2003.
- [49] A. KARMA, *Spiral breakup in model equations of action potential propagation in cardiac tissue*, Physical review letters, 71 (1993), p. 1103.
- [50] ———, *Electrical alternans and spiral wave breakup in cardiac tissue*, Chaos: An Interdisciplinary Journal of Nonlinear Science, 4 (1994), pp. 461–472.
- [51] R. KAUFMANN AND C. BOTHBERGER, *Beitrag zur kenntnis der entstehungsweise extrasystolischer allorhythmien*, Zeitschrift für die gesamte experimentelle Medizin, 5 (1917), pp. 349–370.
- [52] J. KEENER AND J. SNEYD, *Mathematical Physiology*, Springer, 2004.
- [53] J. P. KEENER AND J. J. TYSON, *Spiral waves in the belousov-zhabotinskii reaction*, Physica D: Nonlinear Phenomena, 21 (1986), pp. 307–324.
- [54] E. J. KIRKLAND, *Advanced computing in electron microscopy*, Springer Science & Business Media, 2010.

BIBLIOGRAPHY

- [55] V. KRINSKY AND K. AGLADZE, *Interaction of rotating waves in an active chemical medium*, *Physica D: Nonlinear Phenomena*, 8 (1983), pp. 50–56.
- [56] Y. A. KUZNETSOV, *Elements of applied bifurcation theory*, vol. 112, Springer Science & Business Media, 2013.
- [57] L. RIDGWAY SCOTT, *Numerical Analysis*, Princeton University Press., 2011.
- [58] J. LANGHAM, I. BIKTASHEVA, AND D. BARKLEY, *Asymptotic dynamics of reflecting spiral waves*, *Physical Review E*, 90 (2014), p. 062902.
- [59] J. LIESEN AND V. MEHRMANN, *Linear algebra*, Springer, 2015.
- [60] R.-M. MANTEL AND D. BARKLEY, *Periodic forcing of spiral waves in excitable media*, *Physical Review E*, 54 (1996), p. 4791.
- [61] C. D. MARCOTTE AND R. O. GRIGORIEV, *Unstable spiral waves and local euclidean symmetry in a model of cardiac tissue*, *Chaos: An Interdisciplinary Journal of Nonlinear Science*, 25 (2015), p. 063116.
- [62] C. D. MEYER, *Matrix analysis and applied linear algebra*, vol. 2, Siam, 2000.
- [63] A. B. MOVCHAN, *IUTAM Symposium on Asymptotics, Singularities and Homogenisation in Problems of Mechanics*, vol. 113, Springer Science & Business Media, 2004.
- [64] J. MURRAY, *On travelling wave solutions in a model for the belousov-zhabotinskii reaction*, *Journal of theoretical biology*, 56 (1976), pp. 329–353.
- [65] J. MURRAY, *Mathematical Biology*, Springer: Interdisciplinary Applied Mathematics, 2003.
- [66] J. NAGUMO, S. ARIMOTO, AND S. YOSHIZAWA, *An active pulse transmission line simulating nerve axon*, *Proceedings of the IRE*, 50 (1962), pp. 2061–2070.
- [67] A. PANFILOV, R. KELDERMANN, AND M. NASH, *Drift and breakup of spiral waves in reaction–diffusion–mechanics systems*, *Proceedings of the National Academy of Sciences*, 104 (2007), pp. 7922–7926.

- [68] L. PERKO, *Differential equations and dynamical systems*, vol. 7, Springer Science & Business Media, 2013.
- [69] A. PERTSOV, E. ERMAKOVA, AND A. PANFILOV, *Rotating spiral waves in a modified fitzhugh-nagumo model*, *Physica D: Nonlinear Phenomena*, 14 (1984), pp. 117–124.
- [70] W. H. PRESS, S. A. TEUKOLSKY, W. T. VETTERLING, AND B. P. FLANNERY, *Numerical recipes in C*, vol. 2, Cambridge university press Cambridge, 1982.
- [71] Y. SAAD AND M. H. SCHULTZ, *Gmres: A generalized minimal residual algorithm for solving nonsymmetric linear systems*, *SIAM Journal on scientific and statistical computing*, 7 (1986), pp. 856–869.
- [72] H. SAKAGUCHI AND T. FUJIMOTO, *Elimination of spiral chaos by periodic force for the aliev-panfilov model*, *Physical Review E*, 67 (2003), p. 067202.
- [73] B. SANDSTEDTE AND A. SCHEEL, *Absolute versus convective instability of spiral waves*, *Physical Review E*, 62 (2000), p. 7708.
- [74] J. SCHLESNER, V. ZYKOV, H. ENGEL, AND E. SCHÖLL, *Stabilization of unstable rigid rotation of spiral waves in excitable media*, *Physical Review E*, 74 (2006), p. 046215.
- [75] E. SCHÖLL AND H. G. SCHUSTER, *Handbook of chaos control*, John Wiley & Sons, 2008.
- [76] A. SCOTT ET AL., *Encyclopedia of nonlinear science*, Routledge, 2006.
- [77] N. SHANKS, *Modeling biological systems: the belousov–zhabotinsky reaction*, *Foundations of Chemistry*, 3 (2001), pp. 33–53.
- [78] K. SHOWALTER AND I. R. EPSTEIN, *From chemical systems to systems chemistry: Patterns in space and time*, *Chaos: An Interdisciplinary Journal of Nonlinear Science*, 25 (2015), p. 097613.
- [79] M. STINGL, *Quadratic programming and affine variational inequalities: a qualitative study by gm lee, nn tam and nd yen*, 2007.

BIBLIOGRAPHY

- [80] F. SZABO, *Linear algebra: an introduction using Mathematica*, Academic Press, 2000.
- [81] G. TESCHL, *Ordinary differential equations and dynamical systems*, vol. 140, American Mathematical Society Providence, 2012.
- [82] E. TROFIMCHUK, M. PINTO, AND S. TROFIMCHUK, *Traveling waves for a model of the belousov–zhabotinsky reaction*, *Journal of Differential Equations*, 254 (2013), pp. 3690–3714.
- [83] A. TURING, *The chemical basis of morphogenesis*, *Phil. Trans. Roy. Soc. Londl.*, 237 (1952), pp. 37–72.
- [84] J. J. TYSON AND L. GLASS, *Arthur t. winfree (1942–2002)*, 2004.
- [85] J. WALLECZEK, *Self-organized biological dynamics and nonlinear control: toward understanding complexity, chaos and emergent function in living systems*, Cambridge University Press, 2006.
- [86] D. S. WATKINS, *Fundamentals of matrix computations*, vol. 64, John Wiley & Sons, 2004.
- [87] N. WIENER AND A. ROSENBLUETH, *The mathematical formulation of the problem of conduction of impulses in a network of connected excitable elements, specifically in cardiac muscle.*, *Archivos del instituto de Cardiología de México*, 16 (1946), pp. 205–265.
- [88] J. H. WILKINSON AND J. H. WILKINSON, *The algebraic eigenvalue problem*, vol. 87, Clarendon Press Oxford, 1965.
- [89] A. WINFREE, *Spiral waves of chemical activity*, *Science*, 175 (1972), pp. 634–636.
- [90] A. T. WINFREE, *When time breaks down: the three-dimensional dynamics of electrochemical waves and cardiac arrhythmias*, vol. 14.
- [91] ———, *Rotating chemical reactions*, *Scientific American*, 230 (1974), pp. 82–95.

- [92] ———, *Varieties of spiral wave behavior: An experimentalist's approach to the theory of excitable media*, *Chaos: An Interdisciplinary Journal of Nonlinear Science*, 1 (1991), pp. 303–334.
- [93] C. WULFF, *Spiral waves and euclidean symmetries*, *Zeitschrift für Physikalische Chemie*, 216 (2002), p. 535.
- [94] B. XU, S. BINZAK, S. JACQUIR, O. PONT, AND H. YAHIA, *Parameters analysis of fitzhugh-nagumo model for a reliable simulation*, in 2014 36th Annual International Conference of the IEEE Engineering in Medicine and Biology Society, IEEE, 2014, pp. 4334–4337.
- [95] L. XU, Z. LI, Z. QU, AND Z. DI, *Resonance drifts of spiral waves on media of periodic excitability*, *Physical Review E*, 85 (2012), p. 046216.
- [96] M. YONEYAMA, A. FUJII, AND S. MAEDA, *Wavelength-doubled spiral fragments in photosensitive monolayers*, *Journal of the American Chemical Society*, 117 (1995), pp. 8188–8191.
- [97] G. YUAN, A. XU, G. WANG, AND S. CHEN, *Control of spiral-wave dynamics using feedback signals from line detectors*, *EPL (Europhysics Letters)*, 90 (2010), p. 10013.
- [98] A. ZHABOTINSKY AND A. ZAIKIN, *Autowave processes in a distributed chemical system*, *Journal of theoretical biology*, 40 (1973), pp. 45IN157–56IN361.
- [99] V. S. ZYKOV AND A. T. WINFREE, *Simulation of wave processes in excitable media*, John Wiley & Sons, Inc., 1992.

